SITE CHARACTERIZATION PLAN

Chapter 2.0

GEOENGINEERING

K. Kim
Lead Author

encl. to Site Char. Plan
Chptr. 2.0 rec'd 1/20/87
CONTROLLED DRAFT 0   101.8
NOVEMBER 24, 1986

TABLE OF CONTENTS

TABLE OF CONTENTS (Continued)

TABLE OF CONTENTS (Continued)

TABLE OF CONTENTS (Continued)

LIST OF FIGURES

LIST OF FIGURES (Continued)

LIST OF FIGURES (Continued)

LIST OF FIGURES (Continued)

LIST OF TABLES

LIST OF TABLES (Continued)

LIST OF TABLES (Continued)

Chapter 2

GEOENGINEERING

2.0 INTRODUCTION

Geoengineering is a scientific discipline that deals with the response of rock and rock masses to the force fields of their physical environment. Understanding of geoengineering properties of host rock is of fundamental importance for repository construction feasibility study since the host rock provides a structural barrier to the migration of radionuclides. The shafts, access drifts, emplacement rooms, and emplacement holes should be designed and excavated in such a way that they remain stable during the repository life. To assure adequate performance of the repository in the preclosure and postclosure stages, rock properties and the underground conditions surrounding the repository should be understood thoroughly. Advanced knowledge of underground conditions and rock characteristics has aided design of underground structures significantly; although it is difficult to obtain adequate knowledge when the underground is accessible only through small-diameter boreholes.

This chapter presents a summary of current understanding of geoengineering properties of the repository host rock and underground conditions affecting construction, operation, and decommissioning of the repository being considered at the Hanford Site. They include (1) mechanical and thermal properties of intact basalt and rock mass, (2) in situ stress condition, (3) underground excavation characteristics, and (4) other special geoengineering characteristics. The information presented in the chapter has been used as a guideline for developing strategies for resolving technical issues discussed in Section 8.2.

2.0.1 PURPOSE AND OBJECTIVE

The overall purpose of the geoengineering program is to establish a geotechnical data base for the design and evaluation of a repository system. The geoengineering program also provides input to and interacts with the geologists to develop the site characterization, geohydrology, and backfill and sealing programs. In addition, the geoengineering program provides parameters needed in performance assessment.

The repository system design process includes selection of the underground layout, emplacement room shapes, emplacement configuration, and ground support requirements. The conceptual interaction of components of the overall program leading to a licensable repository design are shown in Figure 2.0-1. The first component, data collection, is an evolutionary process which continues throughout site characterization, site selection, and repository construction.

Geoengineering data will be collected from boreholes, outcrops, and the Exploratory Shaft Facility. Data collection will be guided by the issue resolution strategy as discussed in Chapter 8, and will be constantly modified by the results of data analysis and integration activities, and the evolution of test methodologies. The data will then be used to support site selection, geoengineering numerical modeling, and repository design activities required for performance assessment and license application. The process will continue until all issues have been resolved and a licensable repository design has been produced.

The geoengineering program has played and will continue to play an active role in each stage. Geoengineering numerical modeling provides input to site selection and to the design of emplacement room shape, ground support requirements, and waste emplacement densities. As the design matures from site characterization conceptual design to advanced conceptual design and license application design, more detailed and defensible site-specific design parameters will be required. The geoengineering program will define and provide the geotechnical parameters as the design evolves through its various stages.

The major objectives of this chapter are as follow:

o To provide a compilation of geoengineering data available to date.

o To present conceptual rock mass models supported by current data and numerical predictive models that have been used to interpret in situ test results.

o To define uncertainties in current geoengineering data and areas where further information may be required.

2.0.2 SOURCES OF AVAILABLE INFORMATION

The Basalt Waste Isolation Project (BWIP) geoengineering program has evolved since 1977 to provide the data needed to evaluate the feasibility of constructing a nuclear waste repository in the basalt of the Columbia Plateau. Geoengineering data available to date are from the following sources:

o Surface core hole tests.
o Outcrop mapping.
o Field tests at the Near-Surface Test Facility.
o Case studies on similar rocks (literature).

Data obtained after January 1986 are not included in this report.

The core-hole data consist of downhole tests (hydraulic fracturing), core inspection (logging for joint frequency and fracture infillings), and core testing (laboratory thermal and mechanical properties of intact and jointed rock).

Outcrop mapping provides data on joint continuity, joint spacings, joint roughness, and number of joint sets. This section references sections of Chapter 1 when appropriate.

The Near-Surface Test Facility is located in the northern side of Gable Mountain, a basalt outcrop in the north-central part of the Hanford Site. The facility consists of three tunnels and three rooms as shown in Figure 2.0-2. These tunnels are located in the entablature of the Pomona flow and are approximately 47.5 m (150 ft) below the surface. Therefore, the conditions of stress, water, temperature, and rock mass behavior at the Near-Surface Test Facility are not representative of conditions expected at depth. The geology, construction experience, and preliminary characterization tests involved with the facility were described by Moak and Wintczak (1980).

The Near-Surface Test Facility provided a location to conduct tests in basalt. It was intended to gain a general understanding of basalt rock mass behavior under thermal loading conditions expected in the repository and to develop and demonstrate experimental technology for large-scale rock property measurement. Geoengineering tests that have been completed at the Near-Surface Test Facility include:

o Full-Scale Heater Test 1.
o Full-Scale Heater Test 2.
o The jointed block test.
o Stress measurement technique evaluation/development tests.

The first three tests involved both mechanical and thermomechanical components and are discussed in Sections 2.3 and 2.5. The stress measurement development tests are presented in Section 2.6. Additional field and laboratory tests were carried out in support of these tests in the Near-Surface Test Facility. The Near-Surface Test Facility test results are not directly applicable to repository design. However, the Near-Surface Test

Facility investigations have provided rock mass thermal and mechanical characteristics of basalt and have been useful in evaluating design concepts.

Literature studies and visits to underground excavations in similar rock provide valuable information on the expected response of basalt to excavation and thermal loading. No existing excavation is located in basalt under similar stress conditions, but quantification of existing excavation experience under high in situ stress fields and in jointed crystalline rock similar to basalt provides valuable information for planning and comparing design alternatives.

2.0.3 PLANS FOR OBTAINING ADDITIONAL INFORMATION

The geoengineering program is ongoing and not complete, as evidenced by Section 8.3.3.2. At present, data from the candidate repository horizon are limited, and plans have been made to obtain additional information from core testing and from in situ tests in the Exploratory Shaft Facility.

The Exploratory Shaft Test Program will include geologic characterization and in situ measurements of mechanical and thermal properties and observation of rock mass performance behavior at the repository horizon. These are presented in Section 8.3.2.2.

2.0.4 INFORMATION USE

The current geoengineering program is directed to support repository design, to characterize the site, and to provide data required for performance assessment. The geoengineering data and information will be used to resolve the technical issues identified in Section 8.2.

The data presented in this chapter provided input to the Site Characterization Plan (SCP) conceptual design (KE/PB, 1986) and was used to develop the site characterization program described in Section 8.3.2.2.

Geoengineering information will also be used to support the development of the future performance confirmation program, which is required in 10 CFR 60, Subpart F (NRC, 1985). The performance confirmation program will begin at site characterization and continue until permanent closure. The program will provide data to verify that the subsurface conditions at the repository horizon are within the limits assumed in the licensing review and to confirm that the repository will function as intended or anticipated. The geoengineering program that will be used to support performance confirmation includes such activities as in situ monitoring and laboratory and in situ testing. The data presented in this chapter will be used in part to develop the baseline conditions in the performance confirmation program.

2.0.5 CONCEPTUAL MODELS SUPPORTED BY INFORMATION

A rock mass is composed of blocks of intact rock separated by discontinuities. The transition from intact rock material to a large, heavily jointed rock mass occurs at an increasing scale as illustrated in Figure 2.0-3. All three stages of this transition are related to different aspects of repository design. (1) Intact rock material has a strong influence on the drilling, boring, and blasting operations. (2) The strength of discontinuities is related to excavation stability and support requirements. (3) The stability of the repository depends on the behavior of the entire rock mass surrounding the repository.

A proper conceptual model must, therefore, contain two vital elements: (1) It must be capable of incorporating the complex interaction between intact rock and discontinuities in the behavior of the rock mass; (2) It must be formulated to reflect the scale of concern. Incorporating the first element means that different conceptual models may have to be developed for the deformation, strength, and thermal properties of the rock mass because the degree of interaction between the intact rock material and discontinuities may not be identical in different processes. Incorporating the second element requires that the conceptual models be developed according to the field of application for which these models were intended. For instance, a conceptual model for the rock mass strength used in assessing the stability of repository openings may differ from one that is used for the stability of emplacement holes because different scales are involved. Therefore, there is no universal model that can be used in all geoengineering aspects of repository design, and a number of models have been developed. These models are described in Sections 2.3.3 and 2.3.5.

Two different approaches have been taken in developing rock mass conceptual models for the BWIP geoengineering program. The first approach used empirical methods to correlate the observed rock mass behavior with measured properties of the intact rock material, discontinuities, and fracture characteristics of the rock mass. The second approach developed numerically based constitutive models from first principles. Both approaches will be described in this chapter as there is insufficient data to select one against the other at present. Most of these models, however, were partially supported by the information currently available.

A number of numerical predictive models have been developed to support field testing at the Near-Surface Test Facility and repository design. Discrete element and finite element models were used to study the mechanical response of the basalt rock mass. Thermomechanical response of the basalt rock mass was modeled by boundary element and finite element models. These models were able to predict measured quantities and in many cases correlate reasonably well with measured response. At present, however, there are insufficient data to establish the validity of the models (Sections 2.3.3 and 2.5.3).

2.0.6 DATA ADEQUACY

As stated in Section 2.0.4, the data presented in this chapter were intended to provide input to the SCP conceptual design and to the development of the site characterization program. These data are judged to be adequate for these purposes. The data are, however, not adequate for the next stage of design activities because of uncertainties associated with the data base. The major sources of data uncertainties in the current data base can be summarized as follow:

o Current knowledge of the variation of rock quality both laterally and vertically within the Cohassett flow is not sufficient.

o Many of the test methods used in the present study were in a prototype stage of development.

o Test results were obtained from a limited number of samples and large-scale site-specific tests were not performed.

o Quality assurance procedures meeting present standards were not in place due to the preliminary nature of the investigation.

o Some data were obtained under conditions of stress, water, and temperature not representative of conditions expected at depth.

These uncertainties may not be resolved until access to the repository horizon becomes available. This is because reliable information regarding detailed geological conditions and large-scale rock mass properties cannot be obtained without sufficient exposure of the at-depth rock conditions. The limitations of the existing data are, therefore, primarily due to the lack of access to the repository horizon.

This limitation is more significant for basalt than for other potential host media, because of the jointed nature of the basalt rock mass and because no similar mining or civil excavation in basalt exists from which a meaningful comparison can be made. Further information will be obtained when the Exploratory Shaft is constructed and the development and in situ testing at the proposed repository horizon is complete (Section 8.3.3.2).

2.0.7 PRESENTATION OF TOPICS

The development of the geoengineering program in the BWIP follows a rationale approach starting from an understanding of the behavior of the components of the rock mass to an investigation of the behavior of the rock mass, the in situ stress regime, and the excavation characteristics of basalt. The various topics that will be discussed in this chapter follow.

Mechanical properties of basalt include the strength and deformation properties. These are discussed in Section 2.1 through Section 2.3 and are

used to assess the stability of the repository. Section 2.1 describes the strength, elastic modulus, and porosity of the intact basalt of the Cohassett flow dense interior, flow top, and vesicular zones obtained from laboratory testing of core samples from the reference repository location. Section 2.2 discusses the physical characteristics, strength, and stiffness of basalt joints from the Hanford Site. Specific data from the basalt joints of the Cohassett flow were not available, although the data indicate a likely range of values. Large-scale mechanical properties are discussed in Section 2.3. This section is based on the results of in situ tests carried out at the Near-Surface Test Facility in the Pomona flow. Section 2.3 also contains a general discussion of the conceptual models that have been developed.

Thermal and thermomechanical properties including thermal conductivity, heat capacity, and coefficient of thermal expansion of basalt are discussed in Sections 2.4 and 2.5. These properties are used to estimate the temperature, heat flow, and thermally induced stresses in the repository. The thermal and thermomechanical properties of intact basalt from the Cohassett flow are presented in Section 2.4. Large-scale thermal and thermomechanical properties based on the results of in situ tests in the Near-Surface Test Facility are discussed in Section 2.5. These test results suggest that the large-scale thermal and thermomechanical properties of the Pomona flow are reasonably close to those of the intact rock and that basalt can sustain the high-temperature conditions similar to that expected in the repository.

The in situ stress regime as determined from a number of different approaches is presented in Section 2.6. This is an important parameter in the design of repository layout and room shapes and in assessing the tectonic stability of the repository. Directions and the magnitudes of the in situ stresses were determined from hydraulic fracturing tests conducted in deep boreholes within the reference repository location. The results of the stress orientations from the hydraulic fracturing tests are in general agreement with those obtained from other indirect methods.

Special geoengineering properties as discussed in Section 2.7 include the potential for rock bursting, thermal degradation, and dehydration or saturation of joints between blocks of intact basalt. These properties impact construction, waste isolation, and retrievability.

Section 2.8 presents the excavation characteristics of basalt. These are characteristics that may affect the cost of construction and the safety of workers during the construction of an underground repository. Key characteristics are jointing, water inflow, rock temperature, and potential gas inflow during construction.

2.1 MECHANICAL PROPERTIES OF ROCK UNITS—INTACT ROCK

2.1 Mechanical Properties of Rock Units—Intact Rock
    2.1.0 Introduction
    2.1.1 Mechanical properties of other rocks—intact rock
    2.1.2 Mechanical properties of rocks at the Hanford Site
        2.1.2.1 Results from the Hanford Site outside the
              reference repository location
        2.1.2.2 Results from the reference repository
              location core
        2.1.2.3 Temperature effects
        2.1.2.4 Creep properties
        2.1.2.5 Moisture effects
        2.1.2.6 Anisotropic properties
        2.1.2.7 Discussion of results
    2.1.3 Summary

2.1.0 INTRODUCTION

An understanding of the mechanical properties of intact rock and how they vary with temperature and moisture is the first step toward gaining an understanding of rock mass behavior that is essential for a successful repository design. The two most important properties of intact rock in relation to repository design are the compressive strength and elastic modulus. These are used to assess the constructibility, borability, and other excavation characteristics of the basalt. These are also used as part of the input values for estimating preliminary rock mass properties.

The objective of BWIP mechanical property testing performed to date has been to obtain the average values and ranges of mechanical properties of intact basalt within the reference repository location. Laboratory tests have been performed on intact core samples taken from 14 boreholes drilled from the surface on the Hanford Site. These tests were performed to support in situ testing at the Near-Surface Test Facility and the initial site and horizon selection studies. The completed laboratory studies are listed in Table 2.1-1. Procedures used in the tests performed by the BWIP are contained in BWIP operating procedures. The flow diagram giving the order in which testing is conducted is shown in Figure 2.1-1.

This section summarizes the mechanical properties of intact basalt in general, followed by that of the basalt at the Hanford Site and, specifically, the basalt from the Cohassett flow. Test results of basalt samples from the Hanford Site presented in this section were presented in Sublette (1983, pp. 27-35) and Schmidt et al. (1980, pp. 2-9). The compressive strength, tensile strength, and elastic modulus values presented in this section form the basis for the development of rock mass properties (Section 2.3.3.3) which were used in the SCP Conceptual Design.

The effects of heating and fluid pressure on the mechanical properties and the anisotropic behavior are important considerations in the design analysis and performance assessment of the repository. However, the candidate host rock was changed from the Umtanum flow to the Cohassett flow in August 1984, and these effects have not been studied on intact basalt samples from the Cohassett flow. Thus, the discussion of the effects of heating and fluid pressure will be based on the flows that have been studied for an indication of the possible effects on the Cohassett flow.

2.1.1 MECHANICAL PROPERTIES OF OTHER ROCKS--INTACT ROCK

A list of mechanical property ranges for several basalts is presented for comparison in Table 2.1-2. The term "basalt" refers to a fine-grained, glassy, igneous rock resulting from the rapid cooling of an erupted lava flow. A typical basalt flow can be divided into the following intraflow structures: flow top, flow interior, and flow base. Typical intraflow structures of the Cohassett flow within the reference repository location are shown in Chapter 1, Figure 1.2-35. The flow-top is usually vesicular and brecciated. The flow interior comprises an entablature and colonnade, which are referred to collectively as the dense interior. Vesicular zones may occasionally occur within the flow interior. The flow base usually exists in the form of a glassy, chilled margin or a thin vesicular to brecciated zone. Depending on its location within the flow, the mechanical properties of intact basalt may vary over a wide range. For example, data on the strength of Dresser dense-interior basalt, shown in Table 2.1-2, show that Dresser basalt has the highest mean strength of the eight rock types tested by Krech et. al. (1974). On the other hand, samples containing weathered and flow-top materials may exhibit relatively low strength such as the test results for the Bacon Siphon Tunnel listed in Agapito et al. (1977, pp. 34-35). The strength of intact basalt from the dense flow interior is comparable to dolerites and diorite, and is, in general, stronger than granites and other larger grain, intrusive igneous rocks.

The tensile strength and elastic modulus of intact basalt showed a variation similar to compressive strength. A wide variation of strength and elastic modulus has been reported for the basalts from the Bacon Siphon Tunnel in Washington State, the Ahmeek Copper Mine, in Michigan, and Miocene-time basalt in Oregon. The present data base does not contain sufficient detail for an assessment of the uncertainties and possible ranges of variation of mechanical properties of intact basalt.

Relatively few values of Poisson's ratio for intact basalt have been reported in the literature. Those shown in Table 2.1-2 fall within the range of 0.1 to 0.3.

2.1.2 MECHANICAL PROPERTIES OF ROCKS AT THE HANFORD SITE

The mechanical properties of intact basalt from the Hanford Site have been tested extensively for a number of basalt flows both within and outside the reference repository location. Results from samples taken outside the reference repository location are summarized, followed by results from samples taken from the Cohassett flow within the reference repository location. Finally, anisotropic behavior and the effects of temperature and moisture are discussed with reference to the data available from the Hanford Site.

2.1.2.1 Results from other flows within the Hanford Site

The mechanical property data for intact samples from the entablature of the Pomona flow at the Near-Surface Test Facility and other flows within the Hanford Site are listed in Table 2.1-3. These data are presented in more detail by Sublette (1983, Table 9, pp. 47-48).

As can be seen in Table 2.1-3, the mechanical properties of intact entablature samples from the Umtanum flow showed a wider variation than samples from the Pomona flow. While part of the difference in the range of variation may be accounted for by the apparent differences in the bulk density and apparent porosity of the samples from each flow, the complete cause has not been established.

Data on intact colonnade samples are limited, and the available results suggest that their mechanical properties are probably similar to those of the intact entablature sample. Samples from the flow tops generally exhibit a much lower strength and elastic modulus than those from the dense flow interior. The strength and elastic modulus of samples from the vesicular zones within the flow interior are generally intermediate between those of the flow top and the dense interior.

2.1.2.2 Results from the Cohassett flow within the reference repository location

The results of testing core samples taken from the Cohassett flow within the reference repository location and the procedures used are presented in this section. The test results are shown in Figures 2.1-2 through 2.1-4. As can be seen from these figures, the mechanical properties of intact basalt vary depending on the location of the basalt within the flow. The mechanical properties of samples from the flow top, entablature, colonnade, and vesicular zones will be discussed separately.

2.1.2.2.1 Procedures

The selection of samples and sequence of tests were shown in Figure 2.1-1. In general, the tests were performed in accordance with established BWIP operating procedures. The tests results are summarized in Sublette (1983, p. 47).

The number of cores available for testing were insufficient, therefore, cores from the dense flow interiors were recored to produce 25-mm- (1-in.-) dia. specimens to increase the number of samples. This procedure satisfied the American Society for Testing and Materials Specification D2938 (ASTM, 1986) requirement for a length-to-diameter ratio of 2.0 to 2.5 and the requirement that the minimum specimen size be at least 10 times the size of the largest mineral grain. However, the requirement that the specimen diameter be not less than NX wireline core size, 48 mm (1.9 in.), was not met.

The coring and sample preparation procedure has had the following effects on the test results.

o Those parts of the core damaged during drilling and handling or disked during drilling could not be tested. This introduced a bias in the test results.

o The axis of the sample must coincide with the direction of coring because the diameter of the core was too small to be recored in a direction perpendicular to its axis. Thus, anisotropic behavior could not be studied with the core samples available.

o The use of 25-mm- (1-in.-) dia. samples resulted in higher strengths than would have been determined from that of 50-mm- (2-in.-) dia. samples. Hulstrom and Hanson (1982a, p. 13) performed a linear regression analysis on the data and derived an equation relating compressive strength to nominal sample diameters. Using this equation it can be established that the difference in strength is approximately 6% or 15.5 MPa (2.2×10^3 lbf/in^2). This agreed, in general, with earlier test results reported by Koifman (1963, p. 113). No adjustment to account for size effect has been made to the test results presented in this section.

The combined effect of these procedures is that the test results presented in this section are likely to be biased to a degree that cannot yet be ascertained. These effects will be further studied in future testing of cores extracted from the Exploratory Shaft Facility (Section 8.3.2.2).

2.1.2.2.2 Strength and deformation properties

A comparison of the uniaxial compressive strengths for flow top, entablature, colonnade, and vesicular zones of the Cohassett flow is shown in Figure 2.1-5. The figure was prepared by averaging the values from the

appropriate interflow zones in boreholes RRL-2, -6, and -14. The data indicate that the flow-top zones have a mean unixial compressive strength of 68 MPa (9.86×10^3 lbf/in^2) with a standard deviation of 16 MPa (2.3×10^3 lbf/in^2) and that the dense interior has a mean unixial compressive strength of 292 MPa (42.3×10^3 lbf/in^2) with a standard deviation of 55 MPa (7.9×10^3 lbf/in^2). Vesicular and vuggy colonnade zones have intermediate strength.

Intact rock failure envelopes were developed from the uniaxial and triaxial compression and Brazilian tensile strength test data by Sublette (1983, p. 38) for the Cohassett flow using the failure criterion of Hoek and Brown (1980, pp. 137-139). This criterion has the following form:

$$\sigma_1 = \sigma_3 + \sqrt{m\sigma_c\, \sigma_3 + s\sigma_c^2} \qquad (2.1-1)$$

where

σ_1 = major principal stress at failure

σ_3 = minor principal stress at failure

σ_c = uniaxial compressive strength of intact rock

m = empirical curve fitting parameter, reflecting the curvature of the failure envelope, sensitive to the degree of interlocking of grains in the specimen

s = empirical curve fitting parameter, related to the tensile strength of the rock matrix, reduced as the fracture frequency increases (s = 1 for intact rock).

The scatter diagram and the best-fit failure envelopes for intact basalt samples from the dense interior of the Cohassett flow are shown in Figure 2.1-6. The m values for the entablature and colonnade are 21.7 and 21.4, respectively. The m values for samples from the flow tops and the vesicular zones within the flow interior have not been determined because data are insufficient. According to this criterion, the strength of intact basalt increases rapidly with increasing confining stress as was actually observed in the test results. This failure envelope for the intact basalt samples was used as the starting point to develop an estimate of the rock mass strength failure envelope. This is discussed in greater detail in Section 2.3.3.

Typical stress-strain curves for intact basalt from the Cohassett flow are shown in Figure 2.1-7. Both curves exhibit a predominantly linear response throughout the loading range, similar to the response observed in granite and diabase (Wawersik and Brace, 1971). In the upper curve of Figure 2.1-7, the sample began to dilate as it approached failure. The dilation is commonly associated with the generation of microcracks within the sample. The dilation was absent in samples with stress-strain curve similar

to the lower part of Figure 2.1-7. Disregarding this slight difference, both types of curves are typical of brittle rock of which elastic behavior has commonly been accepted.

Laboratory values of elastic modulus for flow top, entablature, colonnade, and vesicular intraflow structures of the Cohassett flow are shown in Figure 2.1-8. These values were calculated from the tangent of the stress-strain curve at a stress level corresponding to 50% of the failure stress. The dense interior exhibits the highest mean elastic modulus values, 70 to 82 GPa (10,150 to 11,890 kip/in^2); flow top mean modulus values range from 14 to 32 GPa (2,000 to 4,600 kip/in^2); and the vesicular zone has a mean modulus of approximately 51 GPa (7,400 kip/in^2).

For the dense interior, the mean Poisson's ratio ranges from 0.24 to 0.28, which is typical for these types of rocks. The flow tops have lower Poisson's ratios (in the range of 0.11 to 0.27), based on limited samples tested.

Post-failure behavior of basalt under uniaxial and triaxial testing has not been studied. As this may be required in future studies of the stability of repository openings, future tests will be planned (Section 8.3.2.2).

2.1.2.2.3 Bulk density and porosity

The following values of bulk density and porosity have been taken from South (1985, pp. 452-501) and Hulstrom (1985, pp. 66-73). The bulk density of the dense interior of the Cohassett flow ranges from 2.79 to 2.87 g/cm^3 (174.1 to 179.0 lb/ft^3). The flow tops have lower bulk densities, 2.14 to 2.40 g/cm^3 (133.5 to 149.7 lb/ft^3), and the vesicular and vuggy zones have intermediate densities, 2.51 to 2.73 g/cm^3 (156.6 to 170.3 lb/ft^3).

Measured apparent porosities in the dense interior (entablatures and colonnades) are between 0.8% and 3%. Total porosities calculated from grain density measurements ranged from 2.0% to 5.3% in the dense interior (entablatures and colonnades).

Flow tops have apparent porosities that range from 10.5% to 17.7% and total porosities ranging from 18.1% to 28.5%. The higher porosities reflect the brecciated nature of the flow tops.

The mean apparent porosity of the vesicular zone of the Cohassett flow is 4.9%, and the mean total porosity is 12.0%. The high total porosity as compared with the apparent porosity reflects the lack of connectivity between the vesicles.

2.1.2.3 Temperature effects

The results from two series of tests form the basis of discussion in this section. The first series involves testing core samples at elevated temperature. The second series involves testing core samples obtained from different locations in Full-Scale Heater Test 2 at the Near-Surface Test Facility. Each sample in the second series was subjected to a different past maximum temperature during the heater test.

2.1.2.3.1 Elevated temperature tests

One group of basalt samples from the Umtanum flow was tested under a confining pressure of 0.3 MPa (50 lbf/in^2) and at temperatures of 20, 150, 300, and 500 °C (Miller, 1979a, 1979b; Miller and Bishop, 1979). The strength plotted against test temperature for samples taken from the flow interior is shown in Figure 2.1-9. The results of linear regression analysis, with a correlation coefficient of 0.18 (South, 1985, p. 432), is not significant enough to indicate a trend.

The apparent reduction in strength with increasing test temperature has also been observed in the test results of a group of basalt samples taken from the Pomona flow at the Near-Surface Test Facility. These samples were tested under a confining pressure of 0.7 MPa (100 lbf/in^2) and at 150 and 300 °C (FSI, 1980a, p. 6-4; 1980b, p. 6-4; 1981b, p. 6-7). The average strength decreases from 349 MPa (50.6 x 10^3 lbf/in^2) at 150 °C to 285 MPa (41.3 x 10^3 lbf/in^2) at 300 °C (South, 1985, p. 432). As a comparison, the average strength of 20 samples tested in unconfined compression at room temperature (22 °C) is 355.8 MPa (57.4 x 10^3 lbf/in^2) (FSI, 1981b, Table 6.3.1, p. 6-7). The corresponding strength at a confining pressure of 0.7 MPa (100 lbf/in^2) using the Hoek-Brown criterion with an m value of 20 would be of the order of 363 MPa (52.7 x 10^3 lbf/in^2). This is only 4% higher than the mean strength measured at 150 °C and suggests that, within the temperature range of 22 to 150 °C, there is perhaps little strength reduction. The results also suggest that, at temperatures above 150 °C, there may be a significant strength reduction with increasing temperature. However, because of the uncertainties inherent in comparing test results obtained from different samples, these conclusions can only be regarded as preliminary, and additional studies will be required to further clarify this effect (Section 8.3.3.2).

2.1.2.3.2 Post-test characterization, Near-Surface Test Facility Full-Scale Heater Test 2

This series of tests consisted of 54 uniaxial compression tests, 34 Brazilian tensile tests, and associated density, porosity, static, and dynamic elastic modulus measurements performed at room temperature (Hulstrom, 1984; Mitchell, 1984c). The core samples were taken from three vertical and three horizontal boreholes drilled in the location of Full-Scale Heater Test 2

after the completion of the heater test. The maximum temperature that each sample experienced during the heater test was estimated from a numerical modeling analysis in which the results of thermocouple measurements were used as input data.

The elastic modulus and intact compressive strength of these samples are plotted against the maximum exposure temperature in Figures 2.1-10 and 2.1-11. The best-fit line and the correlation coeficient are also shown in each figure. The data in Figure 2.1-11 indicate that samples which experienced a higher past temperature history may have a lower strength. However, the correlation coefficients form the linear regression analysis for both the elastic modulus and the compressive strength were too low for the results to have any statistical significance.

In summary, the results from these two series of tests indicate that both the test temperature and past temperature history may affect the strength of the sample. The effect cannot be quantified from the present data base, which does not contain a sufficient amount of data. Additional testing will be required to confirm and quantify these initial results (Section 8.3.3.2).

2.1.2.4 Creep properties

Since basalt is a strong, brittle rock that has not been known to exhibit time-dependent characteristics in mining and tunneling, activities designed to quantify the creep properties of basalt have not been extensive. The Colorado School of Mines (Miller, 1979a, 1979b; Miller and Bishop, 1979) conducted tests to study the effects of strain rate on compressive strength. Schmidt et al. (1980, pp. 5-19) summarized the Colorado School of Mines test data for various strain rates and concluded that variations in strain rate from 10 $\mu\epsilon$/min to 200 $\mu\epsilon$/min had little effect on strength but that, at a strain rate of 1 $\mu\epsilon$/min, strengths may be measurably lower. The conclusions of Schmidt et al. (1980) need to be verified because of the small number of tests and the inclusion of the flow top and partially jointed samples in the test data. It has been assumed that joints and joint infilling materials are likely to have a greater impact on the time-dependent behavior of the rock mass than the creep properties of intact basalt. Therefore, tests to determine the creep properties of intact basalt are less important than the in situ testing that is planned to evaluate properties and characteristics of the rock mass.

2.1.2.5 Moisture effects

The effect of moisture on the mechanical properties of basalt was studied in an early testing program by Colorado School of Mines (see Miller, 1979a, 1979b; Miller and Bishop, 1979). Tests consisted of uniaxial compression strength tests on Umtanum flow core from boreholes DC-4, -6, and -8 conducted at room temperature under saturated and oven-dried conditions. In general,

the data showed a reduction of strength on saturation. The quoted magnitude of reduction varies from 45% (Schmidt et. al., 1980, pp. 5-19), when samples from all parts of the flow were combined, to 13% (South, 1985, p. 432) when only samples from the dense flow interior were used for the comparison. The actual magnitude of reduction could not be ascertained because the sample description did not contain sufficient detail regarding the degree of jointing in order to separate the influence of jointing from that of moisture.

2.1.2.6 Anisotropic properties

Anisotropic properties of the intact basalt from the Cohassett flow were not studied because of limitations in coring and sample preparation procedures. The only available data on intact basalt taken from drill holes showed isotropic mechanical behavior (Miller, 1979a, 1979b; Miller and Bishop, 1979). Based on this, the assumption of isotropic properties is recommended for the design analysis. This will have to be confirmed by further testing (Section 8.3.3.2).

2.1.2.7 Discussion of results

The results presented in this section showed that the mechanical properties of intact basalt samples from the Cohassett flow vary depending on location within the flow. The strength of intact basalt samples from the dense interior of the Cohassett flow is within the range obtained for other basalts shown in Table 2.1-2.

A number of problems have been identified during the early stages of the testing program. These problems include the limited number of samples available for testing due to the highly jointed nature of the basalt, the presence of healed joints that may become the failure plane in an otherwise apparently intact sample, and disking that limits the amount of intact core available. Furthermore, the process of coring and sample preparation would favor the selection of stronger samples. The combined effect of these factors is that the actual in situ variability of the mechanical properties of intact basalt is unknown and may not be reflected in the present data base. Additional tests will be required to establish the range of variation (Section 8.3.3.2).

2.1.3 SUMMARY

Laboratory tests of dry samples at room temperature indicate that intact basalt from the dense interior of the Cohassett flow is a strong, brittle rock that deforms in a linear-elastic manner throughout most of its pre-peak-strength range. Uniaxial compressive strengths for the dense interior range from approximately 237 to 247 MPa (34 to 50 x10^3 lbf/in^2) with an elastic

modulus in the range of 70 to 82 GPa (10,150 to 11,890 kip/in^2) and a Poisson's ratio in the range of approximately 0.24 to 0.29. Failure strength increases rapidly with confining stress. Measured apparent porosities range from 0.8% to 3.0%, whereas total porosities range from 2.0% to 5.3%, reflecting that the vesicles present are not interconnected. Mean bulk density is approximately 2,830 g/cm^3 (176.6 lb/ft^3).

Flow tops are quite variable in both intact material properties and structural characteristics. The uniaxial strength of samples taken from flow tops ranges from 52 to 84 MPa (7.5 to 12.2 x 10^3 Tbf/in^2). The stress-strain behavior of intact flow-top specimens is linear elastic throughout most of the pre-peak-strength range, elastic modulus ranges from 14 to 32 GPa (2,000 to 4,600 kip/in^2), and Poisson's ratio ranges from 0.11 to 0.27. Measured apparent porosities range from 10.5% to 17.7%; total porosities range from 18.1% to 28.5%. Bulk densities range from 2,140 to 2,310 g/cm^3 (133.5 to 144.1 lb/ft^3). The laboratory strength and porosities of samples from the vesicular zones are intermediate between those from the dense interior and flow-top zones.

The results presented in this section were obtained from a limited number of core samples and therefore may not reflect the in situ variability of the mechanical properties of intact basalt. Furthermore, the test results may be biased due to the process of coring and sample preparation. Because of the limited number of samples available for testing, studies of anisotropy, creep, and the effects of temperature and moisture were limited. The information needs related to the mechanical properties of intact basalt are identified in Section 2.9.3.2 based on an assessment of the deficiency of the present data, and plans for further testing are discussed in Section 8.3.3.2.

2.2. MECHANICAL PROPERTIES OF ROCK UNITS--DISCONTINUITIES

2.2.0 INTRODUCTION

Discontinuities are natural breaks within a rock mass that generally appear as planar features ranging from clean fractures to faults with zones of highly fractured or crushed infill material. Understanding the mechanical properties of discontinuities in basalt is important because of their potential influence on repository safety and performance design limits. Among the wide range of discontinuities described above, the most frequently occurring discontinuities within a basalt rock mass are joints resulting from cooling. Cooling joints are expected to be abundant within the Cohassett flow where the proposed repository is to be located and will fundamentally alter the strength and deformation properties of the rock mass relative to the intact rock properties.

The mechanical properties and the physical characteristics of the joints are summarized in this section. The mechanical properties studied include the shear strength and shear stiffness along the joint and the normal stiffness across the joint. The study of the mechanical properties of joints served two purposes for the BWIP: (1) to provide a rational basis on which the mechanical properties of the rock mass can be developed, and (2) to identify potential problem areas within the assumptions and limitations of treating the rock mass as a continuum in the design analysis. The data presented in this section has not been directly used in the SCP conceptual design (KE/PB, 1986).

The data base on the mechanical properties of discontinuities consists of only a small number of laboratory tests made in core samples. The physical characteristics of fractures were obtained from outcrop mapping and core drilling in deep boreholes at the reference repository location. Data collected from these sources requires considerable interpretation because (1) joints in outcrop have been subjected to destressing and weathering that significantly affect their properties and (2) vertical boreholes sample predominantly horizontal and inclined joints, resulting in a bias in the data base derived from core testing.

The data discussed in this section were obtained from direct shear tests and triaxial tests. The direct shear tests were performed on basalt samples from the Pomona flow as part of the rock mass characterization for the jointed block test (Mitchell, 1984a). The triaxial tests were conducted on jointed core samples from the Grande Ronde and the Pomona flows. Specific tests and corresponding references are listed in Table 2.2-1. The present data base is insufficient to study the effects of time, temperature, pore pressure, and scale on the mechanical properties of joints within the basalt rock mass at the Hanford Site. As a result, the discussion of these effects as presented in Section 2.2.2.4 will be based on previous studies of other rocks.

2.2.1 MECHANICAL PROPERTIES OF JOINTS IN OTHER ROCK

2.2.1.1 Shear strength of joints of similar rocks

The shear strength of joints has been the subject of many laboratory and field studies (e.g., Coulson, 1971; Byerlee, 1978; Bandis et al., 1981; and Barton, 1971), although specific tests on basalt joints are rare. The results of laboratory testing of natural and artificial joints in basalt and rocks similar to basalt are shown in Table 2.2-2. These results were obtained from different testing machines with samples of different sizes. The shear strength of joints is presented in terms of friction angle in Table 2.2-2. The friction angle is defined as the arc tangent of the ratio of shear strength to normal stress applied to the joint surface in the absence of cohesion. This is used as a convenient measure of the shear strength of joints to reflect the commonly observed phenomenon that the shear strength will increase in near proportion with increasing normal stress. Under this definition, a joint surface with a higher friction angle will develop a higher shear resistance under a given normal stress. The first two groups in Table 2.2-2 are data from saw-cut, polished surfaces; the friction angle measured in these surfaces is called basic friction angle because it represents the friction of the surface in the absence of the roughness component. The basic friction angle for most surfaces falls within a narrow range of 25° to 30°. At large shear displacements, some surface damage will occur. This will increase the roughness and area of contact of these surfaces and will result in a higher friction angle in the range of 30° to 38° (Coulson, 1971, p. 101). Friction angles for natural joint surfaces reported by Barton (1973, p. 296) and Duncan (1969, p. 88) are also listed in Table 2.2-2. The peak friction angle for the natural rough joints ranges from 38° to 59°. Artificial extension fractures have an even higher peak friction angle (56° to 72°) because of their rough and tightly interlocked surfaces.

Nieble et al. (1974, pp. 296-297) reported large-scale joint shear tests performed on basalt blocks with a base area of 0.7 to 6.0 m² (7.54 to 64.56 ft²) and with 0.2- to 1-m- (0.66- to 3.28-ft-) thick infillings that contain basalt fragments, sands, and clayey materials. Friction angles ranged from 22° to 35° (Nieble et al., 1974, p. 300).

2.2.1.2 Joint stiffness of similar rocks

Data on joint shear and normal stiffness are relatively scarce and have been summarized by Barton (1982, pp. 23-28, 49-63) and Bandis et al. (1983). The range of shear stiffness quoted in Barton (1982, p. 26) spanned 4 orders of magnitude from 0.01 to 100 MPa/mm (0.4 to 370 x 10^3 lbf/in^2). This variation is caused by differences in normal stress, mechanical properties of the intact rock material, physical characteristics of the joint surfaces, and test scale. Under constant shear stress, the normal stiffness is a function of normal stress. This function has been empirically described by a hyperbolic equation (Goodman, 1976, p. 171; and Bandis et al., 1983, pp. 257-258) that correctly models the behavior that, at high-normal stresses, the joint is tightly closed and the slope of the stress-closure curve of the specimen approaches that of the intact rock. The constants required to define the hyperbolic equation have been correlated empirically with aperture, roughness, wall rock strength, and maximum joint closure (Barton, 1982, pp. 52-56).

2.2.2 MECHANICAL PROPERTIES OF JOINTS IN ROCKS AT THE HANFORD SITE

The mechanical properties and the physical characteristics of the discontinuities at the Hanford Site are described in this section. The mechanical properties of joints were obtained from two series of laboratory testing programs: the first program involved testing of jointed samples from the dense interior of the Pomona and Umtanum flows; the second program involved testing of jointed samples from the dense interior of undifferentiated Grande Ronde flow. The physical characteristics of discontinuities discussed in this section are based on observations of the Rocky Coulee, Cohassett, McCoy Canyon, and Umtanum flows.

2.2.2.1 Physical characteristics of joints

A short summary of the physical characteristics of discontinuities such as frequency, pattern, roughness, and infilling is provided in this section. The discussion will be focused on engineering aspects relevant to the effect of discontinuities on shear strength and deformability. A complete geologic description along with references is provided in Section 1.2.2.1.

2.2.2.1.1 Joint physical characteristics

Most fractures in the Grande Ronde Basalt flows are cooling joints. The dominant cooling joints range from those that define well-formed, regular, polygonal solids to those that form irregular, elongate-to-equant blocks. The dominant, column-defining joints in the colonnade are generally near vertical with no preferred strike. Cooling joints are more frequent and less regular

In the entablature than in the colonnade. An entire spectrum exists from regular, well-formed columns to irregular (hackly) blocks. Both columns and blocks range widely in size, 0.2 to 2.5 m (0.7 to 7.5 ft) for columns and 0.1 to 0.7 m (0.3 to 2.3 ft) for the more equant blocks (Long and WCC, 1984, pp. I.44-I.45). In the colonnade, the fractures are arranged as four-, five-, or six-sided polygons. Single cooling fractures cannot be traced through the entire entablature in the outcrops.

Virtually all columns or blocks are subdivided into smaller blocks by cross fractures. These cross fractures occurred in a wide range of orientations, were formed mainly after the primary column-defining fractures, and typically were terminated by the column-forming joints.

Outcrop observations suggest a fracture frequency of 1 to 37 fractures per meter (less than 1 to 11 fractures per foot) (Long and WCC, 1984, p. I.416). The borehole results were biased to an unknown extent because of the difficulty in sampling near-vertical joints in vertical boreholes.

Measurements of the widths (apertures) of fractures in the Rocky Coulee, Cohassett, McCoy Canyon, and Umtanum flows have been taken from cores extracted from 4 boreholes (RRL-2, -6, -14, and DC-16) within the reference repository location. The results indicate that the distribution of fracture widths follows a log-normal distribution, the mean value of all fractures in the 4 flows is 0.226 mm (0.009 in.). The mean fracture width of the Cohassett flow varies from borehole to borehole between 0.132 and 0.246 mm (0.005 and 0.01 in.) (Lindberg, 1986). No large-scale, in situ measurements of joint profile have been made to determine the roughness of joint surfaces.

2.2.2.1.2 Joint infilling materials

The vast majority of natural fractures observed in core contains infillings of secondary minerals with clay being the most abundant. The proportion of clay in the infilling averaged 89% for joints in the Cohassett flow (Lindberg, 1986, p. 46). The clay is tentatively identified as montmorillonite, generally associated with a low coefficient of friction and a high swelling potential. Other infillings include zeolite, silica, and pyrite. Normally, infilling materials would completely fill the space within the fractures. In the Cohassett flow, these fractures are generally very thin, with a mean value in the range of 0.132 and 0.246 mm (0.005 and 0.01 in.). Accordingly, most of the infillings are also very thin.

2.2.2.2 Strength of joints in basalt

Both direct shear testing and triaxial shear testing have been conducted on basalt joints to develop a data base on joint properties. The results of direct shear tests and triaxial tests on jointed samples from the Pomona flow will be described in Section 2.2.2.2.1. The results of triaxial tests on

jointed samples from the undifferentiated Grande Ronde flow are presented in Section 2.2.2.2.2. The shear strength of the joints in the Cohassett flow could not be studied separately from those of the undifferentiated Grande Ronde flow for lack of data. A summary of the test results and a discussion of the uncertainties associated with these results are provided in Section 2.2.2.2.3.

2.2.2.2.1 Pomona flow

Both direct shear tests and triaxial tests have been conducted on jointed core samples from the Pomona flow. The peak and residual strengths measured during these tests are discussed below. The series of triaxial tests included displacement measurements along and across the test joint. This information was used to calculate the stiffness of joints (Section 2.2.2.3).

The series of direct shear tests included 14 tests (Mitchell, 1984a). The test results show that many joint samples would first develop a peak strength at a small displacement. Then, as the sample underwent further shearing there was a gradual decrease in resistance toward a residual value. Dilation of the joint sample, particularly when the peak resistance was developed, was also observed in most tests. Most of the shear displacements were not recovered upon unloading of the sample. Similar behavior was also observed in the triaxial tests of jointed samples.

The existence of a residual strength was not always apparent, and in some tests the sample even developed a resistance higher than the peak value at large shear displacement. This was possibly due to an increase in surface roughness and contact area as a result of surface damage. Thus, considerable uncertainties were involved in the determination of residual strength and the values reported (Mitchell, 1984a) actually correspond to those measured at large shear displacement, some of which may not strictly be the actual residual strength. Peak and residual strength of jointed samples are shown in Figure 2.2-1. The peak strength obtained from these tests is characterized by an apparent cohesion of 0.8 MPa and a corresonding friction angle of 29.2° (Mitchell, 1984a). There is a very large scatter in the test results and the correlation coefficient of the best fit line is only 0.55. Within the bound of testing error, experience suggests that such a wide scatter may be the result of differences in the aperture, roughness, and infilling characteristics among the jointed samples tested. However, neither sufficient details of the sample exist nor is there a sufficient number of samples available to permit the use of statistical technique to separate the effect of the joint characteristics from the test results. Lacking such evidences, it is not possible to assess the uncertainties of the test results. The residual strength, determined at large shear displacement, is characterized by an apparent cohesion of 1.32 MPa (191.4 lbf/in^2) and a corresponding friction angle of 24.7°. There is less scatter in the results in comparison with those of the peak strength. Again, it is not possible to assess the uncertainties of these results for the same reason presented above for the peak strength.

Twenty basalt core samples, each containing a single inclined joint, were obtained in the Near-Surface Test Facility and tested in a special triaxial setup as described in Section 2.2.2.3 (Brechtel, 1985). The sample diameters ranged between 25.4 and 52.6 mm (1.0 and 2.1 in.), with joint angles ranging between 17.9° and 56.8° from the core axis. Three different groups of samples were tested under different loading conditions:

o Cyclic loading under constant confining pressure.

o Cyclic loading under constant confining pressure with confining pressure increased in increments of 3.5 MPa (0.5×10^3 lbf/in^2) at the beginning of each test stage to a maximum of 13.8 MPa (2×10^3 lbf/in^2).

o Cyclic loading under constant confining pressure with confining pressure in each test stage decreased 3.5 MPa (0.5×10^3 lbf/in^2) from a maximum of 13.8 MPa (2×10^3 lbf/in^2) to a minimum of 3.5 MPa (500 lbf/in^2).

At each confining pressure, the axial load was applied in several cycles for the determination of shear and normal stiffness before the sample was loaded to failure.

The joints in the samples were relatively smooth. The joint roughness coefficient (Barton and Choubey, 1977, p. 19) varies between 5 and 15 out of a possible 20 with an average value of 7.7. Joint apertures varied from less than 0.025 to 0.152 mm (0.001 to 0.006 in.). Infillings had been described previously as a yellow-brown and blue-green clay (Moak and Wintczak, 1980, pp. 3-5).

Peak shear strength and residual shear strength plots for the tests are shown in Figure 2.2-2. The shear strength obtained from these tests shows considerable scatter and was slightly greater than those obtained from direct shear tests. The range of normal stress used in the triaxial tests was, however, well above that used in the direct shear tests.

2.2.2.2.2 Grande Ronde Formation

Multiple-stage triaxial tests were conducted on core samples 54 or 48 mm (2.1 or 1.9 in.) in diameter and transected by a single joint. Samples were tested to peak shear stress under different confining pressure at each stage. More than 100 jointed triaxial tests were performed, in 26 of these tests, failure occurred along the joint surface (Mitchell, 1984b). Of these 26 samples, 7 were tested at elevated temperatures. The results of the remaining 19 tests form the basis of this discussion. The infilling and roughness of joint surfaces tested were not recorded.

Jointed triaxial test results are shown in Figure 2.2-3. The plot of peak or initial strength indicates an apparent cohesion and angle of friction

of 4.1 MPa (0.592 x 10^3 lbf/in^2) and 45.7°, respectively; the apparent cohesion and friction angle at the residual strength are 1.4 MPa (0.203 x 10^3 lbf/in^2) and 42.7°, respectively. These values are higher than the peak and residual values from the direct shear tests of Pomona flow samples, which were 0.8 MPa (116 lbf/in^2) and 29° and 1.3 MPa (0.191 x 10^3 lbf/in^2) and 25°, respectively. The results are also higher than those presented by Byerlee (1978, pp. 619 and 620), which indicate a friction angle of 40.4° at higher normal stress levels.

Uncertainties are inherent in the measurement of residual strength because it is difficult to distinguish between the effects of increased normal stress and accumulated surface damage caused by repeated shearing on the same joint plane.

2.2.2.2.3 Discussion and summary

The results from the three series of tests all exhibit a large scatter. The scatter is caused by differences in physical characteristics, which include roughness, aperture, and infilling. A methodology to quantify the physical characteristics has not been developed. Furthermore, the amount of test data is insufficient for a statistical analysis to be conducted to isolate the effect of each parameter. The present data provide the possible range of variation of the shear strength of basalt joints at the Hanford Site; the strength of joints with specific physical characteristics cannot yet be defined.

Uncertainty in the determination of the residual strength arises mainly from the action of continuous shearing, which will cause an accumulated surface damage to the sample. At present there is insufficient information to determine whether the same surface damage exist under field conditions. Because of this, the measured shear resistance at large shear displacement may not be the same as the residual resistance that may exist under field conditions. Further study will be required to properly define the residual shear strength from the test results (Section 8.3.3.2).

It should be noted that these results were obtained from jointed samples of relatively small scale in comparison with what may be encountered in the repository. The effect of changing scale is not well understood (Section 2.2.2.4), and this represents a major uncertainty in the data. Joint shear strength is known (Barton, 1971) to be dependent on the normal stress applied to the joint, however, this cannot be studied based on current data.

2.2.2.3 Stiffness of joints in basalt

Joint stiffnesses were not measured during the direct shear tests on jointed samples from the Pomona flow or the triaxial tests on jointed samples from the undifferentiated Grande Ronde flow because this would have required

accurate measurements of the displacements along and across the joint surface using special equipment which was not available (Mitchell, 1984a, 1984b). The series of triaxial tests on jointed samples from the Pomona flow used a triaxial cell with a special setup to measure the displacements along and across the joint as shown in Figure 2.2-4. The special setup consisted of a pair of cantilevers oriented to measure displacement parallel and perpendicular to the joint. The displacements along and across the joint were obtained by subtracting the displacements corresponding to the intact rock from those measured in the cantilevers (Brechtel, 1985). The stiffness measurements were not made under constant normal or shear stress conditions as the application of axial loading to the specimen during the test would cause an increase in both the normal and shear stresses on the joint. Thus, the stiffness values reported in this section were obtained under conditions of changing normal and shear stresses. The effects of normal and shear stresses could not be separated, and this constitutes a major uncertainty in the test results.

2.2.2.3.1 Normal stiffness

Two types of normal stress versus normal displacement curves that have been obtained from the tests are shown in Figure 2.2-5. The majority (84%) of the tests showed a regular increase of joint normal stress with joint closure (Fig. 2.2-5a). However, some (16%) of the tests showed most of the joint closure occurring at small initial increments of normal stress (Fig. 2.2-5b) (Brechtel, 1986). This difference in the two types of behavior could not be correlated with the surface characteristics of the joint such as mineral infilling, joint roughness, or aperture.

The joint normal stiffness (K_n) is defined as the change in joint normal stress (σ) per unit change of joint normal displacement (V). As can be seen from the stress-displacement curves shown in Figure 2.2-5(a), the stiffness increases rapidly with increasing normal stress. In order to compare the results with data from other rocks, three stiffness values were calculated from the curve: the first at the beginning of the curve where the normal stress is close to zero, the second at half of the total applied load, and the third at the full load level. These three values, therefore, establish the range of variation of normal stiffness. The results from the hydrostatic loading were shown in Table 2.2-3. It is seen that the stiffness values vary between 0.01 and 3.12 GPa/mm (0.038×10^6 and 11.49×10^6 kip/in.), similar to those reported for other rocks (Bandis et al., 1983, pp. 254, 258, and 262).

2.2.2.3.2 Shear stiffness

Shear stiffness (k_s) is defined as the change in joint shear stress per unit increment of joint shear displacement. The magnitude of shear stiffness will vary with both the shear stress and normal stress. Calculation of the stiffness values is similar to that of normal stiffness. Three values, one at

the beginning of test, one at half the load, and one at full- (peak-) load level were calculated from the shear stress-shear displacement curve. The results obtained from the first cycle of axial load tests are shown in Table 2.2-3. The shear stiffness at the beginning of the test is typically low, which is possibly due to the mismatching of joint surfaces. At the full-load level, the sample is approaching failure, and there is a reduction in shear stiffness from the half-load level.

Note that during the test there also will be a corresponding increase in normal stress, the magnitude of which varies with the inclination of the tested joint in the sample and the applied load. Because of this, the difference in the values given in Table 2.2-3 is due, at least partly, to the fact that different normal stress may be involved. At present, there is no satisfactory way to decouple the effect of normal stress from that of shear stress. However, the stiffness values shown in Table 2.2-3 provide a useful indication of the likely range of variation in the shear stiffness of basalt joints.

2.2.2.4 Effect of various parameters on joint properties

The results presented in the preceding section were obtained from tests conducted over a relatively short period of time under ambient temperature and dry conditions. These conditions are not representative of the conditions expected at the repository horizon where the rock is saturated and at elevated temperature, where the discontinuities exist at a much larger scale than that of the laboratory sample, the loading will be applied over a very long period of time, and the infilling material may possess different characteristics. Thus, in order to apply the results to the design and performance assessment of the repository it is important that the effects of moisture, scale, infilling material, temperature and time on the mechanical properties of discontinuities be assessed. Since the data base for Hanford Site basalt joints is presently very limited, the discussion of these effects is based on information from the literature. The following discussion therefore serves to indicate the trend that may be expected under the repository condition.

2.2.2.4.1 Effect of water

The most important structural effect of water on rock joints is the reduction in effective stress (due to pore water pressure), which will result in a decrease in shear strength. Additionally, the strength of a wet joint surface is sometimes found to be different from that of a dry joint surface. Conflicting evidence has been reported in the literature regarding the effect of wetting the joint surface on shear strength, although the magnitude is usually insignificant (Coulson, 1971, pp. 96, 98, 101-103; Barton, 1973, p. 324; Duncan, 1969, p. 95).

No data are available on the effect of water on joints in basalt from the Hanford Site. The few saturated, jointed triaxial tests performed by Miller (1979a, pp. 37-41; 1979b, pp. 34-37) and Miller and Bishop (1979, pp. 37-41) could not be used because joint failure did not control sample strength (Mitchell, 1984b).

2.2.2.4.2 Effect of infilling

The effect of infilling on shear strength becomes more pronounced with increasing infilling thickness. For joints with thick infillings (thicker than the asperity height), failure can occur entirely through the filling material. With thinner infillings, failure occurs partly through the infilling material and partly through asperities on the joint surface.

At present, there are insufficient data from the testing program to study the effect of infilling on the strength of basalt joints in the Hanford Site. However, limited data from direct shear tests on joints from the Pomona flow seem to indicate that joints with thick infillings will have a lower strength (Mitchell, 1984a). The thickness of more than 90% of the infillings in the joints of the Cohassett flow within the reference repository location is less than 0.37 mm (0.014 in.) (Fig. 1.2-41, Section 1.2.3.1), and thus, the presence of infillings may not significantly affect the shear strength of most joints in the Cohassett flow.

2.2.2.4.3 Effect of scale

Bandis et al. (1981) concluded that the peak shear strength of rock joints is a strongly scale-dependent property with an inverse relationship between strength and joint length; i.e., the shear strength decreases gradually toward a final value as the joint area increases. The magnitude of these scale effects depends on the type of joint roughness. Maximum scale effects are associated with rough, undulating joints; whereas smooth and planar joint types show little scale effect. At present no measurement of the basalt joint profile has been undertaken at the Hanford Site for an assessment of possible effect of scale to be made.

Large-scale shear tests of joints in quartz diorite (Pratt et al., 1974, p. 308) and a comprehensive series of tests performed by Bandis et al. (1981) indicate that larger shear displacements are required to attain peak strength as the length of the joint is increased. As displacement is increased, the larger and less steeply inclined asperities in the surface tend to control peak strength.

Large-scale shear tests on basalt joints at the Hanford Site have not been conducted. The large-scale tests reported on basalt from Brazil by Nieble et al. (1974) showed friction angles between 22° and 35°, similar to that for smaller samples. This absence of scale effect is probably due to the

fact that joint strength in this case was controlled by the thick infilling materials. Thus, the conclusion from this test may not be applicable to the basalt joints at the Hanford Site.

2.2.2.4.4 Creep properties

The effect of time on discontinuity strength is dependent on the presence and properties of infilling (Barton, 1982, p. 84; Dietrich, 1972). For powdered rock debris filling, friction increases with the time that adjacent surfaces are in contact. Other infillings, such as clay, exhibit creep deformations. Fault gouge infilling, if present, would be subject to time-dependent effects.

Friction for clean joints has been found to vary little over a wide range of strain rates (Barton, 1982, p. 84). The studies conducted by Engineers International (1982) in developing a test method for measuring the creep properties of basalt (Section 2.1.1.4) included a small number of tests on jointed samples. Although the results indicated little creep of the samples over the period of test, they cannot be used to support a general conclusion because of the small number of samples tested and the developmental nature of these tests.

2.2.2.4.5 Effect of temperature

The high temperatures of a repository environment could have an adverse effect on discontinuity strength of basalt, particularly for joints filled with clay or zeolite at temperatures greater than 100 °C. Potential chemical and (or) phase changes can occur in these minerals at high temperature. Laboratory tests on fractures in granite (a rock similar in strength but of different crystal structure and mineralogy compared to basalt) at temperatures up to 600 °C (Barton, 1982, p. 79) indicated only a few percent reduction in shear strength over a temperature range of 25 to 300 °C. Significant reductions in shear strength were not seen until temperatures reached 500 to 600 °C.

A series of jointed triaxial tests at elevated temperatures on joints from the Umtanum flow have been performed (Miller, 1979a, pp. 37-41, and 1979b, pp. 34-36; Miller and Bishop, 1979, pp. 37-41; Mitchell, 1984b). The results indicated a reduction of friction angle at elevated temperature. However, because only a small number of samples were tested, it is not known whether this indicated the genuine trend or whether the results were biased by the presence of different infilling materials, surface roughness, and possible polishing effect under continuous shearing.

2.2.2.4.6 Effect of shear displacement

During repository excavation some shear displacements may occur along the joints around the openings as a result of blasting and stress redistribution. Depending on the magnitude of shear displacement, the joint surfaces may become mismatched. This mismatch could alter the stiffness and hydrological properties of the joint. Currently, there is insufficient information to assess this effect and future studies will be required (Section 8.1.1).

2.2.2.5 Discussion of results

The present series of tests revealed the complex nature of the shearing behavior of basalt joint. The range of phenomena observed in the tests include the following (Fig. 2.2-6):

o The joint surface will develop a peak strength at small displacement and there will be a gradual reduction in the resistance toward a residual value.

o Permanent displacement upon unloading/reloading cycles.

o Joint dilation during shear failure.

A continuously yielding joint model has been developed by Hart et al. (1985, pp. 10-14) and the results from preliminary analysis showed some aspects of the observed behavior of real basalt joints. This model has been used to help interpret the observed behavior of the rock mass during the jointed block test (Section 2.3.2.2) and develop a constitutive model for basalt.

Most of the data generated to date was used for preliminary studies and in the development of test procedures. The uncertainties in the data arise from the following factors:

o Alteration of properties of the discontinuities of the core samples due to the drilling process.

o Wide variations in joint and infilling properties, such as roughness, thickness, continuity, and frequency in a small data base.

o Insufficient number of samples of predominantly vertical joints to perform statistical analyses.

o Difficulty of characterizing joint patterns at depth from borehole data.

o Results obtained on a laboratory scale; insufficient information regarding the joint surface profile to extrapolate the results to field scale.

Application of the present data is restricted because of the scatter among the results and the limited number of tests. Most of the problems encountered in determining shear strength also apply to the determination of stiffness. However, since stiffness is more sensitive to surface damage, additional studies will be required to understand the effect on measured stiffness values.

2.2.3 SUMMARY

Specific information regarding the strength and stiffnesses of joints in the Cohassett flow is not available at present. However, the results of direct shear tests and triaxial tests on joint samples from the Pomona flow and the undifferentiated Grande Ronde flow have provided an indication of the range of values likely to be obtained in joints from the Cohassett flow. These results show that, at room temperature and under dry conditions with a normal stress up to the order of 100 MPa (1,450 lbf/in^2), the friction and apparent cohesion of natural basalt joint surfaces at the Hanford Site are probably within the range of 30° to 45° and 0.8 to 4.0 MPa (115 to 600 lbf/in^2), respectively. Considerable scatter has been observed in all results; however, the complete cause of the scatter has not been established.

Measurements of joint normal and shear stiffness were made on Pomona flow samples in a series of triaxial tests on jointed core samples. The results indicate that both normal and shear stiffness are dependent on the magnitude of normal and shear stresses. The stiffness values increase rapidly with increasing normal stress. The values shown in this section vary over more than two orders of magnitude and exhibit large scatter even under the same loading conditions. The results also show that under high normal stresses, such as the condition anticipated in the repository horizon, both the normal and shear stiffness can attain a high value.

The potential effects of moisture, infilling material, test scale, temperature, and time on the joint properties were discussed in general terms in this section because reliable information specific to basalt joints at the Hanford Site is lacking. Based on tests of other rock types, the effects of moisture, temperature, and time on basalt joint properties are expected to be minor. The effect of the test scale could not be assessed because no profile measurements of the joint surfaces were available. The presence of infilling material is not expected to have a significant effect on the shear strength of basalt joints at the Hanford Site because the infillings are generally very thin. The significance of the mechanical properties of joints and impact of these effects on the design and performance of repository will be assessed (Section 8.1.1) and further test programs will be planned (Section 8.3.2).

2.3 MECHANICAL PROPERTIES OF ROCK UNITS--LARGE-SCALE

2.3.0 INTRODUCTION

Rock mass mechanical properties are required in repository design to assess initial opening stability, estimate the canister placement layout, and predict the long-term response of openings subjected to thermally induced stresses as discussed in Section 6.2.6.1. The two properties of most interest in repository design are the rock mass deformability and strength. Data regarding these properties are commonly obtained either by direct measurement in large-scale field testing or by empirical methods that provide correlation between rock mass properties and some easily measurable rock mass characteristics. Available data on large-scale field testing are scarce and often contain a large degree of uncertainty. This is due to the difficulties involved in setting up a test and because neither the procedure nor the equipment have been standardized. The data are summarized in Section 2.3.1. Because of the present uncertainties, the BWIP has directed a significant effort toward identifying those factors that will have significant effects on the mechanical properties of a basalt rock mass and methods suitable for field measurement of these properties.

The tests conducted by BWIP up to January 31, 1986, include borehole jacking tests, large flat-jack test, a jointed block test, and cross-hole seismic studies. Only the deformation properties of the rock mass were measured in these tests; the strength of the rock mass has not been investigated. Test plans and operating procedures are cited in Table 2.3-1. These tests were conducted in the Pomona flow at the Near-Surface Test Facility. The tests were developmental in nature, aiming at establishing a suitable procedure to be used in future field testing of the repository horizon in the Exploratory Shaft Facility described in Section 8.3.2. The test results summarized in Section 2.3.2 provide the initial information on the mechanical responses of a jointed basalt rock mass and were used to develop preliminary design parameters in Section 2.3.3.3.

Rock mass-mechanical response is the result of a complex process of interaction between the intact rock and discontinuities. This process is not completely understood, and part of the BWIP effort has been to develop rock mass models in which the mechanical properties of the intact rock and discontinuities at the Hanford Site can be integrated. The results are still preliminary in nature and will be described in Section 2.3.3. An understanding of this process is crucial toward identifying the parameters that will have a significant effect on the observed mechanical properties and toward generalizing the test results for the design repository.

2.3.1 LARGE-SCALE MECHANICAL PROPERTIES OF OTHER ROCKS

2.3.1.1 Large-scale deformation properties of other rocks

The large-scale deformation properties of rock masses are commonly expressed in terms of deformability modulus, E. The deformability modulus is defined from the stress-strain curve obtained from large-scale field testing in a similar manner as that of the intact rock. Because of the presence of discontinuities in a rock mass, the deformability modulus of a rock mass is invariably lower than the elastic modulus of intact rock. A study by Heuze (1980) on a large number of different types of rocks showed that, in average, the deformaability modulus of a rock mass is approximately one third (0.38 to 0.39) of the elastic modulus of intact rock. Various empirical correlations exist that relate the deformability modulus to measurable rock mass characteristics; some examples are the use of the rock quality designation (Deere et al., 1969) as shown in Figure 2.3-1 and the rock mass rating (Bieniawski, 1978) as shown in Figure 2.3-2. The data base on which the correlations were based typically show wide scatter with a correlation coefficient of 0.665 (see Fig. 2.3-1 and 2.3-2). The scatter can be attributed to many factors, including the use of different testing methods, scale of testing, and natural variability within the rock mass. The studies of Deere et al. (1969) and Bieniawski (1978) showed that the deformability modulus is, perhaps, more closely related to the degree of jointing within the rock mass than to the elastic modulus of the intact rock material. It is, in general, not possible to provide a value, or even a range of values, of deformability modulus for a given type of rock. Because of the wide scatter and the large uncertainty in the data base, the determination of deformability modulus of rock mass must resort to actual measurement by field testing.

Conventional methods of measuring large-scale deformation characteristics of rock masses include plate bearing tests (Stagg, 1968; Dodds, 1974), tunnel pressurization tests, and radial jacking tests (Wallace et al., 1969). A typical stress-deformation curve for a plate loading test in jointed rock is shown in Figure 2.3-3; the response is nonlinear with significant permanent deformation developed with each loading cycle. A variation of the conventional test methods is the block test in which a prism of rock is isolated in situ by line drilling or slot cutting and loaded via pressurized

flat jacks (Pratt et al., 1977; Hardin et al., 1982; Logsters and Voort, 1974). This test was designed to provide better control of the applied stresses to a known volume of rock as compared to the conventional tests.

2.3.1.2 Large-scale strength properties of other rocks

The composite strength of jointed rock is not well understood at present. Field results are scarce, and a satisfactory model that can incorporate the properties of intact rock, discontinuities, and the kinematic restraint caused by the jointing system has not been established. The results of in situ, uniaxial compression tests and laboratory small-scale model triaxial compression tests are summarized below.

2.3.1.2.1 Uniaxial compression

A summary of the results of large-scale uniaxial compression tests is provided in Table 2.3-2. The first seven tests in this table were discussed by Bieniawski and Van Heerden (1975). The granite sample reported by Sundaram et al. (1983, pp. 654-656) included only one throughgoing fracture (sub-horizontal) with a few other discontinuous and healed fractures, whereas the sample tested by Thorpe et al. (1980) was pervasively fractured. In all cases reported, the uniaxial compressive strength of the rock mass is considerably lower than the intact rock material.

In situ uniaxial compressive strengths have also been inferred from the observation of pillar failures in large-scale underground structures. Salamon and Munro (1967) prepared a strength formula for South African coal pillars based on the statistical evaluation of 125 stable and unstable coal pillars. Others (Agapito, 1974; Brady, 1977; Coates et al., 1973; Petersen, 1978) have interpreted rock mass strength by the interpretation of in situ instrumentation and back analysis. The results of these investigations and those of Russell et al. (1984) are summarized in Table 2.3-3.

2.3.1.2.2 Triaxial compression

Rosengren and Jaeger (1968) completed laboratory tests on a marble that had been thermally fractured to induce an interlocking fractured material that Hoek and Brown (1980, p. 168) suggest might be considered as a small-scale analogue of a heavily jointed rock mass. In Figure 2.3-4, the strength envelope for the intact marble is compared to that of the thermally fractured marble. At low confining stress, the strength of the fractured marble sample is considerably lower than that of the intact marble. In contrast, the difference-in-strength was minimal at high confining stress. Rosengren and Jaeger (1968) observed that this effect was due to the degree of interlock of

the grains; and concluded that, with moderate confining pressure, closely jointed rock may retain considerable strength. Also, the slope of the strength envelope of the fractured-marble sample is steep at low confining stress, implying that the fractured-marble sample has a very high internal friction coefficient. Similar behavior has been reported in the results of model tests using plaster blocks at low-confining stress (Brown, 1970, p. 1946; Einstein et al., 1970, p. 98).

2.3.2 LARGE-SCALE MECHANICAL PROPERTIES OF ROCKS AT THE HANFORD SITE

Up to January 31, 1986, the following field tests were conducted in the Pomona flow at the Near-Surface Test Facility.

o <u>Borehole jacking tests</u> (Section 2.3.2.1)--tests performed to measure the deformability modulus of a small volume of rock away from the surface disturbance. The purpose of these tests was to provide input for the predictive analyses of Full-Scale Heater Tests 1 and 2 (Shuri et al., 1980; de la Cruz et al., 1982).

o <u>Jointed block test</u> (Section 2.3.2.2)--a field test designed to allow control of the triaxial stress state and temperature in a 2 m by 2 m by 2 m (6.6 ft by 6.6 ft by 6.6 ft) block of basalt (Cramer and Kim, 1985). This test provided direct measurements of the deformational response of a large block of jointed basalt.

o <u>Cross-hole seismic tests</u> (Section 2.3.2.3)--tests performed to evaluate the dynamic modulus and the extent of damaged rock zone caused by blasting (Myer et al., 1983).

Note that the purpose of these tests was to obtain preliminary data for the conceptual design and to develop testing procedures. The results provided an indication of the magnitude and range of the deformability modulus of the basalt in the Cohassett flow.

2.3.2.1 <u>Borehole jacking tests</u>

The borehole jacking tests were conducted in the Pomona flow at the Near-Surface Test Facility using both the Goodman jack and the modified Goodman jack. The Goodman jack tests were conducted in six boreholes, located in the walls or floor of the Near-Surface Test Facility tunnel in the vicinity of the full-scale heater tests. The tests were conducted within the entablature of the Pomona flow at depths ranging from 1.5 to 7.6 m (5 to 25 ft). The test results are listed in Table 2.3-4.

The modified Goodman jack tests were conducted in vertical holes at the Near-Surface Test Facility (de la Cruz et al., 1982; Voss, 1981). Test depths

ranged from 2.4 to 9.1 m (8 to 30 ft), primarily in the Pomona flow colonnade. The results of the modified Goodman jack tests are shown in Table 2.3-5. The deformability modulus had been calculated from both the tangential strain and the diametrical deformation measurements. The deformability modulus calculated from the tangential strain measurements is significantly higher than that from the diametrical deformation measurements, which is the general observation in this type of test. Possible explanations are that the contact deformation between the rock and the platen may increase the measured value of diametrical deformation, or that the presence of fractures may change the stress distribution around the borehole used to calculate modulus values from tangential strain measurements, or gage slip may have occurred during the test. The values calculated from the two measurements may provide the upper and lower bounds of the in situ deformability modulus of the rock mass (de la Cruz et al., 1982, p. 5).

2.3.2.2 Jointed block test

The jointed block test was located in the west wall of the west access tunnel of the Near-Surface Test Facility (see Fig. 2.0-2). The test block was 2 m by 2 m (6.6 ft by 6.6 ft) square in cross section and 4.5 m (15 ft) deep into the tunnel wall as shown in Figure 2.3-5. The sides of the block (i.e., those in the vertical and north-south (horizontal) direction) were loaded by flat jacks over a 2-m by 2-m (6.6-ft by 6.6-ft) area. Eight hydraulic rams located on the face of the block provided the load in the axial direction through cables anchored beyond the back of the block.

Twenty-six boreholes were drilled within the test block to accommodate the measuring instruments. These holes varried in diameter from 38 to 99 mm (1.50 to 3.90 in.) and were all drilled by coring. The cores were analyzed for joint characterization and were tested in the laboratory for physical and mechanical properties. The rock quality designation values varried between 16% and 47% from borehole to borehole with an average value of 32% (Cramer and Kim, 1985, p. 142). These values are too low to properly correlate between the rock quality designation and the deformability modulus of rock mass as shown in Figure 2.3-1. The values of Q based on the Norwegian Geotechnical Institute Q system (Barton et al., 1974) also show a variation as do the rock quality designation values and have an average value of 8.7. The rock mass rating based on the geomechanics classification system by Bieniawski (1979) was determined for each borehole. The majority of the boreholes have a rating value of 63, while the rating of the remaining boreholes is 58. The average value of all the boreholes is 62, which is very close to values obtained from other locations of the Near-Surface Test Facility (Moak and Wintczak, 1980, pp. 4-58). From the values of the rock mass rating of the test block, the empirical correlation between the deformability modulus and the rock mass rating as shown in Figure 2.3-2 gives a deformability modulus within the range of approximately 15 to 30 GPa (2,175 to 4,350 kip/in^2).

Development and testing of the block was carried out in three steps. Step 1 involved construction and testing of the first slot, which also

included a heater test for a preliminary study of temperature effects. Steps 2 and 3 involved ambient temperature and elevated temperature testing of the block. The important results are presented in the following subsections. Detailed descriptions of construction and test procedures, instrumentation and data acquisition systems, and results and analyses have been presented elsewhere (Black and Cramer, 1983; Cramer et al., 1985; Cramer and Kim, 1985).

2.3.2.2.1 Step 1: slot testing

The slot test was made in the slot that forms the lower horizontal boundary of the test block and was conducted prior to the cutting of the other three slots. The test slot was excavated, as were all other slots, by line drilling followed immediately by grouting two flat jacks within this slot. The relative location of the slot and its associated instrumentation are shown in Figure 2.3-6. The locations of the 15 heaters around the slot are also shown in this figure.

The first stage of the slot test was conducted under ambient temperature by pressurizing the flat jacks. The deformation of the slot was measured by deformation meters installed within the flat jack, and the deformation of the surrounding rock mass was measured by U.S. Bureau of Mines borehole deformation gages installed in the boreholes within the test block. The deformability modulus determined from the deformation of the slot is 40 GPa ($5,800$ kip/in^2), and the deformability modulus determined from the borehole deformation gage is 44 GPa ($6,380$ kip/in^2) (Cramer et al., 1985, p. 19). The modulus obtained from the borehole deformation measurement is slightly higher than that obtained from the slot deformation measurement. One possible explanation is that, because the scale of the borehole is very small in comparison with the joint spacing in the entablature, the readings from the borehole deformation gage may reflect more of the properties of intact rock than those of the rock mass. Note that the deformability modulus determined in this test is considerably higher than that determined from the Goodman jack tests shown in Table 2.3-4.

Subsequent stages of the slot test were conducted by energizing the heaters to study the effect of temperature on the deformability modulus. However, since only one borehole deformation gage survived to the 100 °C temperature level, a conclusion regarding the influence of temperature on rock mass deformation could not properly be made.

2.3.2.2.2 Step 2: ambient temperature tests

The second step of the jointed block test consisted of completing the three slots to form the block, installing the confining cable anchor system, completing the instrumentation, and loading the block under ambient temperatures. While the cutting of the slots was carried out in a carefully controlled sequence to minimize any possible relaxation of the test block, the

deformation of the block during cutting was not monitored for an assessment of the extent of relaxation.

Deformation in all three directions within the test block was measured by the basalt deformation measurement system and three multiple-point borehole extensometers. The basalt deformation measurement system is an electro-optical instrument that remotely monitored the deformation of the test block with a resolution of 1 μm (4 x 10^{-5} in.) and a precision of ± 15 μm (6 x 10^{-4} in.) at a depth of 2.5 m (8.2 ft) from the surface (Cramer and Kim, 1985). The instrumentation plan is shown in Figure 2.3-7. The effect of the presence of 26 instrument holes in the block has been calculated to have a maximum effect of 9% on the displacements as compared to a block without instrumentation holes (Cramer and Kim, 1985, p. 70).

A total of 26 ambient temperature loading tests were conducted during step 2. During each test, a constant confining stress was applied in two of the principal directions while the deviatoric load was cycled between predetermined maximum and minimum levels in the third direction. Confining stress levels varied from 1.5 to 9.0 MPa (0.217 x 10^3 to 1.305 x 10^3 lbf/in^2), while deviatoric stresses went to a maximum of 12.5 MPa (1.812 x 10^3 lbf/in^2). These were selected to minimize gross block deformation through joint slippage or tensile failure (Brady and Hart, 1981). Eleven loading cycles were performed with the deviatoric stress in the horizontal direction, seven in the vertical direction, and six in the axial direction. Two additional tests were run with equal loading in all three directions. A number of cycles were conducted under identical loading conditions to verify the reproducibility of the results. The stress levels attained during the step 2 loading cycles are summarized in Table 2.3-6.

Several examples of the load-deformation curves from the step 2 loading cycles (Cramer et al., 1985) are presented in Figures 2.3-8 (horizontal loading), 2.3-9 (vertical loading), and 2.3-10 (axial loading). Several features of the basalt response are readily apparent from these curves. The most noticeable is the high degree of linearity of the loading portion of the curves. Regression analyses of the loading section demonstrates linearity with a correlation coefficient greater than 0.995 for almost every cycle (Cramer et al., 1985, p. 27). The unloading portions of the curves are generally nonlinear, and the results of many tests showed bilinear response with permanent deformation. Brady et al. (1984) proposed that the slope of the initial unloading region may represent the purely elastic response of the block. Hysteresis is apparent in most of the loading cycles, especially those from loading in the horizontal direction.

The test results also showed a nonuniform deformation pattern within the test block, which had not been anticipated. In particular, it was found that the front portion of the block underwent a larger deformation than the rear portion of the block under the application of axial loading and that the axial deformation was very small when the block was loaded in the horizontal direction. Several numerical models including two- and three-dimensional finite-element analyses (Hardy and Mitchell, 1985) and two-dimensional distinct-element analyses (Cramer and Kim, 1985; Cundall and Hart, 1985) have

been used to model the actual test condition. These studies showed that the particular joint pattern of the basalt rock mass was a major cause of the nonuniform deformation response within the test block.

The finite-element analysis used the ANSYS three-dimensional code with the rock mass assumed to be linearly elastic and orthotropic (Hardy and Mitchell, 1985). The analysis showed the following:

o The horizontal and vertical stresses in the center of the block were significantly less than the applied flat-jack pressure, chiefly as a consequence of the limited area of the block that was loaded by the jacks.

o All stress components were less than that applied by the flat jacks and tendons due to both the friction along the flat jacks and the rock interface and shear stiffness of the flat jacks.

o The axial stress was reduced significantly from the front to the rear portion of the block due to the friction and shear stiffness of the flat jacks.

Based on these findings, the values of deformation modulus were calculated from the average stress obtained from the finite-element analyses. The rock mass deformation modulus in the horizontal and vertical directions are shown in Table 2.3-7 (Cramer and Kim, 1985). The deformation moduli from axial loading are presented in Table 2.3-8 (Cramer and Kim, 1985, p. 324). The moduli values calculated in the axial direction are not as reliable as those of other directions because of greater uncertainties in stress state.

A series of discontinuum analyses using the distinct-element code UDEC (Cundall, 1980) successfully reproduced the hysteresis behavior where the unloading portion of the curve does not follow that of the loading portion and shows a permanent deformation. This behavior was not produced in the finite-element analysis. The observed nonuniform deformation pattern was also explained by the rotation of an individual block. While the discontinuum model showed promise in being able to reproduce actual rock mass behavior more accurately than the equivalent continuum approach, the results are qualitative and further field testing and associated modeling will be required to establish the necessity of discontinuum modeling.

The results from this stage indicate that the deformation of jointed basalt is anisotropic. The axial and vertical moduli are almost twice those measured in the horizontal direction. Poisson's ratio values were generally scattered and did not show directional dependence. Within the range of confining stresses applied during the test, up to 9 MPa (1.30×10^3 lbf/in^2), the deformability modulus was found to increase with increasing confining stress. The moduli values are plotted against the confining stress in Figure 2.3-11. Cramer and Kim (1985, p. 344) fit linear relationships to the experimental deformation modulus as a function of confining stress.

$$Exx = 2.38 \ P + 6.50$$

$$Eyy = 2.39 \ P + 13.5$$

$$Ezz = 1.11 \ P + 20$$

where P is the confining stress in MPa and the modulus is in units of GPa. It should be noted that the anticipated confining stress level around the repository openings is much higher than the test range and that it is not possible to extrapolate the test results to a higher confining stress level since the linear relationships represent only a simplified picture of the true behavior of the block.

2.3.2.2.3 Step 3: elevated temperature tests

The final step of the block test was conducted at elevated temperatures of 100 and 200 °C, with six test runs performed at each temperature (Cramer et al., 1985). Each of the two testing series was identical and based on the pattern of the first six ambient temperature loading cycles. The deformability moduli were evaluated from the test data in the same manner as was used with the ambient temperature results (Cramer and Kim, 1985). The data showed that the deformability modulus at elevated temperature to be higher than those under ambient temperature, which may indicate the locking up of the joint system by the thermally induced stress.

2.3.2.2.4 Preliminary conclusions

The triaxial loading test conducted during the Near-Surface Test Facility block test (Cramer and Kim, 1985, pp. 462-463) generated several basic observations regarding the rock mass deformational response, including the following:

o Anisotropy in the deformational response measured in the three orthogonal loading directions.

o Increase in modulus value with increasing confining stress.

o Linear stress-strain response during loading and the presence of permanent deformation after unloading of the test block.

o Pronounced hysteresis in the stress-strain response to loading, which is not significantly reduced after recycling.

o Column rotation under horizontal loading, resulting in small axial deformation.

These observations were made under relatively low confining stress conditions during the block test and may not represent the actual response of the basalt rock mass in the repository horizon. The potential of the jointed block test as a method for measuring the deformation modulus of jointed basalt has been supported by the present work. Additional study will be required to improve the present data-interpretation method (Section 8.3.3.2).

2.3.2.3 Cross-hole seismic studies

Cross-hole seismic studies have been conducted at the Near-Surface Test Facility at two locations. The first series of tests was associated with pretest and post-test characterization at the full-scale heater test area, while the second series of tests was performed on a series of holes located in close proximity to the jointed block test. The numerical results of the tests from the pretest characterization, cross-hole seismic data for the full-scale heater tests and results from the jointed block area are presented in this section. Post-test cross-hole seismic data from the full-scale heater tests are presented in Section 2.5. Detailed test procedures and full results are described by Myer et al. (1983).

The velocities and dynamic elastic properties obtained in the second series of tests in the block test area are plotted as a function of distance from the tunnel wall surface in Figures 2.3-12 and 2.3-13. The blast-damaged zone is within the zone with lower velocities near the borehole collar, which is generally of the order of 1 to 1.5 m (3.3 to 4.9 ft) in the tunnel sections studied near the block test site (Myer et al., 1983, p. 30). Both the compressional- and shear-wave velocities in the vertical direction were up to approximately 30% greater than those in the horizontal direction away from the blast-damaged zone (Myer et al., 1983, p. 30). This is probably a reflection of the columnar nature of the rock mass jointing. The dynamic modulus calculated from the measured velocities is plotted in Figure 2.3-13. Modulus values in the horizontal direction were approximately 60% of those of the vertical direction away from the blast-damaged zone (Myer et al., 1983, p. 33).

The dynamic modulus values in the blast-damaged zone were considerably lower than those at distance from the tunnel wall. The dynamic modulus of the rock mass within the undisturbed zone is very close to the static modulus determined from intact samples in the laboratory (Myer et al., 1983, p. 33). In comparison, the dynamic modulus is up to four times the value determined from the jointed block test. This agrees with the general experience that the dynamic modulus is higher than the static value.

2.3.2.4 Discussion of results

Three different methods were used to measure the rock mass deformation modulus of the Pomona flow in the Near-Surface Test Facility. Among these,

the borehole jacking test and the cross-hole seismic test have been widely used in site characterization of underground excavations in rock. The jointed block test was specifically designed to measure the deformational response of the basalt rock mass. The advantages of the jointed block test are (1) the test is made on a rock volume appropriate to the size of repository openings; and, (2) deformation within the test block can be determined by direct measurement during the test.

The results are compared in Table 2.3-9, which shows that the moduli values measured in the jointed block test are lower than those obtained from other methods. One explanation is that the test block had been disturbed by the process that created a blast-damaged zone that covered the front portion of the block. Furthermore, the preparation of the test block, where slots were made by line drilling, may have caused relaxation of the rock mass toward the slots. The combination of these effects could cause the measured moduli values to be lower than the actual values. Therefore, the results of the jointed block test are likely to represent a lower bound estimate of the actual deformation moduli. The dynamic moduli obtained from the cross-hole seismic tests provide an upper bound estimate, and the actual deformation moduli may take values between these bounds. The effect of creep and temperature on deformational response of the rock mass have not been studied.

Temperature effects will be important to the repository performance because the repository host rock will experience a temperature cycle during operation of the repository. During the heating phase of the temperature cycle, the rock mass around the repository openings may expand toward the free face. This expansion may result in the opening up of joints around the openings. While it can be reasonably expected that reclosure of joints will occur during the cool-down phase, the possibility that incomplete joint closure, as observed in the post-test inspection of Full-Scale Heater Test 2 (Section 2.5.2.1), cannot be ruled out without further investigation. If this occurs it may affect the mechanical, thermomechanical, and hydrological properties of the rock mass, which may affect the performance of the repository. Thus, further studies are planned, and these studies are described in Section 8.3.2.2.

2.3.3 RELATIONSHIP BETWEEN INTACT ROCK, DISCONTINUITIES, AND LARGE-SCALE ROCK PROPERTIES

2.3.3.1 Introduction

Understanding the relationship between intact rock, discontinuities, and large-scale property is of critical importance in site characterization in basalt because of (1) a need to provide a framework for interpreting the test results; (2) a need to provide a framework to extrapolate the test results throughout the repository; and, (3) the abundance of the cooling joints and their discontinuous nature. This relationship can be used to develop some form of equivalent continuum approach incorporating both joint and intact properties for repository-room-scale design where the rock mass under

consideration contains a sufficient number of discontinuities. It can also be used to develop discontinuous models for the interpretation of intermediate-scale tests (such as the jointed block test) and for end analyses of conditions around the emplacement borehole.

The relationship may be developed by either analytical or empirical approaches. The analytical approach will begin by development of conceptual models for the rock mass and by using these conceptual models as a basis to develop quantitative constitutive models (Section 2.3.3.2). The empirical approach uses some form of rock mass classification system as a basis for correlating empirically the mechanical properties of rock mass with those of the intact rock and discontinuities. Existing rock mass classification systems that had been considered by the BWIP are outlined in Section 2.3.3.3. The rock mass properties used in the SCP conceptual design are summarized in Section 2.3.3.4.

2.3.3.2 Development of analytical models for the mechanical response of basalt rock mass

The development of an analytical model for the mechanical response of a basaltic rock mass consists of two key steps:

o Development of a conceptual model of the basalt rock mass (Section 2.3.3.2.1).

o Development of constitutive equations that describe the mechanical response of a basalt rock mass (Section 2.3.3.2.2).

The conceptual model consists of a qualitative description of the behavior of the rock mass, one that accounts for the contribution of both the intact rock and the discontinuities. This then defines the framework for the development of constitutive equations governing the behavior of the rock mass. These models will eventually be incorporated in geotechnical numerical modeling to support repository design and license application. The computer codes for the numerical modeling that have been developed for the BWIP were described in St. John and Williams (1980), a number of these codes have already been used in the planning and interpretation of the results of field tests in the Near-Surface Test Facility.

2.3.3.2.1 Conceptual models for the basalt rock mass

A number of different two-dimensional conceptual models for a fractured rock mass are illustrated in Figure 2.3-14(a) through (g). These figures represent possible idealizations where Figure 2.3-14(a) may be appropriate when evaluating the behavior of a very large, massive basalt, while Figure 2.3-14(e) or (g) may be appropriate in the entablature and colonnade of the basalt flows where columnar character can be very evident.

Once an idealization has been selected, the next step is to determine whether it is possible to ascribe to the rock mass volume average properties that incorporate the properties of the intact rock and fractures or whether explicit representation of rock and fractures is required. Two alternatives exist: the equivalent continuum and the discontinuum. The fundamental assumptions of the equivalent continuum model, are that it is possible to develop average stress-strain relationships for the rock mass including both intact rock and discontinuities, such that the precise location of the discontinuities is unimportant at the scale of concern. In the discontinuum approach, the rock mass is modeled as an assemblage of blocks; the interaction between the blocks is governed by the mechanical properties of both the intact rock and discontinuities. The construction of such a model requires detailed information regarding the geometry of the jointing system, the stiffnesses and strength of joints, and the mechanical properties of the intact rock material. Because of these reasons, the discontinuum approach will not be discussed further in this section and will be considered in future studies (Section 8.3.2). The continuum model will be discussed in the remaining part of this section.

2.3.3.2.2 Constitutive models for the deformation of basalt rock mass

Four different equivalent continuum models that have been considered by the BWIP are illustrated in Figure 2.3-15(a) through (d). The first model is the simplest case as shown in Figure 2.3-15(a). The material is characterized as linearly elastic and isotropic. Such a simplified approach has been adopted for many scoping and parametric investigations of the Near-Surface Test Facility and in support of the development of repository design concepts. It is a reasonable approximation providing that the fracturing can be considered as intense and random at the scale of concern. If there are relatively few fractures, the deformational response of a rock mass may still be linearly elastic. However, both the deformability and strength of a rock mass can be strongly dependent on the direction of loading.

Based on the results of laboratory tests of intact basalt, the approximation of linear elastic behavior is probably reasonable for the intact material. In contrast, the fractures in basalt exhibit markedly nonlinear behavior under both normal and shear loads. This can be incorporated in the second (nonlinear) model, such as illustrated in Figure 2.3-15(b), in which the joint response dominates at low stress while the intact rock response dominates at higher stresses. This can be further simplified to the third (bilinear) model illustrated in Figure 2.3-15(c), which has been used for some of the predictive analyses performed for the Near-Surface Test Facility experiments (Hocking et al., 1980). The conceptual basis for the bilinear model is that the joints "lock-up" once a certain threshold stress is reached, and thereafter, the intact rock properties dominate.

The fourth model is the hysteretic model illustrated in Figure 2.3-15(d). This model incorporated the hysteresis behavior observed during the jointed block test.

These four models have been applied to the analyses of the field tests conducted at the Near-Surface Test Facility. Possible approaches that can be used to derive the parameters that define the constitutive equations of these models based on the mechanical properties of the intact rock material and the discontinuities and the geometry of the discontinuity system were outlined by Hill (1963), Singh (1973), and Gerrard (1982). Example calculations had been given by Cramer and Kim (1985) and Amadei and Goodman (1981). Other models for equivalent continuum behavior are possible and may eventually prove preferable. For example, the compliant joint model developed by Thomas (1982), in which rock mass response is decomposed into portions for the intact rock and the discontinuities, also may prove to be applicable to the rock mass; however, the current data are insufficient to justify the selection of one model versus another or an adoption of new models.

2.3.3.2.3 Constitutive models for the strength of a basaltic rock mass

The strength of a jointed rock mass is related to the strength of intact rock, strength of discontinuities, and fracture frequency and orientation (Hoek, 1984). This is best demonstrated by the relationship between the strength and size of a rock mass shown in Figure 2.3-16. The data in this figure suggest that rock mass strength decreases with increasing sample size until the sample contains sufficient joints to be representative of the rock mass, hence the term "representative volume." This term is relatively simple to understand but difficult to apply in assessing rock support and allowable waste container placement densities because the dimension of the representative volume depends on both the fracture spacing and the scale of the problem analyzed. Therefore, more fundamental approaches to estimating the rock mass strength have been the subject of evaluation by the BWIP. In the following discussions, hydrologic effects such as pore pressure have not been included. These effects are not well understood at present and will require further study (Section 8.1.1).

The simplest theoretical model is an isotropic, Mohr-Coulomb model with the strength of rock mass completely defined by the uniaxial compressive strength and the internal friction angle. The assumption of isotropy may be valid if fracturing is either absent or so pervading that there is no preferred orientation of fracture. The Mohr-Coulomb model assumes that the intermediate principal stress has only negligible effect. At present, there is insufficient actual testing data to substantiate or disqualify this assumption. Further studies on the yield criteria will be required (Section 8.1.1).

A more common situation is that the presence of one or more sets of discontinuities introduces anisotropy in both the strength and deformability of the rock mass. An unfavorable combination of loading direction and discontinuity orientation may initiate slip along the discontinuities and cause failure to the rock mass. Under such circumstances, the strength of rock will depend on the loading direction, the shear strength along

discontinuity·surfaces, and the persistence of discontinuities. However, even with a simple model containing only one system of joints, a large number of parameters will be required to estimate the mass strength. An accurate determination of these parameters cannot be made in the current stage. The validation and application of theoretical models must, therefore, await until a need is justified and further data can be obtained.

2.3.3.3 Empirical models for the mechanical response of basalt rock mass

The two rock mass classification systems that were used by the BWIP are the South African Council for Scientific and Industrial Research (CSIR) Geomechanics Classification system proposed by Bieniawski (1974, 1976) and the Norwegian Geotechnical Institute (NGI) Tunneling Quality Index proposed by Barton et al. (1974). Both systems incorporate the mechanical properties of the intact rock material and the discontinuities and physical characteristics of the discontinuities in the classification of the rock mass. The application of both systems will result in a numerical value that reflects the overall rating of the rock mass, in the South African Council for Scientific and Industrial Research Geomechanics Classification system this is called the rock mass rating, which varies from 0 to 100; and in the Norwegian Geotechnical Institute Tunneling Quality Index system, this index Q can vary over several orders of magnitude. The ratings from the two systems have been empirically correlated (Bieniawski, 1976). The South African Council for Scientific and Industrial Research Geomechanics Classification system will be the basis of the empirical models described in this section.

2.3.3.3.1 Empirical models for the deformation of basalt rock mass

The empirical correlation between the rock mass rating values and the deformability modulus of the rock mass was discussed in Section 2.3.1.1 with the results shown in Figure 2.3-2. This model shows an increase in deformability modulus in proportion to the rock mass rating value and is applicable only to rock masses with rock mass rating values greater than 50.

In the jointed block test area, the rock mass rating value falls within the range of 58 to 63. According to the empirical model as shown in Figure 2.3-2, the deformability modulus of the rock mass is in the range of 10 to 35 GPa (1,450 to 5,076 kip/in^2). This compares with the actual values being measured, which is in the range of 6.5 to 47 GPa (942 to 6,816 kip/in^2) as shown in Table 2.3-9, and appears to indicate that this empirical model will be applicable to the basalt rock mass at the Hanford Site.

2.3.3.3.2 Empirical models for the strength of basalt rock mass

The majority of empirical models for estimation of rock mass strength applicable to deep underground conditions are based on back analysis of room and pillar geometries of coal mines (Bieniawski and Van Heerden, 1975; Salamon and Munro, 1967). Among the methods applicable to heavily jointed hard rock, the method proposed by Hoek and Brown (1980, p. 166) received a wider acceptance. This method is essentially an extension of the Hoek and Brown failure criterion of intact rock to rock mass strength in which a careful consideration of the choice of the values of empirical constants m and s are required. They extended the method further to correlate the rock mass quality and the constants m and s (Hoek and Brown, 1980, p. 174). The authors have found recently that the initial correlation between rock mass quality, and the constants m and s, are grossly conservative when applied to interlocking rock masses in deep underground (St. John and Kim, 1985, p. 20).

Considering the scarcity of applicable rock mass data to the underground condition at the Hanford Site, the BWIP developed a failure criterion which takes into account the presence of interlocking joint system in basalt. The failure criterion is based on intact basalt strength data that have been adjusted to reflect the presence of joint system in basalt. The degree of weakening due to the joint system is estimated based on the findings of Rosengren and Jaeger (1968) who studied the effect of strength reduction due to the loss of cohesion in grain boundaries in a marble after heating. The findings allow a comparison of the strength of granulated and intact marble specimens under identical confining pressures and provide strength reduction factors. The "reduced" strength data obtained by this method are taken as a reasonable representation of the basalt rock mass, from which the m and s values are calculated. These values are presented in Section 2.3.3.4.

Tests on granulated marble conducted by Gerogiannopoulos (1979) suggest that the strength reduction factors obtained by Rosengren and Jaeger (1968) are likely to be conservative. The validity of the present BWIP approach hinges on the assumption that the granulated marble possesses similar structure to that of the basalt rock mass at the candidate repository horizon. This will be investigated in future studies when access to the repository horizon is made available through the Exploratory Shaft Facility.

2.3.3.4 Rock mass properties for design

The rock mass properties required for design of the underground excavation for a repository reflect, to a considerable extent, the design methodology used. As discussed in Section 6.1.3, the methodology used in the SCP conceptual design of the repository excavation uses simple linear elastic models. It is anticipated that these simple analytical tools will continue to be used but that design verification will be provided by performing detailed analysis based on the best available data on site characteristics and rock mass properties.

Little information is available regarding the mechanical properties of the basalt rock mass in the Cohassett flow. Other than the mechanical properties of the intact rock based on the results of laboratory testing of cores extracted from a few boreholes, the strength, stiffness, and physical characteristics of the joints in the Cohassett flow are generally not available. Thus, the rock mass properties used for the SCP conceptual design were estimated by combining engineering judgment with the following sources of information:

o Results of in situ testing performed in the Pomona flow at the Near-Surface Test Facility.

o Results of laboratory testing of core samples from the dense interior of the Cohassett flow.

o Empirical models using rock mass classification based on the expected geological condition of the Cohassett flow.

The rock mass rating values from the geomechanics classification of the Cohassett flow in the repository horizon were estimated to be in the range of 45 to 67 (Section 2.8.2.2). The upper end of this range is comparable to that of the rock mass in the jointed block test site at the Near-Surface Test Facility. However, because the joints within the Cohassett flow will have a much higher stiffness as a result of high in situ stresses, the deformation modulus of the rock mass in the repository horizon is likely to be closer to the high end of the range obtained from the rock mass in the Pomona flow at the Near-Surface Test Facility. The following are values that were used in the SCP conceptual design (KE/PB, 1986, pp. 7-11):

Unconfined compressive strength   19.8 MPa (2.87×10^3 lbf/in^2)

Deformation modulus   38 GPa (5.51×10^3 kip/in^2)

Poisson's ratio   0.25

The empirical strength criteria developed by Hoek and Brown (1980)

$$\sigma_1 = \sigma_3 + \sqrt{m\sigma_3 \, \sigma_c + S\sigma_c^2} \qquad \text{(2.3-1)}$$

is used for the strength of the rock mass in which

σ_c = intact rock uniaxial strength (305 MPa (44.24×10^3 lbf/in^2))

$m = 22.34$

$S = 0.00421$.

These parameters were obtained by fitting the Hoek and Brown equation to the results of the triaxial testing of intact samples from the Cohassett flow, then reducing the intact strength to that of a fractured rock mass according to the data presented by Rosengren and Jaeger (1968).

Application of the Hoek and Brown criteria in the SCP conceptual design involves calculating a volume average stress at selected points around the excavation or waste emplacement hole. Following the concept developed by Hardy and Hocking (1980), the dimensions of this characteristic volume are defined from the maximum dimensions of the excavation. The stress (σ_1) computed in this manner is then compared to the strength calculated from Equation 2.3-1 and to the computed average confining stress (σ_3). This process, which aims to account for scale effects in a logical manner, is based largely on engineering judgment and has yet to be validated by field testing.

2.3.4 SUMMARY

Rock mass properties, while critical to the design and licensing of a repository, are difficult to measure or calculate. The complex interaction of the intact rock and the discontinuities that compose the rock mass necessitate the use of large-scale tests. Such tests must be performed on volumes of rock sufficiently large to be representative of the rock mass; so the tests are relatively expensive and time consuming.

The large-scale properties of basalt have been investigated through field tests at the Near-Surface Test Facility in the Pomona flow outcrop and through associated numerical modeling. Testing to date has measured the deformability of the basalt rock mass; measurements of rock mass strength have not been made.

The basalt rock mass moduli measured at the Near-Surface Test Facility fall within the range of 10.2 to 47 GPa (0.94 to 6.82 x 10^3 kip/in^2). The deformability modulus of the rock mass of the Cohassett flow in the repository horizon is likely to be near the upper end of this range because of higher joint stiffness at depth caused by higher in situ stresses.

The rock mass strength of basalt is currently represented by the Hoek and Brown formula for estimating strength. The parameters used in this equation are estimated from laboratory data, and correlations are developed for fractured rock.

Numerical modeling has been used extensively to aid in the interpretation of field tests. The jointed block test has provided a comprehensive set of deformational response data, but because it is located at the Near-Surface Test Facility in an outcropping of the Pomona flow where the rock is unsaturated and subjected to low in situ stress, it does not represent the conditions at depth. Further tests are planned to be conducted at depth in the Exploratory Shaft Facility. These are described in Section 8.3.2.

2.4. THERMAL AND THERMOMECHANICAL PROPERTIES--INTACT ROCK

2.4.0 INTRODUCTION

Knowledge of the thermal properties of a nuclear waste repository host rock is necessary to predict the temperature around the repository openings with time. This is used in a number of ways in the design and performance assessment of the repository. The temperature in the host rock caused by the emplacement of containers will be approximately 219 °C (KE/PB, 1986, pp. 6-27), and the confinement around the openings that prevents free thermal expansion of the rock will result in thermally induced stress in the rock mass. The thermally induced stress and its associated displacements significantly influence repository layout and design (Section 6.2.6). The temperature increase will increase the thermal buoyancy of the groundwater and modify the hydraulic conductivity around the storage rooms, both of which will affect the hydrologic calculations describing repository performance.

The thermal and thermomechanical properties of basalt were first estimated from existing literature (Agapito et al., 1977); these were later augmented by site-specific test data from the Umtanum, Pomona, and other Grande Ronde basalt flows. Schmidt et al. (1980) summarized the data available when the conceptual design studies were initiated. Laboratory testing of core from the Full-Scale Heater Tests 1 and 2 locations (FSI, 1980a, 1980b) was completed before test startup and was used in predictive analysis of the tests.

A summary of laboratory testing of core samples to determine thermal and thermomechanical properties of several basalts is given in Table 2.4-1. The test procedure and the corresponding references are listed in Table 2.4-2. Sublette (1983) presents a compilation of the test data from the Cohassett, Umtanum, and Pomona flows. These data are reproduced in Tables 2.4-3 through 2.4-5.

2.4.1 THERMAL AND THERMOMECHANICAL PROPERTIES OF OTHER ROCKS

The thermal conductivities for basalt in general and similar rocks compiled by Clark (1966) are shown in Table 2.4-6. A histogram of thermal conductivity of Columbia River basalt compiled by Roy et al. (1981) is shown in Figure 2.4-1. The temperature at which these measurements were made is not indicated. The results range from 1.12 to 2.38 W/m·°C, with most values between 1.3 and 2.0 W/m·°C. The range of variation of thermal conductivity for basalt as a function of temperature, compiled from a review of 32 sources by Roy et al. (1981), is plotted in Figure 2.4-2, which shows a 25% reduction in thermal conductivity over the expected temperature change for basalt in the repository environment, 40 to 300 °C.

The thermal expansion of basalt and similar rock, as summarized by Clark (1966), is listed in Table 2.4-7. Thirumalai (1970) reported the thermal expansion coefficient for Dresser basalt ranging from 2.9 µε/°C at 24 °C to 11.6 µε/°C at 593 °C.

The heat capacity of basalt, compiled by Roy et al. (1981, p. 436), is shown in Figure 2.4-3 as a function of temperature. The trend shows approximately a 20% increase in the specific heat as the temperature changes from 0 to 300 °C.

2.4.2 THERMAL AND THERMOMECHANICAL PROPERTIES OF ROCKS AT THE HANFORD SITE

2.4.2.1 Pomona and Umtanum flows

Most of the thermomechanical testing on the Pomona flow was completed prior to Full-Scale Heater Tests 1 and 2 at the Near-Surface Test Facility to provide site-specific data for predictive analysis of the tests. The mean values and standard deviations of thermal conductivity, heat capacity, and thermal expansion coefficient are listed in Table 2.4-3. Generally, tests were conducted over a temperature range of 20 to 200 °C. Within this temperature range, heat capacity shows an increase with temperature, while both the thermal conductivity and thermal expansion coefficient appear to be independent of temperature (Sublette, 1983, p. 53). Tests on both the thermal conductivity and thermal expansion coefficient made on samples from vertical and horizontal boreholes indicate no significant difference due to orientation. Similarly, no significant difference was found between the thermal expansion values for samples obtained from Full-Scale Heater Tests 1 and 2; however, half of the thermal conductivity values for Heater Test 2 samples were considerably less than the remaining samples from Heater Test 2 and those from Heater Test 1 (FSI, 1980b, pp. 3-7, 11-7, 14-1).

Results from the thermal and thermomechanical testing of core samples from the Umtanum flow are summarized in Table 2.4-4. Generally, these tests were conducted over a temperature range of 20 to 200 °C. The data on other

<div align="center">2.4-2</div>

Columbia River basalt compiled by Roy et al. (1981) (see Fig. 2.4-1 through 2.4-3) are in general agreement with those otained from the Pomona flow and Umtanum flow. The trends of decreasing thermal conductivity and increasing thermal expansion with increasing temperature reported by Roy et al. (1981) do not agree with the present Hanford Site data which do not appear to be affected by temperature within the range of temperature tested for both Pomona and Umtanum flow samples.

2.4.2.2 Cohassett flow

Results of the thermal and thermomechanical testing of the Cohassett flow are summarized in Table 2.4-5. Generally, these tests were conducted over a temperature range of 20 to 200 °C. Within the range of temperature of these tests, the thermal conductivity and the thermal expansion coefficient do not appear to vary with temperature. These results are comparable to those obtained from the Pomona and Umtanum flow samples. Discussion of the test results and the uncertainties associated with these is provided in Section 2.4.2.4.

2.4.2.3 Effect of various parameters on thermal and thermomechanical properties

The effects of porosity and moisture on the thermal and thermomechanical properties are discussed in this section. Because there are insufficient data from the Hanford Site, some of the discussions will be on other types of rocks.

In general, for the same types of rock in a dry or unsaturated state, the thermal conductivity will be related to its porosity in that those rocks with a higher porosity will possess a lower thermal conductivity. Saturation of the rock will cause an increase in its thermal conductivity and the magnitude of increase will depend on the porosity of the rock (Woodside and Messmer, 1961, p. 1705; Robertson and Peck, 1974, p. 4878). The effects of porosity and moisture on the thermal conductivity of intact rock are therefore interrelated. As an example, using an analytical approach Chan and Jeffrey (1983, p. 296) estimated that the thermal conductivity of saturated, low-porosity (2%) granite is 5% lower than that of solid granite, while drying out the pores will change this figure to 10%. The reduction of thermal conductivity as a function of porosity of a saturated, porous rock is shown in Table 2.4-8. These data are derived from equations presented by Roy et al. (1981, pp. 417 and 418). It can be seen from this table that for a rock whose porosity is already low, the effect of changing moisture conditions on thermal conductivity is very small.

The above discussion suggests that varying porosity and moisture conditions in the basalt dense interior may have little effect on the thermal conductivity because the porosity is already low in the dense interior. The

reduction in thermal conductivity is likely to be significant in the more porous flow tops and vesicular zones. Experimental evidence to verify the above statement has not been obtained at the Hanford Site. However, density measurements that may reflect the variation in porosity were gathered on samples tested for thermal conductivity. The result of correlating density with the thermal conductivity of Grande Ronde Basalt samples indicates lower thermal conductivity for lower density. The results are inconclusive because of the small number of samples and the correlation between density and porosity. The thermal conductivities of flow-top samples are generally lower than those of the dense interior samples (Schmidt et al., 1980, pp. 6-19).

2.4.2.4 Discussion of results

The data presented in this section for basalt from the Hanford Site are in general agreement with that of the Columbia River basalt. However, the temperature dependence of the thermal and thermomechanical properties and the effects of various parameters, such as moisture and jointing, could not be established from the present data base because of insufficient data available and the large scatter exhibited in the data.

The present data base is restricted in that the total number of samples from within the reference repository location consists of only 10 samples from the Umtanum flow and 11 samples from the Cohassett flow (Myer, 1982, pp. 8 and 9). Furthermore, all these samples are from the same borehole. Thus, the variability of the thermal and thermomechanical properties either laterally within the same flow or between flows cannot be assessed from the present data base.

Part of the reason for the large scatter in the test results may be caused by combining the test results from different laboratories. At one instance, identical samples were tested separately by Foundation Sciences, Inc. and the Lawrence Berkeley Laboratory, and the results from these two laboratories were in poor agreement. It is not possible to quantify the degree of uncertainty associated with this. However, future thermal property testing done by the BWIP will rely on common equipment, calibration, and testing and quality assurance procedures to avoid the problem associated with using different laboratories (Section 8.3.2.2).

In addition to the thermal and thermomechanical properties of the intact basalt, the thermal and thermomechanical properties of the infilling material may also have significant effects on the performance of the repository. These are not available at present and future studies will be planned (Section 8.3.3.2).

2.4.3 SUMMARY·

Tests performed to date have included samples from the Pomona, Umtanum, and Cohassett flows. The thermal conductivity and thermal expansion coefficient appear to be independent of temperature, whereas the heat capacity increases by approximately 20% with an increase in temperature of 300 °C (Fig. 2.4-3). The results are in general agreement with those reported in the literature for basalt. For samples from the Cohassett flow the following estimates are currently in use, the mean thermal conductivity is 1.51 W/m·°K, the mean thermal expansion coefficient is 6.02 $\mu\epsilon$/°C, and the mean heat capacity increases from 782 J/kg·°K at 20 °C to 929 J/kg·°K at 200 °C.

The major uncertainty associated with the present data is the effect the test procedure has on the results. This uncertainty is evidenced by the lack of agreement between the results obtained by the laboratories that performed thermal conductivity measurements on identical basalt samples. Future thermal property testing by the BWIP will rely on common equipment, calibration, and testing procedures to avoid the problem caused by using different laboratories (Section 8.3.3.2).

2.5. THERMAL AND THERMOMECHANICAL PROPERTIES--LARGE SCALE

2.5.0 INTRODUCTION

Large-scale thermal and thermomechanical properties are required to calculate the temperature and thermally induced stress in the rock mass surrounding the repository openings (Section 6.1.3) and to assess the potential of thermal fracturing of the rock mass. The thermal and thermomechanical properties of rock mass are affected by the thermal and thermomechanical properties of the intact rock material, the presence of joints, the inhomogenuities within the rock mass, and the in situ moisture condition. At present the potential influence of joints, inhomogenuities, and moisture is generally not understood.

The tests conducted by the BWIP include both Full-Scale Heater Tests 1 and 2 and a single heater test associated with the jointed block test at the Near-Surface Test Facility. The test procedure document for each of these tests is listed in Table 2.5-1.

It should be noted that the full-scale heater tests were designed to demonstrate that the basalt rock mass could withstand high temperature and thermally induced stresses, and the primary purpose of the heater test in the jointed block test was to study the effect of temperature on the mechanical properties of a basalt rock mass. As a result of this, the thermal and thermomechanical properties reported in this section were not directly measured values but were values interpreted from the response of the basalt rock mass during the tests.

In this section, the available data on the large-scale thermal and thermomechanical properties of other rock types (Section 2.5.1) and basalt (Section 2.5.2) are presented. This includes a brief presentation of

representative-results for the Near-Surface Test Facility thermomechanical tests. Next, the relationship between intact and large-scale thermomechanical models is addressed, emphasizing constitutive models that may be applicable when describing the behavior of a basalt rock mass. Since the constitutive models for thermomechanical behavior are substantially the same as the mechanical models discussed in Section 2.3, these are discussed briefly with emphasis on the thermal expansion and thermal dependence of material properties. Finally, values of thermal and thermomechanical properties that were used in the conceptual design are summarized.

2.5.1 LARGE-SCALE THERMAL AND THERMOMECHANICAL PROPERTIES OF OTHER ROCKS

Several large-scale thermal tests have been performed in support of waste repository studies conducted elsewhere. The specific tests, test layouts, and references are listed in Table 2.5-2. These tests consisted of line heaters in rock, with thermocouples used to determine the temperature change with time and distance from the heater. The large-scale thermal properties measured from these tests are shown in Table 2.5-2.

Jeffrey et al. (1979) reported that the large-scale thermal conductivity and thermal diffusivity at the Stripa mine were slightly higher than the laboratory values. For example, the large-scale thermal conductivity is 5% higher than the laboratory value.

The block test reported by Hardin et al. (1982) was conducted on a highly jointed block of granite gneiss. The measured thermal conductivity was in the range of 3.72 to 3.9 W/m·°C, as compared to the average laboratory value of 3.2 W/m·°C for granite. The large-scale thermal expansion coefficient interpreted from the strain measurements varied from 6.07 to 9.86 με/°C when the temperature of the test block was increased from 20 to 80 °C. This is also compatible with the values obtained from laboratory tests for granite.

In summary, available evidence indicates that the large-scale thermal and thermomechanical properties of granite and granite gneiss are very close to those determined in the laboratory from small samples. This will be discussed further in Section 2.5.3.1.

2.5.2 LARGE-SCALE THERMAL AND THERMOMECHANICAL PROPERTIES OF ROCKS AT THE HANFORD SITE

2.5.2.1 Full-scale heater tests

Both Full-Scale Heater Tests 1 and 2 used electric heaters placed vertically in the floor of the test room of the Near-Surface Test Facility. The electric heater was dimensioned to simulate a container of high-level nuclear waste as these tests were intended to demonstrate that the basalt rock mass could withstand high temperatures and thermally induced stresses. The

tests were performed prior to the completion of the preliminary conceptual repository design and followed the configuration of the Stripa tests (Witherspoon and Degerman, 1978).

Full-Scale Heater Test 1 consisted of a single, 2-kW full-scale electric heater surrounded by 8 smaller 1-kW peripheral heaters that will produce a thermal loading of 50 W/m^2 (0.032 W/in^2) (Williams et al., 1981, p. 11). The actual heater power levels and duration of Full-Scale Heater Test 1 are shown in Figure 2.5-1. The test was held with all the heaters powered on for 496 d (step 4) and was monitored for 219 d (step 5) during cooldown. The monitoring system consists of thermocouples, strain monitoring devices, and extensometers installed in vertical holes in the floor of the test room and in horizontal holes from the extensometer room as shown in the layout plan in Figure 2.5-2.

Full-Scale Heater Test 2 used a single, central heater of the same physical dimension as that used in Full-Scale Heater Test 1. The power level to the heater is shown in Figure 2.5-3. After 527 d (steps 1 through 3) of heating, the power was turned off, and the borehole was inspected. Following the cooldown and inspection period (step 4), the heater was reinserted and the power level increased to 9 kW for 21 d (steps 5 through 7) (AMI, 1986, p. 20). The instrumentation layout shown in Figure 2.5-4 was similar to that of the Full-Scale Heater Test 1 with additional instruments to monitor the extent of decrepitation, joint movement, and fracturing in the basalt. The test area was studied thoroughly after completing the test. The post-test characterization studies included coring in the vicinity of the heater hole, laboratory tests on the core, and cross-hole seismic studies.

Predictive and post-test analyses using the computer codes DAMSWEL (Hocking et al., 1980; AMI, 1986) and ANSYS (AMI, 1983; Hardy and Mitchell, 1985) were used to model the temperature and displacement in the rock mass in Full-Scale Heater Test 2. The purpose of this modeling was to interpret and verify the rock mass thermal and thermomechanical properties from field measurements by comparing these with the calculated results. The results of Full-Scale Heater Test 1 have not been analyzed to the same extent as those of Full-Scale Heater Test 2. In the remaining part of this section, only the results from Full-Scale Heater Test 2 will be discussed.

2.5.2.1.1 Thermal results

Temperature measurements were made in approximately 220 locations around Full-Scale Heater Tests 1 and 2. Typical temperature responses measured by the thermocouple during each test are shown in Figures 2.5-5 and 2.5-6. In general, the temperature measurements were considered reliable. The maximum temperatures at the borehole wall reached 429 °C in Full-Scale Heater Test 1 and 679 °C in Full-Scale Heater Test 2 (Kasza, 1985, p. 42).

During the first phase of heating at Full-Scale Heater Test 2, which lasted 90 d, the heater power level was held constant so the thermal properties of the basalt could be interpreted from the test results by fitting

the theoretical curve to the measured value. From these analyses, Ames (1986, p. 9) concluded that the best estimate for the conductivity is 1.71 ± 0.10 W/m °C, with a heat capacity of 845 ± 85 j/kg °C, both very close to those obtained from laboratory tests (Section 2.4.2.1) (Ames, 1986, p. 51).

These values were then used to calculate the temperature history in subsequent steps of the heater tests. As shown in Figures 2.5-5 and 2.5-6, the calculated temperature in the near-field region around the test heaters was within 6.6% of those measured throughout the 900 d of the tests (see AMI, 1986).

2.5.2.1.2 Thermomechanical results

Displacements within the rock mass were measured in Full-Scale Heater Tests 1 and 2 using approximately 25 multiple-position borehole extensometers in each test (AMI, 1986, pp. 17-18). Three- and four-anchor extensometers were used to measure the relative displacement between the anchor point and the extensometer head. Vertical extensometers measured the relative displacement points below, at, and above the midheight level of the heater, relative to the floor of the test room. Horizontal extensometers were installed in boreholes from a lower extensometer room adjacent to the test room. Most of the horizontal extensometers were installed perpendicular to the axis of the test room. The deepest anchor of all horizontal extensometers was located beyond the plane of the heater.

Typical responses of vertical displacement measured during each test are shown in Figures 2.5-7 and 2.5-8. Both predictive analysis (Hocking et al., 1980) and post-test analysis (AMI, 1986) were performed to model the deformation around the heater. In the post-test analysis, the basalt rock mass was modeled as thermally homogeneous and mechanically transversely isotropic with confining-stress-dependent moduli. The deformation modulus and Poisson's ratio were taken from the results of jointed block test. The thermal expansion coefficient used was 6.4 μe/°C (see Table 2.4-5).

Comparisons of the post-test analyses with the field results show that there is a general agreement between the calculated and measured vertical displacements (see Fig. 2.5-7 and 2.5-8). The discrepancy between the calculated and measured horizontal displacements may have been caused by several factors: the magnitude of the displacement was too small to be measured accurately by the instruments; the mechanical properties of the rock mass used in the analysis may not have been appropriate; and the computer code may be inadequate for simulating the three-dimensional nature of the test. Further study is needed to isolate and eliminate the problem (Section 8.3.2.2).

2.5-4

2.5.2.1.3 Post-test characterization

Post-test characterization of the full-scale heater test area has consisted of the visual inspection of empty heater holes, the coring and core analysis of six holes in the heater test area, and the completion of cross-hole seismic surveys.

After the heater tests, six holes were drilled by coring in the test area. The cores were tested in the laboratory to determine tensile strength, uniaxial compressive strength, compressional- and shear-wave velocities, and static and dynamic elastic moduli. These tests were conducted to study whether past temperature history has any effect on the mechanical properties of intact basalt. However, there was considerable scatter in the test results, which could not be used to support any conclusion (Section 2.1.2.3).

All post-test characterization studies have been focused on Full-Scale Heater Test 2, where the central heater had a maximum power output of 9 kW, which produced temperatures at the heater container wall of 679 °C with no noticeable spalling or degradation of the heater wall. The post-test inspection showed some fracture opening or enhancement associated with preexisting fractures but no visually identifiable deterioration of the basalt host rock (Kasza, 1986, pp. 42-43).

The cross-hole seismic survey completed at Full-Scale Heater Test 2 and described by Myer et al. (1983) produced significantly different sonic velocities and dynamic moduli than the pretest survey. A possible explanation involves the opening or dehydration of preexisting fractures during the thermal cycle. The displacement data show a residual upward displacement of up to 1.5 mm (0.1 in.), indicating that, during cooldown, not all thermal expansion was recovered. This and the observed fracture opening in the heater hole suggest that the fracture opening, at least in the vertical sense, may be pervasive and may have contributed to the low seismic velocities.

2.5.2.2 Heated jointed block test

The overall concept of the block test is presented in Section 2.0, and the mechanical test results are presented in Section 2.3.2.2. Thermal properties of the rock mass were measured during step 1, the single-slot phase of the test.

During step 1, a single heater was activated, and temperature changes surrounding the heater were monitored. From these data, the thermal conductivity of the basalt was calculated (Brechtel, 1985, p. 18). The heater was located in instrumentation hole 5H01 (see Section 2.3.2.3) with thermocouples located in instrumentation holes 5F01 and 5F02 approximately 0.3 m (1 ft) below and beside the heater hole. The heater was activated at 1 kW for 210 h. The average horizontal and vertical thermal conductivity

interpreted from the thermocouple data over the temperature range is
1.57 W/m °C (Brechtel, 1985, p. 47). This value compares well with the
1.85 W/m °C measured for Pomona flow laboratory samples (see Table 2.4-5).

2.5.2.3 Discussion of results

The thermal properties presented in this section were not directly
measured but were interpreted from the measured response of the rock mass
under controlled heating conditions. Essentially, the interpretation process
involved finding the set of properties that would produce the best fit between
the theoretical curve and the measured response. The theoretical curve is
based on the assumptions that the rock mass is homogeneous and isotropic and
that the thermal conductivity and heat capacity are constant and independent
of temperature. · Currently, there is no evidence to suggest the existence and
extent of the inhomogenuity and anisotropy of the rock mass in the test area,
nor is there any evidence to suggest that the thermal conductivity and heat
capacity may be temperature dependent. Because of this, anisotropy and the
variation of thermal properties with temperature could not be studied.
Nevertheless, the observation that the interpreted values compared well with
the laboratory results is in agreement with the trend observed in other large-
scale thermal tests conducted in other types of rocks. The thermal
conductivity interpreted from the heated jointed block test is very close to
that interpreted from the first phase of Full-Scale Heater Test 2 (1.57 W/m·°C
versus 1.71 W/m·°C) (Ames, 1986, p. 51).

In the heated jointed block test, the thermocouples located horizontally
and vertically had registered slightly different temperatures during the test.
This may be indicative of a small, thermal anisotropy or the inability to
measure the exact location of the thermocouples with sufficient accuracy.
Further studies will be required (Section 8.3.2.2).

The data developed to date on large-scale thermal and thermomechanical
properties are site-specific to the Pomona flow where stress, jointing, and
moisture conditions may be different from the Cohassett flow. Observation of
jointing and moisture conditions at depth, as well as in situ testing in the
Cohassett flow, should be conducted to obtain data specific to the Cohassett
flow, to provide an understanding of the influence of different rock mass
structure on its thermal and thermomechanical properties, and to further study
the potential of thermal fracturing. The study of thermal fracturing requires
a fracture mechanics model that will be developed in future studies
(Section 8.1.1).

2.5.3 RELATIONSHIP BETWEEN INTACT ROCK, DISCONTINUITIES, AND LARGE-SCALE ROCK PROPERTIES

The first two steps in developing large-scale rock properties for repository design and licensing application include the following:

o Development of a conceptual model of a basalt rock mass (Section 2.5.3.1).

o Development of general constitutive equations that describe the response of a basalt rock mass (Section 2.5.3.2).

Understanding the relationship between intact rock, discontinuities, and large-scale rock properties is important in establishing the conceptual models and the constitutive equations. This is because an essential feature of the models lies in the ability to reproduce the complex interaction of the various components within a rock mass. The conceptual model and constitutive equations are discussed in Sections 2.5.3.1 and 2.5.3.2, respectively. The rock mass thermal and thermomechanical properties used in the SCP conceptual design are summarized in Section 2.5.3.3.

2.5.3.1 Conceptual models for a basalt rock mass

In describing the conceptual models for the mechanical response of a basalt rock mass in Section 2.3.3.1, the possibility of modeling the rock mass as a discontinuum or a continuum material was discussed. The fundamental difference between a discontinuum and a continuum is that in a discontinuum model the properties of the intact rock and discontinuities can be incorporated in the response of the rock mass in an explicit manner whereas in a continuum model it is assumed that it will be sufficient to consider only the apparent mass properties, the properties of the intact rock material and the discontinuities are incorporated in an implicit manner. Only the continuum model has been considered for the thermal and thermomechanical properties of rock mass because (1) a continuum model is considered acceptable for many cases of practical interest, and (2) the effect of the presence of discontinuities on the thermal and thermomechanical properties is not known at present. These models should be capable of accounting for material anisotropy and possible temperature and stress dependency of the pertinent thermal properties (i.e., heat capacity and thermal conductivity). The possibility of temperature and stress dependence of the mechanical and thermomechanical properties, including the coefficient of thermal expansion, also needs to be included in the models.

2.5.3.2 Constitutive equations for a basalt rock mass

Because temperature is a scalar quantity, the thermal conductivity for a material with axes of thermal symmetry (i, j, k) can be defined by three parameters, k_i, k_j, and k_k, which are the thermal conductivities measured in directions parallel to the three axes. For an isotropic material, the three parameters ki, kj, and kk are identical. For a transversely anisotropic material, two of the three parameters will have identical values.

For rock masses, the thermal conductivities k_i, k_j, and k_k should reflect the properties of any discontinuities and discontinuity infillings, as well as the intact rock. For the cases of orthogonal jointing, these properties can be derived by linear summation of the properties of the components. In both the Full-Scale Heater Test 2 and the heated jointed block test, it was found that the thermal conductivity and the heat capacity of a rock mass have values similar to those determined in the laboratory from intact core samples (Section 2.5.2.3). This suggests that the presence of discontinuities within a rock mass would have only an insignificant effect on the thermal behavior of a rock mass. One possible explanation for the absence of a scale effect in heat capacity is that the volume of intact rock within a rock mass is many orders of magnitude larger than those occupied by the discontinuities, and thus, the heat capacity of the intact rock would dominate that of the rock mass. The absence of a scale effect in thermal conductivity suggests that the transfer of heat across a discontinuity does not require any greater effort than that through the intact rock material. It is not possible to substantiate this statement because the process of heat conduction across a discontinuity is not well understood at present.

The logic presented above for heat capacity is equally pertinent to the coefficient of linear thermal expansion. The expansion coefficient of an unconstrained rock mass should be approximately equal to the value of the intact material because the presence of discontinuity will have no effect on the thermal expansion of the intact material and, if the rock mass were allowed to expand freely, its overall thermal expansion must be very close to the sum of the intact blocks. If the rock mass is constrained from expansion, the thermally induced stress may not correspond to that of the intact rock material because the presence of discontinuities will allow a small amount of expansion of the adjacent intact rock. Because of this, the thermally induced stress in the rock mass will be smaller than that of the intact rock. Furthermore, the increase of stress may be a nonlinear function of temperature because the deformation across a discontinuity is generally a nonlinear function of stress. Thus, although the thermally induced stress in a constrained rock mass may appear to be a nonlinear function of temperature, the observed nonlinearity should be accounted by using the proper deformational behavior of the rock mass and not by assuming a nonlinear thermal coefficient of expansion. The conclusion is that in analyzing the thermomechanical response of a constrained rock mass, there is no reason to use a thermal expansion coefficient different from that of an unconstrained rock mass, which should be very close to that of the intact rock. Again, these assessments are consistent with the results from the full-scale heater tests. Observed expansion in the vertical, unconstrained direction agreed

closely with numerical simulations based on the use of the laboratory value
for the coefficient of thermal expansion (AMI, 1986, pp. 83-92). Much greater
difficulty has been experienced when trying to match the displacements in
directions where the rock mass is confined (see Section 2.5.2.1.2).

2.5.3.3 Thermomechanical properties in design

Large-scale thermal or thermomechanical tests have not been performed at
the repository horizon; therefore, preliminary design analyses must use
estimates of at-depth properties based on laboratory-derived core-hole test
data and inferred at-depth conditions. The rock mass in the Cohassett flow is
under considerably higher stress than that in the Pomona flow, which may
produce tighter joints in the Cohassett flow and further reduce the effect of
jointing on the thermal conductivity of the rock mass. Present estimates used
in design have been based on the the laboratory core test values for the dense
interior of the Cohassett flow (Sublette, 1983, p. 57).

The thermal conductivity and thermal expansion coefficient of blast-
damaged or destressed rock around the repository could be reduced if
sufficient joint dilation occurred. This effect is considered small, and the
quantification is uncertain so that no change has been incorporated into the
design analysis for this stage.

The large-scale thermal and thermomechanical properties of flow tops are
not well known at this time. Estimates of flow-top properties are needed for
repository design, regional thermal studies, and regional performance
assessment studies. It is expected that thermal and thermomechanical
properties of the flow tops can be measured in the laboratory. The thermal
conductivities for flow-top material tested by the Colorado School of Mines
and summarized by Schmidt et al. (1980, pp. 19-24) was between 65% and 80% of
that for the dense interior flow material.

The thermal and thermomechanical properties for the dense interior of the
Cohassett flow as used in the SCP conceptual design are listed in Table 2.5-3.

2.5.4 SUMMARY

The large-scale thermomechanical tests completed to date have been
primarily demonstration tests or tests to identify the significant
phenomenology involved in heating a basalt rock mass. The following
observations were made:

o The presence of discontinuities does not appear to affect the
   thermal properties of the rock mass in the Pomona flow entablature
   as evidenced by the agreement between laboratory and field results
   (Huyakorn and Thomas, 1981, p. 70).

o· The·vertical thermal expansion coefficient of the Pomona flow basalt
   inferred from the heater tests is similar to the laboratory-   ·
   determined value. Measured horizontal displacements do not agree
   with predicted values (AMI, 1986, pp. 79-97).

o The cross-hole seismic tests in post-test characterization showed
   that the seismic velocity was lower in regions adjacent to the
   heater hole. However, examination of the heater hole after the test
   did not reveal any new fractures in the wall of the hole, and the
   cause for reduction in seismic velocity has not been established.

   The results from these tests suggest that laboratory-determined values
may provide an approximation of the large-scale thermal and thermomechanical
properties. Therefore, the design values of large-scale thermal and
thermomechanical properties were taken from the laboratory test results of
samples from the Cohassett flow. However, since the above conclusion was
established on a data base that contained only the Pomona flow, questions
relating to the transferability of data from one test area to another (which
may result from changes of basalt mineralogy, fracture infilling thickness,
fracture frequency, moisture, porosity, and in situ stresses) should be
resolved. This can be done by conducting additional tests at the Near-Surface
Test Facility and testing at the Exploratory Shaft Facility (Section 8.3.2).

2.6 EXISTING STRESS REGIME

2.6 Existing stress regime
    2.6.0 Introduction
    2.6.1 Regional stress regime
        2.6.1.1 Tectonic setting
        2.6.1.2 Regional in situ stress regime
    2.6.2 Local stress regime
        2.6.2.1 Stress indicators observed at the Hanford Site
        2.6.2.2 Hydraulic fracturing stress determinations at depth
        2.6.2.3 Stress regime for repository design
    2.6.3 Stress measurements at the Near-Surface Test Facility
    2.6.4 Summary

2.6.0 INTRODUCTION

Knowledge of the state of in situ stress is of fundamental importance in the design of stable underground openings and the prediction of rock mass behavior under static and dynamic loading conditions. The in situ regime at a particular location is a function of the mechanical properties of the rock mass, geologic structure, and tectonic history. Principal stress magnitudes and directions are essential engineering parameters required in the repository design process for evaluation of constructibility and opening stability for calculation of tunnel support requirements and for estimation of the areal density of waste emplacement. Measurement of in situ stress prior to excavation has gained acceptance as an important component in geotechnical investigations for major underground excavations. Early knowledge of the in situ stress regime can result in substantial cost savings in the design and construction of an underground facility.

The orientation of the existing in situ stress field for the Pasco Basin has been assessed through evaluation of geologic structures, geodetic surveys, and focal mechanism solutions for microseismics (Sections 1.3.2.4 and 1.4.1.2). These data, together with the regional tectonic setting, provide a basis for estimating stress orientation but contribute little to a quantitative estimate of stress magnitude. These are summarized in Section 2.6.1. The results of hydraulic fracturing tests conducted in deep boreholes in and around the reference repository location to determine the orientation and magnitude of the in situ stresses in the Cohassett flow are summarized in Section 2.6.2. The results showed high in situ stress conditions and were supported by observations of other stress indicators, such as core disking and borehole wall spalling.

The applicability of stress determination methods in basalt with closely spaced joints has been the subject of extensive study at the Near-Surface Test Facility. These studies included the development of testing methods and comparing the results from hydraulic fracturing and overcoring tests. Preliminary results from these studies are summarized in Section 2.6.3.

2.6.1 REGIONAL STRESS REGIME

This section presents an overview of the tectonic setting and regional stresses. Details of the structural geology and tectonics of the reference repository location and the Hanford Site are presented in Chapter 1.

2.6.1.1 Tectonic setting

Information on past and current tectonic influences in the region and at the reference repository location has been presented by Myers and Price et al. (1979) and Caggiano and Duncan (1983). This information is briefly summarized below.

The Hanford Site lies within the Columbia Plateau. This is an extensive area underlain by Miocene flood basalts erupted from north-northwest trending linear vents in southeastern Washington State, northeastern Oregon, and west-central Idaho. These lavas were very fluid and spread great distances from their source vents, generally flowing westward along gentle slopes into a basin between the ancestral Cascade and Rocky Mountain Ranges between approximately 16.5 and 6 m.y.B.P. The basalts could reach a thickness of greater than 3 km (1.8 mi) in the Pasco Basin.

The Columbia Plateau is located on the western margin of the North American plate in the Cordilleran orogen. The western margin of the Columbia Plateau is approximately 250 km (155 mi) east of the consumptive boundary between the North American plate and the Juan de Fuca plate. The Juan de Fuca plate is a relic of the larger Farallon plate, which was subducted under the overriding North American plate during the Mesozoic and Cenozoic Eras. To the west, the Columbia Plateau is bounded by the north-south trending Cascade Range, which is a volcanic-arc system related to partial melting of the subducting crust of the Juan de Fuca plate. On the north, the Columbia Plateau is bounded by the Okanogan Highlands. The plateau is bounded by the northern Rocky Mountains and the Idaho batholith to the east. On the south, the adjoining tectonic provinces are the High Lava Plains in southeastern Oregon and the Snake River Plain of southwestern Idaho.

The Columbia Plateau can be subdivided on the basis of style of deformation into three subprovinces. These are the Yakima Fold Belt, the Blue Mountains, and the Palouse subprovinces. The Yakima Fold Belt is characterized by east-west trending asymmetric anticlines with intervening, broad sediment-filled synclinal basins. The Blue Mountains subprovince is a broad, east-northeast trending anticlinal uplift affected by northwest trending folds and dip-slip faults. The Palouse subprovince is characterized by a gentle westward slope on which long wavelength, low amplitude north-northwest to northwest trending folds have been superposed.

The reference repository location has been sited in the western part of the Cold Creek syncline, one of several synclinal structures within the Pasco Basin, which is a sediment-filled basin bounded on the north, west, and south by asymmetrical anticlinal structures of the Yakima Fold Belt subprovince.

Regional and local tectonic models are being developed and evaluated to assess the tectonic stability of the Hanford Site. Ideally, a tectonic model should explain existing geologic features, seismicity, and other phenomena related to crustal deformation and tectonic activity, as well as predict future tectonic activity. Such models are somewhat complex and depend heavily on assumptions as to deep subsurface conditions and crustal plate interactions. These aspects of the models are difficult or impossible to verify. Regional and local tectonic models under consideration are summarized in Chapter 7 of Caggiano and Duncan (1983). A common feature of these models is compression along a north-south axis.

2.6.1.2 Regional in situ stress

In situ stress data for the United States have been compiled on a regional basis by Lindner and Halpern (1978) and by Zoback and Zoback (1980). These publications provide a basis for subdivision of the United States into stress provinces, taking into account geologic structure, plate tectonics, seismicity, and available in situ stress determinations. Stress provinces in the United States are shown on a generalized map (Fig. 2.6-1) as prepared by Zoback and Zoback (1980). The Hanford Site is located in the Pacific Northwest stress province. Although somewhat limited, their data indicate a horizontal, north-south compression within this region. It appears that the maximum stress in this region is in the horizontal direction trending north-south, the intermediate stress is in the horizontal east-west direction, and the minimum stress is in the vertical direction.

The regional in situ stress regime for the Pasco Basin can be determined from evaluation of geologic structures, analysis of crustal deformation based on geodetic surveys, and focal mechanism solutions for instrumentally detected earthquakes. However, the magnitude of the stresses cannot be assessed from geologic and seismologic evidence. These data are summarized in Sections 1.3 and 1.4 and in Chapter 6 of Caggiano and Duncan (1983).

The east-west trending anticlines and subparallel thrust and reverse faults suggest that deformation has occurred under a regime of nearly horizontal compression along a north-south axis. The presence of folds and thrust faults suggests that axis of the least compressive stress is vertical. Geologic evidence also suggests that this stress regime has existed for the past 14.5 m.y.

Geodetic surveys across the Pasco Basin show measured strain rates in the same range as instrumental error. However, the data favor crustal compression (see Section 1.3.2.4).

Focal mechanism solutions indicate a general north-south orientation of
the maximum principal stress and a near-vertical minimum principal stress.
Detailed descriptions of regional seismologic investigations can be found in
Section 1.4.1.2.

Seismic monitoring of events in the Pasco Basin tends to corroborate the
north-south orientation of tectonic stresses suggested by geologic evidence
(Caggiano and Duncan 1983, p. iv). Shallow, low-magnitude earthquake swarms
at depths of less than or equal to 6 km (3.7 mi) are common to the Columbia
Plateau, with occasional events at greater depths. Focal mechanism solutions
for both shallow and deep events indicate that they are typically associated
with reverse or thrust faulting (Malone et al., 1975). The events apparently
occur on existing high-angle faults dipping in a northerly or southerly direc-
tion (Arnett et al., 1980). These existing faults parallel the east-west
orientation of the Yakima folds and are associated with the anticlinal
structures of these folds. The seismic activity indicates that a north-south
strain relief, associated with the tectonic stresses, is a continuing process
in the Pasco Basin.

On the basis of the above data, Caggiano and Duncan (1983) concluded that
the present in situ stress regime consists of maximum principal compressive
stress along a generally north-south axis, and minimum principal compressive
stress along a vertical axis. It was concluded that this stress regime has
been relatively unchanged for at least 14 m.y.

2.6.2 LOCAL STRESS REGIME

This section contains discussions of stress indicators at the Hanford
Site and a discussion of the results of hydraulic fracturing stress
determinations in and around the reference repository location. The locations
of the boreholes where hydraulic fracturing tests have been conducted are
shown in Figure 2.6-2.

2.6.2.1 Stress indicators observed at the Hanford Site

Core disking and borehole spalling observed in exploratory boreholes
drilled within the Hanford Site indicate that the state of in situ stress is
relatively high. Core disking, an example of which is shown in Figure 2.6-3,
is a phenomenon wherein the drill core fractures into thin disks during the
drilling process and is known to be an indicator of high stress (Obert and
Stephenson, 1965; Jaeger and Cook, 1963). The disking phenomenon is dependent
on numerous factors, including in situ stress, rock properties, drill bit
pressure, and geometry (Lehnhoff et al., 1982). Core disking at the Hanford
Site has been described by Myers and Price (1981) and DOE (1982). The degree
of core disking experienced in typical Hanford Site boreholes is indicated in
Table 2.6-1. In this table, core disking in boreholes RRL-2, -6, and -14 is
given as a percentage of the dense interior thickness for each horizon (Long
and WCC, 1984).

Spalling in deep boreholes on the Hanford Site has been observed by downhole television surveys, impression packer test results (Rundle and Kim, 1983), and acoustic televiewer techniques (Paillet, 1985). The televiewer is an ultrasonic device that produces a photographic image of the pattern of acoustic reflectivity off the borehole wall. Detailed descriptions of the televiewer logging system and a discussion of imaging techniques employed in the processing of televiewer logs are given by Zemanek et al. (1969). Paillet (1985) has obtained acoustic televiewer logs in boreholes DC-4, DC-12, DC-7, RRL-2, and RRL-6 and concludes that borehole spalling or borehole wall breakouts have a consistent east-west orientation at the Hanford Site. Examples of acoustic televiewer intervals with borehole spalling in borehole RRL-6 and a representation of a horizontal section with spalling are shown in Figure 2.6-4(a) and (b).

The borehole spalling phenomenon is an indication of high deviatoric stresses in the plane perpendicular to the hole. Gough and Bell (1981) first suggested that borehole spalling or breakouts occur in the direction of least horizontal compression as a result of shear failure of the rock in the region where the tangential (compressive) stress adjacent to the borehole is concentrated. Zoback et al. (1985) extended the theoretical analysis of the mechanism in order to better explain the observed breakout shapes. The consistent east-west orientation of borehole spalling at the Hanford Site indicates that the maximum horizontal stress is generally north-south.

Paillet (1985) compared the extent of borehole breakouts or spalling to the extent of core disking in boreholes DC-4, DC-12, and RRL-6. This comparison, presented graphically in Figure 2.6-5, shows relatively good correlation between core disking and borehole spalling and that both are primarily confined to the interior of individual flows.

The frequency of core disking and borehole spalling and the correlation between these phenomena support the premise that the in situ stress distribution at the Hanford Site is not lithostatic. Core disking is generally an indicator of high stress, and borehole spalling is generally an indicator of high horizontal deviatoric stress. Few boreholes exhibited a very low percentage of spalling and disking; the cause of this will be investigated in the study plan discussed in Section 8.3.2.

2.6.2.2 Hydraulic fracturing stress determinations at depth

This section provides a summary of in situ stress determinations by hydraulic fracturing within repository horizons studied at the Hanford Site.

The hydraulic fracturing method is presently the most widely used means for direct determination of in situ stress magnitudes at depth. Other stress determination methods such as overcoring, are generally limited by operational constraints to depths of less than 100 m (300 ft). Hence, hydraulic fracturing has been used exclusively to determine the in situ stress regime for the reference repository location. Overcoring techniques will also be

used for in situ stress determination once the Exploratory Shaft Facility is available to provide access to the repository horizon. The locations of key boreholes used in the BWIP studies are shown in Figure 2.6-2. Hydraulic fracturing tests have been conducted in boreholes DB-15, DC-12, RRL-2, RRL-6, and DC-4. Boreholes DC-12 and DB-15 are located outside the reference repository location, and the tests were conducted within the Umtanum and Rosa flows, respectively. The results from the tests in these two boreholes were summarized by Kim and Haimson (1982) and will not be discussed in this section.

Boreholes RRL-2, RRL-6, and DC-4 are located within the reference repository location. Hydraulic fracturing tests have been conducted in these boreholes in the Cohassett, Grande Ronde 7, McCoy Canyon, and Umtanum flows at depths to 1,195 m (3,900 ft). The results of these tests will be discussed in this section.

2.6.2.2.1 Test description

The hydraulic fracturing method, which has been in use for over 20 yr to determine in situ stress from boreholes, has been described by many authors (Hubbert and Willis, 1957; Fairhurst, 1964; Haimson, 1968; Bredehoeft et al., 1976; Zoback and Haimson, 1982).

The tests were conducted following a consistent procedure in which a 0.61-m (2-ft) section of the borehole was isolated by inflatable packers on both ends and pressurized by injecting water into the test section. As the pressure in the test section was gradually increased, the tangential stress around the borehole decreased and eventually became tensile. Fractures were initiated in the wall of the borehole as soon as the tensile (rupture) strength of the rock was overcome by the induced tensile stress in the tangential direction, the point at which this occurs is generally reflected by a sharp change in the pressure buildup rate, generally referred to as the "breakdown." After breakdown the test section was closed and the pressure within this section was monitored. The pressure within the section dropped rapidly until it became less than the in situ stress normal to the induced fractures. At this point the fractures were closed by the in situ stress, and a change in the rate of pressure decline resulted. This was followed by subsequent repressurizing cycles to reopen the fractures. A typical pressure and flow rate history during one of the tests is shown in Figure 2.6-6.

After the hydraulic fracturing tests were completed, the orientation of the fractures was determined using an impression packer. An example of traces of the fracture impression from one of the tests is shown in Figure 2.6-7. The orientation of the fracture was used to determine the orientation of the in situ stresses as it has been demonstrated that the orientation of the fracture is in a direction normal to the least principal stress in the plane perpendicular to the borehole axis (Hubbert and Willis, 1957). A detailed description of the test procedure used at the Hanford Site is provided by Kim et al. (1986).

The overall character of the pressure-time record and the results of the post-test fracture impression were used as the primary means of determining the acceptability of the test data for each interval. The pressure-time record was examined for evidence of clearly defined breakdown pressures and for consistent values of the fracture reopening and shut-in pressures. The impression was examined to ensure that hydraulic fractures were generated during the test and that little or no borehole spalling existed within the test interval. Test intervals that exhibited little or no spalling were judged to be successful tests, and those with significant spalling were not analyzed because the data analysis method has not been established.

2.6.2.2.2 Data analysis methods

Hydraulic fracturing data for the Hanford Site has been reported and analyzed by Kim and Haimson (1982) and Kim et al. (1986). Under the assumption of plane strain, the Kirsch solution (Kirsch, 1898) for the stress distribution about a circular hole in an infinite plate subjected to biaxial stress is superposed on the stress distribution for an internally pressurized, thick-walled cylinder of infinite outer radius to determine the tangential stress distribution about the borehole. This approach makes the assumption that the borehole is parallel to one of the principal stress axes and that the rock is linearly elastic, homogeneous, and isotropic. While these assumptions are not strictly valid for any rock, available data suggest that intact basalts at the Hanford Site conform reasonably well to these assumptions. An important criteria in the selection of test intervals for hydraulic fracturing is the avoidance of preexisting discontinuities. Test intervals were selected to avoid existing discontinuities if possible.

The minimum horizontal stress is directly measured by the shut-in pressure, which is the pressure in the system immediately after pumping ceases and the system is sealed or "shut-in." In jointed or porous media, a constant shut-in pressure is usually not achieved (Zoback and Haimson, 1982). Estimates of the shut-in pressure are based on changes in the shape of the pressure versus time curve, normally at a point of inflection or change in slope of the pressure-time record. The instantaneous shut-in pressure for the Hanford Site hydraulic fracturing tests has been determined by use of the inflection-point method (Gronseth and Kry, 1983). The inflection point is defined as the point at which the pressure curve diverges from its tangent immediately after the cessation of pumping.

The maximum horizontal stress magnitude can be calculated from the breakdown and shut-in pressures (Haimson, 1968). However, this procedure requires knowledge of the in situ rupture strength, which is usually determined by laboratory testing of cores obtained from the test interval. The significance of the in situ rupture strength on future evaluation of hydraulic fracturing test results will be assessed in Section 8.0. An alternative procedure (Bredehoeft et al., 1976) uses the second and subsequent pressurization cycles to determine fracture reopening pressures. Fracture reopening pressure is defined as the pressure required to open the induced hydraulic fracture

without resistance due to the borehole rupture strength. The fracture
reopening pressure is taken to be the point on the repressurization curve(s)
at which the slope deviates from linearity under constant flow rates (Hickman
and Zoback, 1983). An expanded plot of interval pressure versus time for a
typical repressurization cycle demonstrating the method of determining
fracture reopening and shut-in pressures is shown in Figure 2.6-8..

The equations used to determine in situ stress magnitudes are well
documented (see Hickman and Zoback, 1983). The pore pressure enters into
calculation of the maximum principal stress, and uncertainty arises when
estimating the magnitude of the pore pressure and its influence on stress
determination. One extreme assumes, that in crystalline rocks, pore pressure
at the test interval should be zero (Rummel et al., 1983). The other extreme
is to assume a value of pore pressure equal to the hydrostatic head generated
by the static water level in the borehole. The actual pore pressure is
unknown and is probably somewhere between these two extremes. When using
fracture reopening pressures to determine the maximum stress, it is considered
appropriate to use pore pressures equal to the static hydraulic head because
the tests were conducted in saturated rock below the groundwater table, and
because once the fracture is created and depressurized, the fracture likely
retains some fluid. The results used to establish the stress regime for
repository design have been calculated using pore pressure values equivalent
to the static water level in the borehole.

The two horizontal principal stresses at depth are assumed to be equal to
the stresses determined from hydraulic fracturing data. The vertical stress
is calculated from the density and thickness of the overlying strata.

2.6.2.2.3 Test results

The results of hydraulic fracturing tests in boreholes RRL-2, -6, and
DC-4 within the reference repository location are summarized in Table 2.6-2.
Results presented in Table 2.6-2 are based on the mean values of measured
shut-in and fracture reopening pressures. Stress direction information from
tests that were considered unacceptable for determination of stress magnitude
but acceptable for determination of stress direction is also contained in
Table 2.6-2.

Mean values and standard deviations for in situ stresses calculated from
hydraulic fracturing tests are summarized in Tables 2.6-3 and 2.6-4 by
borehole and by formation, respectively. The stress magnitudes as a function
of depth are shown in Figure 2.6-9.

The mean ratio of average horizontal stress $[(\sigma_H + \sigma_h)/2)]$ to the
vertical stress (σ_V) can be calculated from the data in Table 2.6-2 to be
approximately 1.77 ±0.20. The measured range of stress ratio is compared with
the range of values that had been determined at numerous other locations
worldwide in Figure 2.6-10. These were compiled from the results of many
different in situ stress measurement techniques by Hoek and Brown (1980,

p. 100). It shows that the horizontal stress condition in the basalt flow at the Hanford Site is close to the higher end of known stress conditions at comparable depths in other locations of the world.

Orientations of induced hydraulic fractures and, hence, direction of the maximum horizontal stress are shown in Figure 2.6-11(a) for boreholes within the reference repository location. A plot of hydraulic fracture orientation frequency for the boreholes in the reference repository location is shown in Figure 2.6-11(b). The mean hydraulic fracture orientation in these boreholes is N. 02° E. ±17°, based on 21 fracture impressions. The general north-south orientation of the hydraulically induced fractures, and thus the direction of the maximum horizontal stress, is consistent with east-west borehole spalling as reported by the U.S. Geological Survey (Paillet, 1985).

A direct comparison of mean stress magnitudes and orientations for each borehole and each basalt flow is shown in Tables 2.6-3 and 2.6-4. A comparison between measurements in the Umtanum flow inside and outside the reference repository location is shown in Table 2.6-5. A statistical comparison of the mean values given in these tables (using Student's t test statistic distribution) indicates that principal stress magnitudes and orientations in the various boreholes, flows, and locations are not significantly different at the 95% confidence level.

2.6.2.2.4 Discussion of results

The test results presented in this section demonstrate the applicability of the hydraulic fracturing technique in measuring the in situ stress of a closely jointed basalt rock mass. The uncertainties and possible sources of error associated with the measurement are discussed in this section.

Hydraulic fracturing results indicate that both the maximum and minimum horizontal stresses are greater than the computed vertical stress (based on density and thickness of overlying strata). When the vertical stress is the least principal stress, it is conceivable that horizontal fractures may open at the borehole wall or that vertical fractures initiated at the borehole wall may "roll over" into the horizontal plane with continued fracture propagation. Fracture impressions generally indicated vertical fractures with some degree of branching forming a feather-like appearance. Results from test intervals for which the impression showed evidence of horizontal fractures that intersected the entire circumference of the borehole wall were rejected because the shut-in and reopen pressure may also be affected by the vertical stress, and the effects due to vertical and horizontal stresses cannot be separated by the present data interpretation method.

Fracture rollover at distance from the borehole has been inferred when a significant decrease in shut-in pressure occurs during repressurization cycles (Zoback and Pollard, 1978; Zoback and Haimson, 1982). The occurrence of fracture rollover will result in lower values of horizontal stresses being calculated. The Hanford Site hydraulic fracturing tests did not show a

significant decrease in shut-in pressure but did show a slight decrease in shut-in pressure during most of the repressurization cycles. This result is consistent with observations at other locations (Hickman and Zoback, 1983) and does not independently demonstrate that the fractures have rolled over into the horizontal plane. The induced fractures rolling over into the horizontal plane in the tests performed at the Hanford Site is a possibility that presently cannot be ruled out.

The hydraulic fracturing method has been used by numerous investigators to determine in situ stresses in shallow and deep boreholes and has been studied extensively under controlled conditions in the laboratory. However, uncertainties regarding the accuracy of hydraulic fracturing stress determinations still exist. Comparisons between stress determinations from hydraulic fracturing and from other methods have been made (Haimson, 1983). However, the degree of confidence in deep-borehole hydraulic fracturing stress determinations remains uncertain. Continuing development of the hydraulic fracturing technique and the development of alternative means of stress measurement in jointed rock are required to reduce the level of uncertainty.

Potential sources of error in hydraulic fracturing stress determinations include the following:

o Estimation of the exact pore pressure and the influence of pore pressure on the fracturing process.

o Difficulty of determining exact breakdown, shut-in, and fracture reopening pressures from the pressure-time curves.

o Assumption that the test borehole is parallel to one of the three principal stresses.

o Assumption that the rock deforms in a linearly elastic manner.

o Uncertainties regarding the influence of the preexisting cooling joints in basalt.

o Accumulation of measurement errors from calculating the maximum stress.

Roegiers and McLennan (1983) and McLennan and Roegiers (1983) have identified additional factors that can influence the test data, interpretation, and results of hydraulic fracturing stress determinations. These include the effect of preexisting fractures, fluid viscosity, pumping rate, packer type and configuration, packer bypass, pressure loss by permeations, inclined fracturing, fracture reorientation, and incomplete fracture closure.

The hydraulic fracturing test procedures at the Hanford Site attempted to minimize the uncertainties associated with the above-mentioned factors. However, the degree of influence of these factors on the test results is unknown. This emphasizes the fact that hydraulic fracturing stress

determinations.produce estimates of the conditions at depth and that these estimates should be used with engineering judgment until the results are. confirmed or until additional information becomes available (Section 8.3.2.2).

2.6.2.2.5 In situ stress regime for repository design

Geologic structure, seismicity, core disking, and borehole spalling all indicate relatively high horizontal compressional stresses, with the maximum principal stress oriented approximately north-south, the intermediate principal stress oriented approximately east-west, and the minimum principal stress oriented vertically. Hydraulic fracturing tests in selected boreholes have confirmed these general stress relationships and have provided numerical estimates for the magnitudes of the horizontal stresses. Vertical stresses can be estimated from the thickness and density of overlying strata. Within the reference repository location, the stress regime at the proposed repository (i.e., Cohassett flow) level is calculated to be as follows:

$$\sigma_1 = S_H = 61.5 \pm 5.7 \text{ MPa } (8,922 \pm 827 \text{ lbf/in}^2) \text{ at N. } 06° \text{ E. } \pm 17°$$

$$\sigma_2 = S_h = 32.8 \pm 2.2 \text{ MPa } (4,758 \pm 323 \text{ lbf/in}^2) \text{ at N. } 84° \text{ W. } \pm 17°$$

$$\sigma_3 = S_V = 24.2 \pm 1.1 \text{ MPa } (3,514 \pm 159 \text{ lbf/in}^2) \text{ vertical.}$$

The values of horizontal stresses stated above are obtained from hydraulic fracturing tests using a pore pressure equivalent to the static hydraulic head in the borehole. The other extreme of using zero pore pressure in the calculation, which will result in higher horizontal stresses being calculated, has not been adopted because the test sections are within saturated rock below the groundwater table. These values may be modified as additional data become available.

It should be noted that the in situ stress regime presented in this section did not incorporate possible local variations of in situ stresses within a flow because of the limited number of tests conducted. Local variations in the stress regime are likely to be related to rock properties such as strength and modulus and fracture frequency in different parts of the flow. Attempts will be made to develop a model correlating these parameters with the variation of local stresses. The development of such a model requires an understanding of the causes of borehole spalling and core disking, which are not known with certainty at present. Future studies will be conducted to correlate the occurrence of borehole spalling and core disking with in situ stresses, drilling conditions, and rock properties (Section 8.3.2.2).

The potential for regional long-term tectonic instability depends on a number of factors. Among these factors the most important ones are the occurrence of favorably oriented through-going or local, penny-shaped faults,

the magnitude and direction of the in situ stresses, and the shear strength along the faults. While none of these can be assessed reliably at present, using the stress regime presented above it can be shown that the only possible slip is a reverse displacement along a through-going fault striking east-west and dipping approximately 60° to 65° with an effective friction angle of 33° or less along the fault plane. At present there is no indication that such a fault exists within the reference repository location and available data on the shear strength along possible faults based on Byerlee (1978) and the test results on basalt joints as presented in Section 2.2 all exceed the value required to prevent the occurrence of such a slip (Kim et al., 1986, p. 58). There is therefore no indication from the present data that potential tectonic instability may exist. Further considerations, however, must be given to the effect due to possible stress change resulting from the heat generated after waste emplacement. At present there are insufficient data to address this problem and further studies will be required (Section 8.3.2.2).

2.6.3 STRESS MEASUREMENTS AT THE NEAR-SURFACE TEST FACILITY

Stress measurements were conducted at the Near-Surface Test Facility (NSTF) to develop techniques suitable for jointed rock mass and to provide input parameters for the predictive analysis of heater tests and the jointed block test. The first series of measurements consisted of 6 hydraulic fracturing tests conducted in borehole DC-11 prior to construction (Haimson, 1979) and 16 overcoring tests using the U.S. Bureau of Mines borehole deformation gage after construction in two boreholes (Rockwell, 1980, pp. v-26). Only 4 out of the 16 overcoring tests were partially successful, while the rest yielded unacceptable results mainly because of the jointed nature of the basalt. At corresponding depth, the stress orientations obtained from these two methods were in reasonable agreement, but the stress magnitudes differed by a factor of two. This revealed a significant problem in the determination of the absolute magnitude of stresses in jointed rock.

Since completion of the first series of measurements at the Near-Surface Test Facility, research and development in stress measuring techniques have continued on several fronts. The first has been to improve techniques for monitoring stress changes in the basalt rock mass as part of the in situ testing program (Gregory et al., 1983a), and the second is to evaluate methods of absolute stress measurement by overcoring (Gregory et al., 1983b). Activities to improve the hydraulic fracturing technique for stress measurement at depth have also been ongoing (Kim and Haimson, 1982; Kim et al., 1986; Dischler and Kim, 1985). Vertical stress measurements were made at the Near-Surface Test Facility using flat jacks in the early stages of jointed block test. The results are in general agreement with that calculated from depth and rock density.

As discussed in Gregory et al. (1983b), the following five overcoring techniques have been tested in the process of evaluating methods of absolute stress measurement:

o U.S. Bureau of Mines borehole deformation gage (Hooker and Bickel, 1974).

o Commonwealth Scientific and Industrial Research Organization hollow inclusion stress cell (Worotnicki and Walton, 1976).

o Lulea triaxial gage (Leijon and Stillborg, 1986).

o Council of Scientific and Industrial Researches doorstopper (Leeman and Hayes, 1966).

o Epoxy inclusion of Riley (Riley et al., 1977).

Each gage was tested in vertical boreholes in the floor of the Near-Surface Test Facility at depths ranging from 4.3 to 23.0 m (14.1 to 75.5 ft). From a total of 44 tests, 33 were successful. The results did, however, show a wide scatter. It was concluded that fundamental problems associated with the influence of joints still exist and the methods of dealing with this influence are unresolved. A continuing effort to resolve this situation is being made through laboratory testing, characterization, and field testing at the Near-Surface Test Facility.

2.6.4 SUMMARY

Geological evidence and focal mechanism solutions of microseismic activities that have occurred in the Columbia Plateau suggest a general north-south orientation of the maximum principal stress and a near-vertical minimum stress. Core-disking and borehole spalling that had been observed in boreholes in and around the reference repository location indicate the existence of high in situ stresses at the Hanford Site. These were confirmed by in situ measurements using the hydraulic fracturing technique, which showed a maximum principal stress in the general north-south direction and an intermediate principal stress in the east-west direction. The mean ratio of average horizontal stress to vertical stress in the Cohassett flow within the reference repository location is estimated at 1.96 from the results of hydraulic fracturing tests. The measured in situ stress data have been used in estimating the support requirement for the repository openings (Section 2.8.2) and as input for various analyses in the SCP conceptual design (Section 6.1.3).

2.7 SPECIAL GEOENGINEERING PROPERTIES

2.7 Special Geoengineering Properties
    2.7.0 Introduction
    2.7.1 Potential for rock burst
        2.7.1.1 Rock burst potential in similar rock
        2.7.1.2 Rock burst potential at the Hanford Site
    2.7.2 Potential for thermal degradation
    2.7.3 Swelling and shrinkage of fracture infilling materials
    2.7.4 Coupled effects
    2.7.5 Summary

2.7.0 INTRODUCTION

There are a number of special geoengineering properties pertinent to basalt, which are important to the construction and performance of the repository and which have not been addressed in the preceeding sections. These include (1) the potential for rock burst at the repository horizon, (2) the potential for thermal degradation of the host medium, (3) the impact of dewatering/rehydration of the joint infilling material on the rock mass response, and (4) the coupled effects between mechanical, thermal, hydrological, and chemical effects. These properties will be discussed in this section. The discussion will be conducted in general terms because direct measurements or direct observations are not available for most of the properties discussed.

2.7.1 POTENTIAL FOR ROCK BURST

The combination of high in situ stresses and strong, brittle rock in an underground opening may lead to overstressing of the rock and result in a phenomena commonly known as rock burst. The observed occurrence of core disking and borehole wall spalling indicates that rock bursts may occur in the repository shafts and other excavations. The potential of rock bursts needs to be studied because such phenomena could significantly affect rock support requirements, underground safety, and repository performance.

2.7.1.1 Rock burst potential in similar rock

The term "rock burst" describes a sudden rock failure associated with the release of strain energy in the rock mass. Such failures range in size from minor events that cause no damage and cannot be detected or heard beyond the immediate vicinity of the event, to large bursts that can collapse sections of excavations with a seismic shock wave equivalent to a small-size earthquake. Small-scale rock bursts, generally known as spalling, popping, or spitting,

usually occur as small pieces of rock flying off the face of a drift. In some publications, the term rock burst is used interchangeably for both large and small events. Blake (1984, p. 15) reports that in South Africa the term rock burst is applied only to events that do measurable damage and usually have a Richter magnitude greater than 0.5, which has a major impact on the selection of excavation and support methods. "Spalling" is limited to failures involving no significant rock fallout or failure volumes less than 1 m^3 (35.3 ft^3) and a Richter magnitude of less than 0.5. For these relatively small failures, seismic energy is limited; no air blast or shock wave is created; and, effects on construction are very minor. The definitions of Blake (1984, p. 15) will be used in the present discussion.

Blake (1984, p. 4) states that rock bursts are generally associated with sites that possess all or most of a particular set of rock characteristics and site conditions. These characteristics and conditions are listed below; the first four items are considered present at the Hanford Site.

1. Great depth.

2. High in situ stresses.

3. Narrow and tabular excavation geometry.

4. Strong and brittle rock.

5. Massive rock.

6. High extraction ratio, extensive mined-out area with wide spans.

7. Geologic structural discontinuities.

8. Complex geologic structure.

9. The maximum principal stress essentially perpendicular to the tabular dimension.

The absence of massive rock and high extraction ratio usually results in spalling rather than rock burst.

According to Blake (1984, pp. 22-25), the magnitude of a rock burst will be influenced by the types of excavation activities, which are discussed below in three categories: (1) development openings, (2) multiple mining openings, and (3) extensive mined-out areas. More detailed discussion is given to development openings due to the relevance to repository excavation activities.

2.7.1.1.1 Rock burst potential in development openings

Single openings in rock such as shafts and tunnels are surrounded by a small volume of highly stressed rock, which results in an accumulation of strain energy at or near the face. The popping and spitting that is commonly encountered in brittle rock is a result of the release of small amounts of stored strain energy. When single openings intersect geologic structures such as faults and dikes, a larger volume of highly stressed rock may result, and the rock burst hazard is usually at or very close to the face with a Richter magnitude less than 0.5 (Blake, 1984, p. 22) and is classified as spalling.

Spalling problems in tunnels have been reported by many authors including Saito et al. (1983), Bergman and Stille (1983), Elfman (1969), and Bai et al. (1983). In addition, Lee (1978) summarized stress-induced instabilities in tunnels, many of which included spalling-type phenomena. Curtis (1981) reviewed rock burst phenomena in the gold mines of the Witwatersrand in South Africa and discussed examples of rock bursts in tunnels both influenced by and isolated from mining.

The tunnel and shaft conditions under which spalling/rock bursting has been reported are summarized in Table 2.7-1. Saito et al. (1983) report that spalling of the face occurred in the Kan-Etsu Tunnel when the overburden was greater than 750 m (2,460 ft). It was found that areas of core disking corresponded to those of spalling and that the mechanism of spalling appeared similar to core disking. Bolting of the face was successful in preventing these events. In Sweden, Bergman and Stille (1983) reported spalling in the roof of large tunnels excavated for oil storage. The failures were described as follows: "spalling of thin rock slices and (or) shotcrete occurred occasionally, usually most frequent in the region 20 to 50 m (70 to 160 ft) behind the headings." High horizontal in situ stresses, the brittle nature of the granite, and the possibility of residual stresses were postulated as the cause of the rock spalling by Bergman and Stille (1983).

The last four examples in Table 2.7-1 involve shaft sinking. Vasey (1983) describes the construction of an underground crusher 1,613 m (5,300 ft) below ground surface in granite with the maximum horizontal stress of twice the vertical stress. The spalling during shaft sinking was overcome by the early installation of a shaft liner. Some failures were anticipated during the construction of the crusher and associated tunnels, but adequate planning allowed successful completion of the project.

Rock bursts have been reported during shaft sinking operations in the Caladay Shaft near Osburn, Idaho (Blake, 1984, p. 35). The burst produced an estimated 2 to 3 m^3 (70 to 110 ft^3) of broken rock when the shaft intersected a massive quartzite bed at a depth of 1,400 m (4,600 ft). At the Thierry Shaft in Ontario, Canada, sudden spalling and spitting occurred at depths between 360 and 500 m (1,200 and 1,600 ft) in a massive granite (Blake, 1984, p. 38). In both cases, destress blasting was used to reduce or eliminate the bursting. Spalling and spitting were also reported in the Silver Shaft near Mullen, Idaho, in massive quartzite (Blake, 1984, p. 38).

Rock bursts can occur in underground mine developments where tunnels are excavated in advance of mining. Typical examples are in the Coeur d'Alene district of northern Idaho, and South Africa (Curtis, 1981; Hoek and Brown, 1980). However, apart from the examples listed by Hoek and Brown (1980), specific data are not available. In the Coeur d'Alene district, if bursting becomes a problem during development, preblasting (detonating a blast in a long hole ahead of the face) has sometimes relieved the stresses and reduced the brittleness of the rock mass. This concept of rock softening to reduce the frequency and magnitude of rock bursts is used in the mining industry (Roux et al., 1957; Blake, 1982).

Excavation techniques also affect the potential for rock bursting. Machine boring (Nishida, 1982) or smooth wall blasting techniques leave the walls in a relatively undamaged state, which under high initial stresses, can allow accumulation of strain energy near the roof and wall. Alternatively, conventional blasting can loosen the rock mass, cause stress relief immediately around the opening, and decrease the potential for rock bursts.

2.7.1.1.2 Rock burst potential in multiple mining openings

Multiple excavations from mining can create highly stressed regions between and around these openings, which can involve a large volume of rock. Pillar bursting associated with narrow vein or seam mining is an example of this type of rock bursting. When a highly stressed, relatively isolated pillar fails, a large amount of strain energy is released both from the actual pillar failure and from the closure of the roof and floor. Pillar bursting occurs most commonly when the extraction ratio is greater than 80% (i.e., when a small pillar is left supporting a large, mined-out area) (Blake, 1984, p. 22). Pillar bursts produce seismic activity generally in the Richter magnitude of 1.0 to 3.5 and present a serious hazard to underground personnel.

2.7.1.1.3 Rock burst potential in extensive mined-out areas

As mined-out areas become very extensive (greater than 1 km^2 (0.386 mi^2)), stress transfer due to mining can cause displacements on nearby to distant faults (Blake, 1984, p. 25). The energy release associated with such fault slip can be very large, with Richter magnitudes greater than 5.0. These events can cause damage to surface structures but often do little or no damage underground. Such failures can occur in soft- and hard-rock mines.

2.7.1.1.4 Dealing with rock bursts

Measures have been developed over the years to minimize both the occurrence and the effects of bursts. These methods include (1) modification of the excavation sequence, (2) installation of an appropriate support system, and (3) modification of the excavation method to include the use of preconditioning blasting.

In the mining industry, modification of the extraction sequence to avoid the creation of pillar remnants and to produce stress transfer to the abutments in a gradual manner is often used to decrease the incidence of rock bursting. Burst-prone areas are sometimes mined at a slower rate than normal production rates to allow more time for fracturing and natural destressing.

Spalling in tunneling or shaft sinking has been successfully controlled by the application of rock supports (e.g., bolts and wire mesh) or by softening the rock mass by preblasting. Blake (1984, p. 33) reports that fully grouted untensioned rebar and threadbar with wire mesh and (or) steel fiber-reinforced shotcrete are effective techniques for minimizing spalling. This may be supplemented by cable lacing for more extreme problems. Barton (1984, pp. 81, 82, 84, 85) suggests rock bolting with increased-size bearing plates and notes that the use of fiber-reinforced shotcrete to replace steel mesh has resulted in satisfactory support in Norwegian tunnels driven through burst-prone rock.

Hoek and Brown (1980, pp. 307-311) describe the use of extensive support, including steel sets and concrete, in the deep underground tunnels in South Africa where potentials of massive rock bursts are high. Ortlepp (1970, 1983) emphasizes the use of yielding rock bolts and mesh in South Africa to resist the dynamic loads imposed by rock bursts.

2.7.1.2 Rock burst potential at the Hanford Site

Rock bursts are not expected in the repository excavations. This is based on the guidelines published by Hoek and Brown (1980, p. 218) and the analysis performed by Blake (1984, pp. 71-76) as discussed in the following paragraphs. However, historical evidence of localized rock spalling in underground excavations with low extraction ratios and wide excavation span that are highly stressed and in strong, brittle rock suggests that similar phenomena may be expected during repository construction in basalt. This spalling can be expected to occur shortly after excavation. The potential of spalling caused by the surcharge of thermally induced stress after waste emplacement requires further study because it is not known if the rock mass around the openings will be capable of adjusting to the new stress condition over a period of time and thus reduce the potential of spalling.

Hoek and Brown (1980, p. 218) compiled 21 case histories of deep tunnels in massive quartzite in South Africa and correlated rock failure in these tunnels with the in situ vertical stress, which is the maximum principal

stress in the cases considered, and the uniaxial compressive strength of the intact rock. The correlation, which is reproduced in Figure 2.7-1, shows that spalling occurred in tunnels where the ratio of vertical stress to the uniaxial compressive strength exceeds about 0.2. Hoek and Brown (1980, p. 218) indicate rock burst is unlikely unless this ratio exceeds 0.5. Also plotted in this figure is the range of uniaxial compressive strength of the basalt in the entablature of the Cohassett flow versus that of the maximum principal stress, which acts in the horizontal direction. Within the bounds of uncertainties of these data (which include the strength of intact rock and in situ stresses in the Cohassett flow and other case histories) it is seen that rock burst will be an unlikely event in the repository openings and that only spalling may be expected. It should be noted that a comparison between these tunnels and the repository openings is not strictly valid, and the results will be conservative because these cases are square tunnels in massive quartzite which have a higher potential for rock burst spalling than the arched-shape repository openings in closely jointed basalts.

Several of the conditions Blake (1984, p. 4) cites as being conducive to bursting are present at the candidate horizon at the Hanford Site. The conditions of great depth, high in situ stress, and brittle and strong rock are present; although the brittleness of the rock will be decreased by the high degree of jointing. The repository extraction ratio will be approximately 10%, much less than the 80% which is favorable to bursting (Blake, 1984, p. 22). The 10% repository extraction ratio will preclude any stress interaction between excavations except at intersections. There is not an extensive area of mined-out ground or wide spans necessary to produce a low-stiffness loading system. The geology of the Cohassett flow dense interior is relatively uniform, lacking with a low potential for encountering frequent faults and dikes that could act to concentrate stresses. The maximum stress is parallel rather than perpendicular to the tabular dimension of the repository.

It is expected that the closely spaced and interlocking nature of the basalt joints will tend to dissipate strain energy around the openings through deformation in a nonviolent fashion, reducing the likelihood of rock bursts. Barton (1984, p. 69) suggests that rock bursts are less likely in the entablature than in the colonnade because of the increased fracture density. Blake (1984, p. 73) indicates that construction of repository tunnels by drill-and-blast methods will tend to destress the surrounding rock and further reduce the potential for spalling.

The presence of high stress and strong, brittle rock are conducive to spalling in shafts. Blake (1984, p. 72) calculates that tangential stresses in the shaft wall at repository depth could reach 145 MPa (21 x 10^3 lbf/in^2) or 0.44 of the compressive strength. The use of heavy mud as a drilling medium would reduce the tangential stress and the potential for spalling.

2.7.2 POTENTIAL FOR THERMAL DEGRADATION

Thermal degradation describes changes in the chemistry or physical structure of the geologic medium with changes in rock temperature. Changes in physical structure could be crack formation and spalling caused by thermally induced stress gradients along the mineral grain boundaries. Chemical changes could be caused by secondary mineral dehydration or primary mineral alteration. Neither of these processes are presently considered a real concern at the Hanford Site.

Thermal spalling is observed when heating some rock types. In general, granular rocks with minerals having different coefficients of thermal expansion like quartz and feldspar are susceptible to thermal fracturing and spalling. The potential for rock materials, including basalt, to degrade by thermal fracture, spalling, and slabbing has been tested (Thirumalai, 1975; Thirumalai, 1970). The results show a low potential for thermal degradation of basalt in the laboratory. The slabbing phenomenon at depth is a coupled effect of material weakening by heating and prevailing stresses around the opening.

Information on thermal degradation for the Pomona flow was generated during tests at the Near-Surface Test Facility. Full-Scale Heater Test 2, which was described in Section 2.5, subjected the Pomona flow to temperatures greater than 500 °C at the borehole wall. No spalling or slabbing was observed in visual inspections before and after heating. However, enhancement of existing small fractures was observed (Kasza, 1986, p. 43). If the operations phase of the repository does not raise the rock wall temperature to levels greater than those observed in Full-Scale Heater Test 2, then such phenomena should be limited to the high-temperature areas in the immediate vicinity of the waste emplacement holes. However, if new, thermally induced fractures occur, they will have a significant impact on the performance of the repository and therefore, further study in the Cohassett flow will be required (Section 8.3.2.2). Post-test characterization studies involving laboratory testing of core taken from boreholes drilled adjacent to the heater holes have shown only a small change in mechanical properties; however, preliminary cross-hole seismic studies show a significant decrease in velocity close to the heater (Myer et al., 1983).

2.7.3 SWELLING AND SHRINKAGE OF FRACTURE INFILLING MATERIALS

The possibility of dehydration and the resultant volume reduction of clays and zeolites in fractures during the thermal phase of the repository is of interest because this could affect the water inflow and opening stability. Fractures identified in core from the dense interior of flows at the reference repository location are virtually always filled with secondary minerals (Long and WCC, 1984). The secondary minerals are predominantly clays, zeolites, and silica polymorphs (see Sections 1.2.3.1 and 2.2) with the percentage of clay infilling amounts to 89% in the Cohassett flow. X-ray diffraction studies of infilling material from fractures in the Cohassett flow indicated that a

smectite clay, tentatively identified as montmorillonite, was the dominant phase. The smectite clays possess favorable geochemical aspects with regard to radionuclide retardation (see Section 4.1.3.7) While the smectite clay group possesses unfavorable thermomechanical characteristics because of its tendency to swell or shrink depending on the hydrologic conditions, it is not expected to have significant impact on the repository design because the amount of smectite clay within the basalt flows at the Hanford Site is only in the range of 0.27% to 0.32% (Section 4.1).

The infillings in joints observed in core are generally very thin (typically 0.13 ±0.13 mm (0.005 ±0.005 in.) thick); therefore, testing of infill properties has been limited. Infilling testing has included x-ray diffraction studies performed for mineral identification (Benson and Teague, 1979; Koster van Groos, 1981), differential thermal analyses to identify the effect of pressure on the loss of interlayer water (Koster van Groos, 1981), and shear strength tests performed on jointed basalt core samples containing infill coatings on the joint (see Section 2.2). The differential thermal analysis studies have been reported by DOE (1982, p. 6.1-20) and by Long and WCC (1984, p. I-219).

The differential thermal analysis shows that the loss of interlayer water is unlikely under saturated conditions during postclosure. In regions where temperatures are expected to exceed 130 °C prior to closure, shrinkage associated with the loss of interlayer water can be expected. Although the interaction of the thermal expansion of the basalt and the shrinkage of the joint infilling has not been analyzed, one possible interaction could act to reduce high-stress concentrations around the openings and possibly enhance stability.

The potential for change in moisture condition in the infilling material after construction should be considered. If the clay were distressed and allowed to absorb water, either because of changes in permeability induced by mining or from water introduced for dust control or environmental control, the clay could swell and lose strength. On the other hand, if the clay were allowed to dehydrate it might shrink and lose its binding properties. The clays are likely to desorb rather than absorb water because (1) the water is at a temperature of about 51 °C and therefore will tend to evaporate; and (2) the ventilation air will be at a lower temperature and unsaturated with water when it enters the repository and therefore will tend to absorb water.

The need to do additional joint testing to evaluate the potential shrinkage, swelling, and (or) change in joint strength as a function of changing moisture conditions is dependent on the potential abundance of fracture infillings of measurable thickness. Most joints are filled with a very fine coating of infill material and, thus, may not have a major impact on the joint mechanical properties. However, some thicker infilled joints may be encountered during construction. Further studies will be made on thermal/mechanical and hydrological interaction of joint properties (Section 8.3.2).

2.7.4   COUPLED-EFFECTS

The coupled effects between thermal, mechanical, hydrological, and chemical processes need to be assessed in determining the long-term (postclosure) waste isolation potential of the repository location. Preliminary aspects of the effects of temperature on deformability and strength were discussed in Sections 2.1 through 2.5. The coupled thermal and mechanical effects on hydraulic conductivity and porosity of basalt is not well understood and will be studied further (Section 8.3.2.2).

Coupling between mechanical and hydrological phenomena in a jointed medium is most noticeable in the effect of stress on joint permeability. Coupling between mechanical and hydrological phenomena is discussed partially in Section 2.8 where changes in geoengineering properties due to excavation are presented. Further studies are planned (Section 8.3.2.2).

Couplings between thermal and hydrological phenomena are treated in hydrological/groundwater travel time studies by accounting for the density change in groundwater with temperature. The change in density with temperature introduces a buoyancy force, or upward flow of the groundwater, after waste emplacement.

Mechanical-chemical/thermal-hydrological coupling is potentially important in the basalts because of the occurrence of clays in the basalt joints that (1) can shrink and (or) swell depending on the moisture and temperature conditions and (2) can change in chemical composition as a result of thermal loads. Any change in volume of the clay or clay mechanical properties can affect the mechanical and hydrologic properties of the basalt rock mass. The impact of dewatering/rehydration of the joint infill material was discussed in Section 2.7.3.

2.7.5   SUMMARY

Catastrophic rock bursts are not expected in the repository excavation because of the high degree of natural fracturing present in the basalt, the low extraction ratio, and the relatively uniform geology within the repository construction area. The presence of high stress and strong, brittle rock may result in spalling in the repository openings during excavation, and as the repository heats up and stress increases. However, if spalling proves to be a problem it could be controlled by modifying the excavation methods and support system currently planned.

Available laboratory results suggest that basalt has a low potential for thermal degradation in general. This is supported by full-scale heater tests at the Near-Surface Test Facility where the Pomona flow was subjected to temperature in excess of 500 °C for 21 d with no observable spalling or slabbing. However, the basalts at this location are not under high in situ stress, and the results are indicative of the effects of temperature alone. Thus, further studies of the potential of thermal degradation of basalt in the Cohassett flow are required (Section 8.3.2.2).

The fracture infilling material in the Cohassett flow contains a high percentage of smectite clay, which is susceptible to swelling and shrinkage. Under elevated temperature during repository operation, the clay may desorb water and shrink. However, this may not have a major impact in mechanical properties of the joints encountered as the infilling is very thin. Further studies on thermal/mechanical and hydrological interaction of joint properties are planned (Section 8.3.2.2). A number of coupled effects between thermal, mechanical, hydrological, and chemical processes have been discussed. Most of these effects are not well understood at present and will require further studies (Section 8.3.2.2).

2.8   EXCAVATION CHARACTERISTICS OF BASALT

2.8.0   INTRODUCTION

The purpose of this section is to present (1) a summary of excavation experiences relevant to the excavation of the BWIP repository (Section 2.8.1), (2) a discussion of anticipated conditions during repository excavation and an estimate of the support required (Section 2.8.2), and (3) a discussion of the changes in geoengineering properties during excavation (Section 2.8.3).   The discussions include only the excavation of repository openings; shaft excavation and emplacement hole drilling will be discussed in Chapter 6.

The expected conditions at the candidate repository horizon include the following:

o   High horizontal stress and high stress ratio.

o   High rock temperatures.

o   High fracture frequency.

o   High intact rock strengths.

o   Low water inflow.

These conditions are not duplicated in any one existing excavation. However, case histories that duplicate one or several of the expected conditions do exist and will be reviewed in this section.

2.8.1 EXCAVATION CHARACTERISTICS OF SIMILAR ROCK

The excavation characteristics of similar rocks are presented in the following subsections. Previous experiences of various methods used in underground excavations under conditions similar to the repository are summarized in Section 2.8.1.1. The various rock support systems that had been successfully applied to underground openings under highly stressed conditions and under conditions of changing stress are described in Section 2.8.1.2. A general discussion of methods used to control water inflow in underground excavation is provided in Section 2.8.1.3. The problem associated with gas in underground excavation is briefly outlined in Section 2.8.1.4.

2.8.1.1 Excavation experience

This subsection contains a discussion of excavation experience in basalt and rocks similar to basalt under conditions comparable to the repository environment using both drill-and-blast methods and mechanical boring machines. Many examples of excavation and construction are available in the literature, although none are representative of all expected repository conditions. Experience in basalt is generally from near-surface excavations where stress conditions are not representative of the candidate repository horizon. These studies indicate that available excavation techniques are adequate in dealing with conditions in the proposed repository excavations.

2.8.1.1.1 Drill-and-blast excavations

Four mining projects (one in basalt) under conditions of high stress and high intact rock strength, similar to conditions expected at the repository horizon, are discussed below. Experience with excavations in basalt is also summarized.

South African gold mines

Gold is mined in South Africa from flat-lying, thin (approximately 1-m (3.28-ft)) deposits to depths of 3,500 m (11,000 ft) (DeJongh and Klokow, 1983, p. D1). The ore and surrounding rock are massive, strong quartzites. The average intact rock uniaxial compressive strength is 262 MPa (38.0 x 10^3 lbf/in^2) (Hoek and Brown, 1980, p. 217), compared to 290 MPa (42.0 x 10^3 lbf/in^2) for intact Cohassett basalt (see Section 2.3). Unlike the Cohassett basalt, jointing is infrequent in the South African quartzite (Ortlepp, 1978, p. 2), although fractures develop during seismic events. The

stress in the South African gold mines is of similar magnitude to that in the Cohassett flow, although the direction of maximum principal stress and the stress ratio are generally different. The tunnels were successfully excavated by the drill-and-blast method. The support system used in these tunnels will be discussed in Section 2.8.1.2.

Kolar gold fields

Gold was mined in the Kolar fields of south-central India from vertical quartz veins in metamorphic rock to depths of 3,000 m (10,000 ft) (Taylor, 1961, pp. 575 & 177). The surrounding rock was metamorphosed igneous rocks, mainly basalts and dolerites (Caw, 1956, p. 259). The horizontal in situ stresses at Kolar are reported to be higher than the vertical stress (Krishnamurthy, 1969, p. 100), suggesting a stress state comparable to that measured at the Hanford Site. Joint frequencies, though unreported, are probably lower than those expected in Cohassett flow. Rock bursts were common in the Kolar gold fields, although distinction between "development bursts and bursts in the solid" (Caw, 1956, p. 263) is often obscured.

Coeur d'Alene mining district

From mines in the Coeur d'Alene district of northern Idaho, silver, lead, and zinc are extracted to a depth of 2,400 m (8,000 ft) from near-vertical veins. Rock bursts, often associated with highly stressed pillar remnants, are common in the district (Blake and Leighton, 1968, p. 441; Blake, 1982, p. 1537) where the extraction ratio is typically of the order of 75%. Some of the drifts and shafts in these mines experienced excessive closure and must be rehabitated. Rock is quartzite and argillite with intact strengths on the order of 125 MPa (18 x 10^3 lbf/in^2) (Beus and Chan, 1980, p. 782). Fracturing is heavy along the main fault (ore-bearing) structures and less heavy away from the faults (Miner, 1982, p. 549). In situ stress measurements indicate high horizontal stresses ranging up to 100 MPa (14.5 x 10^3 lbf/in^2).

Michigan copper mining

Copper was mined through basalt in upper Michigan to depths of 1,830 m (6,000 ft) (Crane, 1929a, 1929b; Mendelsohn, 1931; Vivian, 1931). These mines were excavated and operated prior to the widespread use of rock-bolt and shotcrete and had experienced severe ground control problems at deeper levels. Rock bursts, which mainly occurred in the stronger basalt, had been reported, although the occurrence of gradual, nonviolent failure and large closures were more frequently observed in these mines. Intact basalt strengths in these mines are 290 MPa (42 x 10^3 lbf/in^2) (Windes, 1949, 1950, p. 10), approximately equal to that of the Cohassett flow. The ore occurred in interbeds, and possibly flow tops, that were somewhat weaker. Information on jointing or rock structure is not available, although photographs presented by Crane (1929a, 1929b) suggest that fracture frequency is not as high as expected at the repository horizon and that typical colonnade and entablature structures were not encountered in these mines. The in situ stresses were not measured; however because of greater depth, it is likely that in situ stresses were higher than those anticipated in the Cohassett flow.

Excavations in basalt at shallow depth

Many road, rail, and hydroelectric plant tunnels have been excavated in basalt in Washington, Oregon, and other locations around the world using drill-and-blast methods. Pertinent data for many of these excavations are presented in Table 2.8-1 (Hardy and Hocking, 1979). Rock conditions were generally excellent for these excavations. Many of these excavations were constructed without temporary support, some have no final support, and most are still in operation with a minimum of maintenance. Rock conditions during excavation of the Near-Surface Test Facility in the entablature zone were also satisfactory (see Section 2.8.2.1). In comparison with the conditions expected in the repository, the rock mass may have a similar degree of jointing, and there is a significant difference in the in situ stress condition.

2.8.1.1.2 Mechanically mined excavations

Experience with tunnel boring machines under conditions similar to those expected in the repository horizon is from German coal mines, South African gold mines, and a tunnel in England. Several examples of the mechanical mining of basalt are also discussed.

German coal mines

Since 1971, more than 74 km (46 mi) of 5.4- to 6.5-m- (18- to 21-ft-) dia. haulage tunnels have been excavated in the Ruhr area (Loehr, 1983). Openings are between 600 and 1,200 m (2,100 and 4,000 ft) deep in highly stressed, hard-coal-bearing strata (sandstone, siltstone, and shale), with strengths up to 150 MPa (22×10^3 lbf/in^2) (Boldt and Henneke, 1981).

Progress of the tunnel boring machine was adversely effected by difficult ground conditions mostly associated with stress-induced spalling, weaker or highly fractured strata, and faults. Efforts to improve machine performance were primarily concentrated on cutter head design (Loehr, 1983). Rock structure (e.g., jointing and fracture zones) expected in the repository horizon in basalt are likely to be more favorable than those experienced at the deep coal mines of Germany.

South African gold mines

Tunnel boring machines have been used in South Africa at depths of 2,100 m (7,000 ft) (Graham, 1976) in highly stressed, massive, and strong quartzite. Although the rock in the South African mines is more competent than that encountered in the German coal mines, the problems related to overstressed rock and the solutions employed were very similar. Stress-induced slabbing of the brittle wall rock resulted in sidewall overbreak along

the tunnel boring machine and up to the face. This was largely corrected by installing support immediately behind the cutter heads and by making minor machine modifications (Graham, 1976). Short cutter life, related to the hard and abrasive nature of the rock, also had a detrimental effect on tunnel boring progress. In comparison with the expected conditions at the repository horizon, these tunnels were excavated under higher in situ stresses and harder rock.

Kielder water tunnels

The Kielder project in England consisted of a 3.5-m- (11.5-ft-) dia. tunnel that intersected 350 m (1,180 ft) of massive and strong dolerite, a rock similar to basalt (Korbin, 1979). The average rock strength was 350 MPa (50×10^3 lbf/in^2), and the depth was 360 m (1,180 ft). This section was therefore excavated in a stronger rock and under lower in situ stresses than those of the repository horizon. Tunnel boring machine performance was poor, with penetration rates of only 0.4 m/h (1.3 ft/h). Sections of both relatively massive and highly fractured rock were encountered. Penetration rates increased by a factor of three in the jointed areas as compared to the massive sections. Stability problems within the fractured regions were minor due to the rough, closed, and partly healed character of the joints.

Mechanical mining of basalt

Experience in the mechanical mining of basalt is extremely limited. The Baltimore tunnel in Scotland was bored through approximately 4.8 km (3 mi) of basalt (Hardy and Hocking, 1979). Depth and rock strength were not specified. The tunnel boring machine performed well in zones of competent basalt but had to be withdrawn and replaced by drill-and-blast excavation when the tunnel passed through a flow-top breccia.

A 2.3-m (90-in.) hole was drilled vertically through various igneous and sedimentary rock types (including some basalt) on Amchitka Island, Alaska, for the U.S. Atomic Energy Commission. Total basalt thickness drilled was approximately 100 m (330 ft), with an additional 170 m (560 ft) of basaltic pillow lava (Morris, 1968, Fig. 1). Information on jointing is not available. Uniaxial compressive strengths of the basalt and pillow lava averaged 122 MPa (17.7×10^3 lbf/in^2) and 80 MPa (11.6×10^3 lbf/in^2), respectively (Lee, 1969a, Table 13). Drilling through the basalt and pillow lava was rated as excellent, with no mining problems (Lee, 1969b).

2.8.1.1.3 Excavations mined by other methods

Other methods of excavation such as the use of hydraulic water jet and large saws or cutter bars are available. However, these are generally not suitable in rock as hard and strong as basalt and were not considered in the SCP conceptual design as described in Section 6.2.

2.8.1.2 Rock support

Tunneling, construction, and mining operations employ a variety of ground-support systems depending on various geomechanical, economic, and longevity considerations associated with an underground structure. Support system components can include rock bolts, cable bolts (wire rope), metal straps or plates between bolts, wire mesh (held in place by bolts), shotcrete (or gunite), mesh or fiber reinforced shotcrete, steel or timber sets with mesh and (or) lagging, cast concrete, and backfill. Often, two or more types of support are combined into an integrated rock support system.

This subsection describes several support systems that have been used successfully in excavations associated with either high-stress environments or subjected to significant stress increases. These examples are presented because they represent a relatively new type of support that might find application to the particular conditions expected in the repository. None of these systems described, however, had been used under elevated temperature conditions similar to that expected in the repository, and further studies will be required (Section 8.3.2).

2.8.1.2.1 Deep hard-rock tunnels in South Africa

The rock reinforcing system of tunnel support used in the South African gold mining industry (Ortlepp, 1983) is often referred to as "wire mesh support." The essential components of this system are rock reinforcement tendons, lacing, and wire mesh, and these were designed to withstand the high and changing stress conditions encountered in the gold mines. The rationale of the support design is that the support must preserve the integrity of the fractured rock surrounding the tunnel while accommodating the inevitable bulk movement of the fractured mass.

Rock reinforcement tendons are invariably anchored by "full-column" grouting using cement slurry, resin, or cementitious cartridges. Tendons generally range from 12 to 20 mm (approximately 0.5 to 0.75 in.) in diameter, and their length and spacing tend to be based on broad, empirical guidelines. Support tendons are provided with pigtails or looped ends to accommodate support lacing.

The type and size of wire rope used for lacing is determined largely by practical considerations and availability rather than by design. Most mines use single strands of discarded scraper (slusher) rope as lacing. Thus, the diameter of rope or strand used for lacing ranges from 9 to 16 mm (0.35 to 0.63 in.). The lacing method is determined by the density and position of support tendons.

With few exceptions, diamond mesh (chain link) is used in tunnels, and weld mesh is used in larger chambers. Diamond mesh used for support is usually made of 3.2- to 4.0-mm (0.13- to 0.16-in.) wire, with apertures ranging from 50 to 100 mm (2 to 4 in.). The stiffness of weld mesh makes it

somewhat difficult to mold to rough surfaces. However, the apertures of welded mesh are larger than those of diamond mesh. Thus, if shotcrete is required, welded mesh allows better shotcreting than does diamond mesh.

2.8.1.2.2 Experimental tunnel at the East Rand Property Mines

Over a 5-yr period starting in 1976, the Chamber of Mines of South Africa developed and monitored an experimental research tunnel (Fig. 2.8-1) at the East Rand Property Mines (Ortlepp and Gay, 1984). This tunnel, 170 m (557 ft) long and approximately 3,075 m (10,090 ft) below the ground surface, was driven across a strong, massive quartzite in the hanging wall. The tunnel was developed from a low-stress, undermined area into a highly stressed abutment zone. Subsequently, the southern portion of the tunnel was undermined, leaving it straddling a 55-m- (180-ft-) wide stabilizing pillar some 50 m (160 ft) vertically below. The experience with this tunnel under both high initial stress and high-stress change conditions might provide some similarities to repository conditions at the Hanford Site where additional thermally induced stress changes are applied to the support system.

The jointing in the rock mass consisted of groups of closely spaced (0.1- to 1-m (0.3- to 3-ft)) joints, orthogonal near-vertical joints, and minor quartz veins. The mean uniaxial compressive strength of the quartzite is 350 MPa (50.75 x 10^3 lbf/in^2). The magnitude of stresses in the destressed portion and the central stressed portion of the tunnel was estimated by the computer program MINSIM to be 50 MPa (7.25 x 10^3 lbf/in^2) and 140 MPa (20.3 x 10^3 lbf/in^2), respectively.

Permanent tunnel support consisted of cement-grouted steel tendons (on 1-m (3-ft) spacing in rows 0.5 m (1.5 ft) apart), wire mesh, and wire-rope lacing. Over the 4-yr period following completion of the tunnel, stoping and the establishment of the stabilizing pillar below the tunnel created significant stress changes. By 1981, it was estimated that the stress in the central portion of the tunnel had increased by 62% to a value of 225 MPa (32.6 x 10^3 lbf/in^2). During this time and after undermining was completed, no further deterioration of the tunnel occurred, and the investigators concluded that "the relatively weak constraint provided by the cladding of lacing and mesh was sufficient to prevent further degradation of the stable shape," and that "in a regime dominated by strong, massive rock and limited depth of fracturing, is clear that a tunnel can be designed in terms of shape and support to resist very large quasi-static stress changes" (Ortlepp and Gay, 1984, pp. 345 and 346).

2.8.1.2.3 Blyvooruitzicht Gold Mine and the Vaal Reefs Gold Mining Complex

Dempster et al. (1983) describe the use of rock bolt and grouted loop in the Blyvooruitzicht Gold Mine and at the Vaal Reefs Gold Mining Complex in highly stressed ground and in areas of changing stress. At the Blyvooruitzicht Mine, the Carbon Leader Reef is extracted at depths up to 2,380 m (7,810 ft) below ground surface. In the Klerksdrop Gold Field, the Vaal Reefs Exploration and Mining Company is mining at depths up to 2,500 m (8,200 ft). These mines are in a geologically disturbed area, with much of the seismic activity occurring along fault planes. The depth of mining indicates that in situ stresses are high. The mining methods that often leave abutment or remnant areas produced significant mining-induced stress changes in the vicinity of the development entries. Magnitudes of in situ stresses and stress changes induced by mining are not reported.

Support systems for tunnels in these mines have evolved from passive timber or steel set supports to active rock bolt and grouted tendon supports. Dempster et al. (1983) note that support must be installed before induced stresses endanger the stability of the excavation. The combination of these support elements with wire mesh and lacing ropes between the support tendons has resulted in an integrated support system that is capable of controlling most rock burst damage and quasi-static load changes.

2.8.1.3 Water Inflow

Occurrence of water in deep excavations can create problems ranging from minor to extremely difficult and can have an important effect on the cost and progress of an excavation. Prediction of water inflow can be based on rainfall, topography, drainage, lithology, and structure. The reliability of the inflow predictions is not high.

Sources of water include the sea, surface lakes, rivers, swamps, rainfall, snow and ice, unconfined near-surface aquifers, confined aquifers, isolated subsurface pockets or caverns, and magmatic waters. Conduits through which water reaches underground workings may be simple (a single fault plane or permeable layer) or complex (several joint sets), natural (flow along joints or through porous rock) or induced (leakage around shafts or tunnels). The permeabilities of fractures and fissures are generally orders of magnitude greater than the permeabilities of intact rock. Intersection of a shaft or tunnel with an aquifer is the most likely cause of water inflow. An aquifer may owe its water conducting property to primary (connected pore space) or secondary (joints and other discontinuities) permeability. Water inflow may be increased by blasting and other mining procedures.

Many techniques have been developed to minimize the effect of groundwater inflow on excavation operations. These techniques can be classified as detection, isolation, and removal. Detection by pilot-hole probing or seismic

techniques can permit better isolation by means of grouting, or adequate preparation to handle the water via a collection and pumping system. Removal refers to pumping in order to predrain the area where groundwater is known to exist.

Several examples of water inflows recorded during tunneling and mining operations are listed in Table 2.8-2. Also listed in the table is the recovery method used. Though some exceptionally high-peak inflows have been encountered, recovery techniques were available to handle the inflow. Zones of significant water inflow requiring engineered water control measures usually occur along relatively small, anomolous zones (Baker, 1985, p. 10).

2.8.1.4 Gas

Flammable gases encountered underground include methane, hydrogen, and hydrogen sulfide, with methane occurrence being most common in coal and other sediments having some organic content. Methane in smaller quantities, usually occurring in solution with the groundwater, can also be present in hard-rock mines (i.e., igneous and metamorphic rocks). The presence of inflammable gas in large quantity is a major safety concern and may affect the progress of excavation. The Mineral Resources Code of Federal Regulation 30 CFR 57, Subpart T, Gassy Mines (MSHA, 1985), provides the guidelines for the identification of gassy mines.

The danger associated with gassy mines can be averted by appropriate mining practice and by proper ventilation systems that provide fresh air to working areas. Ventilation air dilutes and sweeps away dangerous gases if present. The coal mining industry has demonstrated that ventilation systems and mining practices can be devised to mitigate the hazards in gassy conditions. General excavation experiences in similar rock indicate that harmful gases have not been a significant problem in basalt or similar rocks.

2.8.1.5 Summary of excavation characteristics of similar rock

The case histories described in this section showed that present excavation technology and support systems were successful in underground excavations at great depth under high-stress conditions. Support systems had been successfully developed to cope with changing stress conditions in underground excavations. Methods dealing with water inflow and the presence of inflammable gas were also available. These include the use of advance detection techniques, dewatering by pumping, sealing, and ventilation.

2.8.2 EXCAVATION CHARACTERISTICS AT THE HANFORD SITE

Based on experiences obtained from excavations in similar rocks as summarized in the preceding section and the estimated characteristics of the basalt rock mass in the repository horizon, this section attempts to describe the excavation characteristics that may be anticipated in the repository excavation and the support system that may be used. The problem of water inflow and gas will be addressed. Finally, the monitoring system that may be used during excavation and the method for analyzing the results will be briefly discussed.

2.8.2.1 Excavation experience

The only underground excavation experience in basalt at the Hanford Site is from the excavation of the Near-Surface Test Facility. The Near-Surface Test Facility was excavated by drill-and-blast, without controlled blasting techniques such as presplitting or smooth-wall blasting. Inconsistently drilled and loaded rounds resulted in overblasting and rock damage in some areas (Moak and Wintczak, 1980, p. 3-20).

Shotcrete with or without rock bolts was generally used for support in the dense interior of the Pomona flow. Steel sets were used at the portals. Two small rock falls occurred near one of the portals when support was lagging behind the excavation face by as much as 8.5 m (28 ft) (Moak and Wintczak, 1980, p. 3-23). This experience is consistent with other construction experience; most major problems of ground control occur at the portals where rock is weathered and destressed.

The conditions that may be anticipated during the excavation of the repository were addressed in Section 2.7.1.2. It was concluded that rock burst will be an unlikely event, and some spalling may be expected during repository excavation.

2.8.2.2 Rock support

The rock support system at the Hanford Site will be required to maintain stability in the underground openings during the operation of the repository. The support system must prevent major roof falls or stress-induced problems in the ribs and must minimize minor rock falls that could endanger personnel or waste emplacement operations.

The repository will be built, operated, and decommissioned in phases over a period of approximately 90 yr as described in Section 6.2.2.4. Excavation dimensions will have a large influence on required support. The dimensions of the main excavations proposed in the SCP conceptual design (KE/PB, 1986) are shown in Table 2.8-3.

Ideally, the rock support system installed during construction should remain functional for the life of repository; this, however, may not be feasible or cost effective. It is possible that the support system will be repaired or reapplied at one or more stages during the repository operating period.

The following subsections discuss the BWIP repository support recommendations based on rock mass classification systems.

2.8.2.2.1 Rock mass classification

This section provides an assessment of the range of rock mass quality likely to be encountered in the repository horizon in the Cohassett flow using the Norwegian Geotechnical Institute-Q system. An assessment of the support required based on the rock mass quality was made. This is essentially an empirical method. The basis of the Norwegian Geotechnical Institute-Q system and its application in support design for underground openings are described in Barton et al. (1974).

Barton (1984, p. 73) determined the rock mass quality rating in the repository under two different conditions: those during the repository excavation and those after the waste emplacement where thermal loading to the rock mass will be considered. The ratings corresponding to both conditions are shown in Table 2.8.4. Under the condition of repository excavation, the rock mass quality ratings for the Cohassett flow are "very poor to fair rock" (rock mass quality = 0.4 to 8.3) for the entablature and "very poor to poor rock" (rock mass quality = 0.5 to 1.9) for the colonnade. To account for the long-term effect of thermal loading, Barton (1984, p. 72) adjusted the rock mass quality ratings by increasing the stress reduction factor parameter to simulate the stress increase due to temperature changes. The rock mass quality ratings calculated for the thermal case are also shown at the bottom of Table 2.8-4.

2.8.2.2.2 Support recommendation

The ranges of span/excavation support ratio and rock mass rating values for the repository excavations are plotted on the rock mass quality support chart in Figure 2.8-2. The design ranges of rock mass quality ratings for thermally loaded conditions are shown by the shaded areas; extreme ratings are shown also. Several support categories with somewhat different support are indicated in the figure. Barton (1984, p. 85) simplified the support recommendations and his recommendations for the rock support system are as follows:

o Emplacement rooms, panel entries, and main entries in the colonnade--bolts on 0.8-m (2.5-ft) spacing with 5 cm (2 in.) of fiber-reinforced shotcrete.

o · Emplacement rooms, panel entries, and main entries in the entablature--5 cm (2 in.) of fiber-reinforced shotcrete.

o Confinement returns, panel crosscuts, and backreaming drifts in the colonnade--bolts on 1.0-m (3-ft) spacing with 2.5 cm (1 in.) of fiber-reinforced shotcrete.

o Confinement returns, panel crosscuts, and backreaming drifts in the entablature--2.5 cm (1 in.) of fiber-reinforced shotcrete.

o Intersections--bolts on 0.8-m (2.5-ft) spacing with 5 cm (2 in.) of fiber-reinforced shotcrete.

Barton (1984, p. 65) also suggested that stress-related ground control problems such as spalling will be more difficult to control in the colonnade than in the entablature. When these occur, heavier support systems than those suggested may have to be used.

Finally, it should be noted that the combination of conditions likely to be encountered in the repository have little or no precedence in terms of underground construction and rock mechanics. These include variable rock conditions, high horizontal stresses, great depth, development of high temperature due to heat generation from the decay of radioactive waste, and changing groundwater conditions. Consequently, the repository excavations are beyond the data bases from which the empirical support design method was developed and heavier support may be necessary due to one or a combination of these conditions.

2.8.2.3 Water Inflow

Large inflows sufficient to produce flooding are not expected, although some water inflow into the repository excavations is anticipated. Hydrologic studies suggest that water inflow into the repository excavations will be low due to the very low permeability of the basalt dense interior. The possibility of any significant water inflow into the repository from the surface flood or the upper aquifers will be minimized by the installation of minimized surface protection structures and shaft seals. However, the possible existence of localized water-bearing zones dictates that precautions (i.e., excess pumping capacity) be taken to provide the capability of removing large quantities of water.

Under normal conditions, the permeability of the dense interior is sufficiently low that most water entering the repository will be from drilled holes and from the small quantities of water passing the shaft seals. The measured permeabilities for repository intraflow zones are shown in Table 2.8-5. The inflow values used in previous repository designs are shown in Table 2.8-6. Preliminary calculations indicate that the seepage into the repository located in the Cohassett flow will be only 5.8 L/s (91 gal/min) (Baker, 1985, Figure 3), compares to the 19.58 L/s (310 gal/min) calculated

for the Conceptual System Design Description (RKE/PB, 1983) as shown in
Table 2.8-6. The flow rates under abnormal conditions result from
intersecting a fracture that connects directly to the flow top or breaching
the flow top directly. Uncertainties in the calculation of these maximum
inflows are large. It is likely that these high inflow rates will drop off
significantly with time due to the limited storage in the flow top aquifer;
maximum probable peak inflow of 219 L/s (3,400 gal/min) has been calculated,
which will decay to 130 L/s (2,000 gal/min) after 1 h (Baker, 1985).
Currently there is a large uncertainty in the estimates of water inflow.

Several measures will be taken to ensure that the repository is not
inundated with water (Section 6.2.6.2). Exploration programs such as drilling
in advance of mining, geophysical exploration to detect anomalous zones of
rock, and pilot drifts around large development areas are measures designed to
detect water-bearing zones. If a water-bearing zone is detected or
intersected, it will be grouted and (or) the direction or elevation of the
drift will be altered to avoid the potential water-bearing zone. Adequate
backup or reserve pump, sump, piping, and power capacity will be installed to
handle any larger-than-normal inflows (Section 6.2.6.2). Ample techniques
exist to detect and seal water-bearing zones and to pump larger quantities of
water than indicated above to prevent flooding of the repository.

2.8.2.4 Gas

Precautions will be taken to ensure that the presence of gas will not
create hazardous conditions. The occurrence of significant quantities of
methane and other harmful gases are not expected in the repository
excavations. Groundwater from the Grande Ronde basalt in the reference
repository location is approximately 50% saturated with methane gas at
formation conditions. Methane would enter the repository in solution in the
groundwater, and its quantity is directly related to the amount of groundwater
inflow. The precautions which will be taken include controlling groundwater
inflow, dilution with ventilation air, and monitoring of ventilation air for
the concentration of methane. Preliminary calculations indicate that
ventilation required for cooling will provide many times the air volume
necessary to dilute the expected methane inflow to safe concentrations. It
should be noted that because the quantity of methane inflow was estimated on
the basis of estimated water inflow into the repository, this estimate is
subjected to large uncertainty as that of the water inflow.

2.8.2.5 Monitoring and analysis

The repository excavation will be monitored to assess stability. Back
analysis of excavation behavior will be performed to estimate or verify rock
mass properties in conformance with the performance confirmation requirements
of 10 CFR 60, Subpart F (NRC, 1985). These are described in detail in
Section 8.3.3.2.

Precise measurements of rock movements via convergence stations and (or) borehole extensometers will be used to evaluate excavation stability and the adequacy of empirical models. Instrumentation should be installed in all critical areas (i.e., major intersections, loading pockets) as well as at random drift sections and intersections throughout the repository to monitor stability.

A microseismic system may be used to detect any zones of stress buildup as indicated by microseismic activity. Such activity can be a precursor to, or accompany, rock bursting or spalling and could indicate where additional support or destressing techniques would be appropriate.

Back analyses of repository excavations under a variety of conditions will be used to estimate or verify rock mass properties through the comparison of measured and predicted behavior. The use of rock mass properties verified by such back analysis can allow model validation as well as more confident predictive analyses.

2.8.3 CHANGES IN GEOENGINEERING PROPERTIES DUE TO EXCAVATION

The excavation of repository openings will cause disturbance to the surrounding rock that may affect the excavation stability and the permeability around the excavation. This disturbance consists of a blast-damaged zone immediately adjacent to the opening and stress redistribution zone beyond the blast-damaged zone. The effect on the rock from blasting is caused by the dissipation of energy imparted to the rock mass. The effect on the rock due to stress redistribution is dependent on the size of the opening, the in situ stress, and the rock mass strength.

There are large uncertainties in the parameters that control the extent and properties of the blast-damaged and stress redistribution zones. The theoretical basis for predicting changes in rock properties due to excavation is poorly developed, and there is very little experimental data on which to base projections. Cross-hole seismic data from the Near-Surface Test Facility and information in the literature provide some data on the extent of the disturbed zone and the change in mechanical properties due to excavation. The extent of the blast-damaged and stress redistribution zones is discussed below; the effects of the disturbance on rock properties are discussed in the following subsections.

The effects of the stress redistribution caused by an excavation can be considered as (1) the plastic zone surrounding the damaged rock zone of the opening, and (2) the zone of changed stresses caused by the excavation locally disrupting the in situ stress field. The plastic zone is where the strength of rock is fully mobilized. The thickness of the plastic zone in basalt under repository conditions has been estimated to be from 51 mm (2 in.) (for a 12-ft dia. shaft in the Cohassett dense interior, Cottam, 1983, p. 16) to approximately 1 tunnel or shaft radius (Kelsall et al., 1982, p. 30). On the other hand, Ortlepp (1983, p. D181) states that stress-induced wall failure is

typically in the range of 0.4 to 0.7 times the height of the sidewall. Beyond the plastic zone, the changed stress zone extends out to several excavation radii, although the most significant stress changes are confined to within 2 radii of the excavation wall. In a jointed rock mass, the stress change may cause opening or closing of the aperture and thus change the permeability of the rock mass.

Several studies available in the literature quantify the extent blasting may affect the surrounding rock. Case history data presented by Kelsall et al. (1982, p. 49-75) and Cottam (1983, p. 103) indicate that blast damage resulting from conventional blasting in hard rock such as granite would extend 1.0 to 1.5 m (3.3 to 4.9 ft) into the rock. For controlled blasting such as smooth wall, the damage would be limited to a region within 0.5 m (1.6 ft) of the excavation surface. Cross-hole seismic data from the Near-Surface Test Facility indicate lower seismic velocities, due presumably to blast damage, for a distance of 1 to 2 m (3.3 to 6.6 ft) (see Section 2.3.2.4).

2.8.3.1 Mechanical properties

Information on changes in mechanical properties due to excavation can be derived from literature sources and from cross-hole seismic measurements at the Near-Surface Test Facility. Theoretically, the strength of rock within the plastic zone would be reduced to residual or postfailure values with a corresponding decrease in deformation modulus. The ultimate mechanical properties of rock in the disturbed zone cannot be predicted until physical and chemical changes are quantified.

2.8.3.1.1 Strength

Limited data are available on the residual strength of rock masses. Most data in the literature are for coal pillars, which are not relevant to excavations in basalt. Hoek and Brown (1980, p. 283 and 176) propose guidelines on residual strength that depend on the quality of the undamaged rock mass as well as on the amount of damage inflicted on the rock by the excavation method. These guidelines indicate a reduction in uniaxial strength on the order of a factor of three or more. The reduction in strength from intact to residual is less at higher confining stresses.

2.8.3.1.2 Deformation

Information on the reduction in deformation modulus around an excavation in basalt can be obtained from the cross-hole seismic studies performed at the Near-Surface Test Facility. As discussed in Section 2.3.2.4, these tests measured the seismic velocity as a function of depth into the tunnel wall. The dynamic elastic moduli calculated from the measured seismic velocities are

shown in Figure 2.3-13. The modulus in the vertical direction is very low
near the excavation wall and rises quickly to asymptotically approach the
undisturbed value approximately 2.5 m (8.2 ft) into the rock. The modulus in
the horizontal direction rises less rapidly to reach its premining value
approximately 2.5 m (8.2 ft) into the rock. Extrapolation of these data to
the conditions around the proposed repository excavations is difficult due to
the different stress state, geologic conditions, and excavation techniques at
the repository horizon.

2.8.3.2 Thermal and thermomechanical properties

The rock thermal properties in the disturbed zone will probably be
similar to those of both the intact rock mass and laboratory samples, although
there are no data on the effect of rock damage on thermal and thermomechanical
properties of basalt. Analysis of the full-scale heater tests has shown that
the rock mass thermal properties are comparable to the laboratory-determined
values (see Section 2.5), indicating the effect of jointing on these proper-
ties is probably minor. Because joint conditions (i.e., intact or in various
states of failure) are the major differences between the disturbed zone and
the intact rock mass and because jointing does not significantly affect
thermal properties, the disturbed zone should have thermal properties of
comparable magnitudes to both the rock mass and laboratory-determined values.
Data on thermomechanical behavior (thermal expansion coefficient) in the
disturbed rock are lacking.

2.8.3.3 Hydraulic properties

Changes in hydraulic conductivity due to excavation can result from three
mechanisms: (1) the creation of new fractures by blasting and (or) rock
failure immediately around the excavation, (2) the change in the conductivity
due to stress changes across existing joints induced by the excavation, and
(3) dislocation along the joints. The first mechanism causes an increase in
conductivity, whereas the second and the third can cause either an increase or
a decrease in conductivity, depending on the sign of the stress change.

There have been very few measurements of hydraulic properties close to
the excavation in other rocks and none in basalt. Tests at both Idaho Springs
(Montazer et al., 1982) and Stripa (Nelson and Wilson, 1980) in granite
indicated a reduction in radial permeability of 1 to 2 orders of magnitude due
to the increase in tangential stress caused by the opening and an increase of
several orders of magnitude in axial permeability close to the tunnel walls
(Kelsall et al., 1984, p. 130). Both tests were in relatively competent
granite; at greater depths, the rock mass may exhibit a plastic zone close to
the excavation wall.

Preliminary scoping studies performed to estimate the effect of the disturbed zone on hydraulic conductivity at the Hanford Site indicate that significant disturbance (permeability increased by a least an order of magnitude) may be contained within 1 excavation radii (Cottam, 1983, p. 112). This includes the effect of both stress redistribution and blast damage.

2.8.3.4 Methods of investigating damage

Several of the techniques mentioned below could be used to investigate the extent and properties of the disturbed rock zone. A more complete description of the methods is contained in Kelsall et al. (1982, p. 93-109). Tests available to investigate the disturbed rock zone include:

o Hydraulic tests such as packer tests in boreholes, tracer tests between boreholes, and macropermeability tests that would measure radial permeability along an entire tunnel cross section.

o Geologic tests such as detailed geologic mapping and core and borehole logging.

o Geophysical tests such as seismic refraction, micro-seismic, cross-hole seismic, borehole geophysical logging, and ground probing radar.

o Mechanical tests such as borehole jacking, flat-jack tests, plate loading tests, and extensometer measurements.

Among these tests, the hydraulic tests which measure permeability directly appear to be the most useful, since the permeability of the disturbed zone is the characteristic of interest to repository design and sealing.

2.8.3.5 Impact on repository design

Damage to the rock mass due to the excavation has two main effects on repository design and performance: (1) the damaged rock may require additional support to maintain stability, and (2) the increased permeability of the damaged rock could act as a preferential pathway to groundwater flow and affect the postclosure performance of the repository.

The damaged rock is not a serious obstacle to support design and excavation stability because the effect of the damaged rock is implicitly included in the empirical support design methods (Section 2.8.2.2.1). In addition, instrumentation will be used to monitor excavation stability, and additional support could be installed if considered appropriate based on instrumentation measurements. Several years after waste emplacement, the thermally induced stress may cause additional disturbance to the rock. The

combination of damaged rock with thermally induced stress may have impact on the stability of the opening and the retrievability of the canisters if the support design does not take this into account.

The damaged rock will be a potential pathway for groundwater flow along the shafts and tunnels. The permeability increase in the damaged rock may be mitigated by a combination of careful excavation and properly constructed cutoffs (Section 6.2.3.2). Grouting may not be sufficient to reduce the permeability because of the low permeability of dense interior basalt even in the damaged zone. Natural or induced precipitation of secondary minerals in fresh fractures may in geologic time decrease the permeability of the host rock.

Information related to the excavation characteristics of basalt required to address preclosure safety in the repository is not known with certainty at present. These include the performance of support system under elevated temperature conditions, the availability of suitable analytical tools to predict the interaction of rock mass and the support system, and the geology of the Cohassett flow at the repository horizon. The last item includes rock mass quality data taking into account the presence of healed fractures and core disking, identification of "weak" zones within the Cohassett flow which may create unfavorable conditions for excavation and potential anomalous geologic conditions which may connect to flow top or bottom aquifers and result in large water inflow during excavation. These are likely to have a significant impact on the excavation of repository and need to be studied (Section 8.1.1). Information related to the excavation characteristics of basalt which may affect the post-closure performance of the repository include the thickness of the disturbed zone and the characteristics of the damaged rock. Further studies will be planned to obtain this information (Section 8.3.3.2).

2.8.4 SUMMARY

The expected conditions in the repository excavations are not duplicated in any one existing excavation. However, case histories from deep mines and from engineering projects provide an indication of the situation that may occur under one or several of the conditions expected at the repository horizon. Engineering and construction techniques have been developed in deep mining and tunneling to deal with high stresses of the same magnitude as those expected at the repository horizon. Other conditions, such as elevated temperatures, will require additional study.

The Norwegian Geotechnical Institute Q system was used to estimate the support requirement for the proposed repository excavations. The present recommendation consists of pattern bolts with shotcrete.

A zone adjacent to the openings consisting of damaged rock is created by a combination of blasting operations and stress redistribution. In this zone the mechanical, thermomechanical, and hydrological properties will be changed

from those existing prior to the opening. New surfaces will be created, and
joint slip and some rotation of blocks can be expected in this zone.
Quantification of these changes for engineering design is difficult.

Two consequences of the rock damage caused by excavation are potentially
important: (1) the effect on the support system and (2) the influence on the
hydraulic conductivity. The empirical method of rock support selection
implicitly includes a portion of the effect of the disturbed zone on support
requirements. The additional disturbance caused by the stress changes induced
by thermal load after waste emplacement has been evaluated by comparison with
other mining examples where stress changes are induced on a supported exca-
vation by mining in an adjoining area. For the analytical schemes of
evaluation of rock support requirement, a knowledge of the mechanical
properties of the damaged rock is required. This can be met partly by seismic
methods, but the effect on the strength characteristics will have to be
determined from back analysis of monitored excavations in basalt at the
candidate repository horizon (Cohassett flow). Plans to obtain this
information will be addressed in Section 8.3.2.

2.9 SUMMARY OF CHAPTER 2

The geoengineering program is developing a data base on the mechanical, thermal, and thermomechanical properties and the excavation characteristics of Columbia Plateau basalt, in general, and the Cohassett flow, in particular. This process involves reviewing literature sources for characteristics and phenomena evident in similar rocks, laboratory testing of core from the Cohassett and surrounding flows, and field testing in the Near-Surface Test Facility.

The geoengineering program is concerned with understanding and predicting the in situ mechanical and thermomechanical responses of the rock mass to changes imposed by excavation and waste emplacement. These are essential for the design and performance assessment of the repository. The more significant results from the geoengineering program completed before January 31, 1986, as well as its relation to the repository design, are presented in this section. Currently available data suggest that a repository can be built with existing technology.

It is not yet possible to predict with certainty the properties of basalt rock mass at the repository horizon because of the jointed nature of the basalt, insufficient exposure of the basalt rock mass at depth, and limited quantities of samples available for testing. Further information are required to remove some of the uncertainties and to support future design and

performance assessment activities of the repository. The information needs
are identified in Section 2.9.3. These will be used in Section 8.1.1 to
develop plans for future tests and analyses (Section 8.3.2.2).

2.9.1 SUMMARY OF SIGNIFICANT RESULTS

2.9.1.1 Mechanical properties of rock units--intact rock

Intact basalt from the dense interior of the Cohassett flow is a hard,
brittle rock with a mean uniaxial compressive strength of 290 MPa
(42×10^3 lbf/in^2) and mean elastic modulus within the range of 70 to 80 GPa
(10 to 12 kip/in^2). The uniaxial compressive strength of samples from the
flow top is generally less than 100 MPa (15×10^3 lbf/in^2) with mean elastic
modulus within the range of 14 to 32 GPa (2 to 4.6 kip/in^2). In the vesicular
zones, the uniaxial compressive strength is generally of the order of 162 MPa
(23×10^3 lbf/in^2) and the mean elastic modulus is approximately 51 GPa
(7.4 kip/in^2). The limited amount of test results showed little lateral
variation in the mechanical properties measured in samples from different
boreholes.

2.9.1.2 Mechanical properties of rock units--discontinuities

Site-specific testing of joints from the Cohassett flow has not been
completed. Joints are generally characterized as tight, with a thin coating
of clay minerals which does not appear to dominate the shear strength.
Presently available evidence suggests that the discontinuous cooling joints
will be the most abundant in the dense interior of the Cohassett flow. The
friction angle of laboratory-scale basalt joints at the Hanford Site is
probably within the range of 30 to 45 with some apparent cohesion within the
range of normal stress of 0 to 100 MPa (0 to 14.5×10^3 lbf/in^2). Normal and
shear stiffness tests on cores from the jointed block test area at the Near-
Surface Test Facility showed large variation in stiffness over the range of
stress level used in the test. The results indicate that very high stiffness
values can be expected in the joints at the repository horizon.

2.9.1.3 Mechanical properties of rock units--large scale

The large-scale mechanical deformation properties of basalt have been
assessed in the Pomona flow at the Near-Surface Test Facility. No large-scale
rock mass strength determinations have been made.

Modulus values determined at the Near-Surface Test Facility using
borehole jacking, cross-hole seismic tests, and jointed block tests, differed
significantly. The jointed block test has produced the most complete set of
data on the directional and stress dependence of the modulus in the Pomona

flow basalt. The results indicate a modulus of 8% to 56% of the intact laboratory value, depending on direction and confining stress level. The Hoek and Brown formula is used to describe the strength of basalt rock mass in the Cohassett flow. The parameters required to define the strength are estimated from the fracture characteristics and intact properties of the dense interior of the Cohassett flow.

2.9.1.4 Thermal and thermomechanical properties--intact rock

Intact basalt from the dense interior of the Cohassett flow has a low thermal conductivity of 1.51 W/m·K and thermal expansion coefficient of 6.02 $\mu\epsilon$/°C. Variations in temperature within the test range appear to have little effect on the measured thermal conductivity and thermal expansion coefficient. The heat capacity of intact basalt increases from 782 J/kg·K at 20 °C to 929 J/kg·K at 200 °C. The variability of thermal and thermomechanical properties, either within the flow or laterally, has not been assessed. The thermal properties are expected to be influenced by porosity and moisture conditions and will vary in the flow top and vesicular zones from that of the dense interiors.

2.9.1.5 Thermal and thermomechanical properties--large scale

Large-scale thermal and thermomechanical properties have been interpreted from the results of the full-scale heater tests in the Pomona flow. The thermal and thermomechanical properties inferred from these tests are very close to those measured in the laboratory. No apparent thermal anisotropy was observed in the tests. Based on these findings, the thermal and thermomechanical properties of the basalt rock mass in the Cohassett flow were estimated from those measured in the intact basalt samples.

2.9.1.6 Stress regime

Stress measurements by hydraulic fracturing in three boreholes within the reference repository location in the Cohassett, Grande Ronde 7, McCoy Canyon and Umtanum flows have produced a consistent pattern of in situ stresses. The horizontal stresses do not show any significant trend with depth within the flows or between the four flows tested. In the Cohassett flow within the reference repository location, the maximum horizontal stress is estimated to be 61.5 MPa (8.9 x 10^3 lbf/in^2), the intermediate (horizontal) stress is 32.8 MPa (4.8 x 10^3 lbf/in^2) with a minimum (vertical) stress of 24.2 MPa (3.5 x 10^3 lbf/in^2). The maximum principal stress is generally north-south; the intermediate stress is east-west (both in the horizontal plane); and the minimum stress is vertical. The stress levels are high and consistent with observed borehole spalling, core disking, and seismic activity in the area.

2.9.1.7 Special geoengineering properties

The basalt host rock is generally chemically stable over the temperature ranges anticipated during the thermal phase of waste storage. The secondary minerals found as infill material in joints are not as chemically stable as the basalt and could be dehydrated, or modified mineralogically at repository temperatures, thereby influencing the rock mass properties. Thermal degradation was not seen in the full-scale heater tests at the Near-Surface Test Facility.

Rock bursting is a function of the in situ stress state, the mechanical properties of the rock mass, opening dimensions, and stress change caused by heating. Previous experiences in underground and tunnel excavations in similar rock suggest that the low extraction ratio and the jointed nature of basalt may mitigate the potential for rock bursts since the jointed nature of the basalt will relieve the high stress concentrations around openings, rock spalling is the only likely event during excavation.

2.9.1.8 Excavation characteristics

The excavation characteristics of basalt have been assessed by comparison to underground mining and tunneling experience in similar rocks under similar stress conditions. Examples of mining under high stress conditions at depth in similar rock (hard, brittle rock) are common. These examples include the gold mines of South Africa, the Kolar gold fields in India, the Coeur d'Alene mining district of Idaho, and the copper mines of upper Michigan. All of these projects experienced rock spalling and rock bursting, but the rock bursting is generally associated with high-stress concentrations caused by extensive mining. Rock spalling in tunnels, under similar conditions expected in a repository layout, is generally minor in extent and mitigated by application of rock supports such as bolts and shotcrete.

Existing empirical methods of estimating the rock support requirements using the Norwegian Geotechnical Institute Q system for a repository in the dense interior flows have indicated that shotcrete and bolts should be sufficient. The data base for the Norwegian Geotechnical Institute Q system does not include a case with conditions similar to that of the repository. However, the resulting support requirements even under conservative estimates of rock mass qualities, rock strengths, stress field, and stability requirements are well within the range of conventional underground construction experience. Confirmation of the suitability of the empirical method for the conditions at the Hanford Site at depth must await at-depth testing.

2.9.2 RELATION TO DESIGN

The geoengineering properties provide a significant input to the design characteristics presented in Chapters 6 and 7. The properties used in the SCP conceptual design (KE/PB, 1986) are summarized in Table 2.9-1.

The mechanical and thermomechanical properties are used extensively in establishing the waste emplacement layout, emplacement density, and rock support systems, while providing important mechanical boundary conditions for assessment of long-term stability and performance assessment. The mechanical, thermal, and thermomechanical properties are used directly in the layout and waste emplacement design studies. The empirical design methods for rock support system selection use laboratory mechanical strength data, joint frequencies, orientations, roughness and moisture conditions, and the in situ stress data. Thermal properties are used in regional postclosure performance assessment studies. In Sections 2.3, 2.5, and 2.6, properties on data used in design are presented with the rationale for selection as appropriate. In some cases, the mean of measured values is used, while in others such as the in situ rock mass strength, the estimated value is based on intact properties and known fracture characteristics of the rock mass. Not all the data presented in Chapter 2 are intended to be used in design but are used to develop positions for licensing the data for performance assessment.

2.9.3 IDENTIFICATION OF INFORMATION NEEDS

2.9.3.1 General

A brief summary of the geoengineering data available to date on basalt and similar rock types on which repository design has been based is presented in Chapter 2. Although most data were not obtained from the site-specific candidate repository horizon, they provided a basis for estimation of properties or ranges of properties that were used in the conceptual and preliminary designs developed to date. Additional data are needed to define and confirm the estimates based on nonsite-specific data. Some of these data can be developed from core extracted from the repository horizon but most, especially rock mass properties, can only be developed once access is available to the repository horizon via the Exploratory Shaft.

Specific information, which is required but is not known to sufficient detail for resolving issues and satisfying system requirements, is presented in this section. This information is identified by synthesizing the data presented in Sections 2.1 through 2.8, and the issue resolution strategy is discussed in Section 8.2.1. The information needs are presented following the major subheadings of this chapter for ease of referencing and are listed in order of preliminary priorities. The information needs and prioritization will be discussed again in Section 8.1.1 and Section 8.1.2, which will then be fully coordinated with and cross referenced to specific elements of the overall project plan.

2.9.3.2 Mechanical properties of rock units--intact rock

The data base on mechanical properties of basalt from the Hanford Site is near sufficient for such properties as the uniaxial compressive strength of dense interior flow basalt, but the extent to which the strength will be affected by various factors needs to be defined further. Additional laboratory testing of core is planned to identify or further define the following.

o Lateral and vertical variation in strength and elastic properties.

o Effect of sample size and orientation on the strength and deformation of intact, partially jointed, and multiple-jointed samples.

o Effect of temperature, porosity, and moisture on the strength of intact basalt.

o Creep characteristics of basalt under elevated temperature conditions.

o Postfailure characteristics under compressive stresses and confining stress.

2.9.3.3 Mechanical properties of rock units--discontinuities

Currently there are no specific data on the mechanical properties of basalt joints from the Cohassett flow at the repository horizon. The effects of various parameters such as moisture, temperature, and test scale on the mechanical properties of joints are also not well understood. Since these are required for the development of rock mass models, additional site-specific testing of the basalt joints in the Cohassett flow is needed.

Information needs are identified in the following areas.

o Physical characteristics of joints in the Cohassett flow.

o Strength and deformational response of joints from the Cohassett flow.

o Effect of moisture and temperature on mechanical properties of joints with infill materials typical of repository conditions.

o Effect of joint size on mechanical properties.

o Creep of joints.

o· Effect of shear displacement on mechanical properties to evaluate the effect of disturbance due to excavation and (or) blasting on joints.

o Continued development of a joint deformation--strength models.

2.9.3.4 Mechanical properties of rock units--large scale

The large-scale mechanical properties of the basalt rock mass in the Cohassett flow have not been measured. The accuracy of constitutive models based on intact and joint mechanical properties are inadequate for repository design. Since the rock mass strength and deformability have a sufficient impact on the interpretation of constructibility and repository layout, a significant effort will be devoted to this information need.

Information needs are identified in the following areas.

o Deformational properties of in situ basalt rock mass in the Cohassett flow.

o Deformational properties of the disturbed basalt rock mass in the Cohassett flow.

o Yield criteria of rock mass.

o Effect of temperature on the mechanical properties of the rock mass.

o Hydrologic effects on the strength of the rock mass.

o Development of a rock mass constitutive model based on joint and intact mechanical properties and core hole or mapping data.

o Development of a fracture mechanics model of rock mass.

o Coupling between rock mass properties, stress, and hydraulic conductivity.

o Creep of rock mass.

2.9.3.5 Thermal and thermomechanical properties--intact rock

Information needs for thermal and thermomechanical properties of intact rock include the following:

o Site-specific data from Cohassett flow to demonstrate lateral and vertical variation within flows and flow tops.

o · Thermal and thermomechanical properties of secondary minerals, specifically joint infill materials.

o Correlation of thermal and thermomechanical properties with mineral content.

o Effect of moisture on properties.

2.9.3.6 Thermal and thermomechanical properties--large scale

Large-scale thermal and thermomechanical properties of the rock mass are required for repository design and performance assessment studies such as emplacement density of waste canisters, temperature profile of the repository, and thermal fracturing of rock. Tests conducted at the Near-Surface Test Facility on the Pomona flow indicate that these properties are reasonably close to the values determined from laboratory core samples. Further information needs are as follows:

o Thermal and thermomechanical properties of rock mass of the Cohassett dense interior, flow top, vesicular zone and surrounding flows.

o Anistropy effect.

o Influence of different rock mass structure on thermal and thermomechanical properties of rock mass.

o Potential of thermally induced fracture in the rock mass of the Cohassett flow.

2.9.3.7 Stress regime

The existing stress regime has been estimated by hydraulic fracturing tests from surface core holes. Because of the importance of the in situ stress conditions on the stability of the repository openings, continuing development of the hydraulic fracturing technique will be required and the results from these tests need to be confirmed by alternate borehole overcoring techniques. When subsurface access is available, specific information needs include the following.

o Validate lateral and vertical variations in stress both in the dense interior, flow tops, and vesicular zones of potential repository horizons.

o Study further the causes of borehole spalling and core disking and relate these occurrences to in situ stress, drilling conditions, and intact rock strengths.

o · Develop a model to incorporate the variation of site-specific
   vertical and lateral variation of rock quality and joint frequency
   in the variation of local stress.

o Develop alternate means of stress measurement in jointed rock at
   depth from core holes including either the hydraulic fracturing,
   crack reopening, modified fracturing fluids, or alternate schemes to
   provide a redundant method to measure stress throughout the
   reference repository location prior to extensive subsurface
   exploration and development.

o Continue development and testing to validate the hydraulic frac-
   turing technique under similar conditions to that of the Hanford
   Site to further quantify the uncertainties related to the pore
   pressure effect, shut-in pressure, and crack reopening pressure.

2.9.3.8 Special geoengineering properties

Special geoengineering properties that have been discussed include
stress-induced failure of openings, thermal degradation, potential for
shrinkage and swelling of joint infilling materials, and coupled effects.
Information needs are identified as follows:

o Potential of thermal fracturing of basalt in the Cohassett flow.

o Potential for shrinkage and swelling of joint infilling materials
   due to pressure, elevated temperature, or change in mineralogy.

o Mechanical/hydrological coupling.

o Mechanical-chemical/thermal-hydrological coupling.

o Coupled thermal/mechanical effects on conductivity and porosity of
   basalt.

o Potential of rock spalling and rock bursts in the repository
   openings and shafts.

2.9.3.9 Excavation characteristics

Excavation characteristics are important to the design of the repository. Most information needs in this area relate directly to design needs and the selected design methodology. For both empirical and analytical design methods, the following information needs are identified:

o Rock mass quality data from fresh core from the horizons studied and surrounding strata, incorporating rational method of accounting for core disking and healed (intact) fractures.

o Further definition of potential "weak" zones where fracture frequencies are high or joint orientations or conditions unfavorable.

o Response of excavation support systems to heat and temperature cycles.

o Development of analytical tools to model the interaction of the rock mass and the rock support system and demonstration that these tools are adequate by comparison of support loads with prediction in the Exploratory Shaft Facility.

o Further quantification of potential anomalous geologic conditions that could cause hydrologic connection with the flow top or bottom aquifers and cause high water inflow during construction.

o Boundary of disturbed zone.

o Thickness of damaged zone, its porosity, diffusion coefficient, hydraulic conductivity, and sorption coefficient.

2.9.4 RELATION TO REGULATORY GUIDE 4.17

The content of this chapter follows the annotated outline developed by the DOE from the Regulatory Guide 4.17 (NRC, 1983). Changes from Regulatory Guide 4.17 involve minor changes in nomenclature and changes in order of presentation to aid the development of the data package as shown in Table 2.9-2.

2.10 REFERENCES

Agapito, J. F. T., 1974. Rock Mechanics Applications to the Design of Oil Shale Pillars, Preprint Number 74-AIME-26, Society of Mining Engineers of Aime, New York, New York. [MF 2002; NV; C-4; NHC]

Agapito, J. F. T., M. P. Hardy, and D. R. St. Laurent, 1977. Geoengineering Review and Proposed Program Outline for the Structural Design of a Radioactive Waste Repository in Columbia Plateau Basalt, RHO-ST-6, Rockwell Hanford Operations, Richland, Washington. [MF 1044; V; C-N; HC]

Amadei, B., and R. E. Goodman, 1981. "A Three-Dimensional Constitutive Relationship for Fractured Rock Masses," Proceedings, Part B, International Symposium on the Mechanical Behavior of Structured Media, Ottawa, Selvadurai, A.P.S. (ed.), pp. 249-268. [MF 3232; NV; C-__; NHC]

Ames, R. R., 1986. Near-Surface Test Facility Phase I Tests Rock Mass Thermal Property Determinations, SD-BWI-TI-314, REV 0, Applied Mechanics, Inc., for Rockwell Hanford Operations, Richland, Washington. [MF 1203; V; C-N; HC]

AMI, 1983. Task IV Report on Thermal Modeling of Near-Surface Test Facility Heater Tests Using ANSYS and DAMSWEL, Applied Mechanics, Incorporated for Rockwell Hanford Operations, Richland, Washington.

AMI, 1986. Thermomechanical Analysis of Full-Scale Heater Tests 1 and 2 Conducted at the Near-Surface Test Facility, SD-BWI-TI-315, Applied Mechanics, Incorporated, Richland, Washington. [MF 2011; NV; C-N; NHC]

Arnett, R. C., R. G. Baca, J. A. Caggiano, S. M. Price, R. E. Gephart, and S. E. Logan, 1980. Preliminary Hydrologic Release Scenarios for a Candidate Repository Site in the Columbia River Basalts, RHO-BWI-ST-12, Rockwell Hanford Operations, Richland, Washington. [MF 0105; V; C-N; HC]

ASTM, 1986. Unconfined Compressive Strength of Intact Rock Core Specimens, Vol. 04.08, D2938, American Society of Testing and Materials, pp. 486-489. [MF 3252; NV; C-__; NHC]

Bai, S., W. Zhu, and K. Wang, 1983. "Some Rock Mechanics Problems Related to a Large Underground Power Station in a Region with High Rock Stress," Proceedings, 5th Congress, International Society of Rock Mechanics, Melbourne, Australia, pp. D271-D273.

Baker, S. M., 1985. A Preliminary Assessment of Water Inflow into Proposed Excavations in the Cohassett Flow Interior, SD-BWI-TI-274, REV 0, Rockwell Hanford Operations, Richland, Washington. [MF 1708; V; C-N; HC]

Bandis, S., A. C. Lumsden, and N. R. Barton, 1981. "Experimental Studies of Scale Effects on the Shear Behavior of Rock Joints," International Journal of Rock Mechanics and Mining Sciences and Geomechanics Abstracts, Vol. 18, pp. 1-21. [MF 0107; V; C-6; HC]

Bandis, S. C., A. C. Lumsden, and N. R. Barton, 1983. "Fundamentals of Rock Joint Deformation," International Journal of Rock Mechanics and Mining Sciences and Geomechanics Abstracts, Vol. 20, No. 6, pp. 249-268. [MF 3218; V; C-6; HC]

Barton, N. R., 1971. "A Relationship Between Joint Roughness and Joint Shear Strength," Proceedings, International Symposium on Rock Mechanics, Nancy, Paper 1-8. [MF 2029; NV; C-18; NHC]

Barton, N. R., 1973. "Review of a New Shear-Strength Criterion for Rock Joints," Engineering Geology, Vol. 7. [MF 0112; V; C-17; HC]

Barton, N. R., 1982. Modeling Rock Joint Behavior from In Situ Block Tests: Implications for Nuclear Waste Repository Design, ONWI-308. [MF 0114; V; C-N; HC]

Barton, N. R., 1984. Rock Mass Quality and Support Recommendations for Basalt at the Candidate Repository Horizon, Based on the Q-System, SD-BWI-ER-012, REV 1, Terra Tek Engineering for Rockwell Hanford Operations, Richland, Washington. [MF 1989; V; C-N; HC]

Barton, N. R., R. Lien, and J. Lunde, 1974. "Engineering Classification of Rock Masses for the Design of Tunnel Support," Rock Mechanics, Vol. 6, No. 4, pp. 189-236. [MF 0014; V; C-16; HC]

Barton, N. R., and V. Choubey, 1977. "The Shear Strength of Rock Joints in Theory and Practice," Rock Mechanics, Vol. 10, No. 1-2, pp. 1-54. [MF 2600; V; C-16; HC]

Benson, L. V., and L. S. Teague, 1979. A Study of Rock-Water-Nuclear Waste Interactions in the Pasco Basin, Washington, LBL-9677, Lawrence Berkeley Laboratory, Berkeley, California. [MF 0512; NV; C-N; NHC]

Bergman, S. G. A., and H. Stille, 1983. "Rock Burst Problems in a 2.6 Million M^3 Underground Crude Oil Storage in Granite," Proceedings, 5th Congress of the International Society of Rock Mechanics, Melbourne, Australia, pp. D301-D309. [MF 2039; V; C-18; HC]

Beus, M. J., and S. S. M. Chan, 1980. "A Structural Approach to Shaft Design for Deep Mines in Hard Rock," Proceedings, 21st U.S. Symposium on Rock Mechanics, University of Missouri, Rolla, Missouri, pp. 780-786. [MF 0126; V; C-18; HC]

Bieniawski, Z. T., 1974. Advances in Rock Mechanics, Vol. II, Part A, "Geomechanics Classification of Rock Masses and Its Application in Tunneling," in Proceedings, 3rd International Congress of the International Society for Rock Mechanics, September 1-7, Denver, Colorado, pp. 27-32. [MF 2602; V; C-42; HC]

Bieniawski, Z..T., 1976. "Rock Mass Classifications in Rock Engineering,"
Proceedings, Symposium on Exploration for Rock Engineering,
Johannesburg, South Africa, pp. 97-106. [MF 1008; V; C-32; HC]

Bieniawski, Z. T., 1978. "Determining Rock Mass Deformability: Experience
from Case Histories," International Journal of Rock Mechanics and Mining
Sciences & Geomechanics Abstracts, Vol. 15, pp. 237-247. [MF 0127; V;
C-6; HC]

Bieniawski, Z. T., 1979. "The Geomechanics Classification in Rock Engineering
Applications," Proceedings, 4th International Congress on Rock Mechanics,
International Society of Rock Mechanics, Montreaux, Switzerland, Vol. 2,
pp. 41-48. [MF 1009; V; C-N; HC]

Bieniawski, Z. T., and W. L. Van Heerden, 1975. "The Significance of In Situ
Tests on Large Rock Specimens," International Journal of Rock Mechanics
and Mining Sciences & Geomechanics Abstracts, Vol. 12, No. 4,
pp. 101-113. [MF 0128; V; C-6; HC]

Black, M. T., and M. L. Cramer, 1983. The Design and Construction of a Block
Test in Closely Jointed Rock, RHO-BW-SA-286 P, Rockwell Hanford
Operations, Richland, Washington. [MF 2045; V; C-N; HC]

Blake, W., 1982. "Destressing to Control Rock Bursting," Underground Mining
Methods Handbook, W. Hustrulid (ed.), Society of Mining
Engineers-American Institute of Mining, Metallurgical, and Petroleum
Engineers, pp. 1535-1539. [MF 0133; V; C-4; HC]

Blake, W., 1984. Assessment of the Rock Burst Potential in Basalt at the
Hanford Site, SD-BWI-ER-010, REV 0, Rockwell Hanford Operations,
Richland, Washington, 82 pp. [MF 1718; V; C-N; HC]

Blake, W., and F. Leighton, 1968. "Recent Developments and Applications of
the Microseismic Method in Dep. Mines," Proceedings, 8th U.S. Symposium
on Rock Mechanics, University of Minnesota. [MF 2048; NV; C-19; NHC]

Boldt and Henneke, 1981. "Tunnel Boring Under Coal Mining Conditions,"
Proceedings, Vol. 1, Rapid Excavation and Tunneling Conference,
San Francisco, California, May 3-7, pp. 722-737. [MF 2049; V; C-4; HC]

Brady, B. H. G., 1977. "An Analysis of Rock Behaviour in an Experimental
Stoping Block at the Mount Isa Mine, Queensland, Australia,"
International Journal of Rock Mechanics and Mining Sciences &
Geomechanics Abstracts, Vol. 14, pp. 59-66. [MF 2061; V; C-6; HC]

Brady, B. H. G., M. L. Cramer, and R. D. Hart, 1984. Preliminary Analysis of
a Loading Test on a Large Basalt Block, RHO-BW-SA-432 P, Rockwell Hanford
Operations, Richland, Washington. [MF 3233; NV; C-N; NHC]

Brady, B. H. G., and R. D. Hart, 1981. Pre-Test Analysis of Step 2 of the Jointed Block Test, RSD-BWI-TI-059, REV A000, Rockwell Hanford Operations, Richland, Washington. [MF 3227; NV; C-N; NHC]

Brechtel, 1985. Triaxial Shear Testing of Twenty Jointed Basalt Core Samples, SD-BWI-TD-018, Rockwell Hanford Operations, Richland, Washington.

Brechtel, C. E., 1986. Further Data Analysis for Triaxial Shear Testing of Joint Pomona Basalt Cores, Computational Brief No. (   ), Rockwell Hanford Operations, Richland, Washington. (Not released) [MF 2608; NV; C-N; NHC]

Bredehoeft, J. D., R. G. Wolff, W. S. Keys, and E. Shuter, 1976. "Hydraulic Fracturing to Determine the Regional In-Situ Stress Field, in the Piceance Basin, Colorado," Geological Society of America Bulletin, Vol. 87, pp. 250-258. [MF 0139; V; C-13; HC]

Brown, E. T., 1970. "Strength of Models of Rock with Intermittent Joints ASCE," Journal of the Soil Mechanics and Foundation Division, pp. 1935-1949. [MF 0148; V; C-45; HC]

Byerlee, J., 1978. "Friction of Rocks," Pure and Applied Geophysics, Vol. 116, pp. 615-626. [MF 0155; V; C-16; HC]

Caggiano, J. A., and D. W. Duncan (eds.), 1983. Preliminary Interpretation of the Tectonic Stability of the Reference Repository Location, Cold Creek Syncline, Hanford Site, RHO-BW-ST-19 P, Rockwell Hanford Operations, Richland, Washington. [MF 1045; V; C-N; HC]

Caw, J. M., 1956. "The Kolar Gold Field," Mine and Quarry Engineering, pp. 258-268. [MF 2078; NV; C-__; NHC]

Chan, T., N. Littlestone, and O. Wan, 1980. "Thermomechanical Modeling and Data Analysis for Heating Experiments at Stripa, Sweden," Rock Mechanics a State of the Art, Proceedings, 21st Symposium on Rock Mechanics, Rolla, Missouri, May 28-30, pp. 16-25. [MF 2673; V; C-42; HC]

Chan, T., and J. A. Jeffrey, 1983. "Scale and Water-Saturation Effects for Thermal Properties of Low-Porosity Rock," Rock Mechanics Theory - Experiment - Practice, C. C. Mathewson (ed.), Proceedings of the 24th U.S. Symposium on Rock Mechanics, June 20-23, pp. 287-301. [MF 2609; V; C-31; HC]

Chaoui, A., M. Mariotti, and M. Orliac, 1970. "In Situ Calcareos Marls Strain and Shear Strength - Comparison Between Different Tests-Characteristics," Proceedings of the Second Congress of the International Society for Rock Mechanics, Vol. 2, Paper 3-50, Belgrade, Yugoslavia. [MF 0162; V; C-18; HC]

Clark, Jr., S. P., 1966. "Thermal Conductivity," Handbook of Physical Constants, Memoir 97, S. P. Clark, Jr. (ed.), The Geological Society of America, Inc., New York, New York, pp. 94 and 461. [MF 2081; V; C-13; HC]

Coates, D. F., H. U. Bielonstein, and D. G. F. Hedley, 1973. "A Rock Mechanics Case History of Elliot Lake," Canadian Journal of Earth Science, Vol. 10, No. 7, pp. 1023-1057. [MF 0522; V; C-12; HC]

Cottam, A. E., 1983. An Evaluation of the Extent and Properties of the Zone of Disturbed Rock Around a Vertical Shaft Excavated Through Basalt Flows at the Basalt Waste Isolation Project Site, SD-BWI-TI-128, REV 0-0, Rockwell Hanford Operations, Richland, Washington. [MF 2649; V; C-N; HC]

Coulson, J. H., 1971. "Shear Strength of Flat Surfaces in Rock," Stability of Rock Slopes, E. J. Cording (ed.), Proceedings, Thirteenth Symposium on Rock Mechanics, Urbana, Illinois, August 30-September 1, pp. 77-105. [MF 2649; V; C-45; HC]

Cramer, M. L., 1984. Supporting Document Test Plan for Jointed Block Test #1, SD-BWI-TP-001, REV 2, Rockwell Hanford Operations, Richland, Washington. [MF 0405; V; C-N; HC]

Cramer, M. L., 1985. Triaxial Shear Testing of Twenty Jointed Basalt Core Samples, SD-BWI-TD-018, J. F. T. Agapito and Associates, Inc., for Rockwell Hanford Operations, Richland, Washington. [MF 2607; V; C-N; HC]

Cramer, M. L., and K. Kim, 1985, Block Test #1 Interim Report: Results from Experimental and Numerical Analyses at Ambient Temperature, SD-BWI-TD-015, REV 0, Rockwell Hanford Operations, Richland, Washington. [MF 3201; V; C-N; HC]

Cramer, M. L., G. T. Berlin, R. E. Heath, and J. J. Keating, 1985. Block Test #1 Final Report: Results from Experimental and Numerical Analyses at Elevated Temperature, SD-BWI-TD-023, REV 0, Rockwell Hanford Operations, Richland, Washington. [MF 3234; NV; C-N; NHC]

Crane, W. R., 1929a. "Mining Methods and Practice in the Michigan Copper Mines," U.S. Bureau of Mines Bulletin 306, U. S. Department of Commerce, Washington, D.C. [MF 0181; V; C-N; HC]

Crane, W. R., 1929b. "Rock Bursts in the Lake Superior Copper Mines, Keweenaw Point, Mich.," U.S. Bureau of Mines Bulletin 309, U.S. Department of Commerce, Washington, D.C. [MF 0182; V; C-N; HC]

Cross, R. W., 1985. Deep Borehole Stratigraphic Correlation Charts, SD-BWI-DP-035, REV 3, Rockwell Hanford Operations, Richland, Washington. [MF 0407; V; C-N; HC]

CSM, 1978. Final Report for the Fiscal Year 1978 on the Physical and Thermal Properties of Basalt Core, RHO-BWI-C-38, Colorado School of Mines Excavation Engineering and Earth Mechanic Institute for Rockwell Hanford Operations, Richland, Washington. [MF 0523; V; C-N; HC]

Cundall, P. A., 1980. UDEC - A Generalized Distinct Element Program for Modeling in Jointed Rock, Final Report, PCAR-1-80, Peter Cundall Associates, Virginia Waters, England. [MF 0186; V; C-N; HC]

Cundall, P. A., and R. D. Hart, 1985. Development of a Generalized 2-D and 3-D Distinct Element Program for Modeling Jointed Rock, Final Report, Miscellaneous Paper SL-85-1, ITASCA Consulting Group, Inc., for the Department of the Army, U.S. Army Corps of Engineers, Washington, D.C.

Curtis, J. F., 1981. "Rockburst Phenomena in the Gold Mines of the Witwatersrand: a Review," Transactions, Sec. A, Vol. 90, pp. A163-A176. [MF 2097; V; C-55; HC]

Deere, D. U., A. H. Merritt, and R. F. Coon, 1969. Engineering Classification of In Situ Rock, AFWL-TR-67-144, Department of Civil Engineering, University of Illinois, for Air Force Weapons Laboratory, Air Force Systems Command, Kirtland Air Force Base, New Mexico. [MF 3235; NV; C-N; NHC]

de la Cruz, R. V., M. Karfakis, and K. Kim, 1982. Analysis of Displacement of Strain Data for the Determination of the In Situ Deformability of Rock Masses, RHO-BW-SA-197 P, Rockwell Hanford Operations, Richland, Washington. [MF 0199; V; C-N; HC]

DeJongh, C. L., and J. W. Klokow, 1983. "The Use of a Seismic Network as a Management Tool, " International Congress on Rock Mechanics, Vol. 2, International Society of Rock Mechanics, Melbourne, Australia, pp. D1-D7. [MF 2103; V; C-18; HC]

Dempster, E. L., J. A. Tyser, and H. Wagner, 1983. "Regional Aspects of Mining-Induced Seismicity: Theoretical and Management Considerations," Rockbursts: Prediction and Control, Institution of Mining and Metallurgy, London W1, England, pp. 37-52. [MF 2611; V; C-55; HC]

De Reeper, F., 1966. "Design and Execution of Field-Pressure Tests up to Pressures of 2000 kg/cm^2," Proceedings of the First Congress of the International Society for Rock Mechanics, Lisbon, Portugal, pp. 613-619. [MF 0200; V; C-18; HC]

Dietrich, J. H., 1972. "Time-dependent Friction in Rocks," Journal of Geophysical Research, Vol. 77, No. 20, pp. 3690-3697. [MF 2109; NV; C-9; NHC]

Dischler, S. A., and K. Kim, 1985. "Determination of Rock Mass Deformation Modulus During Hydraulic Fracturing," Research and Engineering Applications in Rock Masses, Proceedings of the 26th U.S. Symposium on Rock Mechanics, Rapid City, South Dakota. [MF 3236; NV; C-16; NHC]

Dodds, D. J., 1974. Interpretation of Plate Loading Results, Field Testing and Instrumentation of Rock, ASTM STP-554, American Society for Testing and Materials, pp. 20-34. [MF 2113; V; C-58; HC]

DOE, 1982. Site Characterization Report for the Basalt Waste Isolation Project, DOE/RL 82-3, 3 Vol., Rockwell Hanford Operations for the U.S. Department of Energy, Washington, D.C. [MF 2119; V; C-N; HC]

DOE, 1985. Draft Environmental Assessment, Reference Repository Location, Hanford Site, Washington, DOE/RW-0017, Rockwell Hanford Operations for the U.S. Department of Energy, Washington, D.C. [MF 2125; V; C-N; HC]

Duncan, N., 1969. Engineering Geology and Rock Mechanics, Vol. II, International Textbook Co. Ltd., London, England, pp. 88-95. [MF 2134; V; C-16; HC]

Duvall, W. I., R. J. Miller, and F. D. Wang, 1978. Preliminary Report on Physical and Thermal Properties of Basalt, Drill Hole DC-10, Pomona Flow, Gable Mountain, RHO-BWI-C-11, Rockwell Hanford Operations, Richland, Washington. [MF 0207; V; C-N; HC]

Einstein, H. H., R. A. Nelson, R. W. Bruhn, and R. C. Hirschfeld, 1970. "Model Studies of Jointed-Rock Behavior," Rock Mechanics - Theory and Practice, Proceedings, Eleventh Symposium on Rock Mechanics, American Institute of Mining, Metallurgical, and Petroleum Engineers, Inc., New York, New York, pp. 83-103. [MF 2147; V; C-55; HC]

Elfman, S., 1969. "Design of a Tunnel in a Rock Burst Zone," Proceedings, International Symposium on Large, Permanent Underground Openings, Oslo, Norway, pp. 79-85. [MF 2148; V; C-__; HC]

Engineers International, Inc., 1982. Evaluation of the Joint Creep Response of Basalt, Subcontract #SA-581, Engineers International, Inc., for Rockwell Hanford Operations, Richland, Washington. [MF 2150; NV; C-N; NHC]

Erikson, R. L., and K. M. Krupka, 1980. Thermal Property Measurements of Pomona Member Basalt from Core Holes DB-5 and DB-15, Hanford Site, Southeastern Washington, RHO-BWI-C-76, Rockwell Hanford Operations, Richland, Washington. [MF 2158; V; C-N; HC]

Fairhurst, C., 1964. "Measurement of In Situ Rock Stresses, with Particular Reference to Hydraulic Fracturing," Rock Mechanics and Engineering Geology, Vol. II, No. 3-4, pp. 129-147. [MF 2163; V; C-16; HC]

FSI, 1980a. Thermal/Mechanical Properties of Pomona Member Basalt - Full-Scale Heater Test #1 (Area 1), RHO-BWI-C-77, Foundation Sciences, Inc., for Rockwell Hanford Operations, Richland, Washington. [MF 0217; V; C-N; HC]

FSI, 1980b. Thermal/Mechanical Properties of Pomona Member Basalt - Full-Scale Heater Test #2 (Area 2), RHO-BWI-C-85, Foundation Sciences, Inc., for Rockwell Hanford Operations, Richland, Washington. [MF 0218; V; C-N; HC]

FSI, 1980c. Thermal/Mechanical Properties of Pomona and Umtanum Basalts--Elevated Temperature Comparative Triaxial Test, RHO-BWI-C-91, Foundation Sciences, Inc., for Rockwell Hanford Operations, Richland, Washington.

FSI, 1981a. Thermal/Mechanical Properties of Umtanum Basalt--Borehole DC-2, RHO-BWI-C-92, Foundation Sciences, Inc., for Rockwell Hanford Operations, Richland, Washington. [MF 2175; V; C-N; HC]

FSI, 1981b. Thermal/Mechanical Properties of Pomona Member Basalt - Area 3 and Summary, RHO-BWI-C-100, Foundation Sciences, Inc., for Rockwell Hanford Operations, Richland, Washington. [MF 2176; V; C-N; HC]

Georgi, F., K. H. Hofer, P. Knoll, W. Menzel, and K. Thoma, 1970. "Investigations About the Fracture and Deformation Behaviour of Rock Masses," Proceedings of the Congress of the International Society for Rock Mechanics, Vol. 2, Paper 3-43, Belgrade, Yugoslavia. [MF 0227; V; C-18; HC]

Gerogiannopoulos, N. G., 1979. A Critical State Approach to Rock Mechanics, Ph.D. dissertation, Imperial College, London, England. [MF 3237; NV; C-__; NHC]

Gerrard, C. M., 1982. "Elastic Models of Rock Masses Having One, Two and Three Sets of Joints," International Journal of Rock Mechanics and Mining Science & Geomechanics Abstracts, Vol. 19, pp. 15-23. [MF 3221; V; C-6; HC]

Gimm, W. A. R., E. Richter, and G. P. Rosetz, 1966. "A Study of the Deformation and Strength Properties of Rocks by Block Tests In Situ in Iron-Ore Mines," Proceedings of the Congress of the International Society for Rock Mechanics, Libson, Portugal, pp. 457-463. [MF 0228; V; C-18; HC]

Goodman, R. E., 1976. Methods of Geological Engineering in Discontinuous Rocks, West Publishing Company, St. Paul, Minnesota, p. 171. [MF 2192; NV; C-74; NHC]

Goodman, R. E., 1980. Introduction to Rock Mechanics, John Wiley & Sons, New York, New York, p. 58. [MF 2193; V; C-__; HC]

Gough, D. I., and J. S. Bell, 1981. "Stress Orientations from Oil-Well Fractures in Alberta and Texas," Canadian Journal of Earth Science, Vol. 18, pp. 638-645. [MF 2194; V; C-12; HC]

Graham, P. C., 1976. "Some Problems Associated with the Use of a Tunnel Machine in Deep-Level Gold Mines," Tunneling '76, M. J. Jones (ed.), Proceedings of an International Symposium, the Institution of Mining and Metallurgy, London, England, March 1-5, pp. 397-410. [MF 2195; V; C-55; HC]

Gregory, C., M. Cramer, R. Ames, and J. McHenry, 1983a. "Applicability of Borehole Stress Measurement Instrumentation to Closely Jointed Rock," Rock Mechanics Theory - Experiment - Practice, Proceedings, 24th U.S. Symposium on Rock Mechanics, College Station, Texas, pp. 283-285. [MF 0234; NV; C-31; NHC]

Gregory, E. C., T. A. Rundle, J. M. McHenry, W. M. McCabe, K. Kim, B. A. Leijon, R. M. Nolting, and R. E. Goodman, 1983b. An Assessment of the Suitability of Five Overcoring Techniques for Stress Determination in a Jointed Basalt, SD-BWI-TI-129, Rockwell Hanford Operations, Richland, Washington. [MF 2617; NV; C-N; NHC]

Gronseth, J. M., and P. R. Kry, 1983. "Instantaneous Shut-In Pressure and Its Relationship to the Minimum In-Situ Stress," Proceedings of a Workshop on Hydraulic Fracturing Stress Measurements, National Academy Press, pp. 55-60. [MF 3238; NV; C-__; NHC]

Haimson, B. C., 1968. Hydraulic Fracturing in Porous and Nonporous Rock and its Potential for Determining In-Situ Stresses at Great Depth, Technical Report No. 4-68, U.S. Army Corps of Engineers; also published as Ph.D. dissertation, University of Minnesota, Minneapolis, Minnesota. [MF 3239; NV; C-19; NHC]

Haimson, B. C., 1979. "Hydrofracturing Tests for In Situ Stress Measurement-Near-Surface Test Facility, Hole DC-11, Hanford Reservation," Heater Test Planning for the Near-Surface Test Facility at the Hanford Reservation, LBL 8730, Vol. 2, Lawrence Berkeley Laboratory, Berkeley, California, pp. 10-1 to 10-19. [MF 2205; V; C-N; HC]

Haimson, B. C., 1983. "A Comparative Study of Deep Hydrofracturing and Overcoring Stress Measurements at Six Locations With Particular Interest to the Nevada Test Site," Proceedings of a Workshop on Hydraulic Fracturing Stress Measurements, National Academy Press, pp. 107-118. [MF 3240; NV; C-__; NHC]

Handin, J., 1966. "Strength and Ductility," Handbook of Physical Constants, Memoir 97, S. P. Clark (ed.), The Geological Society of America, Inc., New York, New York, pp. 223-289. [MF 2214; V; C-13; HC]

Hardin, E., N. Barton, D. Lingle, M. Board, and M. Voegele, 1982. A Heated Flatjack Test Series to Measure the Thermomechanical and Transport Properties of In Situ Rock Masses ("Heated Block Test"), ONWI-260, Terra Tek, Inc., for the Office of Nuclear Waste Isolation. [MF 2213; V; C-N; HC]

Hardy, M. P., and G. Hocking, 1979. Rock Mechanics Design Criteria for a Repository in Basalt, for Rockwell Hanford Operations, Richland, Washington.

Hardy, M. P., and G. Hocking, 1980. Rock Mechanics Design Criteria for Repository Design in Hard Rock, American Society of Civil Engineers Annual Meeting, Portland. [MF 3229; HC; C-45; NHC]

Hardy, M. P., and S. J. Mitchell, 1985. Boundary Conditions on the Jointed Block Test, A Two-Dimensional and Three-Dimensional Finite Element Analysis of Stresses and Temperatures, SD-BWI-TD-016, REV 0, Rockwell Hanford Operations, Richland, Washington. [MF 2217; V; C-N; HC]

Hart, R. D., P. A. Cundall, and J. V. Lemos, 1985. Analysis of Block Test No. 1 Inelastic Rock Mass Behavior Phase 4, Further Evaluation of Basalt Joint Behavior, for Rockwell Hanford Operations, Richland, Washington. [MF 2618; NV; C-N; NHC]

Heuze, F. E., 1980, "Scale Effects in the Determination of Rock Mass Strength and Deformability," Rock Mechanics, Vol. 12, No. 3-4, pp. 167-192. [MF 3202; V; C-16; HC]

Hickman, S. H., and M. D. Zoback, 1983. "Interpretation of Hydraulic Fracturing Pressure-Time Data for In Situ Stress Determination," Proceedings of Workshop XVII, Workshop on Hydraulic Fracturing Stress Measurements, Open-File Report 82-1075, Vol. I, U.S. Geological Survey, Menlo Park, California, pp. 103-146. [MF 3241; NV; C-__; NHC]

Hill, R., 1963. "Elastic Properties of Reinforced Solids: Some Theoretical Principles," Journal of the Mechanics and Physics of Solids, Vol. 11, pp. 357-372. [MF 3217; V; C-6; HC]

Hocking, G., J. R. Williams, P. Boonlualohr, I. Mathews, and G. Mustoe, 1980. Numerical Prediction of Basalt Response for Near Surface Test Facility Heater Test #1 and #2, RHO-BWI-C-86, Rockwell Hanford Operations, Richland, Washington. [MF 0247; V; C-N; HC]

Hoek, E., 1984. "Strength of Jointed Rock Masses, 1983 Rankine Lecture," Geotechnique, Vol. 33, No. 187, pp. 187-223. [MF 3242; NV; C-__; NHC]

Hoek, E., and E. T. Brown, 1980. Underground Excavations in Rock, Institution of Mining and Metallurgy, London, England, pp. 98, 132, 137-139, 168, 174, 176, 217, 218, and 283. [MF 2231; V; C-55; HC]

Hooker, V. E., and D. L. Bickel, 1974. Overcoring Equipment and Techniques Used in Rock Stress Determination, Information Circular No. 8618, U.S. Bureau of Mines. [MF 2238; V; C-N; HC]

Hubbert, M. K., and D. G. Willis, 1957. "Mechanics of Hydraulic Fracturing," Trans. American Institute of Mining, Metallurgical, and Petroleum Engineers, Vol. 210, pp. 153-166. [MF 2243; V; C-4; HC]

Hulstrom, L. C., and D. J. Hanson, 1982a. The Effect of Sample Size on the
Uniaxial Compressive Strength of Core from the Umatilla Flow,
SD-BWI-TI-106, Rockwell Hanford Operations, Richland, Washington.
[MF 0412; V; C-N; HC]

Hulstrom, L. C., and D. J. Hanson, 1982b. Tabulation of Physical and
Mechanical Property Data from Borehole RRL-2, SD-BWI-TD-002, REV 0-1,
Rockwell Hanford Operations, Richland, Washington. [MF 0413; V; C-N; HC]

Hulstrom, L. C., and D. J. Hanson, 1983a. Tabulation of Physical and
Mechanical Property Data from Borehole RRL-14, SD-BWI-TD-004, REV 0-1,
Rockwell Hanford Operations, Richland, Washington. [MF 0414; V; C-N; HC]

Hulstrom, L. C., and D. J. Hanson, 1983b. Tabulation of Physical and
Mechanical Property Data from Borehole RRL-6, SD-BWI-TD-003, REV 0-0,
Rockwell Hanford Operations, Richland, Washington. [MF 0415; V; C-N; HC]

Hulstrom, L. C., 1984. Tabulation of Physical and Mechanical Property Data
Supporting Post-Test Data Characterization of the Full Scale Heater
Test #2 Area at the NSTF, SD-BWI-TD-008, REV 0-0, Rockwell Hanford
Operations, Richland, Washington. [MF 2244; V; C-N; HC]

Hulstrom, L. C., 1985. Supplemental Calculations to Support Section 2.1,
'Mechanical Properties of Rock Units-Intact Rock' of BWIP SCP,
Computational Brief No. 00218, Rockwell Hanford Operations, Richland,
Washington. [MF 2622; V; C-N; HC]

Huyakorn, W., and J. R. Thomas, 1981. Analysis of Thermal Properties of
Basalt from Heater Test #2 Experiement, RSD-BWI-TI-023, Rockwell Hanford
Operations, Richland, Washington.

Jaeger, J. C., and N. G. W. Cook, 1963. "Pinching-Off and Disking of Rocks,"
Journal of Geophysical Research, Vol. 68, No. 6, pp. 1759-1765.
[MF 2254; V; C-9; HC]

Jahns, H., 1966. "Measuring the Strength of Rock In Situ at an Increasing
Scale," Proceedings of the Congress of the International Society for Rock
Mechanics, Lisbon, Portugal, pp. 477-482. [MF 0257; V; C-18; HC]

Jansson, G., 1979. "Problems Associated with Heavy Water Leakage during
Construction of Large Area Tunnels in Granite, Limestone and Chalk,"
Tunnelling Under Difficult Conditions, I. Kitamura (ed.), Proceedings of
the International Tunnel Symposium, Tokyo, Japan, pp. 187-192. [MF 3207;
V; C-6; HC]

Jeffrey, J. A., T. Chan, N. G. W. Cook, and P. A. Witherspoon, 1979.
Determination of In-Situ Thermal Properties of Stripa Granite from
Temperature Measurements in the Full Scale Heater Experiements, Method
and Preliminary Results, LBL-8423, Swedish-American Cooperative Program
on Radioactive Waste Storage in Mined Carvers in Crystalline Rock,
Lawrence Berkeley Laboratory, Berkeley, California. [MF 0258; V; C-N;
HC]

KE/PB, 1986. Site Characterization Plan, Conceptual Design Report, Project B-301, Task V Engineering Study 10, Kaiser Engineers, Inc./Parsons Brinkerhoff Quade & Douglas for Rockwell Hanford Operations, Richland, Washington. [MF 3243; NV; C-N; NHC]

Kasza, G. L., 1986. Photographic Comparison of the Pre-Test and Post-Test Heater Hole Wall Condition in the Full Scale Heater Tests, RHO-BWI-TI-276, REV 0, Hanford Operations, Richland, Washington. [MF 1108; V; C-N; HC]

Kelsall, P. C., J. B. Case, and C. R. Chabannes, 1982. A Preliminary Evaluation of the Rock Mass Disturbance Resulting from Shaft, Tunnel, or Borehole Excavation, ONWI-411, Office of Nuclear Waste Isolation, Battelle Memorial Institute, Columbus, Ohio. [MF 2269; V; C-__; HC]

Kelsall, P. C., J. B. Case, and C. R. Chabannes, 1984. "Evaluation of Excavation-induced Changes in Rock Permeability," International Journal of Rock Mechanics and Mining Science & Geomechanical Abstracts, Vol. 21, No. 3, pp. 123-135. [MF 2626; V; C-6; HC]

Keyser, D. J., and N. M. Krige, 1978. "Construction Problems in Water Tunnels in the Republic of South Africa," Tunnelling Under Difficult Conditions, I. Kitamura (ed.), Proceedings of the International Tunnel Symposium, Tokyo, Japan, pp. 223-232. [MF 3203; V; C-6; HC]

Kim, K., and B. C. Haimson, 1982. "In Situ Stress Measurement at a Candidate Repository Horizon," Proceedings of the 1982 National Waste Terminal Storage Program Information Meeting, DOE/NWTS-30, Office of NWTS Integration, Battelle Project Management Division for the U.S. Department of Energy, Washington, D.C., pp. 54-58. [MF 0049; V; C-N; HC]

Kim, K., S. A. Dischler, J. R. Aggson, and M. P. Hardy, 1986. The State of In Situ Stress Determined by Hydraulic Fracturing at the Hanford Site, RHO-BW-ST-73 P, Rockwell Hanford Operations, Richland, Washington. [MF 1075; V; C-N; HC]

King, M. S., L. R. Myer, and J. J. Rezowalli, 1984. "Cross-Hole Acoustic Measurements in Basalt," Rock Mechanics in Productivity and Protection, Proceedings of the Twenty-Fifth Symposium on Rock Mechanics, Evanston, Illinois, June 25-27, pp. 1053-1062. [MF 2276; V; C-4; HC]

Kirsch, G., 1898. "Die Theorie der Elastizitat und die Bedurforisse der Festigkeitslehre," Zietschrift des Vereines Duetscner Ingenieure, Vol. 42, p. 797. [MF 2277; NV; C-__; NHC]

Koifman, M. I., 1963. "The Size Factor in Rock-Pressure Investigations," Mechanical Properties of Rocks, M. M. Protod'yakonov, M. I. Koifman et al. (eds.), Academy of Sciences of the USSR (Union of Soviet Socialist Republics), translated by the Israel Program for Scientific Translations, Jerusalem, Israel (1969), pp. 109-117. [MF 2627; V; C-__; HC]

Korbin, C. E., 1979. Technical Services to Develop a Test Plan for Tunnel
    Boring Machine Demonstration, for Rockwell Hanford Operations, Richland,
    Washington. (not released) [MF 2280; NV; C-N; NHC]

Koster van Groos, A. F., 1981. Determination of Dehydration Temperatures of a
    Secondary Vug-Filling Mineral (Smectite Clay) Using a Differential
    Thermal Analysis at Various Pressures, RHO-BWI-C-102, Rockwell Hanford
    Operations, Richland, Washington. [MF 0268; V; C-N; HC]

Krech, W. A., F. A. Henderson, and K. E. Hjelmstad, 1974. A Standard Rock
    Suite for Rapid Excavation Research, Report of Investigations 7865, .
    U.S. Bureau of Mines, U.S. Department of Interior, Washington, D.C.
    [MF 0269; V; C-N; HC]

Krishnamurthy, R., 1969. "Investigations of Problems of Ground Control and
    Rockbursts in the Kolar Gold Field," I. E. (I) Journal - MM, Vol. 49,
    pp. 98-103. [MF 2628; V; C-__; HC]

Landon, R. D., 1983. Geologic Thickness Data - Candidate Repository Horizons,
    SD-BWI-DP-011, Rev. A-0, Rockwell Hanford Operations, Richland,
    Washington. [MF 0418; V; C-N; HC]

Lee, W. H., 1969a. Some Physical Properties of Rocks in Drill Hole UAe-2,
    Amchitka Island, Alaska, USGS-474-5, U.S. Geological Survey,
    Washington, D.C. [MF 0274; V; C-N; HC]

Lee, W. H., 1969b. Lithologic Log of Emplacement Drill Hole UA-1 from 5,000
    to 60,900 feet, Amchitka Island, Alaska, USGS-474-4, U.S. Geological
    Survey. [MF 2295; NV; C-N; NHC]

Lee, C. F., 1978. "Stress Induced Instability in Underground Excavations,"
    Proceedings, 19th U.S. Symposium on Rock Mechanics, Reno, Nevada,
    pp. 165-173. [MF 2294; V; C-__; HC]

Leeman, E. R., and A. J. Hayes, 1966. "A Technique for Determining the
    Complete State of Stress in Rock Using a Single Borehole," Proceedings,
    1st International Conference on Rock Mechanics, Lisbon, Portugal,
    pp. 17-24. [MF 0275; V; C-18; HC]

Lehnhoff, T. F., B. Stefansson, K. Thirumalai, and T. M. Wintczak, 1982. The
    Core Disking Phenomenon and Its Relation to In-Situ Stress at Hanford,
    SD-BWI-TI-085, Rockwell Hanford Operations, Richland, Washington.
    [MF 0051; V; C-N; HC]

Leijon, B. A., and B. L. Stillborg, 1986. "A Comparative Study Between Two
    Rock Stress Measurement Techniques at Luossavaara Mine," Rock Mechanics
    and Rock Engineering, Vol. 19, pp. 143-163. [MF 3244: NV; C-__; NHC]

Lindberg, J. W., 1986. Width and Infilling of Fractures in Four Grande Ronde Basalt Flows Beneath the Reference Repository Location, SD-BWI-TI-282, Rev. 0.0, Rockwell Hanford Operations, Richland, Washington, pp. 3-17. [MF 1797; V; C-N; HC]

Lindner, E. N., and J. A. Halpern, 1978. "In Situ Stress in North America: A Compilation," International Journal of Rock Mechanics and Mining Sciences & Geomechanics Abstracts, Vol. 15, pp. 183-203. [MF 2630; V; C-6; HC]

Loehr, 1983. "Specific Problems Connected with the Application of Full Face Tunneling Machines in German Coal Mines," Proceedings, Rapid Excavation and Tunneling Conference, Chicago, Illinois, June, pp. 761-768. [MF 2301; NV; C-__; NHC]

Logsters, G., and H. Voort, 1974. "In Situ Determination of the Deformational Behaviour of a Cubical Rock-Mass Sample Under Tri-Axial Load," Rock Mechanics, Vol. 6, No. 2, pp. 65-79. [MF 0277; V; C-16; HC]

Long, P. E., and WCC, 1984. Repository Horizon Identification Report, SD-BWI-TY-001 DRAFT, Vols. 1 and 2, Woodward-Clyde Consultants for Rockwell Hanford Operations, Richland, Washington. [MF 0057; V; C-N; HC]

Malone, S. D., G. H. Rothe, and S. W. Smith, 1975. "Details of Microearthquake Swarms in the Columbia Basin, Washington," Bulletin of the Seismological Society of America, Vol. 65, No. 4, pp. 855-864. [MF 2313; V; C-1; HC]

Martinez-Baez, L. F., and C. H. Amick, 1978. Thermal Properties of Gable Mountain Basalt Cores, Hanford Nuclear Reservation, LBL-7038, Lawrence Berkeley Laboratory for Rockwell Hanford Operations, Richland, Washington. [MF 0288; V; C-N; HC]

McLennan, J. D., and J. C. Roegiers, 1983. "Do Instantaneous Shut-In Pressures Accurately Represent the Minimum Principal Stress?" Proceedings, Hydraulic Fracturing Stress Measurements, National Academy Press, pp. 68-78. [MF 3245; NV; C-__; NHC]

Mendelsohn, A., 1931. Mining Methods and Costs at the Champion Copper Mine, Painesdale, Mich., Information Circular No. 6515, U.S. Department of Commerce, U.S. Bureau of Mines. [MF 2338; V; C-N; HC]

Miller, R. J., 1979a. Determination of Basalt Physical and Thermal Properties at Varying Temperatures, Pressures, and Moisture Contents, Third Progress Report, Fiscal Year 1979, RHO-BWI-C-55, Rockwell Hanford Operations, Richland, Washington. [MF 2331; V; C-N; HC]

Miller, R. J., 1979b. Determination of Basalt Physical and Thermal Properties at Varying Temperatures, Pressures, and Moisture Contents, Second Progress Report, Fiscal Year 1979, RHO-BWI-C-54, Rockwell Hanford Operations, Richland, Washington. [MF 2332; V; C-N; HC]

Miller, R. J., and R. C. Bishop, 1979. Determination of Basalt Physical and Thermal Properties at Varying Temperatures, Pressures, and Moisture Contents, RHO-BWI-C-50, Rockwell Hanford Operations, Richland, Washington. [MF 2333; V; C-N; HC]

Miner, G., 1982. "Cut- and Fill-Stoping at Star Mine," Underground Mining Methods Handbook, W. Hustrulid (ed.), Society of Mining Engineers-American Institute of Mining, Metallurgical, and Petroleum Engineers, pp. 549-553. [MF 2334; V; C-4; HC]

Mitchell, S. J., 1984a. Direct Shear Testing Data Reduction, Computational Brief No. 00066, Rockwell Hanford Operations, Richland, Washington. [MF 1078; V; C-N; HC]

Mitchell, S. J., 1984b. CSM (Colorado School of Mines) Jointed Triaxial Testing, Computational Brief No. 00208, Rockwell Hanford Operations, Richland, Washington. [MF 2339; V; C-N; HC]

Mitchell, S. J., 1984c. FS#2 Post-Test Lab-Testing, Computational Brief No. 00207, Rockwell Hanford Operations, Richland, Washington. [MF 2340; NV; C-N; NHC]

Moak, D. J., and T. M. Wintczak, 1980. Near-Surface Test Facility Phase I Geologic Site Characterization Report, RHO-BWI-ST-8, Rockwell Hanford Operations, Richland, Washington. [MF 0294; V; C-N; HC]

Mochida, Y., 1979. "Excavation of Expansive Ground Formation for the Seikan Undersea Tunnel Project," Tunneling '79, M. J. Jones (ed.), Proceedings of the Second International Symposium, the Institution of Mining and Metallurgy, London, England, March 12-16, pp. 220-241. [MF 3208; V; C-55; HC]

Montazer P., G. Chitombo, R. King, and W. Ubbes, 1982. "Spatial Distribution of Permeability Around CSM/ONWI Room Edgar Mine, Idaho Springs, Colorado," Issues in Rock Mechanics, Proceedings of the Twenty-Third Symposium on Rock Mechanics, Berkeley, California, August 25-27, pp. 47-56. [MF 2634; V; C-4; HC]

Morris, R. H., 1968. Technical Letter: Amchitka-11, Preliminary Lithologic Log of Drill Hole UAe-6C from 0- to 6,999 feet, Amchitka Island, Alaska, USGS-474-54, U.S. Geological Survey for the U.S. Atomic Energy Commission. [MF 2346; V; C-N; HC]

MSHA, 1985. Safety and Health Standards-Underground Metal and Nonmetal Mines, Title 30, Code of Federal Regulations, Part 57, U.S. Department of Labor, Mine Safety and Health Administration, Washington, D.C., pp. 4082-4126. [MF 3224; V; C-N; HC]

Myer, L., 1982. Results of Thermomechanical Tests on Specimens of Hanford Basalts, SD-BWI-TD-017, Rev. 0, Lawrence Berkeley Laboratory for Rockwell Hanford Operations, Richland, Washington. [MF 2329; NV; C-N; NHC]

Myer, L. R., J. J. Rezowalli, and M. S. King, 1983. Crosshole Seismic Tests at the Near-Surface Test Facility, SD-BWI-__-__, Lawrence Berkeley Laboratory for Rockwell Hanford Operations, Richland, Washington.

Myers, C. W., S. M. Price, J. A. Caggiano, M. P. Cockran, W. J. Czimer, N. J. Davidson, R. C. Edwards, K. R. Fecht, G. E. Holmes, M. G. Jones, J. R. Kunk, R. D. Landon, R. K. Legerwood, J. T. Lillie, P. E. Long, T. H. Mitchell, E. H. Price, S. P. Reidel, and A. M. Tallman, 1979. Geologic Studies of the Columbia Plateau: A Status Report, RHO-BWI-ST-4, Rockwell Hanford Operations, Richland, Washington. [MF 0001; V; C-N; HC]

Myers, C. W., and S. M. Price (eds.), 1981. Subsurface Geology of the Cold Creek Syncline, RHO-BWI-ST-14, Rockwell Hanford Operations, Richland, Washington. [MF 0067; V; C-N; HC]

Nelson, P., and C. Wilson, 1980. "Thermomechanical and Macropermeability Experiments in the Stripa Granite - Status Report," Proceedings, Workshop on Thermomechanical-Hydrochemical Modeling for a Hardrock Waste Repository, LBL-11204, Lawrence Berkeley Laboratory, Berkeley, California, pp. 45-55. [MF 2636; V; C-N; HC]

Nieble, C., N. F. Midea, F. Fujimura, and S. B. Neto, 1974. "Shear Strength of Typical Features of Basaltic Rock Masses--Parana Basin, Brazil," Proceedings, 3rd Congress, International Society of Rock Mechanics, Denver, Colorado, pp. 294-301. [MF 0299; V; C-36; HC]

Nishida, T., 1982. "Excavation of an Inclined Tunnel by Tunnel-Boring Machine," Tunneling 82, M. J. Jones (ed.), The Third International Symposium organized by the Institution of Mining and Metallurgy, London, England, pp. 145-152. [MF 2637; V; C-55; HC]

Nose, M., 1964. "Rock Tests In Situ, Conventional Tests on Rock Properties and Design of Kurobegawa No. 4 Dam Based Thereon," Trans., 8th Congress, Large Dams, ICOLD, Edinburgh, Scotland, pp. 219-252. [MF 2365, V; C __; HC]

NRC, 1983. Standard Format and Content of Site Characterization Plans for High-Level-Waste Geologic Repositories, Draft Regulatory Guide 4.17, U.S. Nuclear Regulatory Commission.

NRC, 1985. Disposal of High-Level Radioactive Wastes in Geologic Repositories; Licensing Procedures, Title 10, Code of Federal Regulations, Part 60, U.S. Nuclear Regulatory Commission, Washington, D.C. [MF 1986; V; C-N; HC]

Obert, L., and D. E. Stephenson, 1965. "Stress Conditions Under Which Core Discing Occurs," Society of Mining Engineers Transactions, Vol. 232, pp. 227-234. [MF 2375; V; C-4; HC]

Ortlepp, W. D., 1970. "An Empirical Determination of the Effectiveness of Rockbolt Support under Impulse Loading," Proceedings, International Symposium on Large Permanent Underground Openings, T. C. Brekke and F. A. Jorstad (eds.), Universitetsforlaget, Oslo, Norway, pp. 197-205. [MF 2382; V; C-__; HC]

Ortlepp, W. D., 1978. "The Mechanism of a Rockburst," Proceedings, 19th U.S. Symposium on Rock Mechanics, Reno, Nevada, pp. 476-483. [MF 2383; NV; C-__; NHC]

Ortlepp, W. D., 1983. "Considerations in the Design of Support for Deep Hard-Rock Tunnels," Proceedings, 5th International Congress on Rock Mechanics, International Society for Rock Mechanics, Melbourne, Australia, pp. D179-D187. [MF 2384; V; C-32; HC]

Ortlepp, W. D., and N. C. Gay, 1984. "Performance of an Experimental Tunnel Subjected to Stresses Ranging from 50 MPa to 230 MPa," Design and Performance of Underground Excavations, International Society of Rock Mechanics Symposium, Cambridge, United Kingdom, September 3-6, pp. 337-346. [MF 2641; V; C-18; HC]

Paillet, F. L., 1985. Acoustic-Televiewer and Acoustic-Waveform Logs Used to Characterize Deeply Buried Basalt Flows, Hanford Site, Benton County, Washington, Open-File Report 85-419, U.S. Geological Survey, Washington, D.C. [MF 2389; V; C-N; HC]

Patricio, J. G., 1985. Description of Spirit Lake Outlet Tunnel Project, Trip Report 10420-85-JGP-010, Rockwell Hanford Operations, Richland, Washington, January 18. [MF 2644; V; C-N; HC]

Petersen, D. L., 1978. Estimating the Strength of St. Peter Sandstone Pillars, M.S. thesis, University of Minnesota, Department of Civil and Mining Engineering, Minneapolis, Minnesota. [MF 2395; NV; C-__; NHC]

Pratt, H. R., A. D. Black, W. S. Brown, and W. F. Brace, 1972. "The Effect of Specimen Size on the Mechanical Properties of Unjointed Diorite," International Journal of Rock Mechanics and Mining Sciences & Geomechanics Abstracts, Vol. 9, pp. 513-529. [MF 2646; V; C-6; HC]

Pratt, H. R., A. D. Black, and W. F. Brace, 1974. "Friction and Deformation of Jointed Quartz Diorite," Proceedings, 3rd Congress, International Society of Rock Mechanics, Denver, Colorado, pp. 306-310. [MF 0310; V; C-18; HC]

Pratt, H. R., H. S. Swolfs, W. F. Brace, A. D. Black, and J. W. Handin, 1977. "Elastic and Transport Properties of an In Situ Jointed Granite," International Journal of Rock Mechanics and Mining Sciences & Geomechanics Abstracts, Vol. 14, pp. 35-45. [MF 1534; V; C-6; HC]

Ramspott, L. D., L. B. Ballou, and W. C. Patrick, 1982. Status Report on the Spent Fuel Test-Climax, Nevada Test Site: A Test of Dry Storage of Spent Fuel in the Deep Granite Location, UCRL-87448, Lawrence Livermore National Laboratory, Livermore, California, pp. 131-142. [MF 0313; V; C-N; HC]

Richter, E., 1968. Druckversuche In Situ Zur Bestimmung Von Verformungs-Und Festigkeitsparametern Des Kluftigen Gebirges, Bergakademie 20, pp. 721-724.

Riley, P. B., R. E. Goodman, and R. M. Nolting, 1977. "Stress Measurement by Overcoring Cast Photoelastic Inclusions," Energy Resources and Excavation Technology, F. Wang and G. B. Clark (eds.), Proceedings, 18th U.S. Symposium on Rock Mechanics, Keystone, Colorado, pp. 4C4-1 through 4C4-5. [MF 2426; V; C-36; HC]

RKE/PB, 1983. Conceptual System Design Description - Nuclear Waste Repository in Basalt, Project B-301, SD-BWI-SD-005, REV. 0-0, Vol. 1, Raymond Kaiser Engineers, Inc./Parsons Brinckerhoff Quade & Douglas for Rockwell Hanford Operations, Richland, Washington, p. C-14. [MF 2428; NV; C-N; NHC]

Robertson, E. C., and D. L. Peck, 1974. "Thermal Conductivity of Vesicular Basalt from Hawaii," Journal of Geophysical Research, Vol. 79, No. 32, pp. 4875-4888. [MF 2648; NV; C-9; NHC]

Rockwell, 1978. Final Report for Fiscal Year 1978 on the Physical and Thermal Properties of Basalt Cores, RHO-BWI-C-38, Colorado School of Mines for Rockwell Hanford Operations, Richland, Washington. [MF 0523; V; C-N; HC]

Rockwell, 1980b. "Rock Mechanics Field Test Results to Date," Basalt Waste Isolation Project Annual Report - Fiscal Year 1980, RHO-BWI-80-100, Rockwell Hanford Operations, Richland, Washington, pp. V26-V34. [MF 3204; V; C-N; HC]

Roegiers, J. C., and J. D. McLennan, 1983. "Factors Influencing the Initiation and Orientation of Hydraulically Induced Fractures," Proceedings, Workshop on Hydraulic Fracturing Stress Measurements, National Academy Press, pp. 176-180. [MF 3248; NV; C-__; NHC]

Rosengren, K. J., and J. C. Jaeger, 1968. "The Mechanical Properties of an Interlocked Low-Porosity Aggregate," Geotechnique, Vol. 18, pp. 317-326. [MF 1068; V; C-108; HC]

Roux, A. J. A., E. R. Leeman, and H. G. Denkhaus, 1957. "De-stressing: A Means of Ameliorating Rockburst Conditions," Journal of the South African Institute of Mining and Metallurgy, Vol. 58, pp. 101-119. [MF 2441; V; C-94; HC]

Roy, R. F., A. E. Beck, and Y. S. Touloukian, 1981. "Thermophysical Properties of Rocks," Physical Properties of Rocks and Minerals, Book 6, Chapter 12, Y. S. Touloukian and C. Y. Ho (eds.), McGraw-Hill, New York, New York, pp. 412-435. [MF 2442; V; C-59; HC]

Rummel, F., J. Baumgärtner, and H. J. Alheid, 1983. "Hydraulic Fracturing Stress Measurements along the Eastern Boundary of the SW-German Block," Proceedings, Workshop on Hydraulic Fracturing Stress Measurements, National Academy Press, pp. 3-17. [MF 3249; NV; C-__; NHC]

Rundle, T. A., and K. Kim, 1983. Summary of Borehole RRL-2 Hydraulic Fracturing Test Data and Data Analysis Methods, SD-BWI-TD-006, Rockwell Hanford Operations, Richland, Washington. [MF 0431; V; C-N; HC]

Russel, F. M., D. R. M. Armstrong, and R. Talbot, 1984. "Analysis of Stoping Sequence and Support Requirements in a High-Stress Environment - ZCCM, Mufulira Division," Rockbursts: Prediction and Control, Mining Industry, Institution of Mining and Metallurgy, Transactions, Section A, Vol. 93, pp. A1-A9. [MF 3211; V; C-55; HC]

Saito, T., K. Tsukada, E. Inami, H. Inoma, and Y. Ito, 1983. "Study on Rock Bursts at the Face of a Deep Tunnel (the Kon-Etsu Tunnel in Japan being an example)," Proceedings, 5th Congress, International Society of Rock Mechanics, Melbourne, Australia, pp. B9-B12. [MF 1004; V; C-18; HC]

Salamon, M. D. G., and A. H. Munro, 1967. "A Study of the Strength of Coal Pillars," Journal of the South African Institute of Mining & Metallurgy, Vol. 68, pp. 55-67. [MF 2447; V; C-94; HC]

Schmidt, B., W. F. Daly, S. W. Bradley, P. R. Squire, and L. C. Hulstrom, 1980. Thermal and Mechanical Properties of Hanford Basalt: Compilation and Analyses, RHO-BWI-C-90, Rockwell Hanford Operations, Richland, Washington. [MF 0327; V; C-N; HC]

Schneider, B., 1967. "Moyens Nouveaux de Reconnaissance des Massifs Rocheux," Supp. to Annales de L'Inst. Tech. de Batiment et des Travaux Publics, Vol. 20, No. 235-236, pp. 1055-1093. [MF 2454; NV; C-__; NHC]

Shiwie, B., and L. Guangyu, 1982. "Stress Measurement of Rock Mass In Situ and the Law of Stress Distribution in a Large Dam Site," Issues in Rock Mechanics, R. E. Goodman and F. G. Heuze (eds.), Proceedings of the 23rd Symposium on Rock Mechanics, Berkeley, California, August 25-27, pp. 230-237. [MF 2460; V; C-__; HC]

Shuri, F. S., D. J. Dodds, and K. Kim, 1980. Measurement of Rock-Mass Deformation Properties by the Borehole Jacking Method at the Near-Surface Testing Facility, RHO-BWI-C-89, Rockwell Hanford Operations, Richland, Washington. [MF 0332; V; C-N; HC]

Singh, B., 1973. "Continuum Characterization of Jointed Rock Masses, Part I - The Constitutive Equations," _International Journal of Rock Mechanics and Mining Sciences & Geomechanics Abstracts_, Vol. 10, pp. 311-335. [MF 3215; V; C-6; HC]

South, D. L., 1985. _Computations to Support Section 4.3, 'Mechanical Properties - Continua,' of the BWIP Site Characterization Plan_, Computational Brief No. 00072, Rockwell Hanford Operations, Richland, Washington, pp. 329-432. [MF 2479; V; C-N; HC]

Stagg, K. G., 1968. "In Situ Tests on the Rock Mass," _Rock Mechanics in Engineering Practice_, K. G. Stagg and O. C. Zienkiewicz (eds.), John Wiley & Sons, Inc., New York, New York. [MF 0342; V; C-24; HC]

St. John, C. M., and K. Kim, 1985. "Geoengineering Design Parameters Workshop," _Proceedings_, Rapid City, South Dakota; also SD-BWI-TI-299, Rockwell Hanford Operations, Richland, Washington. [MF 3250; NV; C-N; NHC]

St. John, C. M., and J. R. Williams, 1980, _Geotechnical Numerical Models, Annual Report-Fiscal Year 1980_, RHO-BWI-C-88, Rockwell Hanford Operations, Richland, Washington. [MF 3205; V; C-N; HC]

Sublette, W. R., 1983. _Rock Mechanics Data Package_, SD-BWI-DP-041, REV 0-0, Rockwell Hanford Operations, Richland, Washington. [MF 2492; V; C-N; HC]

Sundaram, P. N., D. J. Watkins, W. E. Ralph, and D. Frink, 1983. "Large Scale Compression Test on Fractured Rock-Application to Room and Pillar Mine Design," _Rock Mechanics, Theory - Experiment - Practice_, Proceedings, 24th U.S. Symposium on Rock Mechanics, Texas A&M, College Station, Texas, pp. 653-664. [MF 0349; V; C-__; HC]

Tammemagi, H. Y., and J. D. Chieslar, 1985. _Interim Rock Mass Properties and Conditions for Analyses of a Repository in Crystalline Rock_, BMI/OCRD-18, for the Office of Crystalline Repository Development, Battelle Memorial Institute, Columbus, Ohio. [MF 2660; V; C-__; HC]

Taylor, J. T. M., 1961. "Mining Practice on the Kolar Gold Field, India," _Transactions Institution Mining and Metallurgy_, Vol. 70, pp. 575-604. [MF 2512; V; C-55; HC]

Thirumalai, K., 1970. _Rock Fragmentation by Creating a Thermal Inclusion with Dielectric Heating_, Report of Investigations 7424, U.S. Bureau of Mines, Minneapolis, Minnesota. [MF 2515; V; C-N; HC]

Thirumalai, K., 1975. "Rock Mechanics and Development of Advanced Hard Rock Breaking Methods," _Proceedings_, Fifteenth Symposium on Rock Mechanics, South Dakota, American Society of Civil Engineers, New York, New York, pp. 449-467. [MF 0356; V; C-45; HC]

Thomas, R. K., 1982. A Continuum Description for Jointed Media, SAND81-2615, Sandia National Laboratories, Albuquerque, New Mexico. [MF 3209; V; C-N; HC]

Thorpe, R., D. J. Watkins, W. E. Ralph, R. Hsu, and S. Flexser, 1980. Strength and Permeability Tests on Ultra-Large Stripa Granite Core, LBL-11203, Lawrence Berkeley Laboratory, Berkeley, California. [MF 2661; V; C-N; HC]

Thorpe, R. K., D. J. Watkins, and W. E. Ralph, 1983. "Strength and Permeability of an Ultra-Large Specimen of Granitic Rock," Rock Mechanics, Theory - Experiment - Practice, Proceedings, 24th U.S. Symposium on Rock Mechanics, Texas A&M, College Station, Texas, pp. 511-518. [MF 0357; V; C-__; HC]

Vasey, J., 1983. "Design and Support of Excavations Subjected to High Horizontal Stress," Proceedings, First International Conference on Stability in Underground Mining, Vancouver, B.C., Canada, American Institute of Mining, Metallurgical, and Petroleum Engineers, Littleton, Colorado, pp. 428-449. [MF 2537; V; C-4; HC]

Vivian, H., 1931. Deep Mining Methods, Conglomerate Mine of the Calumet and Hecla Consolidated Copper Co., Information Circular No. 6526, U.S. Bureau of Mines. [MF 2538; V; C-N; HC]

Voss, C. F., 1981. Field Measurements of the Elastic Properties of Basalt at the Near-Surface Test Facility Using the Modified Borehole Jack, RHO-BWI-SA-200A P, Rockwell Hanford Operations, Richland, Washington.

Wallace, G. B., E. J. Slebir, and F. A. Andersen, 1969. In Situ Methods for Determining Deformation Modulus Used by the Bureau of Reclamation, STP 477, American Society for Testing and Materials, Philadelphia, Pennsylvania. [MF 0368; V; C-58; HC]

Wawersik, W. R., and W. F. Brace, 1971. "Post-Failure Behavior of a Granite and Diabase," Rock Mechanics, Vol. 3, No. 2, pp. 61-85. [MF 2550; V; C-16; HC]

Williams, J. R., G. Mustoe, I. Mathews, and J. Sharp, 1981. Preliminary Results for Full-Scale Heater Tests 1 and 2, RSD-BWI-TI-061, Rockwell Hanford Operations, Richland, Washington. [MF 3251; NV; C-N; NHC]

Windes, S. L., 1949. Physical Properties of Mine Rock, Part I, Report of Investigations 4459, U.S. Bureau of Mines, College Park, Maryland.

Windes, S. L., 1950. Physical Properties of Mine Rock, Part II, Report of Investigations 4727, U.S. Bureau of Mines, College Park, Maryland, pp. 1-37. [MF 2569; V; C-N; HC]

Witherspoon, P. A., and O. Degerman, 1978. Swedish-American Cooperative Program on Radioactive Waste Storage in Mined Caverns, Program Summary, LBL-7049, Lawrence Berkeley Laboratory, Berkeley, California. [MF 2572; V; C-N; HC]

Wolmarans, J. F., and F. H. Guise-Brown, 1978. "The Water Hazard in Deep Gold Mining of the Far West Witwatersrand - South Africa," Siamos - 78, El agua en la Mineria y Trabajos Subterraneos, Water in Mining and Underground Works, Vol. I, Associacion National Ingenieros de Minas, Spain, pp. 329-346. [MF 3225; V; C-__; HC]

Woodside, W., and J. H. Messmer, 1961. "Thermal Conductivity of Porous Media. II. Consolidated Rocks," Journal of Applied Physics, Vol. 32, No. 9, pp. 1699-1706. [MF 2667; V; C-__; HC]

Worotnicki, G., and R. J. Walton, 1976. "Triaxial 'Hollow Inclusion' Gauges for Determination of Rock Stresses In Situ," Proceedings, International Symposium on Rock Mechanics on the Investigation of Rock and Advances in Stress Measurement, Sydney, Australia, pp. 1-8.

Yano, T., et al., 1979. "Construction of the Enasan Tunnel and the Design of the Second Stage," Proceedings of the International Tunnel Symposium, Tokyo, 1978.

Yokayama, A., 1979. "Tunneling under High Water Pressure in Soft Ground," Proceedings of the International Tunnel Symposium, Tokyo, 1978.

Zemanek, J., R. L. Caldwell, E. E. Glenn, Jr., S. V. Holcomb, J. L. Norton, and A. J. D. Straus, 1969. "The Borehole Televiewer--A New Logging Concept for Fracture Location and Other Types of Borehole Inspection," Journal of Petroleum Technology, Vol. 21, pp. 762-774.

Zoback, M. D., and D. D. Pollard, 1978. "Hydraulic Fracture Propagation and the Interpretation of Pressure-Time Records for In Situ Stress Determinations," Proceedings, 19th U.S. Symposium of Rock Mechanics, Stateline, Nevada, May 1-3, pp. 14-22. [MF 2582; V; C-42; HC]

Zoback, M. L., and M. D. Zoback, 1980. "State of Stress in the Conterminous United States," Journal of Geophysical Research, Vol. 85, No. B11, pp. 6113-6156.

Zoback, M. D., and B. C. Haimson, 1982. "Status of the Hydraulic Fracturing Method for In-Situ Stress Measurements," Proceedings, 23rd U.S. Symposium on Rock Mechanics, University of California, Berkeley, California, pp. 143-156. [MF 0622; V; C-__; HC]

Zoback, M. D., D. Moos, L. Mastin, and R. N. Anderson, 1985. "Wellbore Breakouts and In-Situ Stress," Journal of Geophysical Research, Vol. 90, No. B7, pp. 5523-5530. [MF 2581; V; C-9; HC]

Figure 2.0-1. The conceptual interaction of components
of the overall program leading to licensable
repository design. PS84-2042-2.0-1

(on Star)
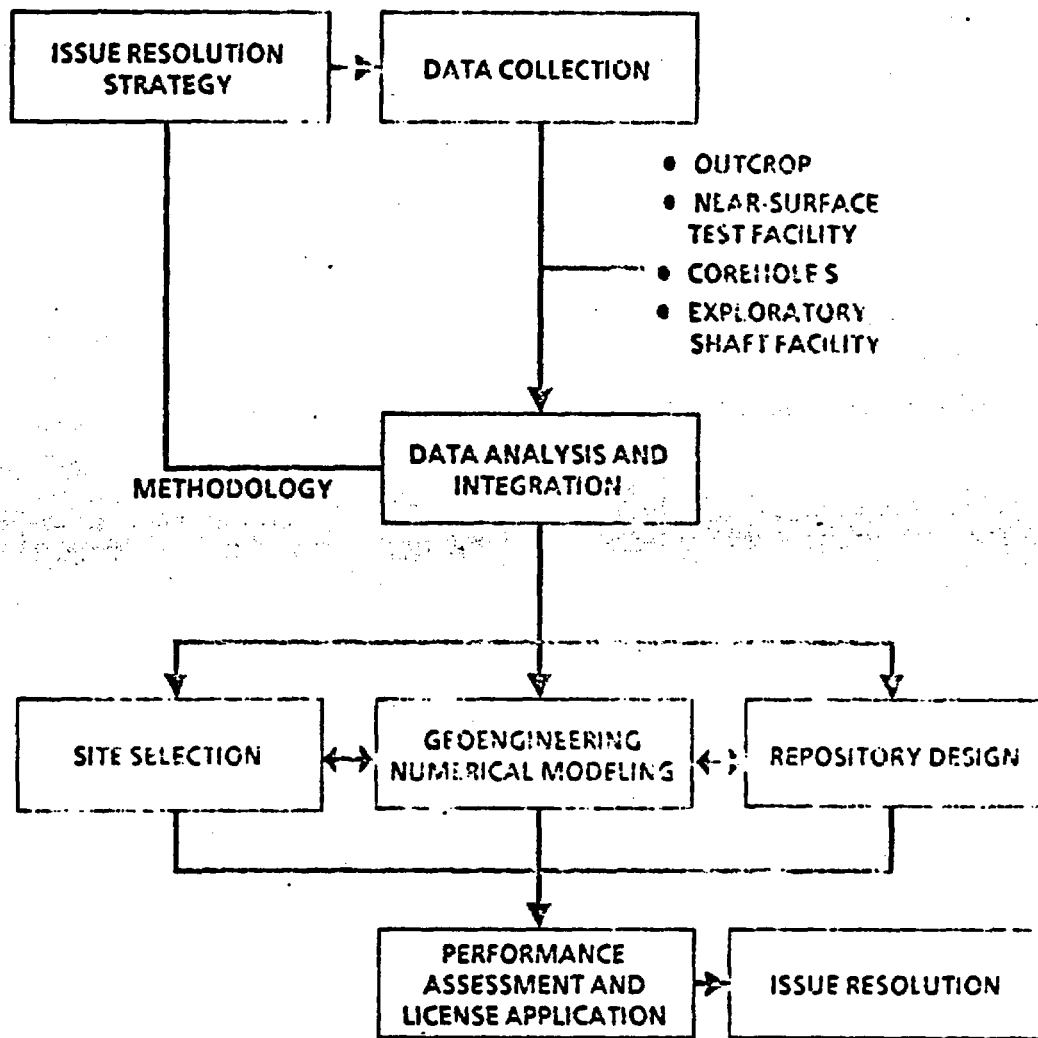
Figure 2.0-1. The conceptual interaction of components of the overall program leading to licensable repository design.

Figure 2.0-2. Plan view of
near-surface test facility.

PS8407-111

FULL-SCALE HEATER TEST 1

FULL-SCALE HEATER TEST 2

TRANSFER ROOM

TRANSFER ROOM

STRESS MEASUREMENT TECHNIQUE EVALUATION/ DEVELOPMENT TESTS

JOINTED BLOCK TEST

EXTENSOMETER ROOM

TUNNEL 3 (EAST ACCESS)

TUNNEL 2 (WEST ACCESS)

TUNNEL 1

NOT TO SCALE

PS8407-1118
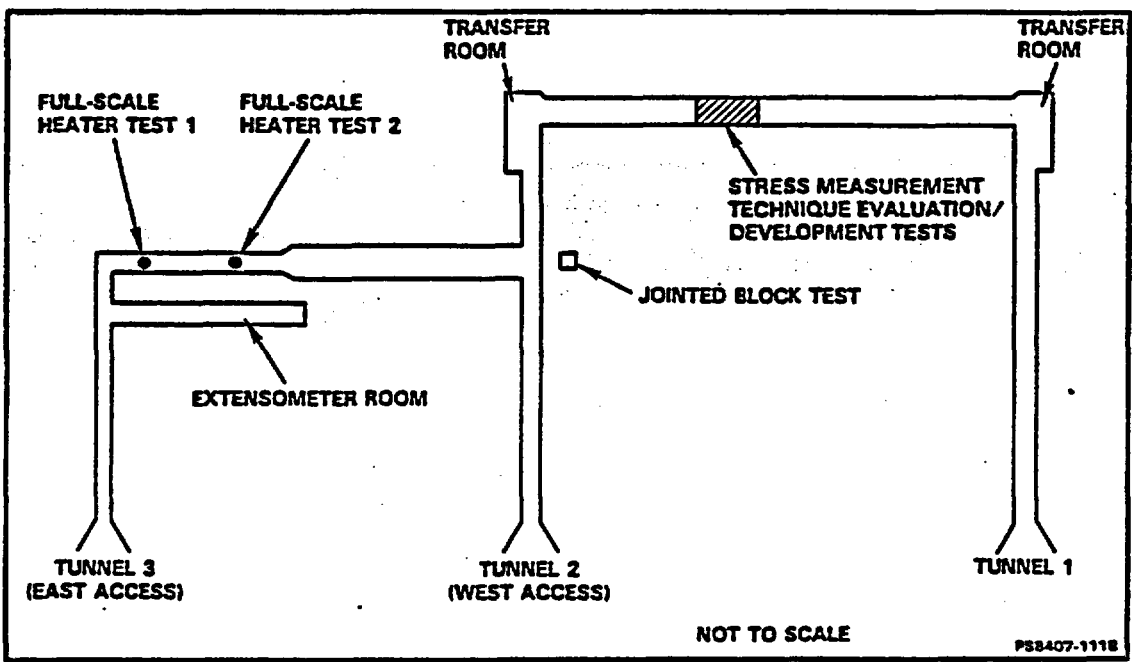
PS8508-37

Figure 2.0-3. Idealized diagram of the transition from intact rock to a
heavily jointed rock mass with increasing sample size (Hoek and Brown, 1980,
p. 132).

INTACT ROCK

SINGLE DISCONTINUITY

TWO DISCONTINUITIES

SEVERAL DISCONTINUITIES

ROCK MASS

UNDERGROUND EXCAVATION

PS8508-37
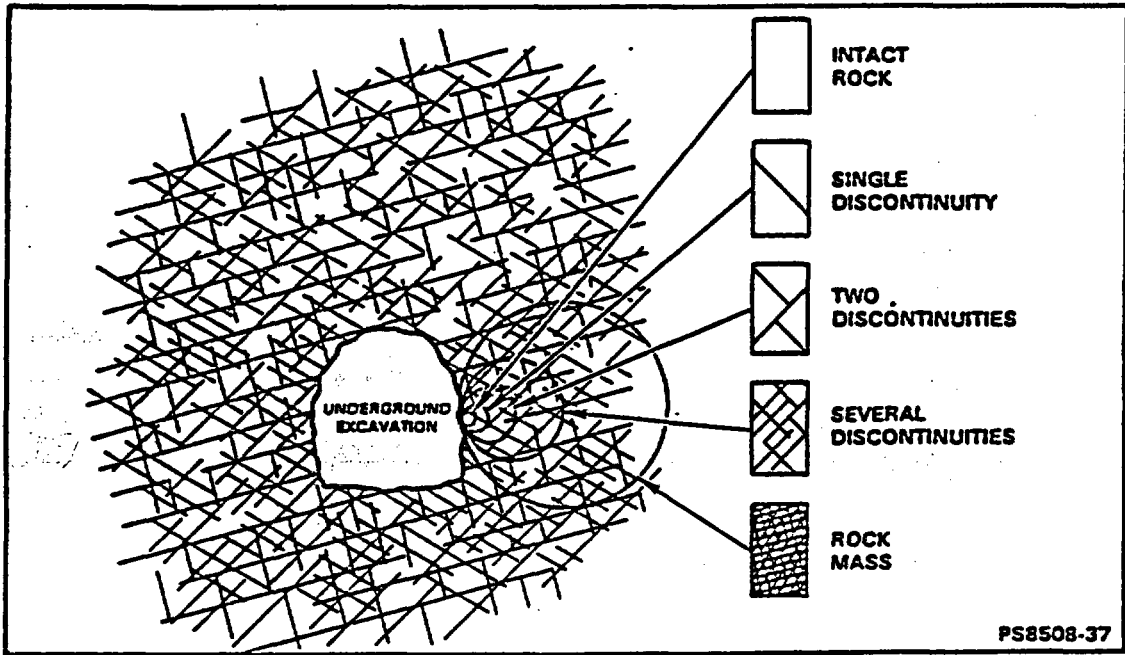
Figure 2.1-1. Flow diagram of conducting
laboratory tests by the Basalt Waste
Isolation Project Rock Mechanics Laboratory.

RCP8207-156A

```
                          │
                          ▼
              ┌───────────────────────┐
              │   REVIEW CORE BOXES   │
              │    IN CORE LIBRARY    │
              └───────────────────────┘
                          │
                          ▼
              ┌───────────────────────┐
              │     SELECT SAMPLES    │
              └───────────────────────┘
                          │
                          ▼
          ┌───────────────────────────────┐
          │ MARK AND LOG SAMPLES AND INSERT│
          │  SPACER TUBES INTO CORE BOXES  │
          └───────────────────────────────┘
                          │
                          ▼
              ┌───────────────────────┐
              │     CHARACTERIZE      │
              │       SAMPLES         │
              └───────────────────────┘
                          │
                          ▼
          ┌───────────────────────────────┐
          │  MARK SAMPLES INTO SPECIMEN    │
          │ LENGTHS. LOG AND MARK SPECIMENS│
          └───────────────────────────────┘
                          │
                          ▼
          ┌──────────────────┐        ┌──────────────────┐
          │ CUT SAMPLES INTO │───────▶│  SURFACE GRIND   │
          │    SPECIMENS     │        │  ENDS AS REQUIRED│
          └──────────────────┘        └──────────────────┘
                                               │
                                               ▼
                                      ┌──────────────────┐
                                      │    APPARENT      │
                                      │    POROSITY      │
                                      └──────────────────┘
                                               │
                                               ▼
                                      ┌──────────────────┐
                                      │      DRYING      │
                                      └──────────────────┘
                                               │
                                               ▼
                                      ┌──────────────────┐
                                      │   BULK DENSITY   │
                                      └──────────────────┘
                                               │
                                               ▼
    ┌──────────────┐                  ┌──────────────────┐
    │   MODULUS    │◀─────────────────│ DYNAMIC ELASTIC  │
    │  OF RUPTURE  │                  │    PROPERTIES    │
    └──────────────┘                  └──────────────────┘
                                               │
    ┌──────────────┐                           ▼
    │   BRAZILIAN  │◀─────────────────┌──────────────────┐
    │ TENSILE TEST │                  │  STATIC ELASTIC  │
    └──────────────┘                  │    PROPERTIES    │
                                      └──────────────────┘
                                               │
                                               ▼
    ┌───────────────────────────────┐  ┌──────────────────┐
    │ GRAIN DENSITY AND/OR RETURN   │◀─│   STRENGTH TEST  │
    │  SPECIMEN TO CORE LIBRARY     │  │   1. UNIAXIAL    │
    └───────────────────────────────┘  │   2. TRIAXIAL    │
                    │                   └──────────────────┘
        ┌───────────┤
        ▼           ▼
┌──────────────┐  ┌───────────────────────────┐
│TOTAL POROSITY│─▶│   DATA OUT TO RECORDS     │
│ AS REQUIRED  │  │ AND REDUCTION (STATISTICS)│
└──────────────┘  └───────────────────────────┘
```
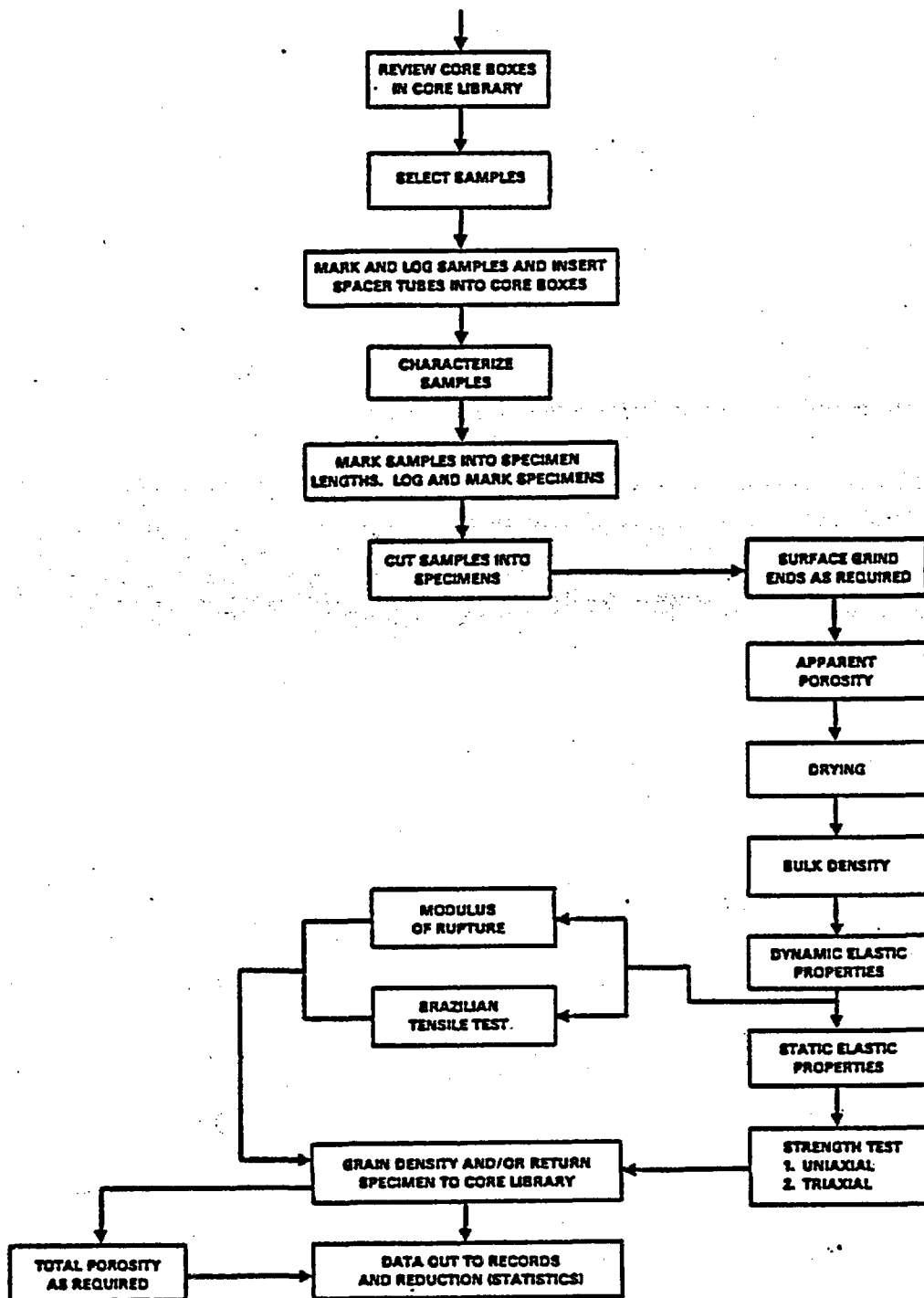
RCP8207-156C

Figure 2.1-2.   Laboratory test results on intact samples
from the Cohassett flow in borehole RRL-2.

PS8407-120

GEOLOGIC LOG

DEPTH (ft)	DEPTH (m)	DISKING	DEPTH (m)	INTRAFLOW STRUCTURE	BRAZILIAN TENSILE STRENGTH (MPa) MEAN	STD DEV	n	UNIAXIAL COMPRESSIVE STRENGTH (MPa) MEAN	STD DEV	n	YOUNG'S MODULUS (GPa) MEAN	STD DEV	n	POISSON'S RATIO MEAN	STD DEV	n	BULK DENSITY (g/cm³) MEAN	STD DEV	n	APPARENT POROSITY (%) MEAN	STD DEV	n
			2,993	TOP CONTACT / FLOW TOP *	7.89	2.64	8	69.99	29.10	8							2.29	0.19	13	12.95	2.31	13
3,020	920		3,016	UPPER COLONNADE	17.46	2.24	4										2.72	0.05	4	4.82	1.29	4
3,060	930		3,071	ENTABLATURE																		
	940		3,076 / 3,083	COLONNADE																		
3,100				VESICULAR ZONE *	13.06	1.96	3	195.77	34.45	3	52.40	6.39	3	0.27	0.06	3	2.71	0.01	8	2.73	0.76	8
	950		3,107	ENTABLATURE	13.03	4.16	8	261.19	7.90	4	74.35	2.20	4	0.26	0.02	4	2.83	0.03	13	1.16	0.37	13
3,140	960		3,134.5 / 3,147	COLONNADE	16.66	1.29	2	263.24	–	1	78.12	–	1	0.25	–	1	2.86	0.01	4	1.32	0.41	4
			3,167.5	ENTABLATURE				248.57	29.59	3	78.72	8.31	3	0.29	0.02	3	2.86	0.01	8	0.89	0.23	8
3,180	970		3,183	COLONNADE				332.26	–	1	86.57	–	1	0.25	–	1	2.86	0.01	3	0.57	0.42	3
			3,200	COLUMNAR ENTABLATURE																		
3,220	980			COLONNADE	13.60	2.26	2	279.44	19.42	2	76.87	5.62	2	0.27	0.00	2	2.83	0.02	8	1.29	0.96	8
	990		3,256	BOTTOM CONTACT																		

STD DEV = STANDARD DEVIATION
n = NUMBER OF SAMPLES
* COMPRESSIVE STRENGTH SAMPLES TESTED AT >25-mm- (1-in.-) DIA

TO CONVERT: MPa TO lbf/in², MULTIPLY BY 145
GPa TO Mp/in², MULTIPLY BY 145
g/cm³ TO lb/in³, MULTIPLY BY 62.4

LANDON (1983, p. 43) SOUTH (1985, pp. 29-70)

Figure 2.1-3. Laboratory test results on intact samples
from the Cohassett flow in borehole RRL-6.

PS8407-121

GEOLOGIC LOG					BRAZILIAN TENSILE STRENGTH (MPa)			UNIAXIAL COMPRESSIVE STRENGTH (MPa)			YOUNG'S MODULUS (GPa)			POISSON'S RATIO			BULK DENSITY (g/cm³)			APPARENT POROSITY (%)		
DEPTH (ft)	(m)	JOINTING	DEPTH (ft)	INTRAFLOW STRUCTURE	MEAN	STD DEV	n	MEAN	STD DEV	n	MEAN	STD DEV	n	MEAN	STD DEV	n	MEAN	STD DEV	n	MEAN	STD DEV	n
			3,092.5	TOP CONTACT FLOW TOP ✦	8.43	0.78	3	84.82	9.34	2	31.75	4.87	2	0.19	0.03	2	2.33	0.11	8	18.25	2.44	8
			3,102	PART OF UPPER COLONNADE	11.53	2.49	3	234.48	—	1	81.78	—	1	0.24	—	1	2.68	0.02	6	7.42	1.06	6
3,130	950		3,132	UPPER COLONNADE	12.06	4.10	3	205.80	72.04	2	77.22	8.24	2	0.26	0.01	2	2.82	0.01	6	2.90	0.76	6
3,160	960		3,163	COLUMNAR ENTABLATURE																		
			3,169																			
	970		3,175	ENTABLATURE																		
3,200				VESICULAR ✦	9.36	2.29	8	169.39	84.87	4	48.64	—	1	0.33	—	1	2.66	0.12	9	8.61	2.31	9
	980		3,201																			
3,240				ENTABLATURE	14.56	3.43	3	270.31	18.22	8	74.67	7.82	8	0.25	0.02	8	2.83	0.02	14	1.96	0.43	14
	990		3,237	COLONNADE	19.57	—	1										2.82	—	1	2.40	—	1
			3,261	ENTABLATURE	18.24	—	1	266.89	—	1	78.39	—	1	0.21	—	1	2.84	0.06	4	1.77	0.13	4
3,280	1,000		3,281	COLUMNAR ENTABLATURE	14.56	2.41	8	259.22	—	1	84.13	—	1	0.27	—	1	2.87	0.01	8	1.71	0.22	8
			3,300																			
3,320	1,010			BASAL COLONNADE	17.52	—	1	266.42	—	1	81.77	—	1	0.27	—	1	2.84	0.02	4	1.82	0.17	4
			3,344	BOTTOM CONTACT																		

STD DEV = STANDARD DEVIATION

n = NUMBER OF SAMPLES

✦ COMPRESSIVE STRENGTH SAMPLES TESTED AT >25-mm- (1-in.-)DIA

TO CONVERT: MPa TO lbf/in², MULTIPLY BY 145
GPa TO lbf/in², MULTIPLY BY 145
g/cm³ TO lb/ft³, MULTIPLY BY 62.4

LANDON (1983, p. 44) SOUTH (1985, pp. 76-127)

PS8407-121

Figure 2.1-4. Laboratory test results on intact samples
from the Cohassett flow in borehole RRL-14.

PS8407-122

GEOLOGIC LOG			BRAZILIAN TENSILE STRENGTH (MPa)			UNIAXIAL COMPRESSIVE STRENGTH (MPa)			YOUNG'S MODULUS (GPa)			POISSON'S RATIO			BULK DENSITY (g/cm³)			APPARENT POROSITY (%)		
DEPTH (m) / DISKING	DEPTH (m)	INTRAFLOW STRUCTURE	MEAN	STD DEV	n	MEAN	STD DEV	n	MEAN	STD DEV	n	MEAN	STD DEV	n	MEAN	STD DEV	n	MEAN	STD DEV	n
3,082	TOP CONTACT ●		4.61	1.77	4	39.29	27.71	2							2.17	0.16	6	15.73	8.06	6
3,113.5 / 3,116	COLONNADE		16.54	—	1										2.79	—	1	3.16	—	1
3,125	COLUMNAR ENTABLATURE														2.82	0.00	2	2.25	0.07	2
3,130	COLONNADE																			
3,147.5	ENTABLATURE		18.70	—	1	369.67	—	1	87.96	—	1	0.23	—	1	2.84	0.00	4	2.27	0.39	4
3,165.5 / 3,174	COLONNADE																			
	ENTABLATURE																			
3,193	VESICULAR		6.56	—	1	163.92	8.99	2							2.55	0.06	3	6.57	1.04	3
3,203	ENTABLATURE		16.51	2.93	3	392.92	19.00	3	82.37	6.81	3	0.29	0.06	3	2.83	0.04	17	1.97	1.30	12
3,282 / 3,291	COLUMNAR ENTABLATURE																			
	BASAL COLONNADE		16.25	1.19	6	332.69	23.43	3	76.96	4.20	3	0.28	0.01	3	2.85	0.02	21	1.91	0.57	21
3,321	BOTTOM CONTACT																			

STD DEV = STANDARD DEVIATION

n = NUMBER OF SAMPLES

● COMPRESSIVE STRENGTH SAMPLES TESTED AT >25-mm- (1-in.-) DIA

TO CONVERT: MPa TO lbf/in², MULTIPLY BY 145
GPa TO lbf/in², MULTIPLY BY 145
g/cm³ TO lb/ft³, MULTIPLY BY 62.4

LANDON (1963, p. 45) SOUTH (1985, pp. 139-190)
HULSTROM (1985, pp. 11-19)

PS8407-122

Figure 2.1-5. Uniaxial compressive strength of flow top,
entablature, colonnade, and vesicular zones of
Cohassett flow in boreholes RRL-2, -6,
and -14 (South, 1985, pp. 329-376;
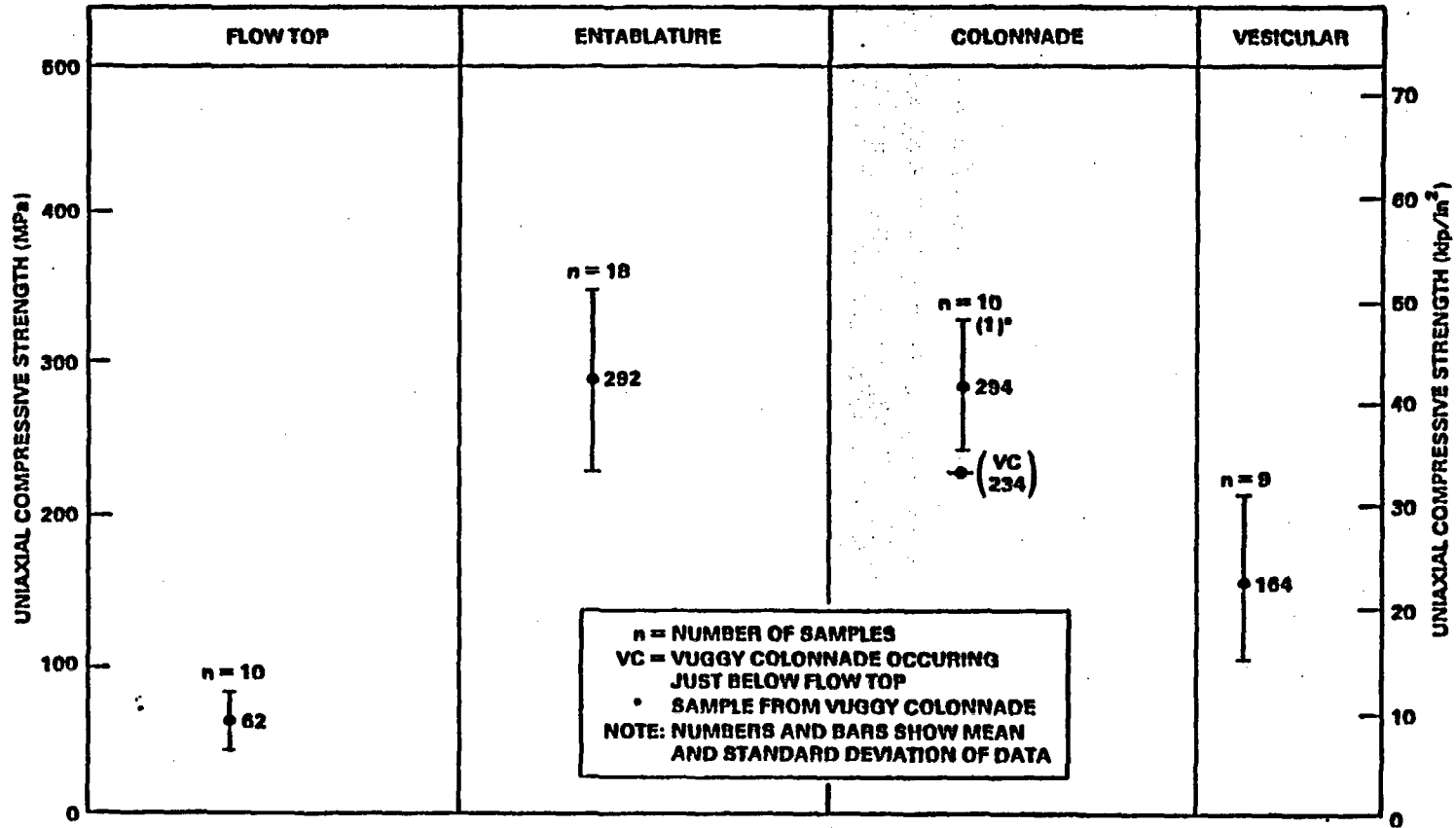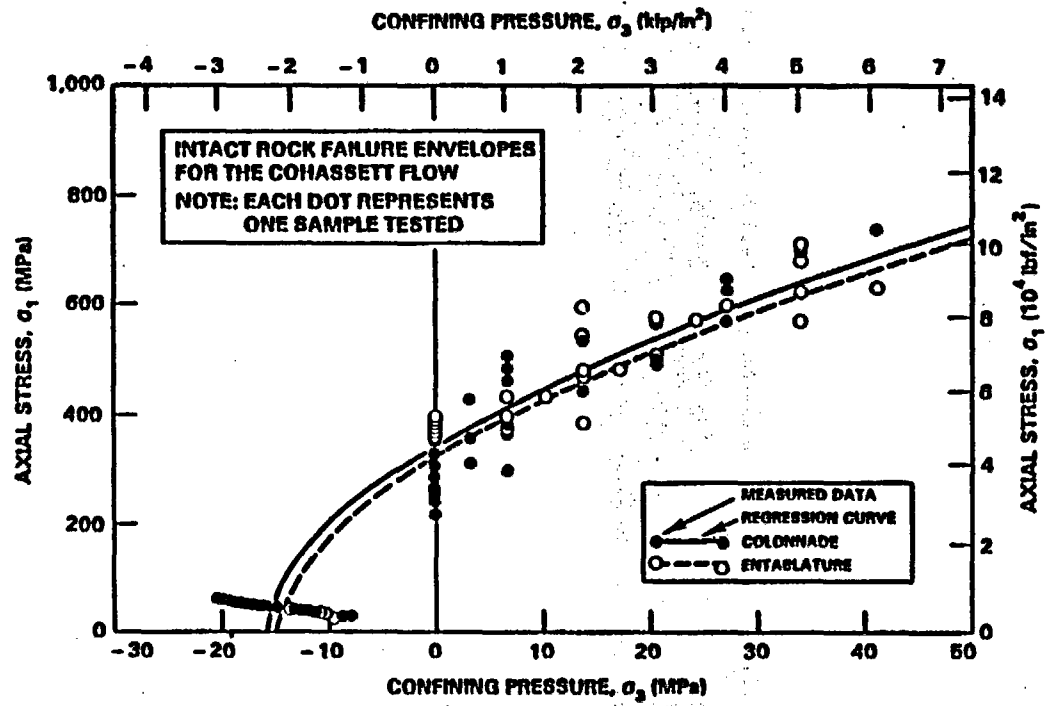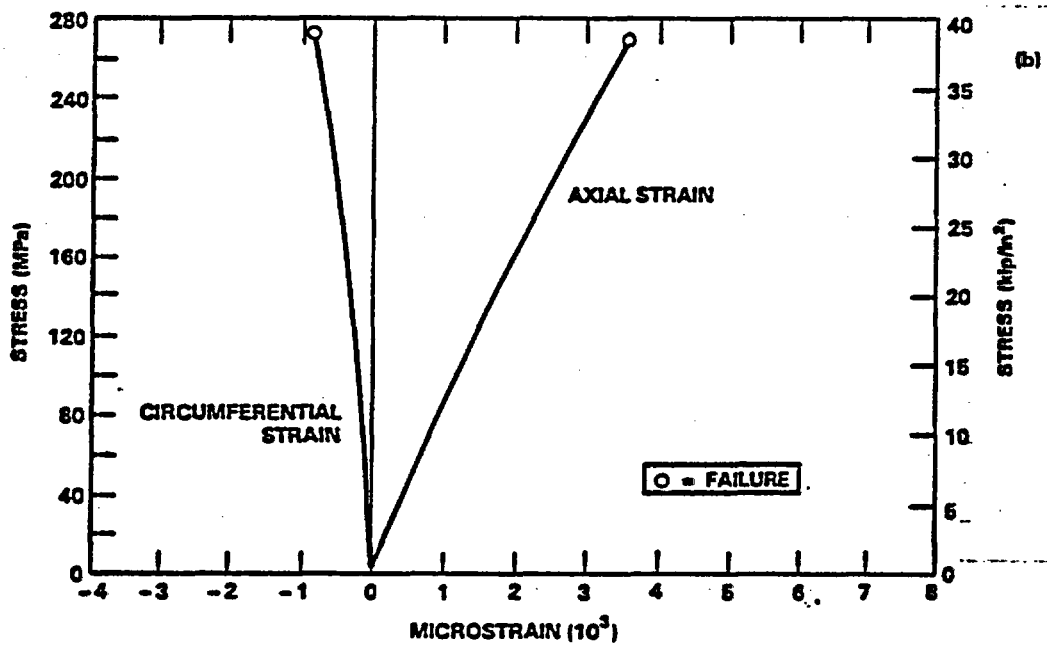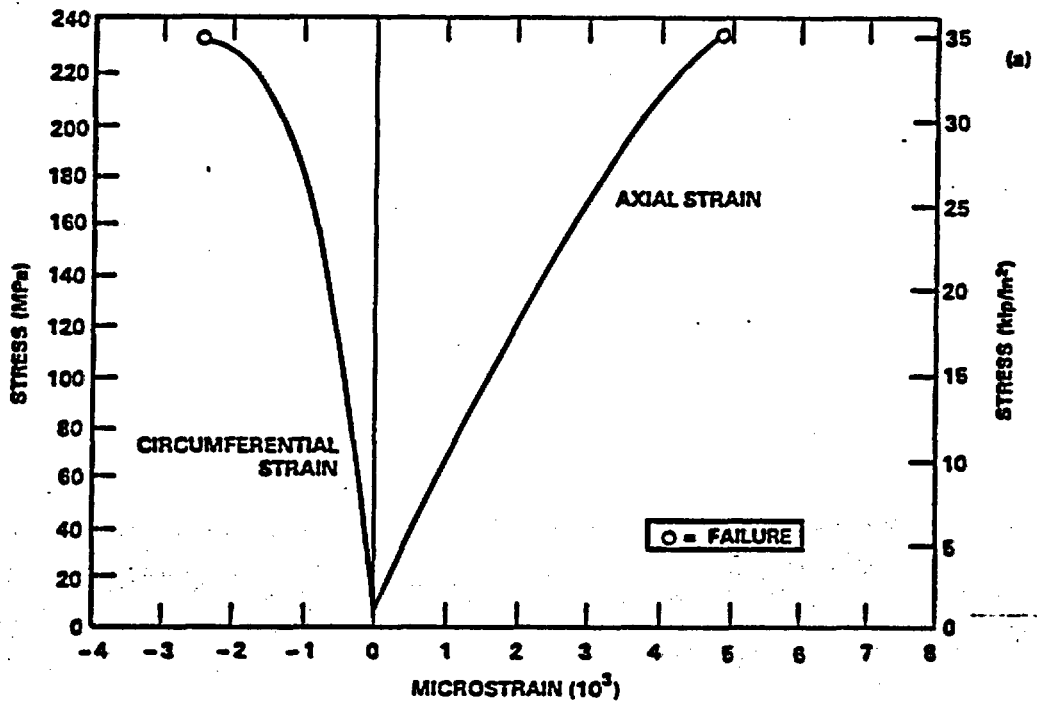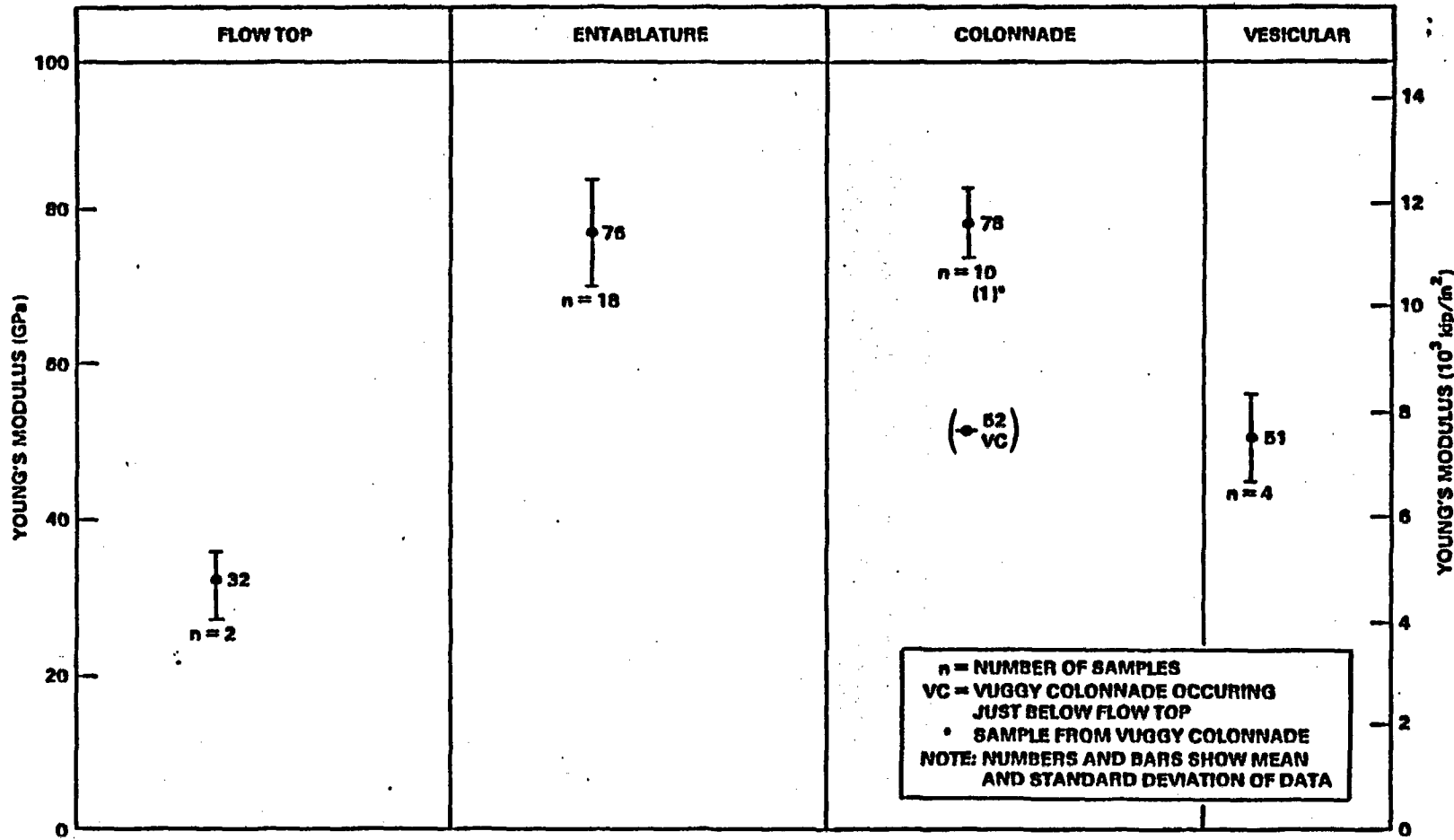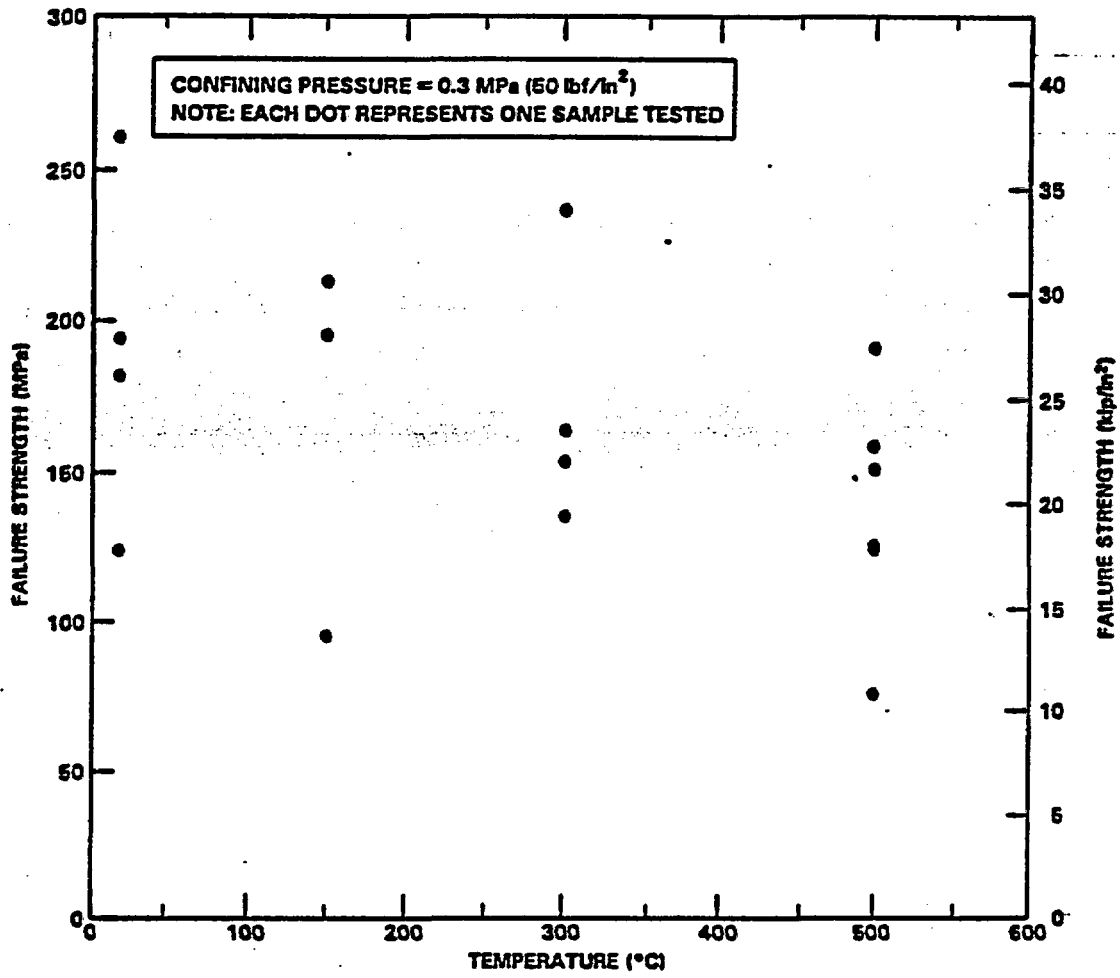Hulstrom, 1985, pp. 57-65).

PS8407-127

FLOW TOP   ENTABLATURE   COLONNADE   VESICULAR

n = NUMBER OF SAMPLES
VC = VUGGY COLONNADE OCCURING
JUST BELOW FLOW TOP
• SAMPLE FROM VUGGY COLONNADE
NOTE: NUMBERS AND BARS SHOW MEAN
AND STANDARD DEVIATION OF DATA

PS9407-127A

Figure 2.1-6. Failure envelopes for intact basalt
from dense interior of the Cohassett flow
(South, 1985, pp. 377-402).

PS8407-214

CONFINING PRESSURE, σ_3 (kip/in²)

-4   -3   -2   -1   0   1   2   3   4   5   6   7

**INTACT ROCK FAILURE ENVELOPES
FOR THE COHASSETT FLOW**

**NOTE: EACH DOT REPRESENTS
ONE SAMPLE TESTED**

AXIAL STRESS, σ_1 (MPa)

AXIAL STRESS, σ_1 (10⁴ lbf/in²)

	MEASURED DATA	REGRESSION CURVE
COLONNADE		
ENTABLATURE		

-30   -20   -10   0   10   20   30   40   50

CONFINING PRESSURE, σ_3 (MPa)

(a)

P89407-128A

Figure 2.1-7. Typical stress-strain curves
for intraflow zones of the Cohassett flow
(South, 1985, pp. 403-430).

PS8407-130

PS8407-130

Figure 2.1-8. Young's modulus of flow top, entablature,
colonnade, and vesicular zones of Cohassett flow
in boreholes RRL-2, -6, and -14
(South, 1985, pp. 329-376; Hulstrom, 1985, pp. 57-65).

PS8407-129

FLOW TOP	ENTABLATURE	COLONNADE	VESICULAR

YOUNG'S MODULUS (GPa)

YOUNG'S MODULUS (10^3 kip/in^2)

32
n = 2

76
n = 18

78
n = 10
(1)*

(←52)
VC

51
n = 4

n = NUMBER OF SAMPLES
VC = VUGGY COLONNADE OCCURING
    JUST BELOW FLOW TOP
*   SAMPLE FROM VUGGY COLONNADE
NOTE: NUMBERS AND BARS SHOW MEAN
    AND STANDARD DEVIATION OF DATA

P88407-129A

Figure 2.1-9. Failure strength of intact Umtanum flow
   basalt as a function of temperature (after Miller
      and Bishop, 1979; Miller, 1979b) (graph from
            South, 1985, pp. 431).

PS8407-132

CONFINING PRESSURE = 0.3 MPa (50 lbf/in²)
NOTE: EACH DOT REPRESENTS ONE SAMPLE TESTED

FAILURE STRENGTH (MPa) vs TEMPERATURE (°C)

FAILURE STRENGTH (kip/in²)

PS8407-132A

Figure 2.1-10. Scatter diagram and best-fit line
of static elastic modulus versus maximum temperature
during exposed Full-Scale Heater Test 2
(after Mitchell, 1984c, p. 34).

PS8407-189

BEST FIT LINE
Y = A + B · X
A = 79.403
B = +0.016795
CORRELATION
COEFFICIENT = 0.07

PS5407-189A
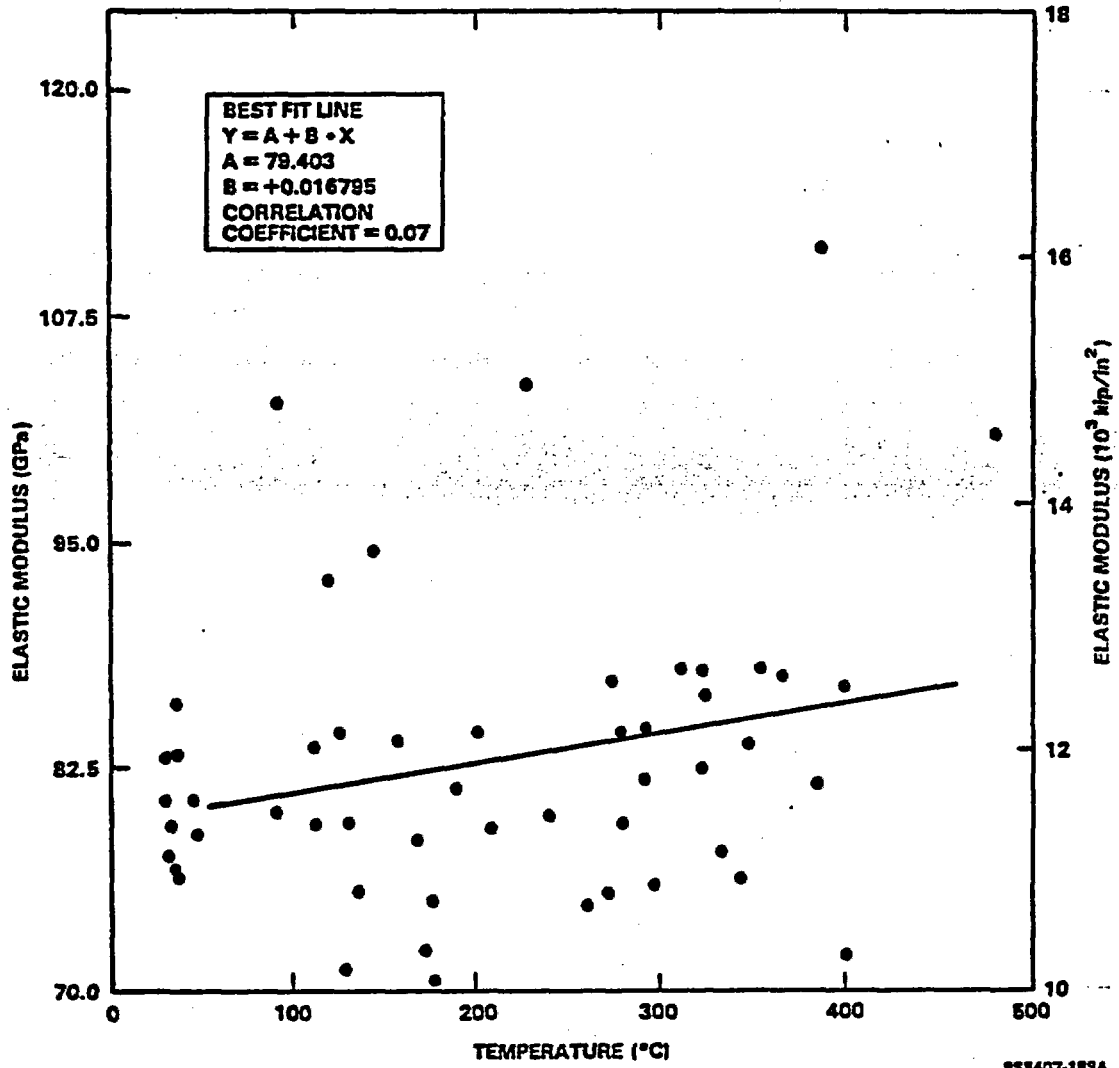
Figure 2.1-11. Scatter diagram and best-fit line of uniaxial
compressive strength versus maximum temperature of intact
samples from the post-test characterization core from
Full-Scale Heater Test 2 (Mitchell, 1984c, p. 38).

PS8407-133

BEST FIT LINE
Y = A + B · X
A = 317.98
B = −0.19146
CORRELATION
COEFFICIENT = 0.14
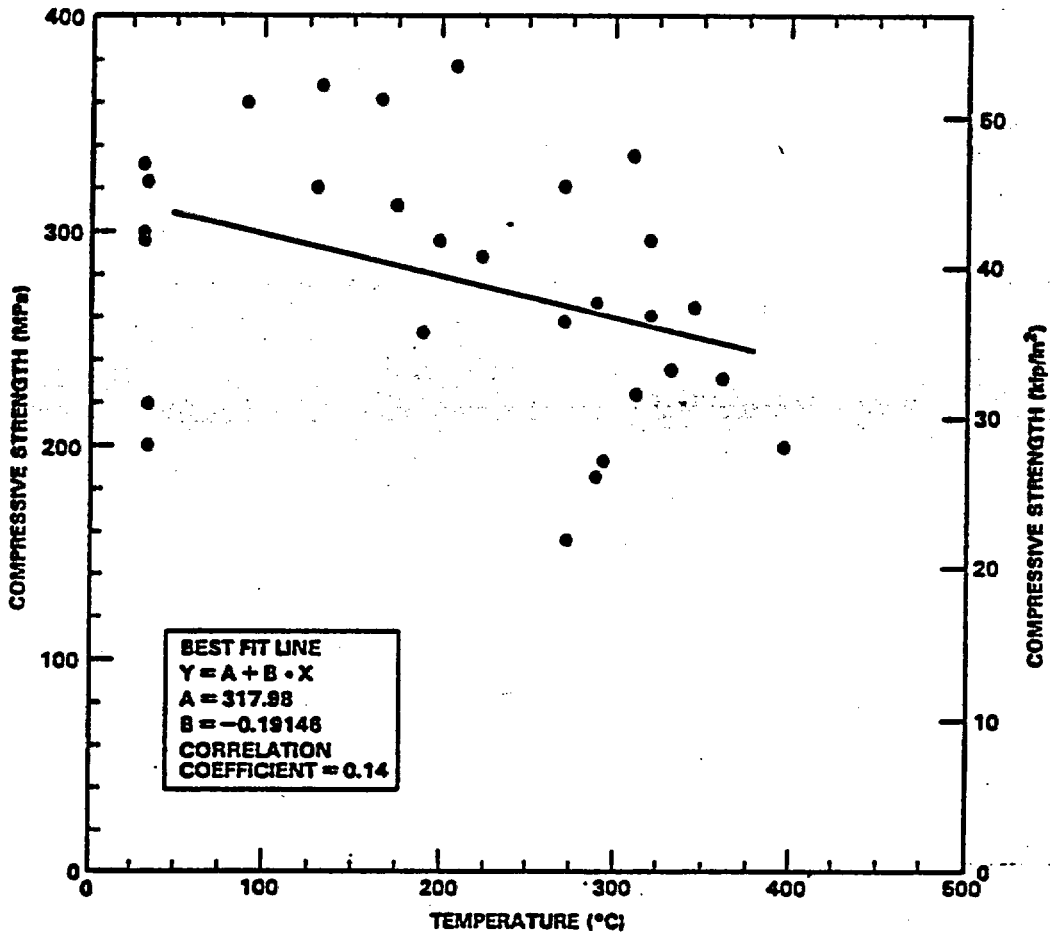
PS8407-133A

Figure 2.2-1. Peak and residual strength
of joint samples from Pomona flow by
direct shear test (Mitchell,
1984a, p. 34).

PS8407-137

NORMAL STRESS (kip/in²)

PEAK STRENGTH

BEST FIT LINE
C = 0.8 MPa (116 lbf/in²)
ϕ = 29.2°
CORRELATION
COEFFICIENT = 0.55

SHEAR STRESS (MPa)

SHEAR STRESS (kip/in²)

NORMAL STRESS (MPa)

NORMAL STRESS (kip/in²)

RESIDUAL STRENGTH

BEST FIT LINE
C = 1.32 MPa (191 lbf/in²)
ϕ = 24.7°
CORRELATION
COEFFICIENT = 0.88

SHEAR STRESS (MPa)

SHEAR STRESS (kip/in²)

NORMAL STRESS (MPa)
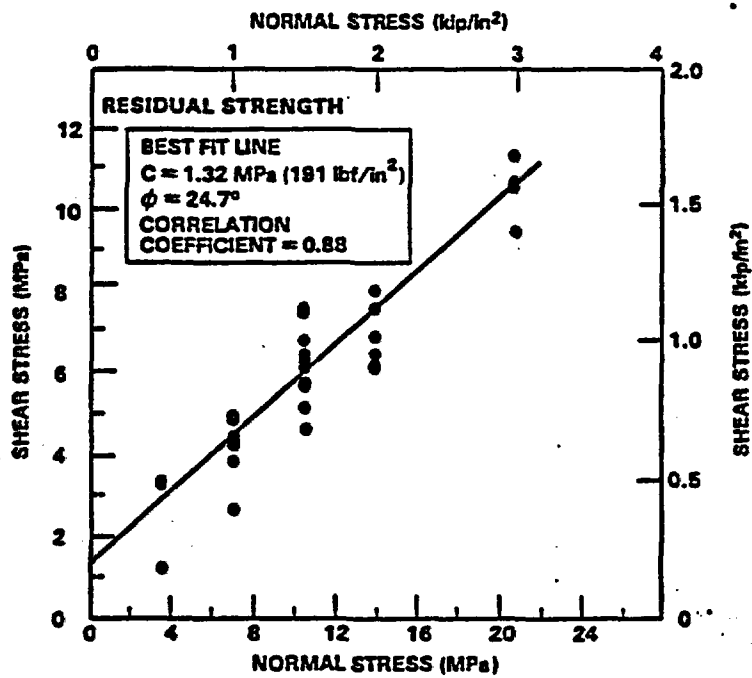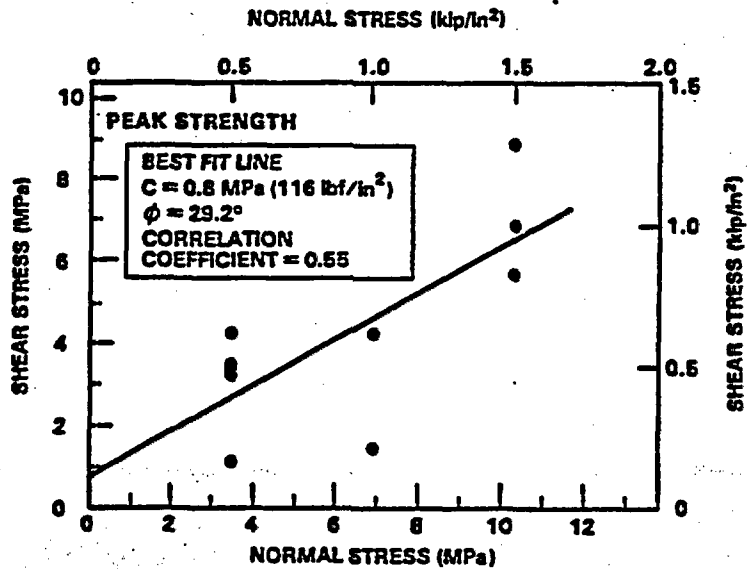
PS8407-137A

Figure 2.2-2. Peak and residual shear strength of
joint samples from Pomona flow by triaxial
tests (Brechtel, 1985, pp. 39-41).

PS8508-28

NORMAL STRESS (kip/in²)

SHEAR STRESS (MPa)

SHEAR STRESS (kip/in²)

PEAK STRENGH

BEST FIT LINE
C = 1.6 MPa
ϕ = 35°
CORRELATION
COEFFICIENT = 0.88

NORMAL STRESS (MPa)

NORMAL STRESS (kip/in²)

SHEAR STRESS (MPa)

SHEAR STRESS (kip/in²)

RESIDUAL STRENGTH

BEST FIT LINE
C = 1.9 MPa
ϕ = 34°
CORRELATION
COEFFICIENT = 0.83

NORMAL STRESS (MPa)

PS8508-23A
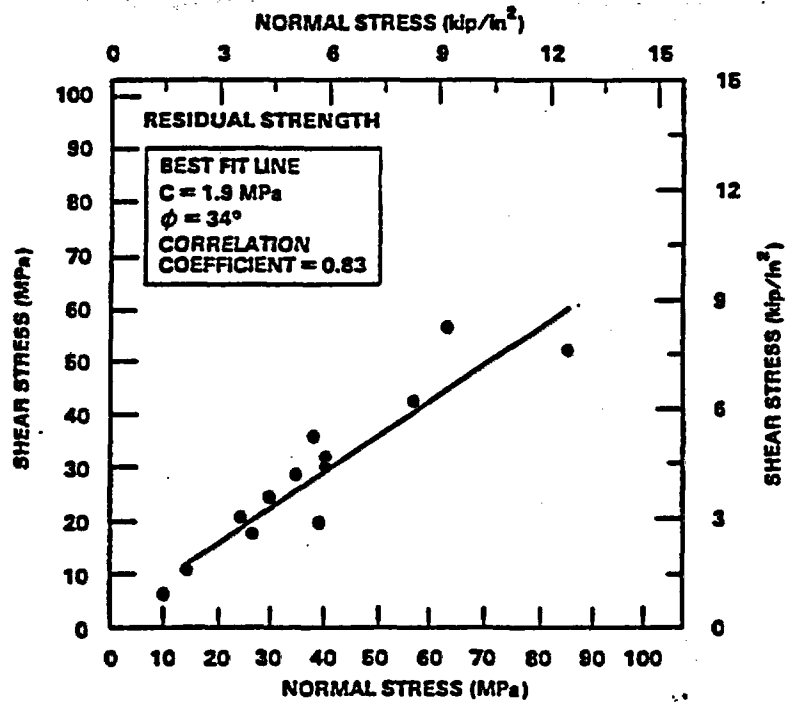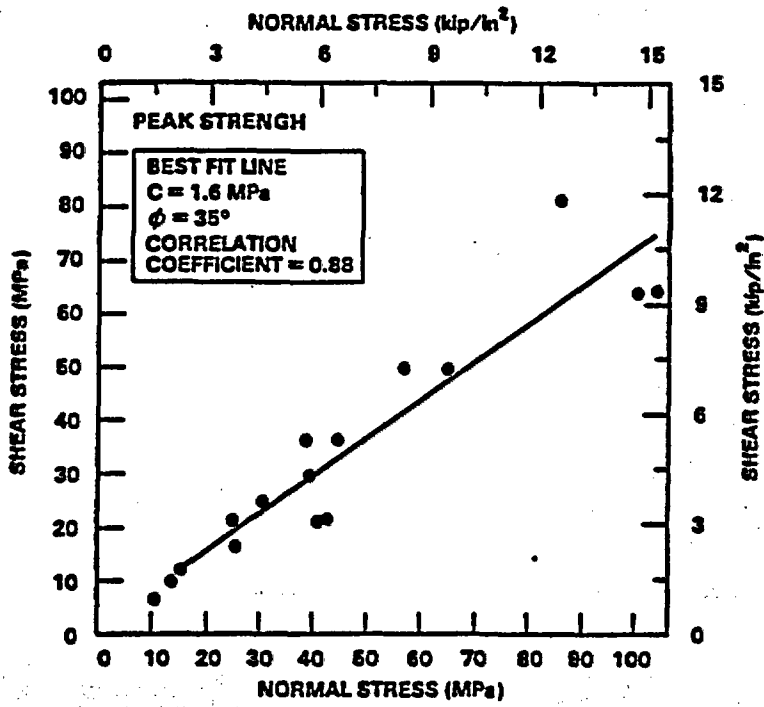
Figure 2.2-3. Peak and residual shear strength
of joint samples from undifferentiated
Grande Ronde flow by triaxial tests
(Mitchell, 1984b, pp. 21-22).

PS8407-138

NORMAL STRESS (kip/in²)

PEAK STRENGTH

SHEAR STRESS (MPa)

SHEAR STRESS (kip/in²)

BEST FIT LINE
C = 4.08 MPa (592 lb/in²)
ϕ = 45.7°
CORRELATION
COEFFICIENT = 0.95

NORMAL STRESS (MPa)

NORMAL STRESS (kip/in²)

RESIDUAL STRENGTH

SHEAR STRESS (MPa)

SHEAR STRESS (kip/in²)

BEST FIT LINE
C = 1.40 MPa (203 lb/in²)
ϕ = 42.7°
CORRELATION
COEFFICIENT = 0.93

NORMAL STRESS (MPa)

PS8407-138A
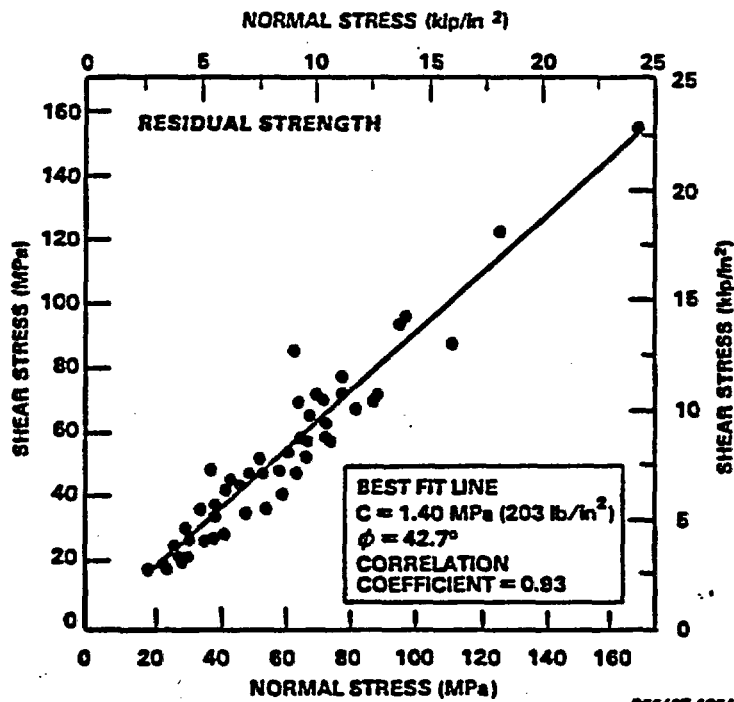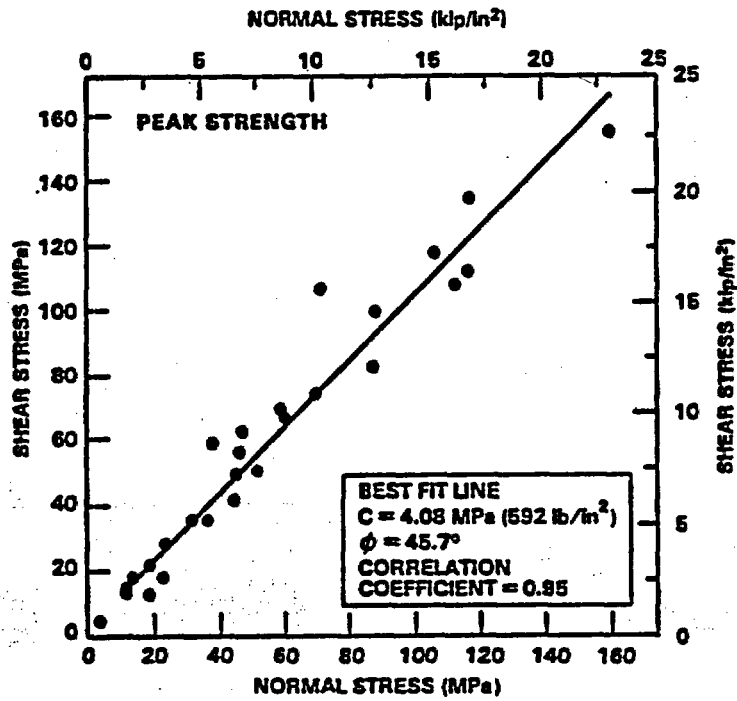
Figure 2.2-4. Schematic of the triaxial testing
system illustrating the measurement of joint
displacement (Brechtel, 1985, p.10).

PISTON

PISTON GUIDE

PLATEN

PLATEN

JOINTED SAMPLE

LOW FRICTION SURFACE

DISPLACEMENT GAGE ATTACHMENT

SAMPLE JACKET

PRESSURE VESSEL

SHEAR DISPLACEMENT CANTILEVER

NORMAL DISPLACEMENT CANTILEVER

BASE PLUG
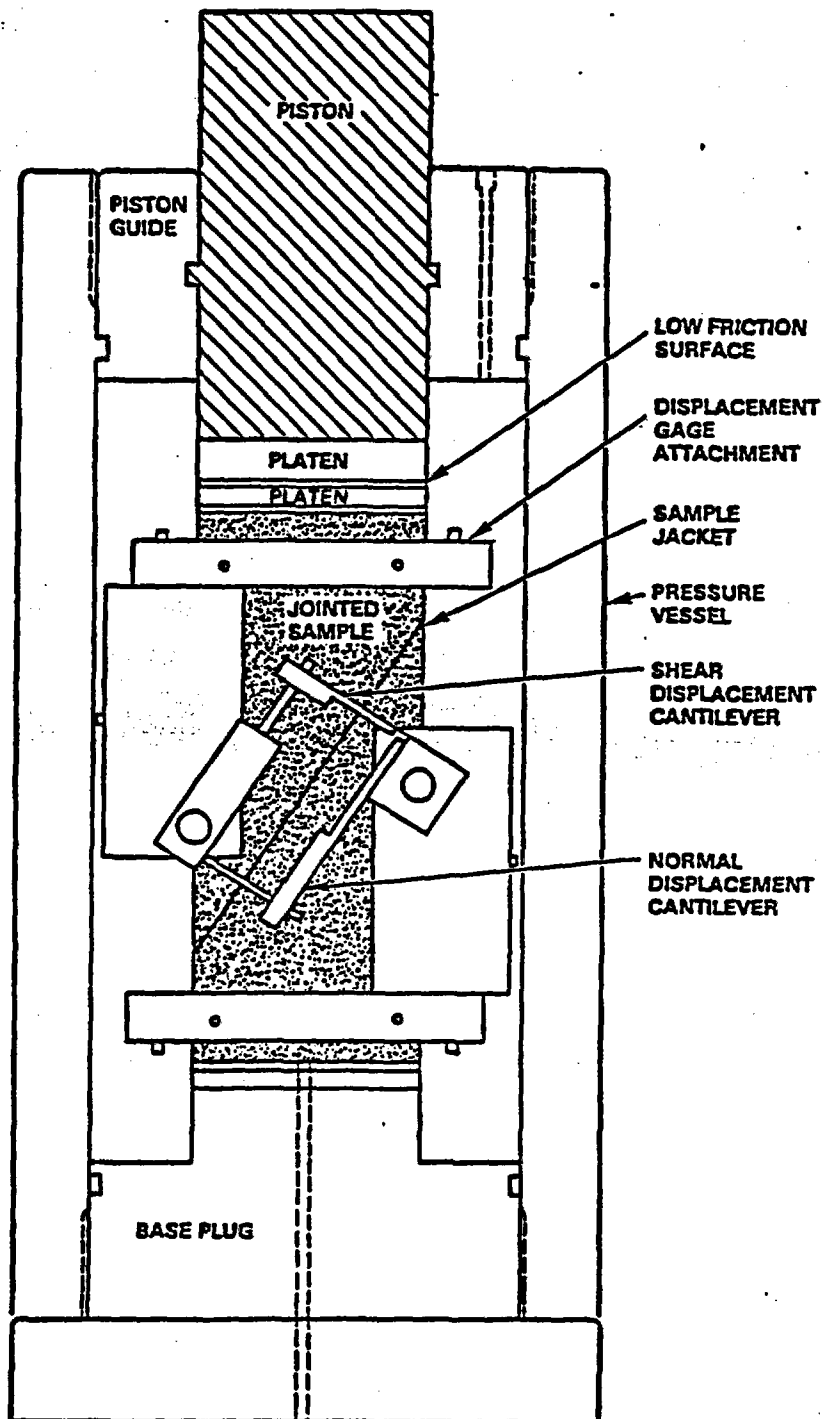
PS8508-29

Figure 2.2-5.   Range of joint normal displacement versus joint
normal stress for hydrostatic compression in basalt
cores.   (a) Test curves showing gradual closure
of a joint under increasing normal stress.
(b) Test curves showing rapid initial closure
of joint at early stage of loading
(Brechtel, 1985, p. 35).

PS8508-32

(a)

(b)
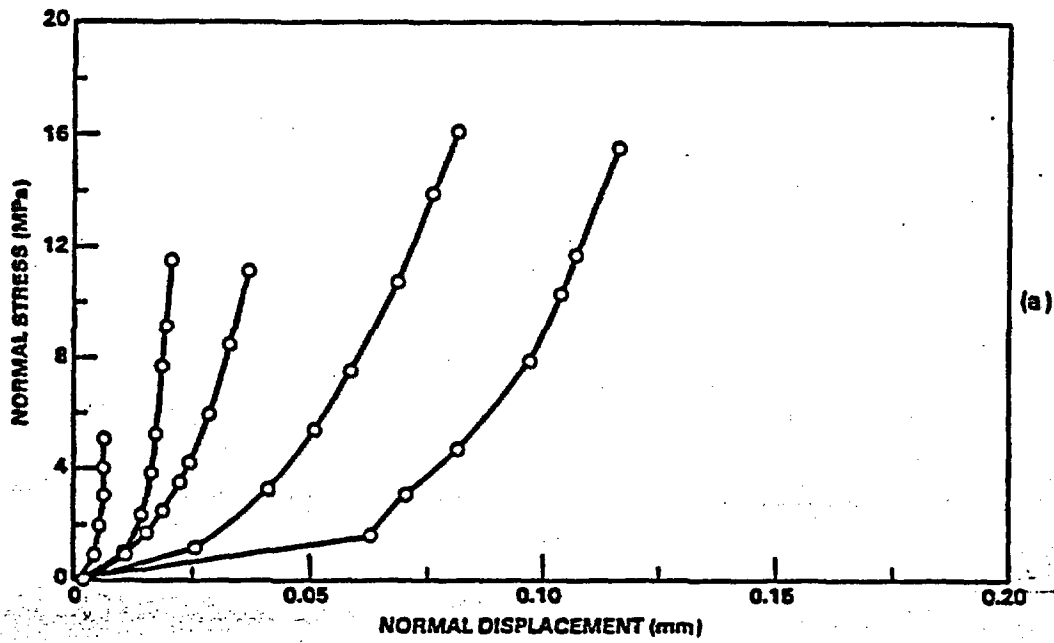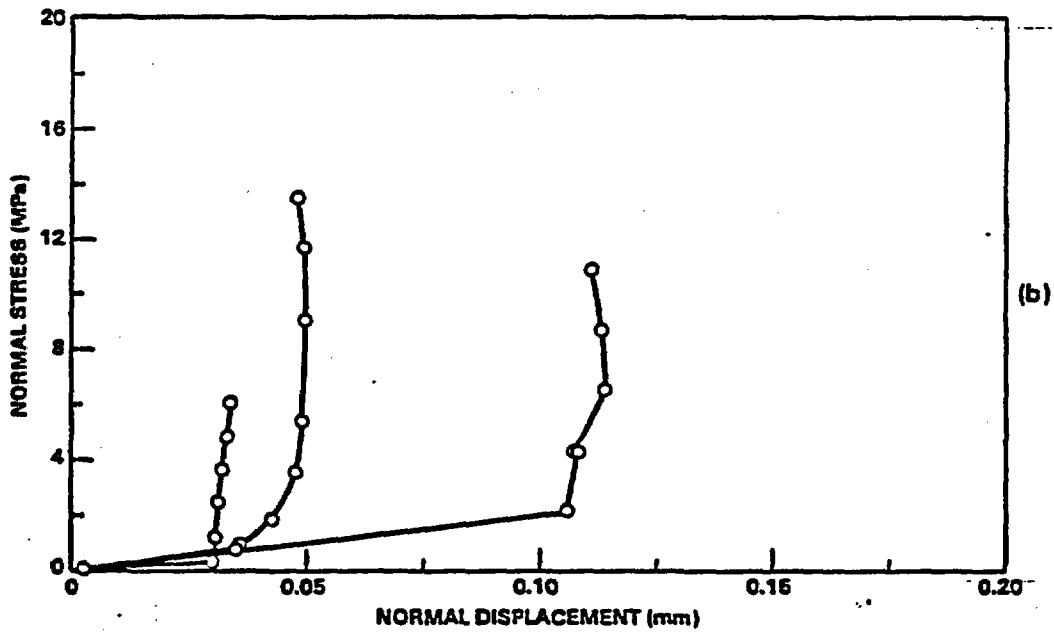
PS8508-32

Figure 2.2-6. Idealized stress-displacement curves
illustrating complex mechanical response of rock joints.

PS8508-35

Left plot: SHEAR STRESS (τ) vs. SHEAR DISPLACEMENT (μ_s) — labeled PEAK/RESIDUAL BEHAVIOR, STABLE SLIDING, HYSTERISIS

Right plot: NORMAL DISPLACEMENT (μ_n) / JOINT DILATION vs. SHEAR DISPLACEMENT (μ_s)
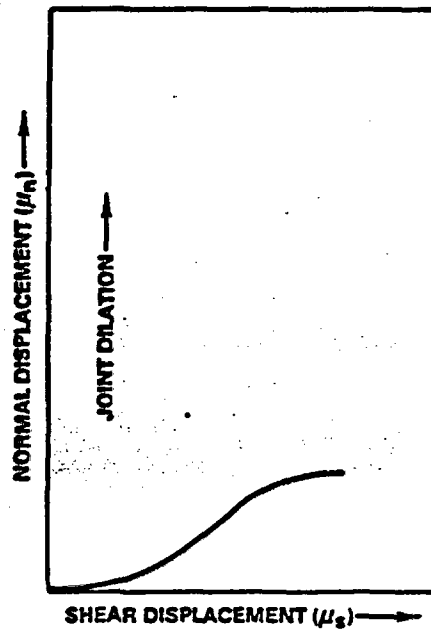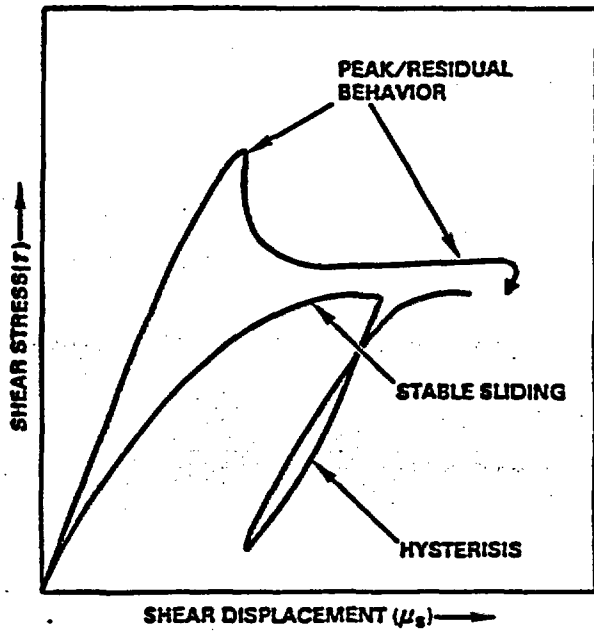
PS8508-35

PS8407-143

Figure 2.3-1. Comparison in in situ deformability modulus and rock quality
designation (after Deere et al., 1969, p. 171).

Legend:

r = 0.665
SL = 0.001
● DWORSHAK DAM, GRANITE GNEISS, SURFACE GAGES
○ DWORSHAK DAM, GRANITE GNEISS, BURIED GAGES
▲ GLEN CANYON DAM, SANDSTONE
□ TWO FORKS DAMSITE, GNEISS
■ YELLOWTAIL DAM, LIMESTONE

X-axis: ROCK QUALITY DESIGNATION, RQD (%)

Left Y-axis: DEFORMABILITY MODULUS (FIELD, STATIC), E (GPa)

Right Y-axis: DEFORMABILITY MODULUS (FIELD, STATIC), E (10^6 kip/in²)

P38407-143A
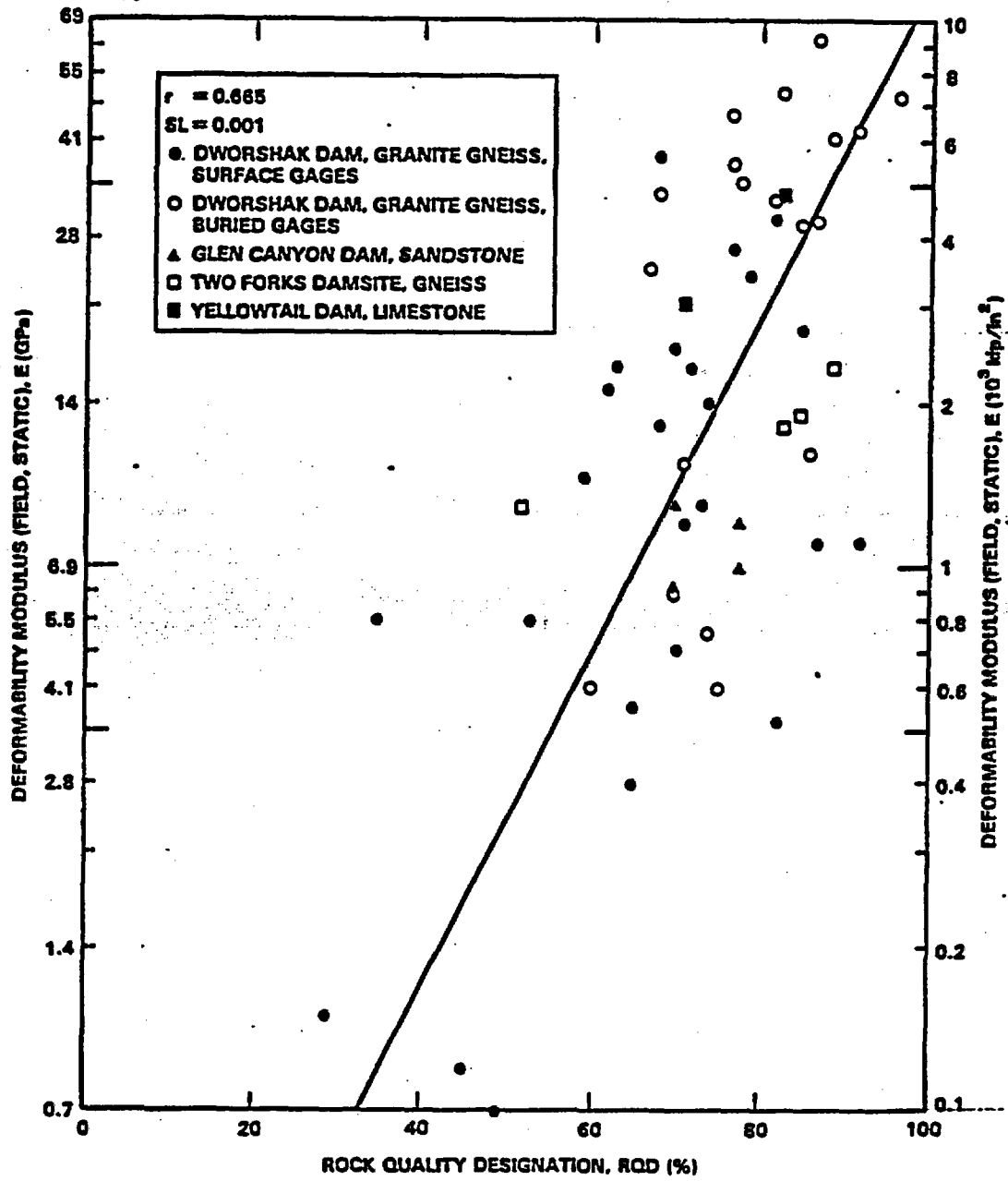
Figure 2.3-2. Relationship between in situ deformability modulus and geomechanics classification rock mass rating (after Bieniawski, 1978, p. 245).

GEOMECHANICS ROCK-MASS RATING (RMR)
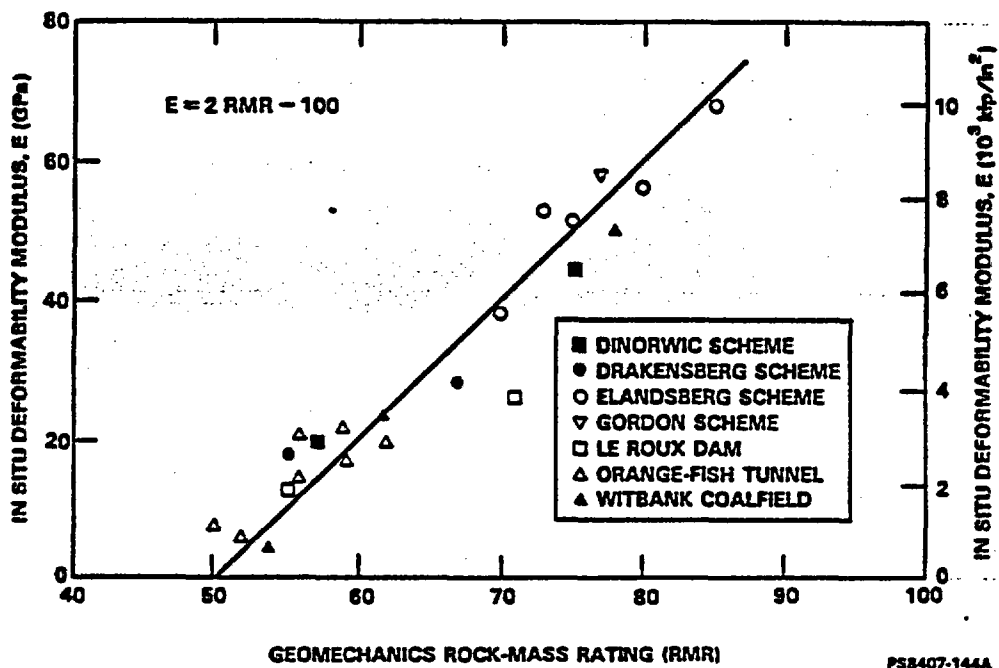
PS8407-144A

PS8407-142

Figure 2.3-3. Typical stress-deformation curve from plate bearing tests in fractured rock including cyclic loading (Schneider, 1967).

FRACTURED ROCKS

ρ = AVERAGE PRESSURE ON THE PLATE
$\bar{\omega}$ = AVERAGE DISPLACEMENT OF THE PLATE

STRESS (ρ) →
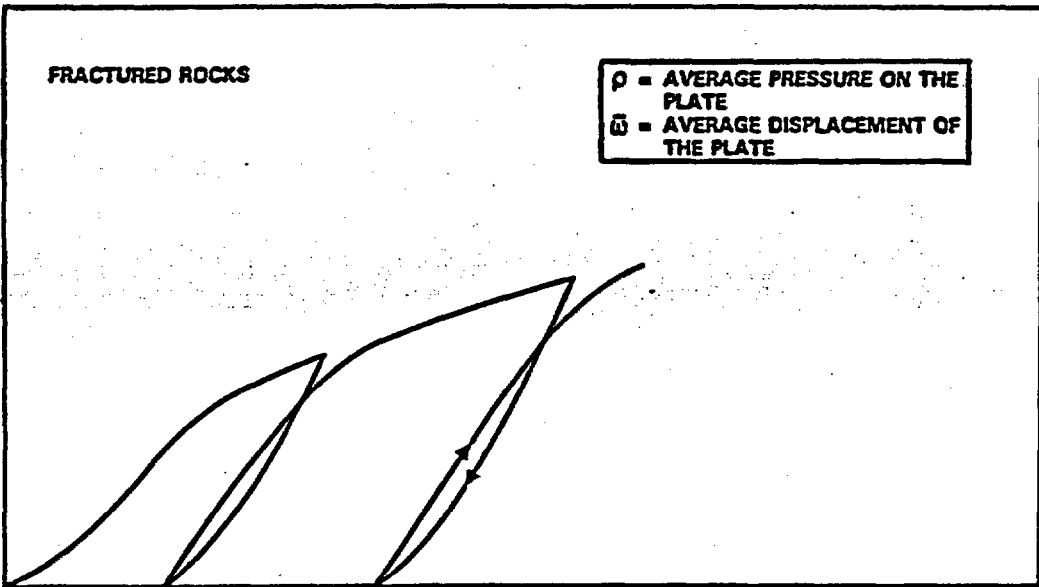
STRAIN ($\bar{\omega}$) →

PS8407-142

PS8407-147

Figure 2.3-4. The triaxial strength of Wombeyan marble (after Rosengren and Jaeger, 1968, p. 321).

MAJOR PRINCIPAL STRESS, σ_1 (kip/in^2)

MINOR PRINCIPAL STRESS, σ_3 (kip/in^2)

MINOR PRINCIPAL STRESS, σ_3 (MPa)

MAJOR PRINCIPAL STRESS, σ_1 (MPa)

WOMBEYAN MARBLE

I = INTACT MARBLE
II = HEAT-TREATED MARBLE
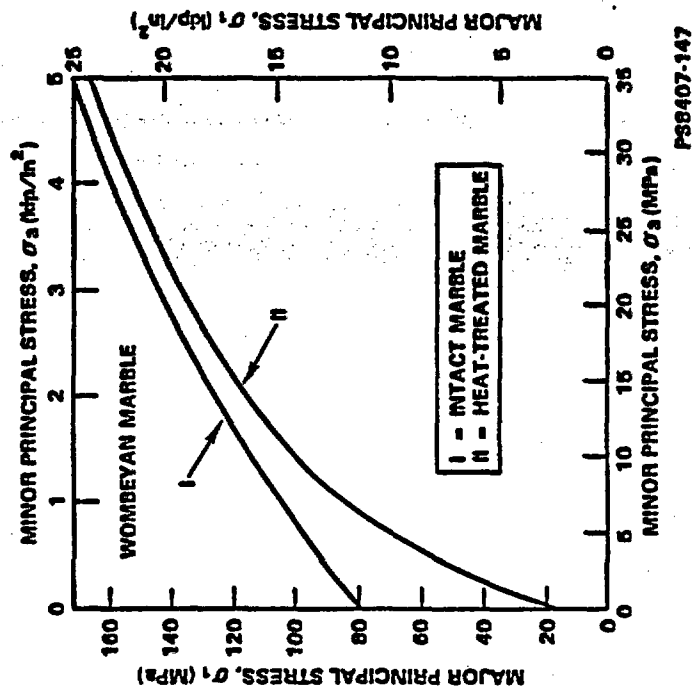
PS8407-147

Figure 2.3-5. Schematic of the jointed test block, flat jack and grouting
boxes in the Near-Surface Test Facility, after Cramer and Kim (1985).

PS8407-116

FLAT JACK

THERMOCOUPLES

GROUTING BOX

VERTICAL, Y

E-W, z

N-S, x

FACE

HYDRAULIC LINES
AND VALVES

~2 m
(6.6 ft)

~2 m
(6.6 ft)

~1 m
(3.3 ft)

~2 m
(6.6 ft)

~1.5 m
(4.5 ft)

TUNNEL 2
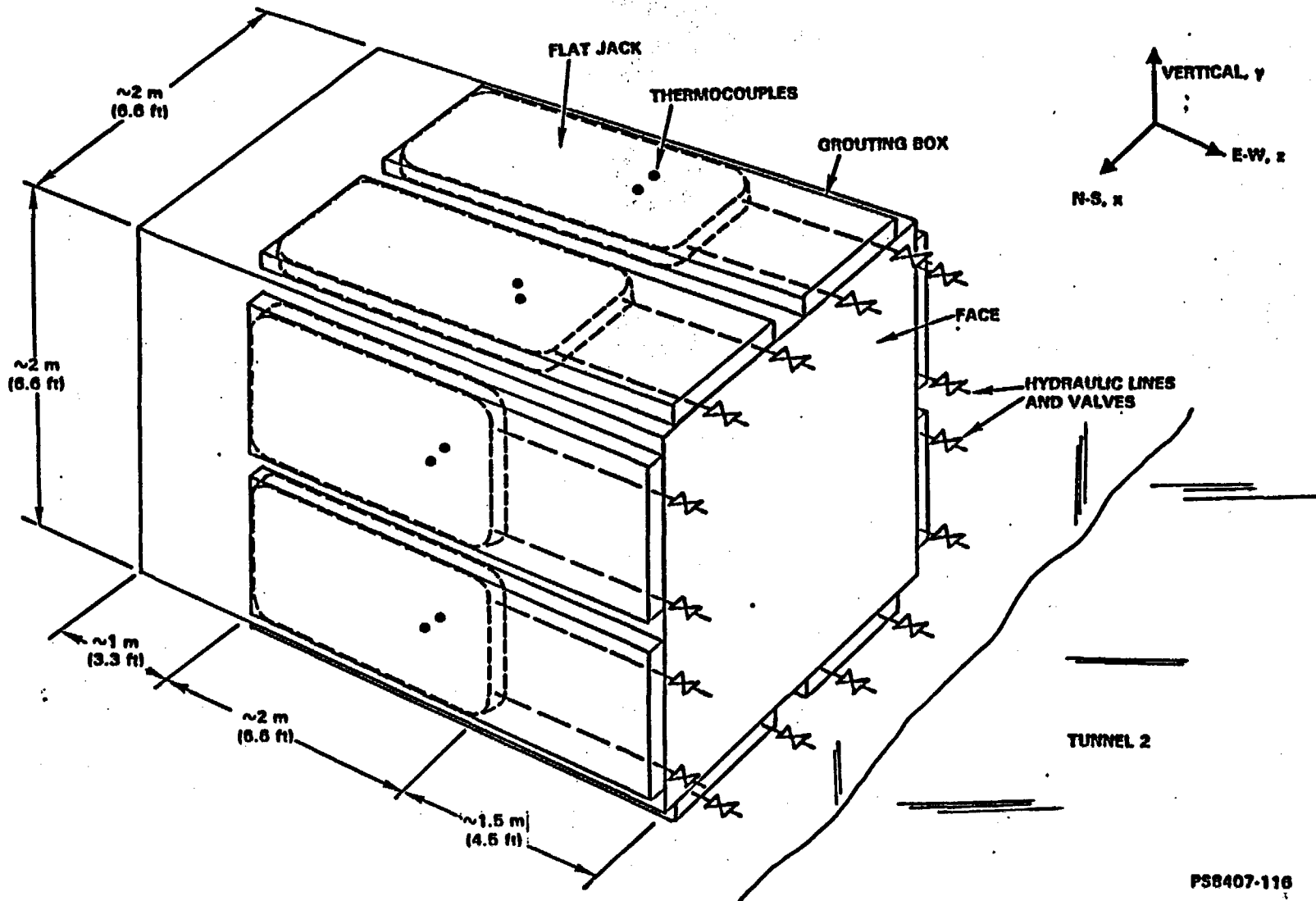
PS8407-116

Figure 2.3-6. Jointed block test step 1 heater and instrumentation (after Cramer, 1984, p. 12).

PS8407-153
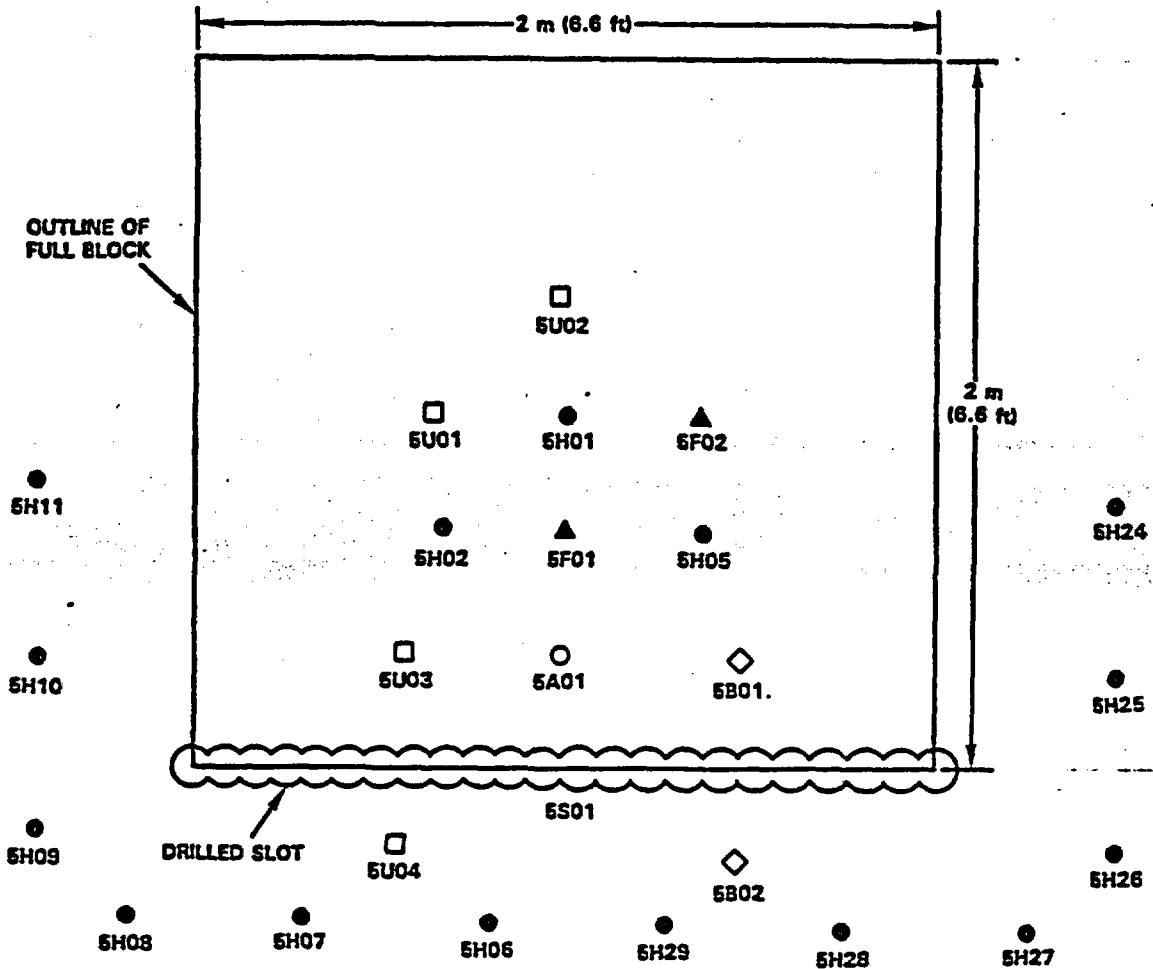
◇ CSIRO STRESS METER	CSIRO	= COMMONWEALTH SCIENTIFIC AND INDUSTRIAL RESEARCH ORGANIZATION	
● HEATER			
○ MONITORING HOLE	IRAD	= IRAD MANUFACTURING COMPANY	
▲ THERMOCOUPLE	USBM	= U.S. BUREAU OF MINES	
□ USBM/IRAD STRESS METER	NOTE: EACH INSTRUMENT AND HEATER SHOWN CONTAINS A THERMOCOUPLE		

PS8407-153

Figure 2.3-7. Jointed block test instrument layout and borehole designation
(after Cramer, 1984, p. 15).

PS8407-117
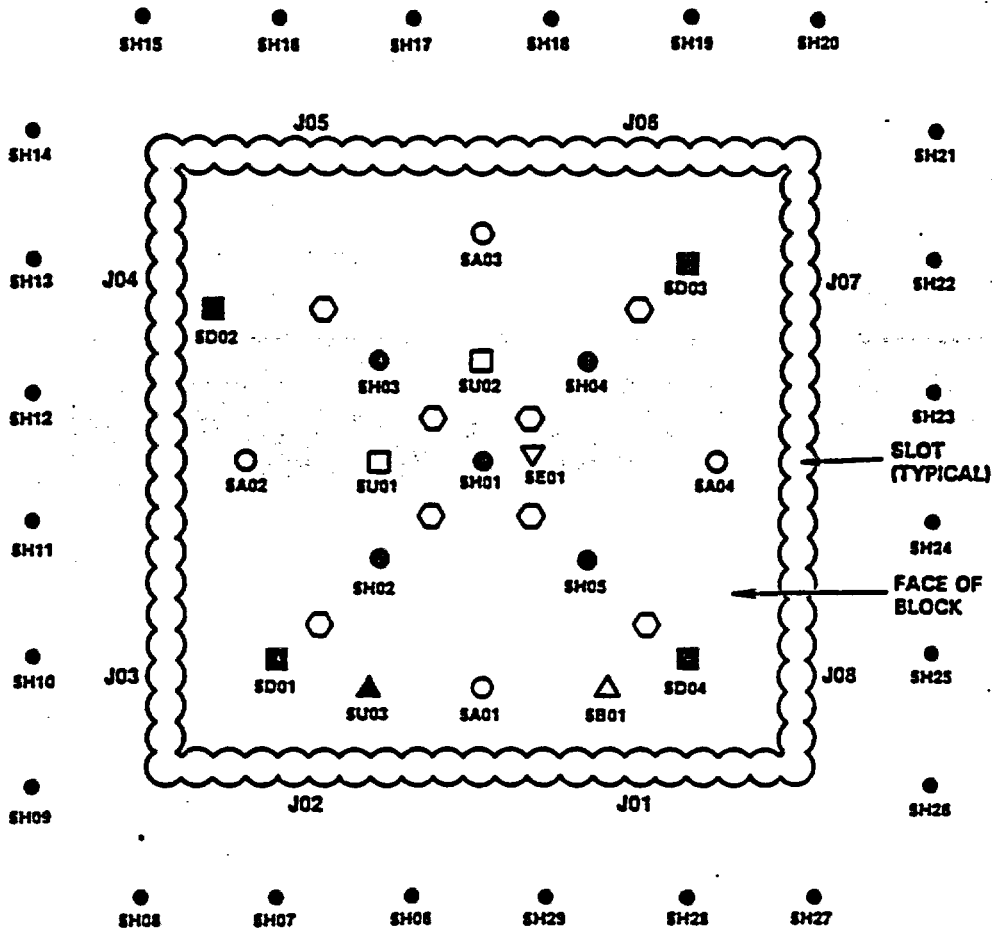
	BOREHOLE DEFORMATION GAGE		MONITORING HOLE
▲	BOREHOLE DEFORMATION GAGE AND VIBRATING WIRE STRESSMETER	○	OPTICAL TARGET
○	CABLE TENDON HOLE	△	VIBRATING WIRE STRESSMETER
▽	EXTENSOMETER		
●	HEATER		

NOTE: EACH INSTRUMENT AND HEATER SHOWN CONTAINS A THERMOCOUPLE;
J INDICATES FLAT JACK

PS8407-117

Figure 2.3-8. Deformational response of the test block during horizontal loading cycles at ambient temperature (Cramer et al., 1985, p. 24)

PS8407-154

FLAT JACK PRESSURE (lbf/in²)
(HORIZONTAL STRESSING)

FLAT JACK PRESSURE (MPa)
(HORIZONTAL STRESSING)

STRAIN (10⁻⁴)

PS8407-154

CYCLE 3R
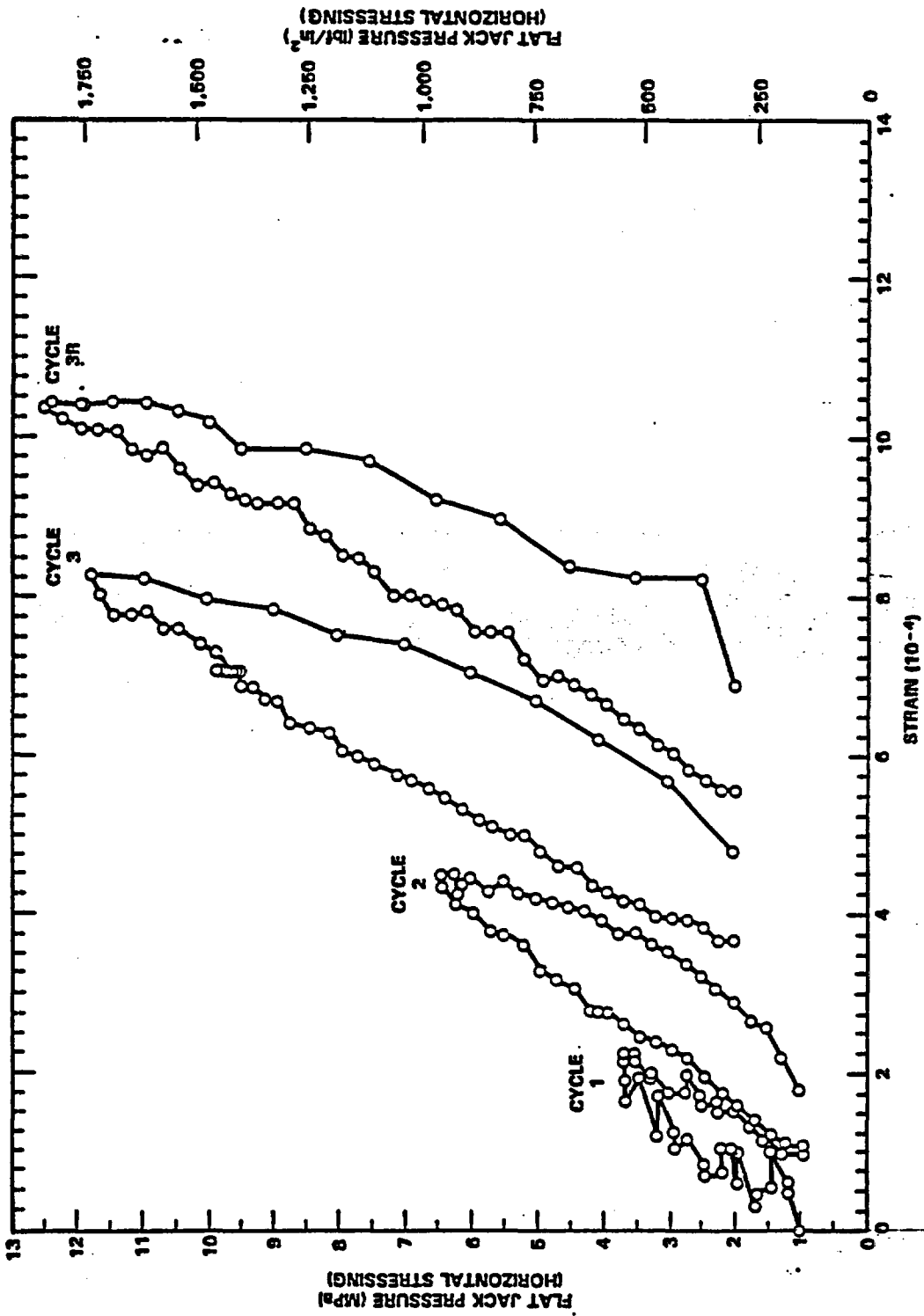
CYCLE 3

CYCLE 2

CYCLE 1

Figure 2.3-9. Deformational response of the block test during vertical
loading cycles at ambient temperature (Cramer et al., 1985, p. 24).

PS8407-155

FLAT JACK PRESSURE (lbf/in²)
(VERTICAL STRESSING)

1,750
1,500
1,250
1,000
750
500
250
0

STRAIN (10-4)

14   12   10   8   6   4   2   0

CYCLE 6

CYCLE 5

CYCLE 4

12   10   8   6   4   2

FLAT JACK PRESSURE (MPa)
(VERTICAL STRESSING)
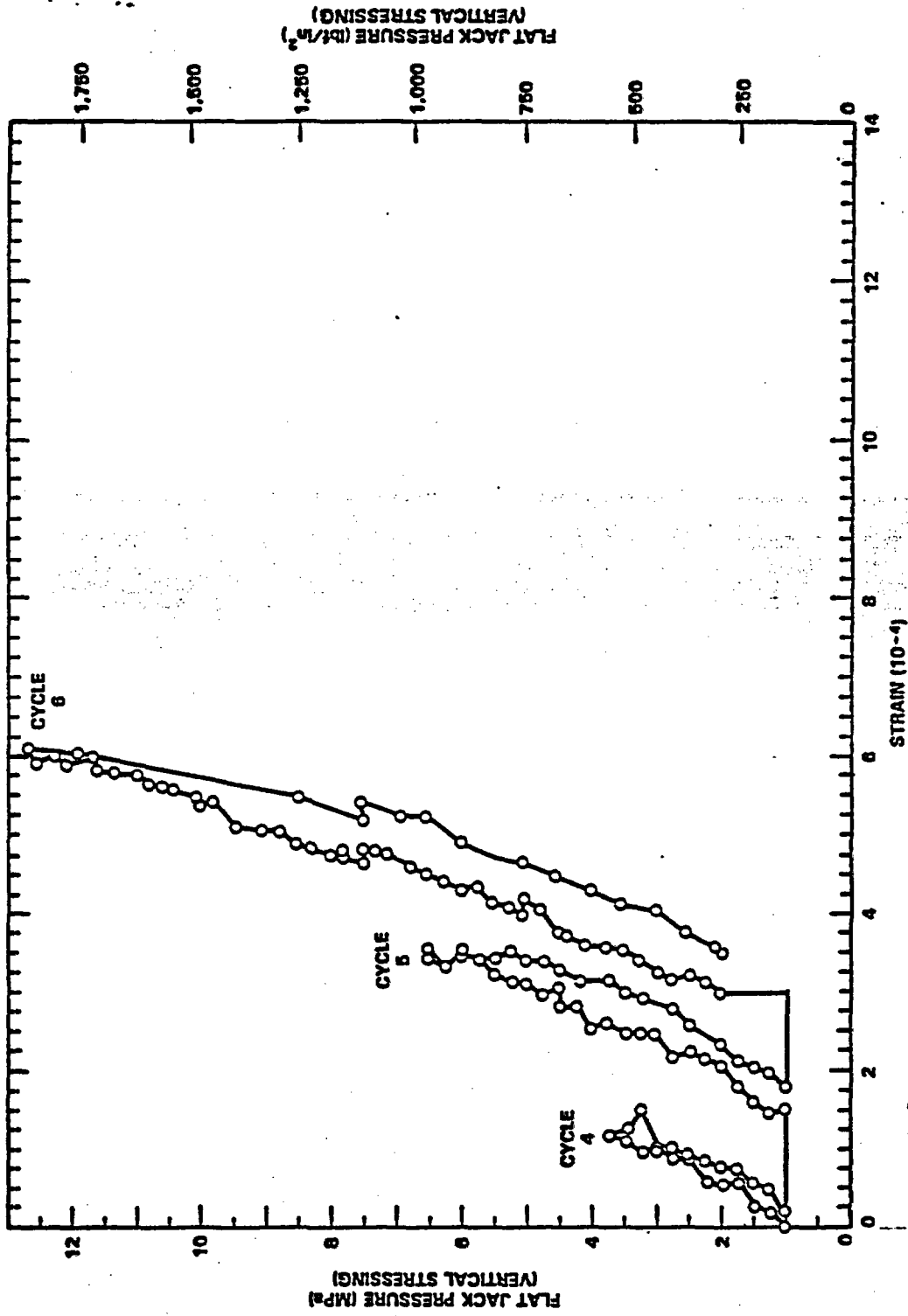
Figure 2.3-10. Deformational response of the test block during axial
loading cycles at ambient temperature (Cramer et al., 1985, p. 28).

PS8407-156

RELATIVE DISPLACEMENT (10^{-3} in.)

CYCLE 11

CYCLE 12

CYCLE 13

CYCLE 15

APPLIED LOAD (MN)

APPLIED LOAD (10^6 lb)

RELATIVE DISPLACEMENT (mm)
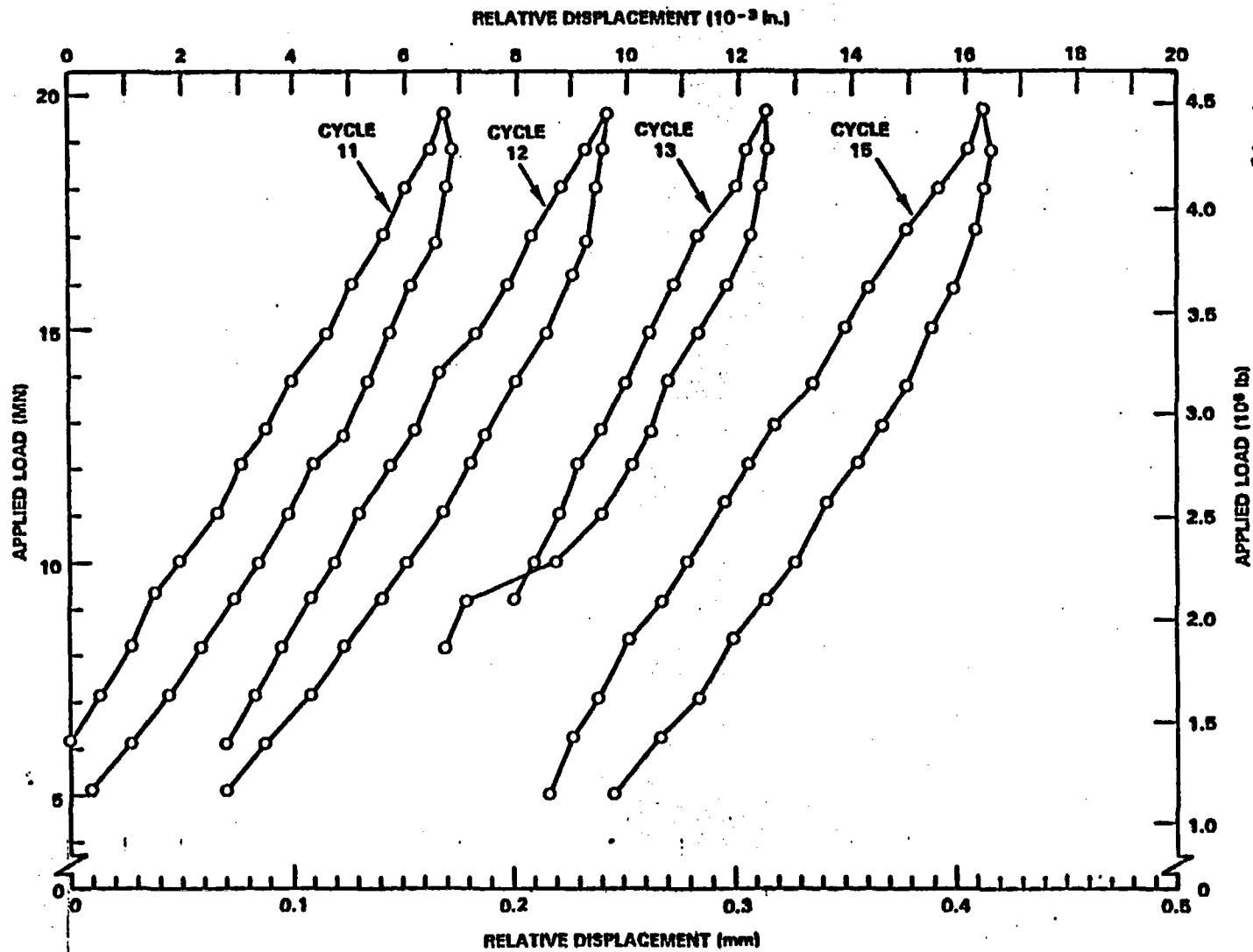
PS8407-156

Figure 2.3-11. Deformation moduli versus confining stress of the block test during ambient temperature testing (after Cramer and Kim, 1985, p. 345).

PS8508-40

PS8508-40
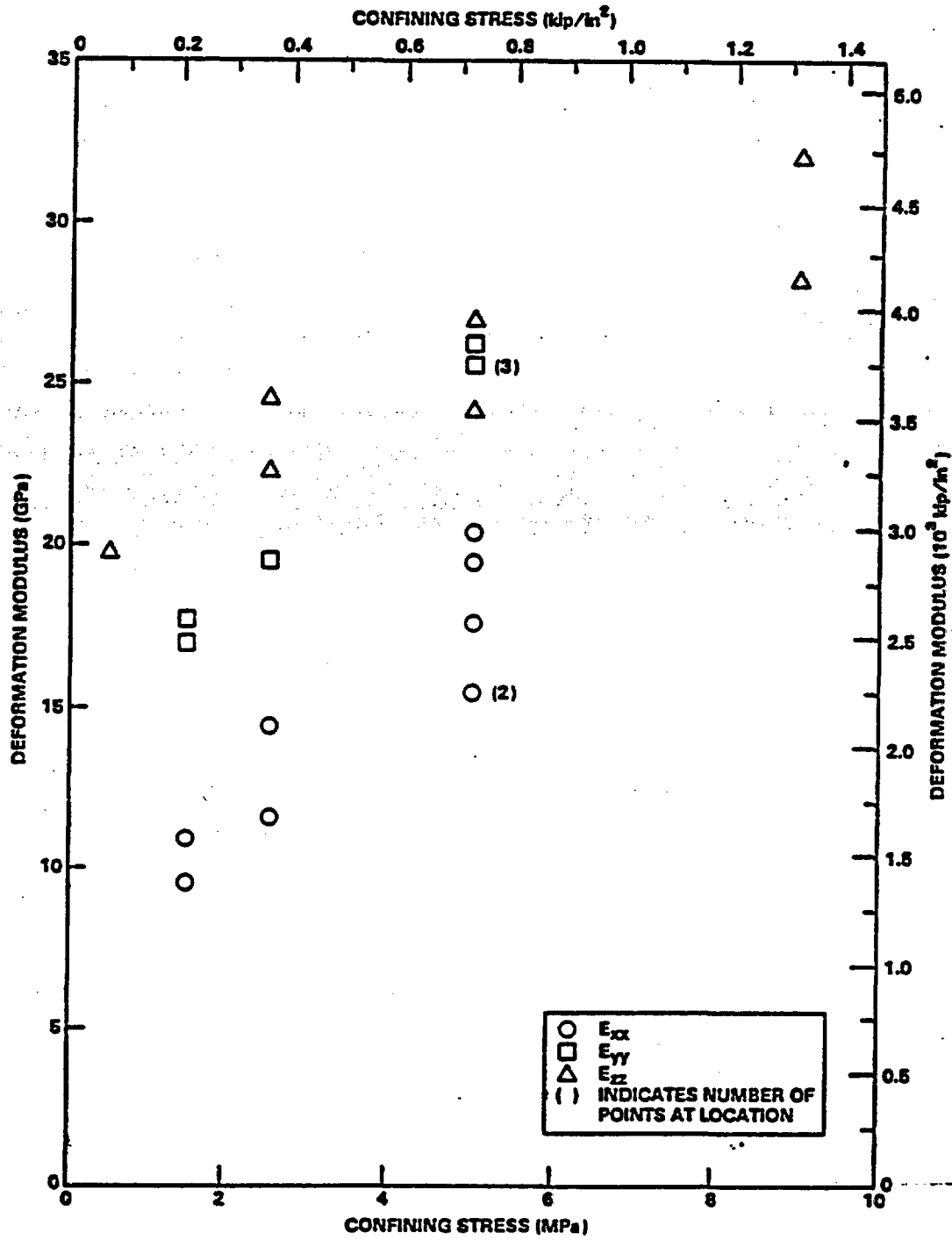
PS8407-173

Figure 2.3-12. Compressional-wave velocity (V_p) and shear-wave velocity (V_s) as a function of distance from the tunnel wall surface in vertical and horizontal directions (Myer et al., 1983, p. 28).
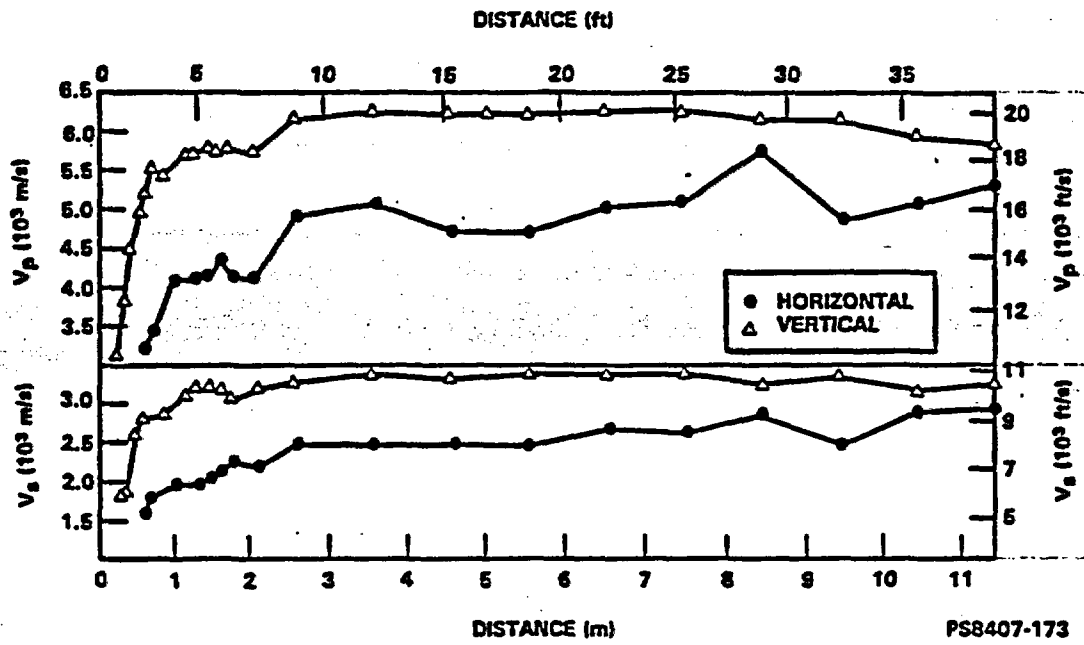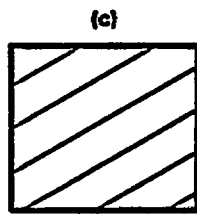
PS8407-173

PS8407-174

Figure 2.3-13. Dynamic elastic properties as a function of distance from the tunnel wall surface in vertical and horizontal directions (Myer et al., 1983, p. 34).
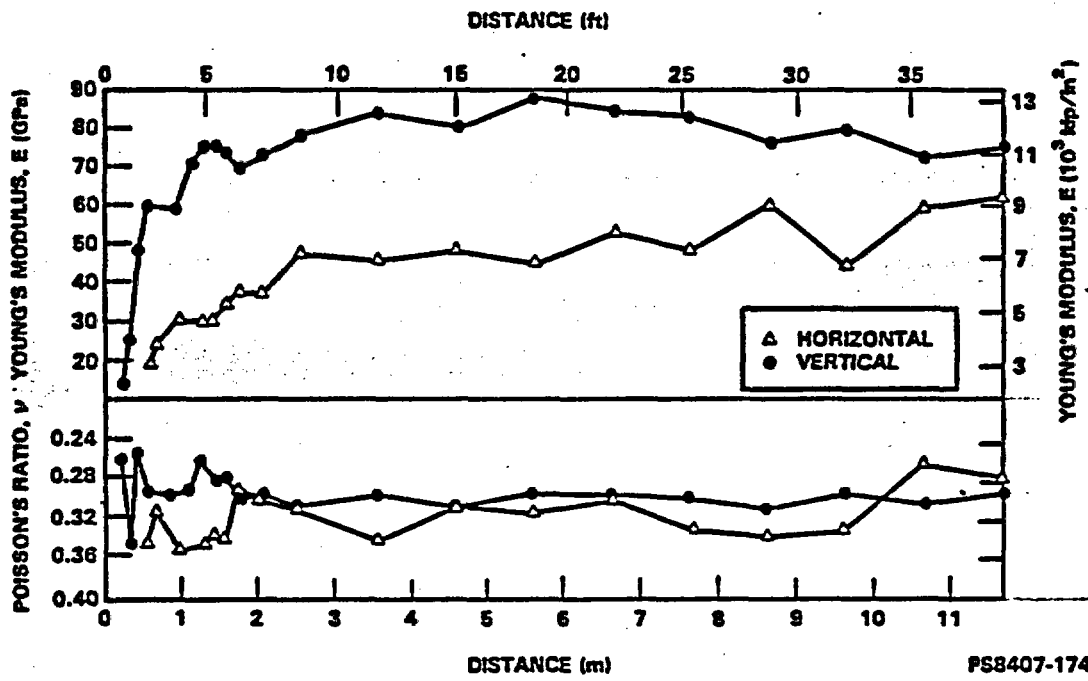
PS8407-174

PS8508-44

Figure 2.3-14(a) through (g). Conceptual models for a basaltic rock mass.
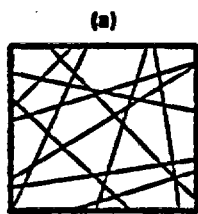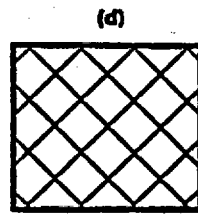
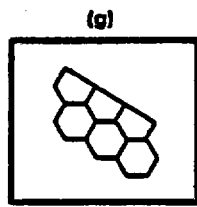| (a)	(b)	(c)	(d)
RANDOMLY FRACTURED	GRANULAR MATERIAL	SINGLE SET OF JOINTS (CONTINUOUS)	TWO SETS OF JOINTS (THROUGH GOING)
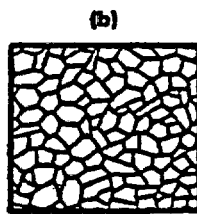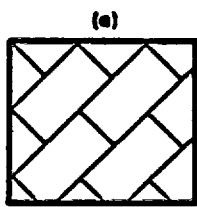
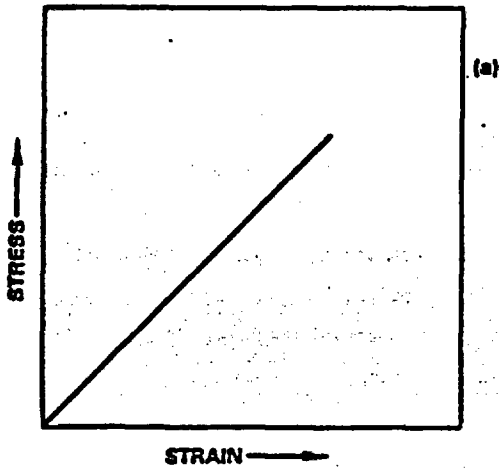| (e)	(f)	(g)
TWO SETS OF JOINTS (STEPPED)	FINITE FRACTURES	HEXAGONAL JOINTLY
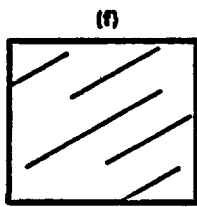
PS8508-44
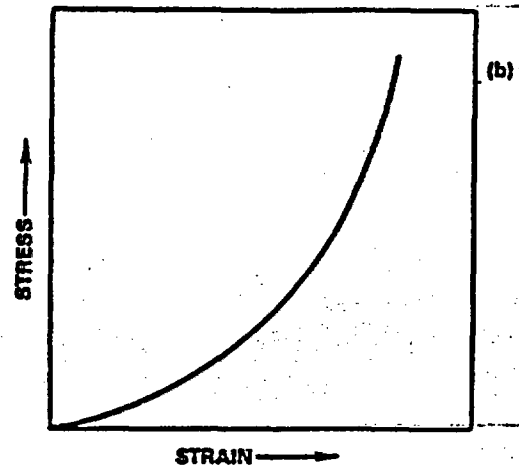
Figure 2.3-15(a) through (d). Equivalent continuum models for rock mass
deformation.

PS8508-45

LINEAR
ELASTIC

STRESS

STRAIN

(a)

NONLINEAR
ELASTIC

STRESS

STRAIN

(b)

BILINEAR

STRESS

STRAIN

(c)

HYSTERETIC

STRESS

STRAIN

(d)

PS8508-45
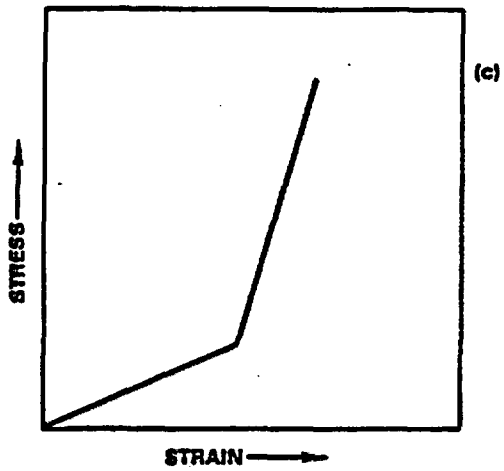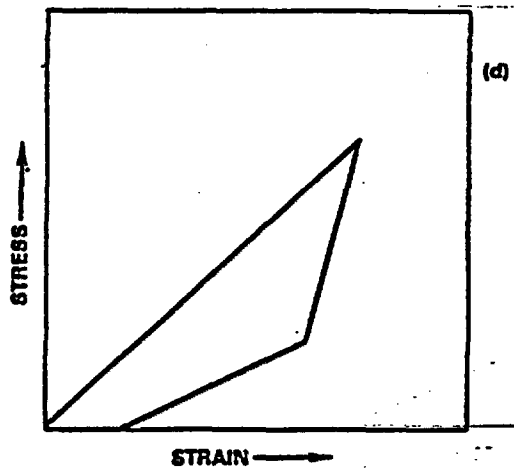
PS8407-146

Figure 2.3-16. Relationship between the strength and size of a rock specimen
as observed from large-scale compression tests (from Bieniawski and
Van Heerden, 1975, p. 104).

SPECIMEN SIDE LENGTH (ft)
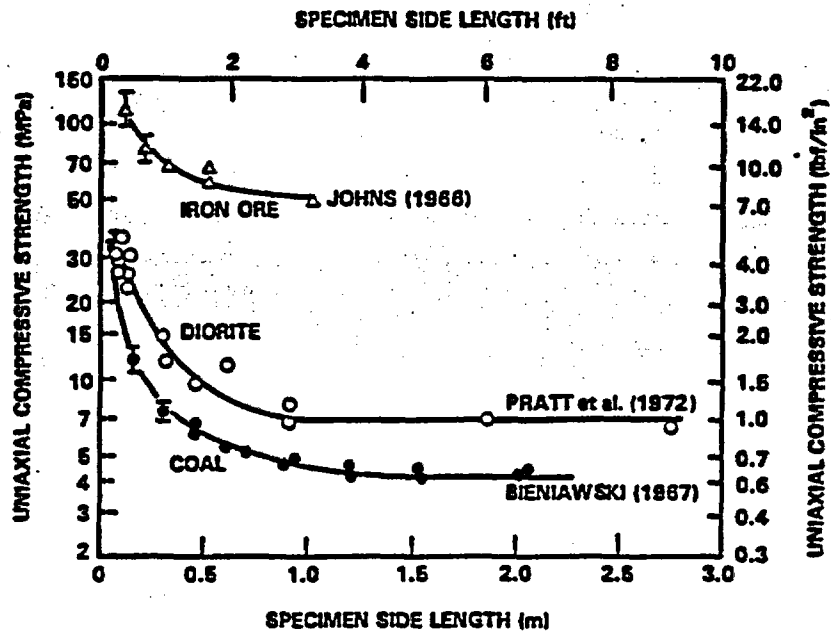
FS5407-146A

PS8407-96

Figure 2.4-1. Histogram of the thermal conductivity of basalt (Columbia River Plateau, Washington; Roy et al., 1981).

NUMBER OF SAMPLES = 72
K_{min} = 1.12
K_{max} = 2.38

(TO CONVERT W/m-K TO cal/cm-s-°C
DIVIDE BY 418.4)

THERMAL CONDUCTIVITY (W/m-K)

NUMBER OF SAMPLES
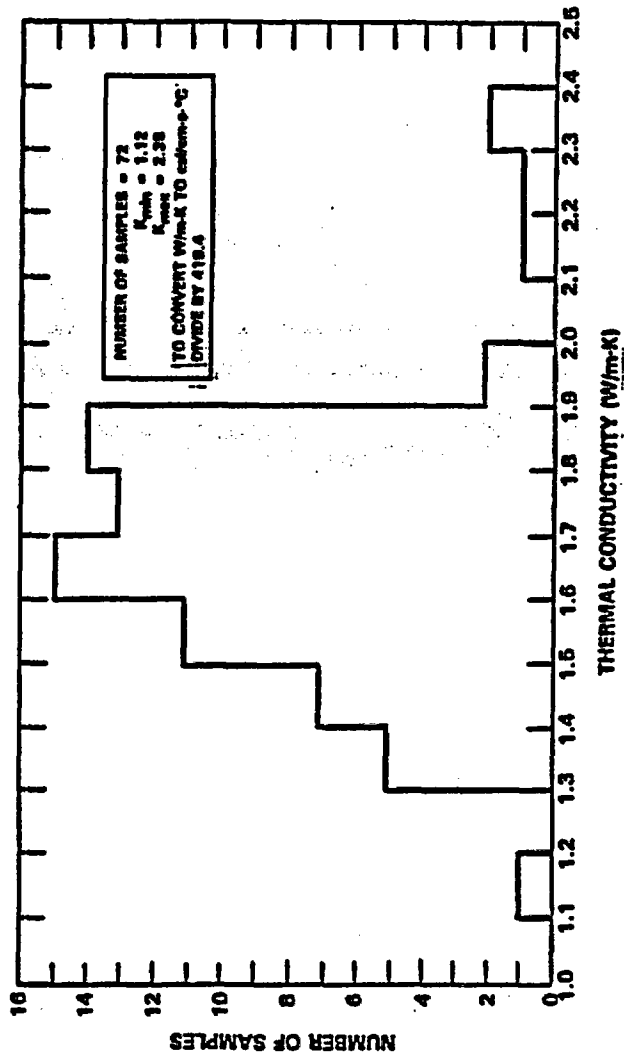
PS8407-86

PS8407-97

Figure 2.4-2. Range of probable thermal conductivity values for basalt
(Roy et al., 1981).

TO CONVERT W/m·K TO cal/cm·s·°C, DIVIDE BY 418.4
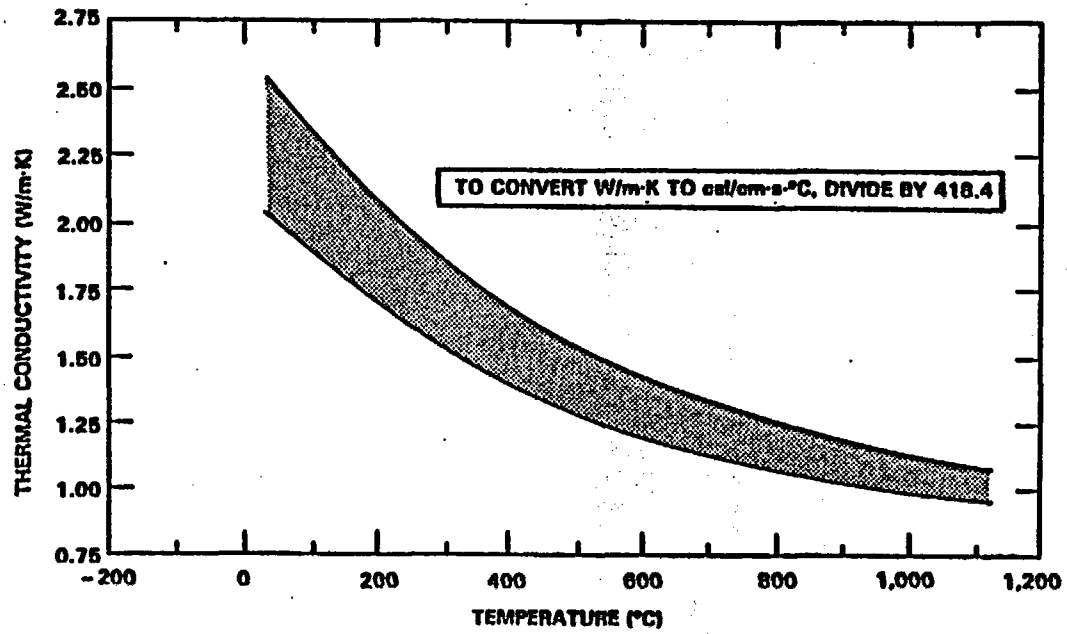
PS8407-97

PS8407-98

Figure 2.4-3. Range of probable heat capacity values for basalt (Roy et al., 1981).

TO CONVERT J/kg-K TO cal/g-°C, DIVIDE BY 4,184

DRESSER BASALT

TRANSITION ~570°C

HEAT CAPACITY (J/kg-K)

TEMPERATURE (°C)
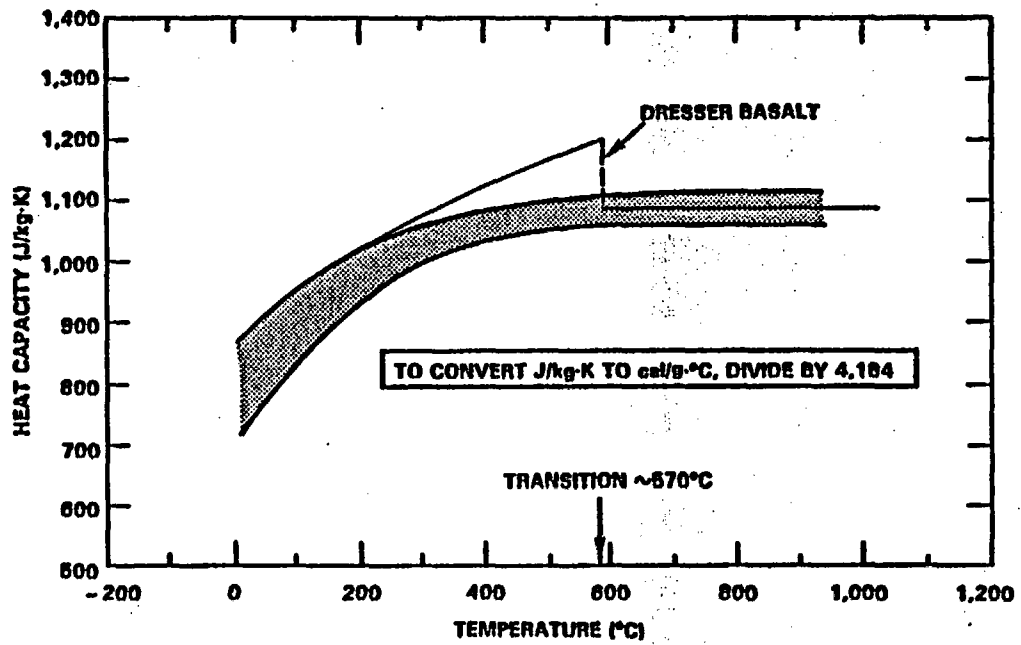
PS8407-98

Figure 2.5.1. Heater power levels for Full-Scale
Heater Test 1 (Williams et al., 1981, pp. 11-12).

PS8407-113
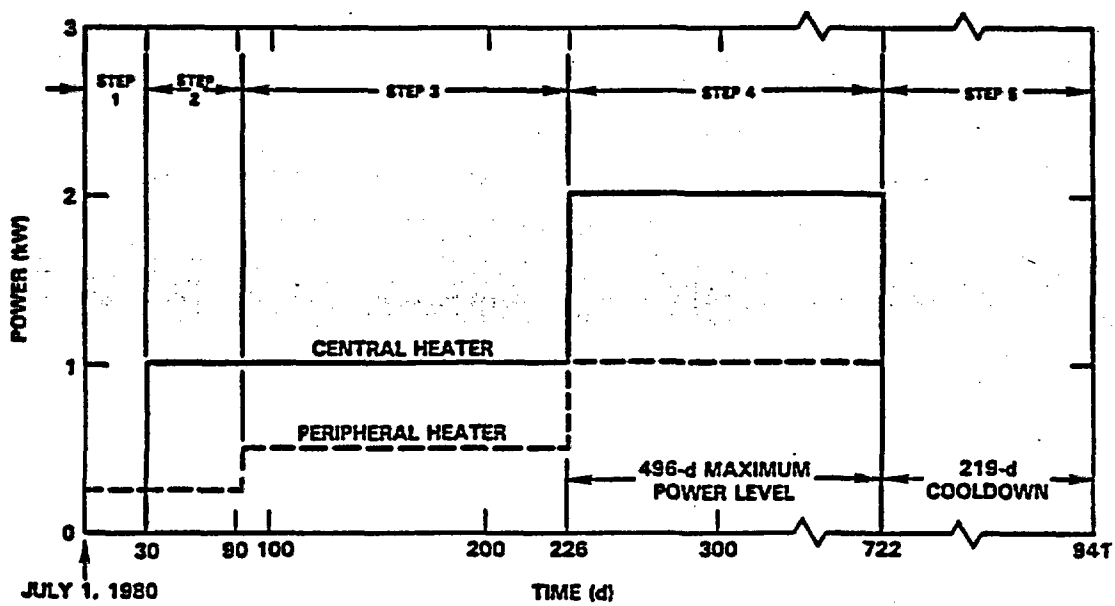
NOTE: A TOTAL OF 8 PERIPHERAL HEATERS HAD BEEN INSTALLED, EACH POWERED AT THE SAME LEVEL AS SHOWN IN FIGURE.

PS8407-113

Figure 2.5-2. Instrumentation layout for Full-Scale
Heater Test 1 (AMI, 1986, p. 17).

PS8407-112

CL OF ARRAY

CABLEWAY 1 →

HOLES DRILLED FROM
EXTENSOMETER ROOM

CL

CL

-N-

CL

```
0        1        2        3 METERS
```

```
0            4            6 FEET
```
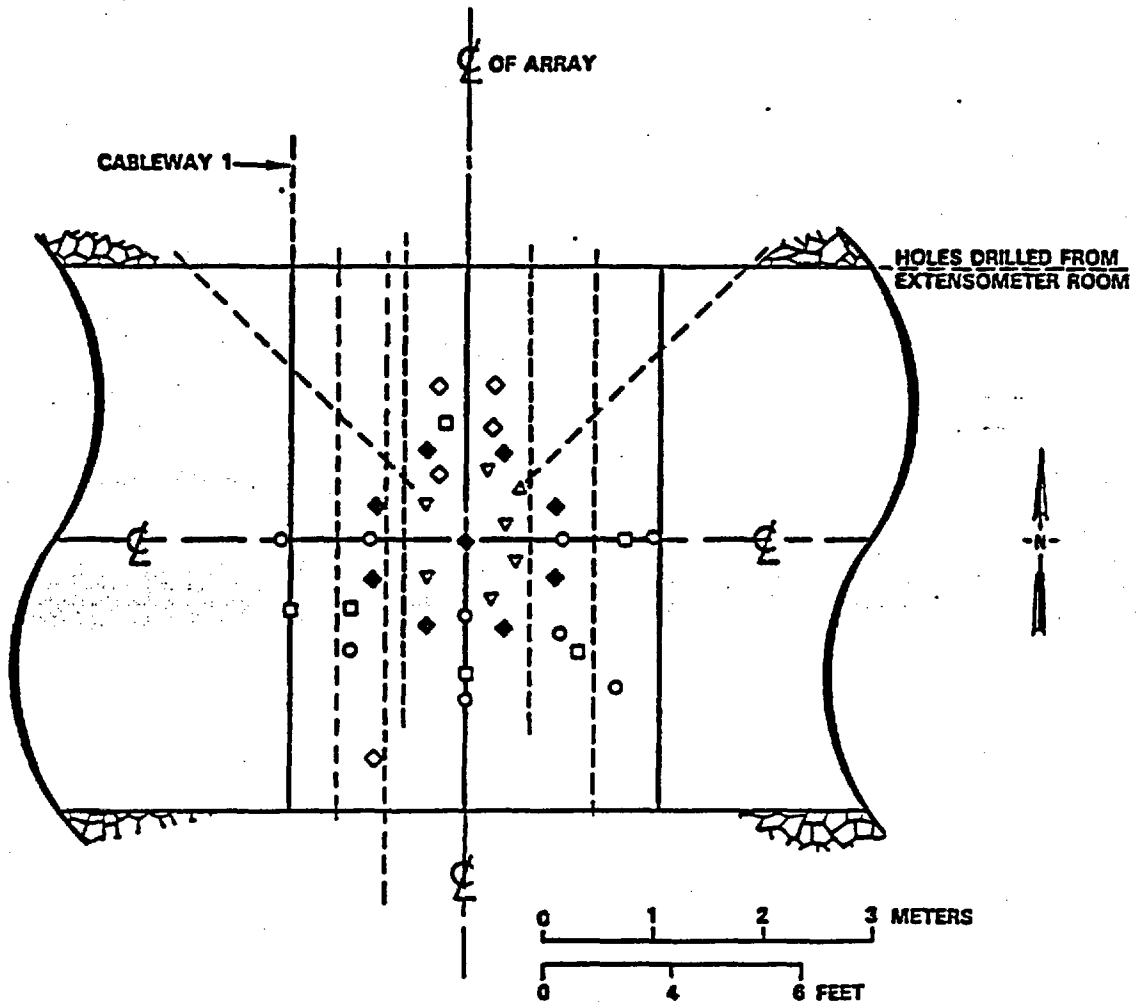
IRAD = IRAD MANUFACTURING COMPANY
USBM = U.S. BUREAU OF MINES

HOLE SYMBOLS	INSTRUMENTS
○	EXTENSOMETER
◆	HEATER
◇	MONITOR
▽	THERMOCOUPLE
□	USBM/IRAD

PS8407-112

Figure 2.5-3. Heater power levels for Full-Scale
Heater Test 2 (Williams et al., 1981, pp. 13-15).
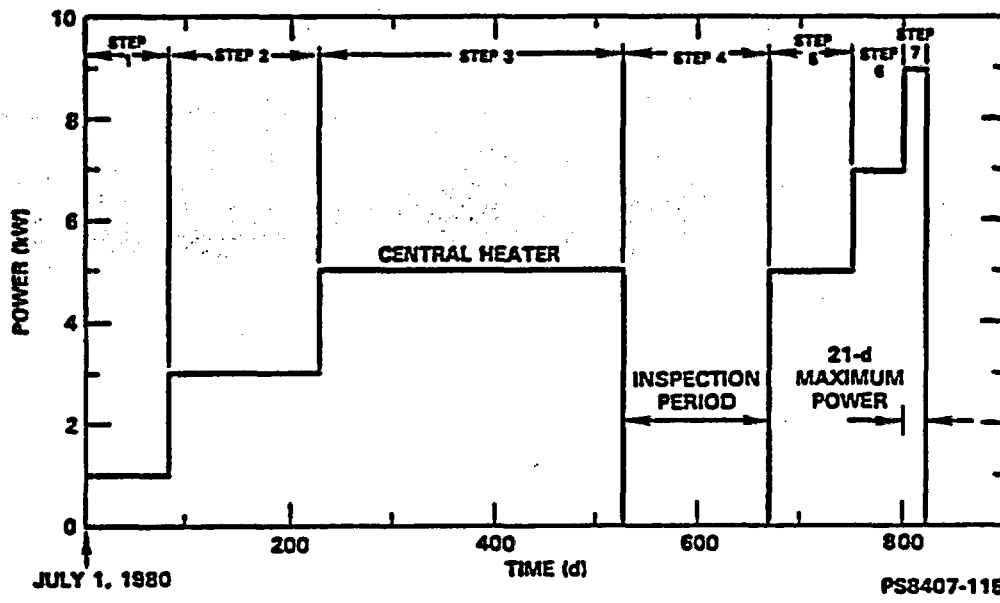
.PS8407-115

Figure 2.5-4. Instrumentation layout for Full-Scale
Heater Test 2 (AMI, 1986, p. 18).

PS8407-114

Ҁ OF ARRAY

← CABLEWAY 2

HOLES DRILLED FROM
EXTENSOMETER ROOM

Ҁ

Ҁ

-N-

Ҁ
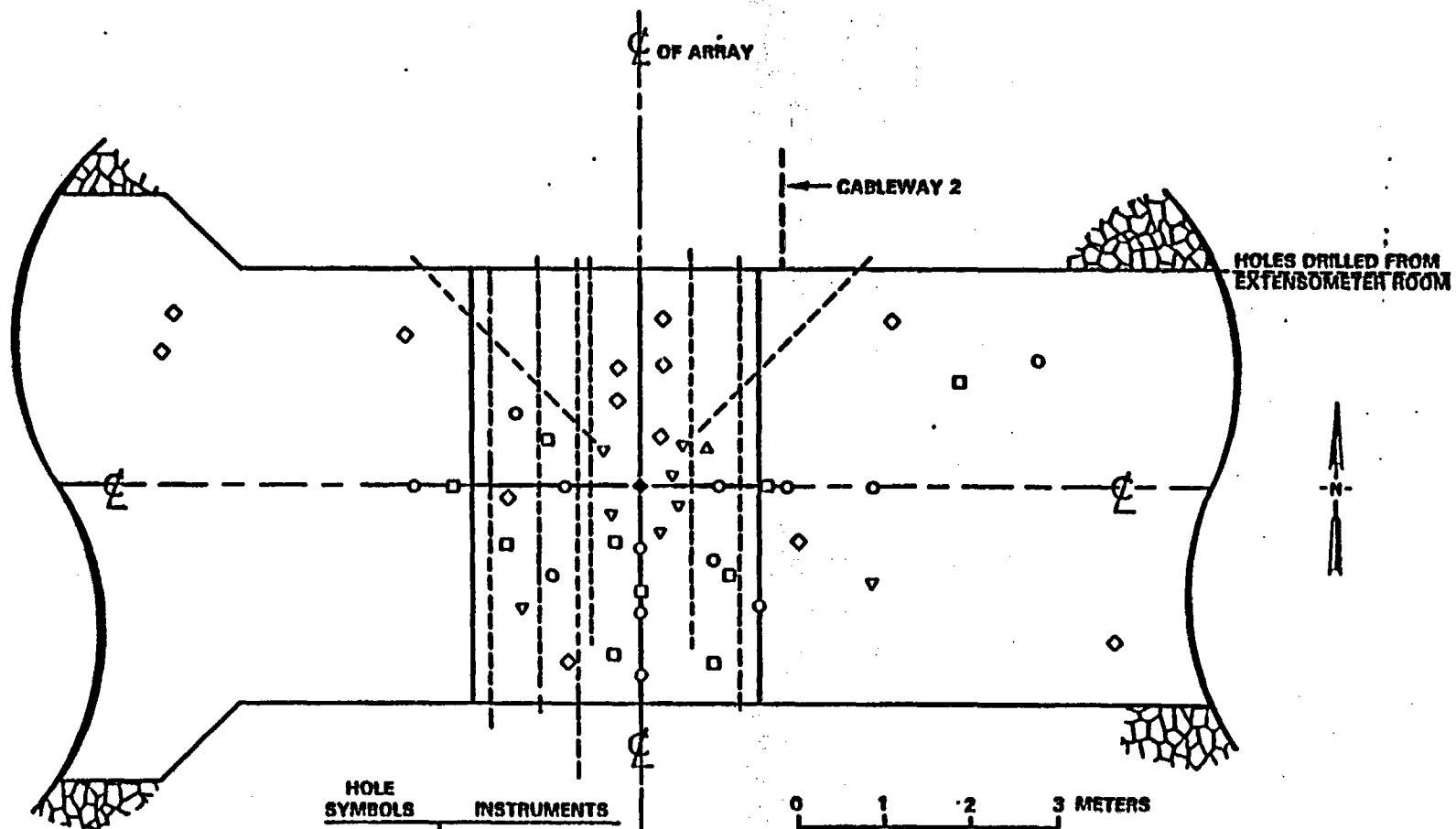
HOLE SYMBOLS	INSTRUMENTS
○	EXTENSOMETER
◆	HEATER
◇	MONITOR
▽	THERMOCOUPLE
□	USBM/IRAD STRESS METER

0   1   2   3 METERS

0   4   8 FEET
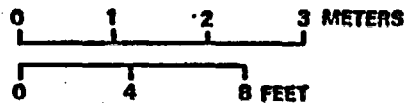
IRAD = IRAD MANUFACTURING COMPANY
USBM = U.S. BUREAU OF MINES

PS8407-114

Figure 2.5-5. Full-Scale Heater Test 1 measured and
predicted temperatures for themocouple 1T01T03
(AMI, 1986, p. 69).

PS8407-175
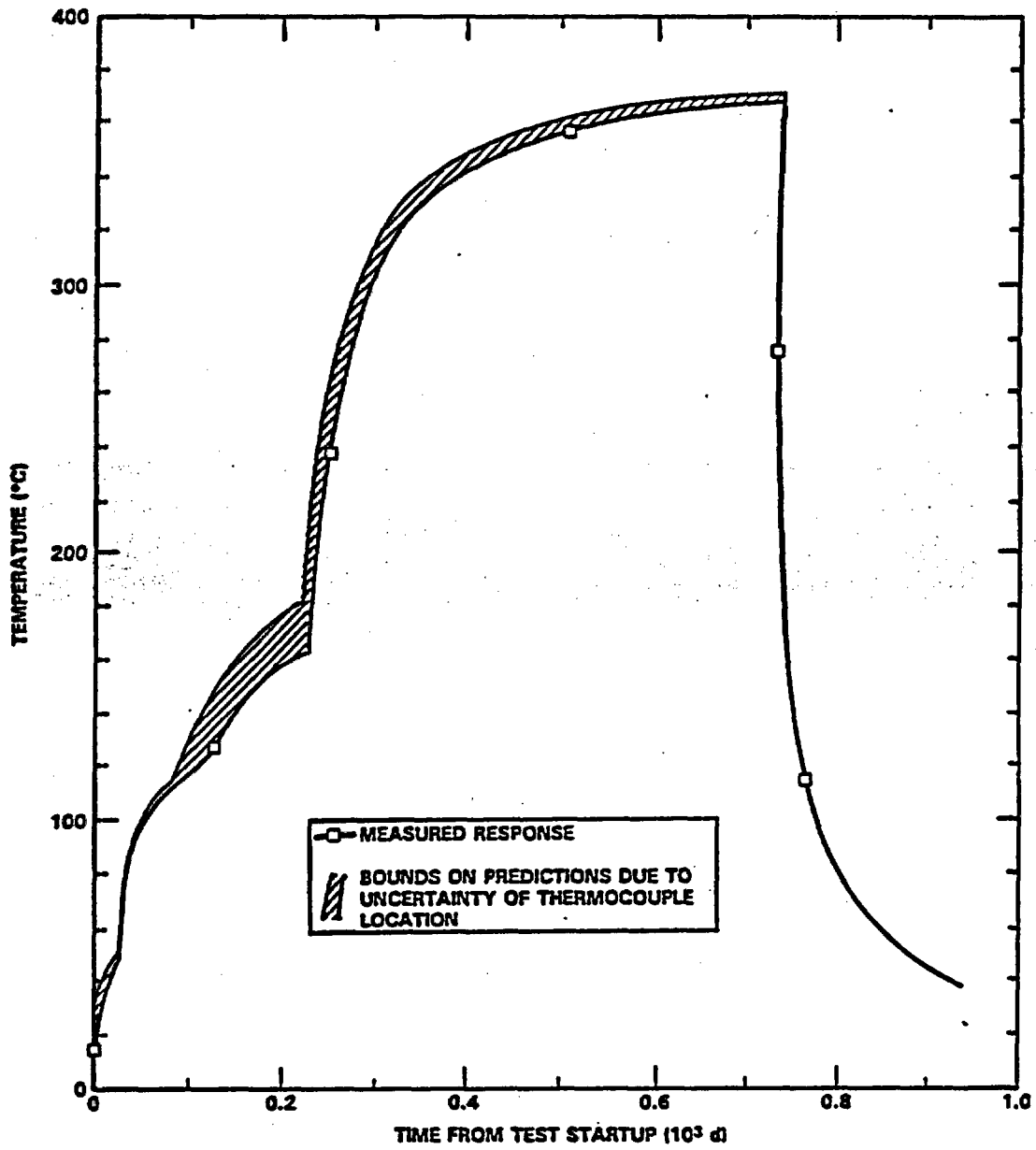
PS8407-175

Figure 2.5-6. Full-Scale Heater Test 2 measured and
predicted temperatures for thermocouple 2T01T03
(AMI, 1986, p. 70).

PS8407-176

TIME FROM TEST STARTUP (10³ d)
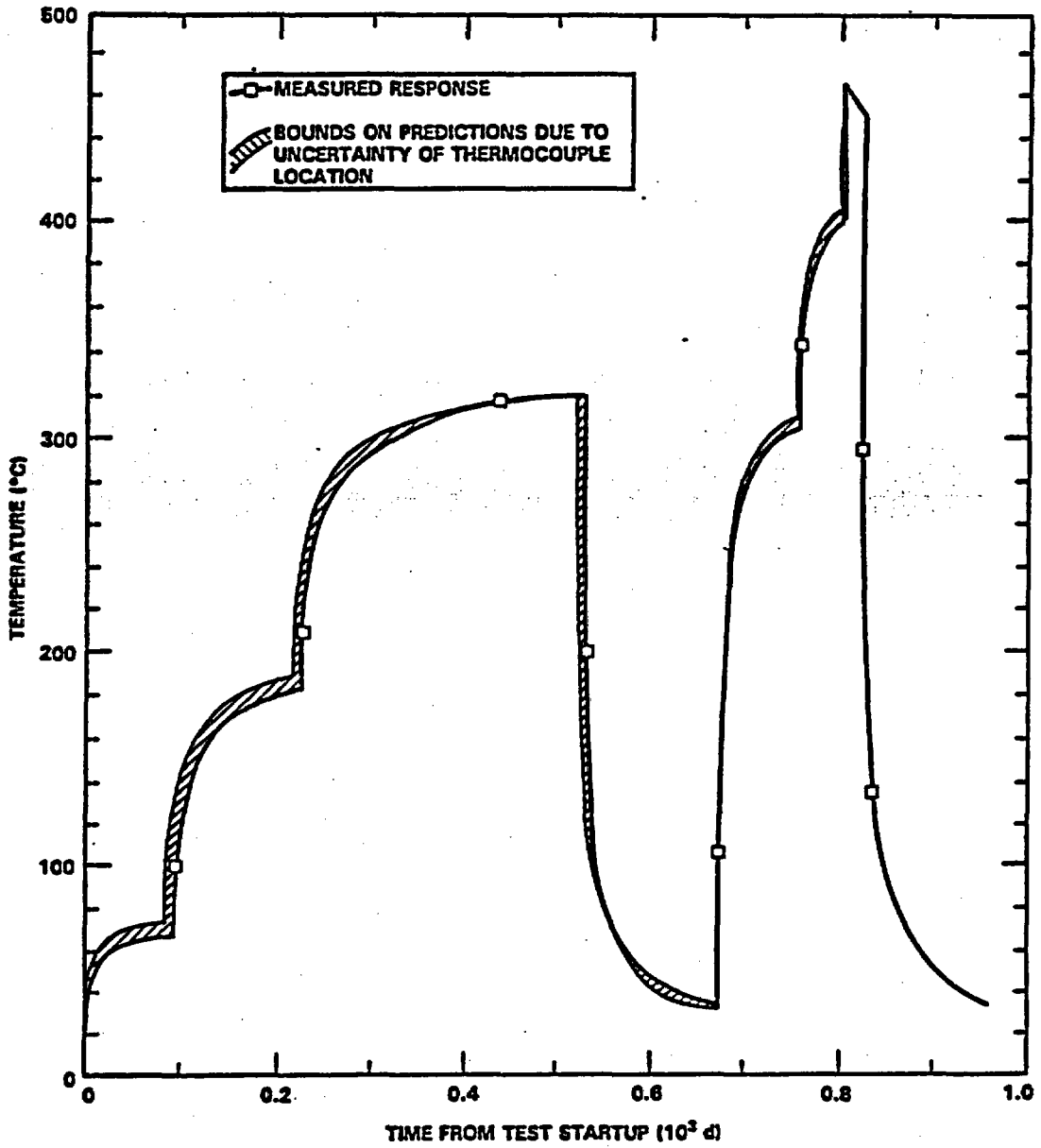
PS8407-176

Figure 2.5-7. Time history vertical displacement response and
predicted displacement for a location at a radius 0.95 m (3.12 ft)
from the center of the main heater for Full-Scale Heater Test 1
(AMI, 1986, pp. 84-85).

PS8407-180
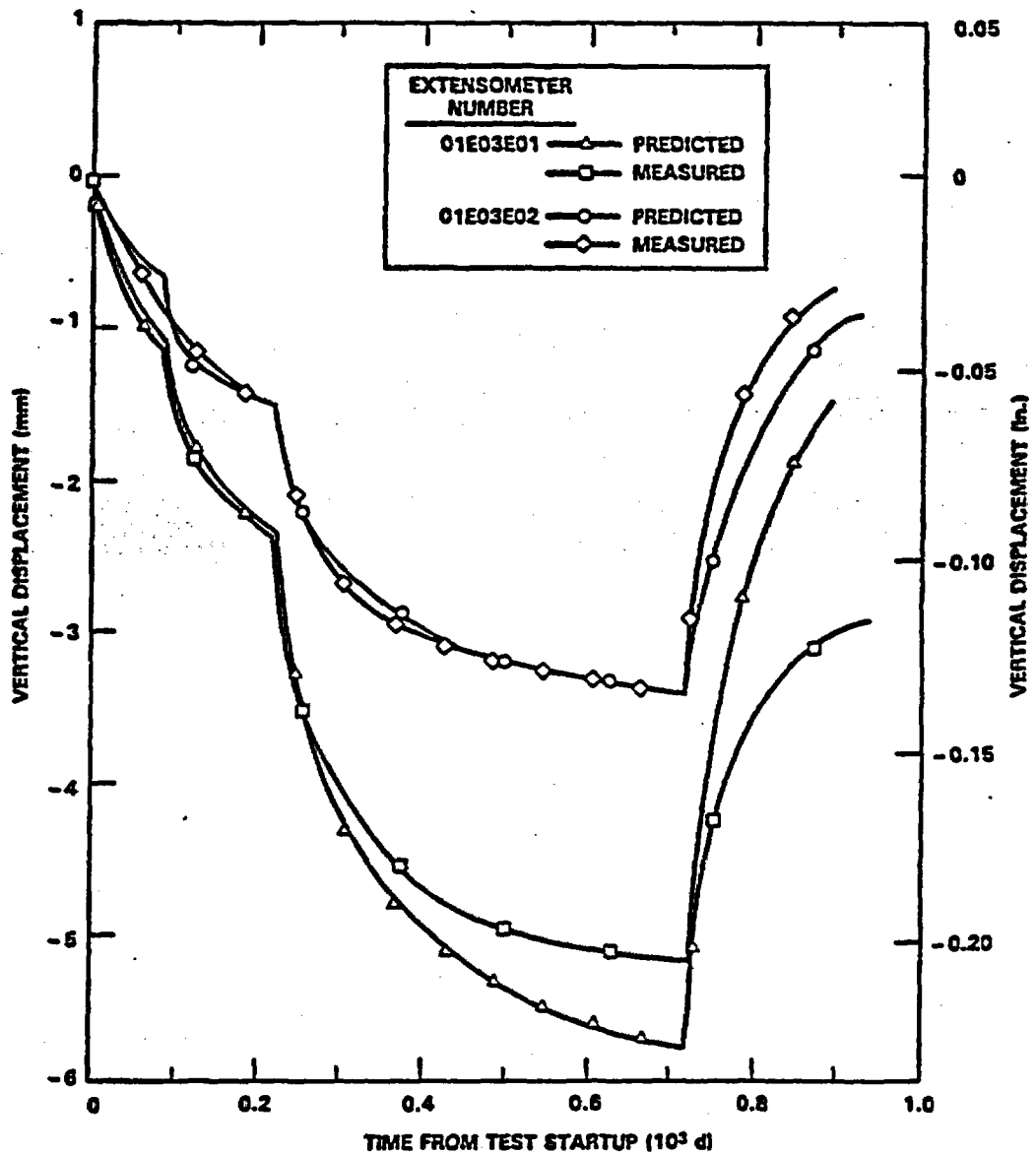
PS8407-180

Figure 2.5-8. Time history vertical displacement response and
predicted displacement for a location at a radius 0.9 m (2.95 ft)
from the center of the main heater for Full-Scale Heater Test 2
(AMI, 1986, p. 87).

PS8407-181
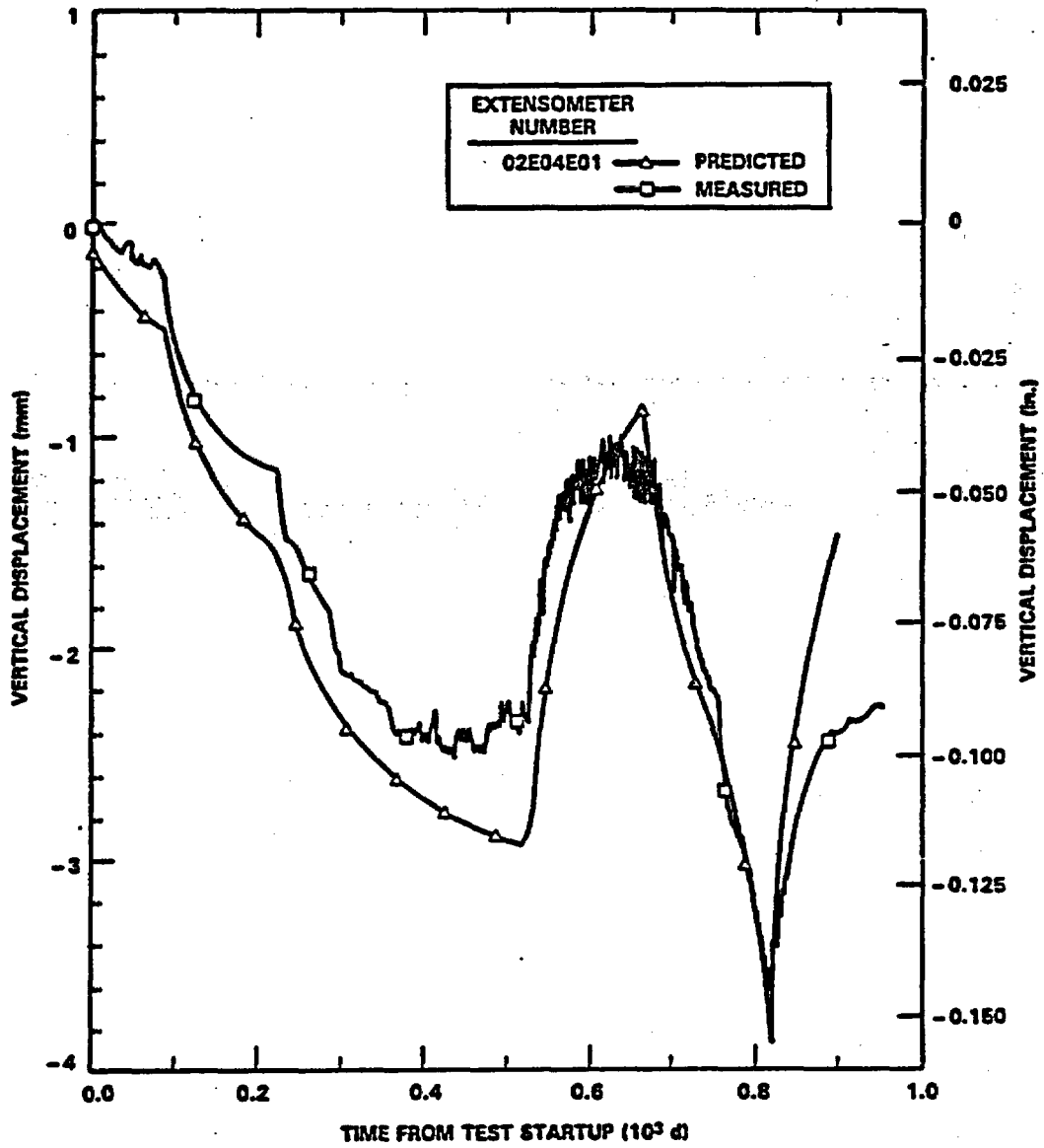
PS8407-181

Figure 2.6-1. Generalized stress map of the conterminous United States,
arrowheads indicate the direction of maximum in situ stresses (after
Zoback and Zobak, 1980, Fig. 5).

STRESS PROVINCES
CP = COLORADO PLATEAU
NBR = NORTHERN BASIN AND RANGE
NRM = NORTHERN ROCKY MOUNTAINS
PNW = PACIFIC NORTHWEST
RGR = RIO GRANDE RIFT
SA = SAN ANDREAS
SBR = SOUTHERN BASIN AND RANGE
SGP = SOUTHERN GREAT PLAINS
SN = SIERRA NEVADA
SRP = SNAKE RIVER PLAIN

RRL = REFERENCE
REPOSITORY
LOCATION

P28809-342
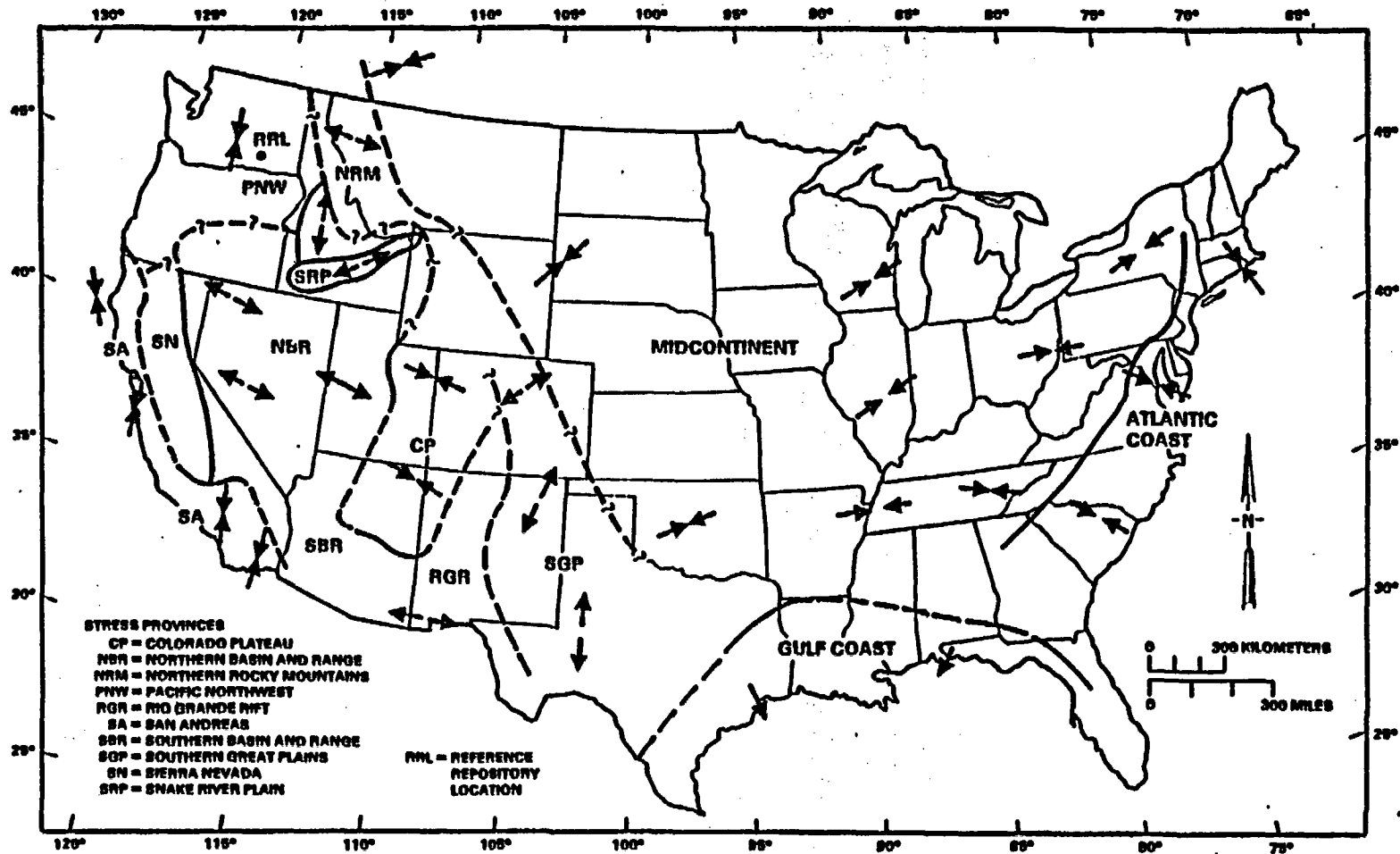
Figure 2.6-2. Location map of key boreholes used in
Basalt Waste Isolation Project studies.

RCPB108-145E

SHELL OIL COMPANY WELL

HANFORD SITE BOUNDARY

DH-5

DH-4

COLUMBIA RIVER

DC-14

NEAR-SURFACE TEST FACILITY
HAYNES STOCK WELL
GABLE MOUNTAIN
DH-18

DB-12
GABLE BUTTE
DB-5
BH-5
GRAHAM RIDGE
DC-6

DB9-K3-103
DB-6
BDH-1
DB-10
DB9-K3-117
DC-4/5
RRL-6
DH-9b
DH-6/DB-11
RRL-7
RRL-3
RRL-14
RRL-2
200 WEST AREA
DC-3
200 EAST AREA
DH-9a
RRL-2S
RRL-6
DB-8
DH-8
RRL-4
RRL-5
REFERENCE REPOSITORY LOCATION
YAKIMA RIDGE
DC-16A,B,C
DB-4
DB-14
DH-12
BENSON RANCH
DB-13
OC-12
DC-7/8
DB-2
RATTLESNAKE MOUNTAIN
199-5-2
BH-3
PFTF
DB-1
RSH-1
RATTLESNAKE HILLS GAS FIELD (DEPLETED)
DB-7
WW-4
DC-15
RIVER
DDH-3
RICHLAND
YAKIMA

BOREHOLE
GAS WELL
REFERENCE REPOSITORY LOCATION BOREHOLE
GENERALIZED OUTCROP OF BASALT WITHIN THE HANFORD SITE
HYDRAULIC FRACTURING BOREHOLE

0   5   10 KILOMETERS

0 1 2 3 4 5   MILES

RCP8108-145E

Figure 2.6-3. Examples of core disking.

8103615-21cn, 8202239-4

( )
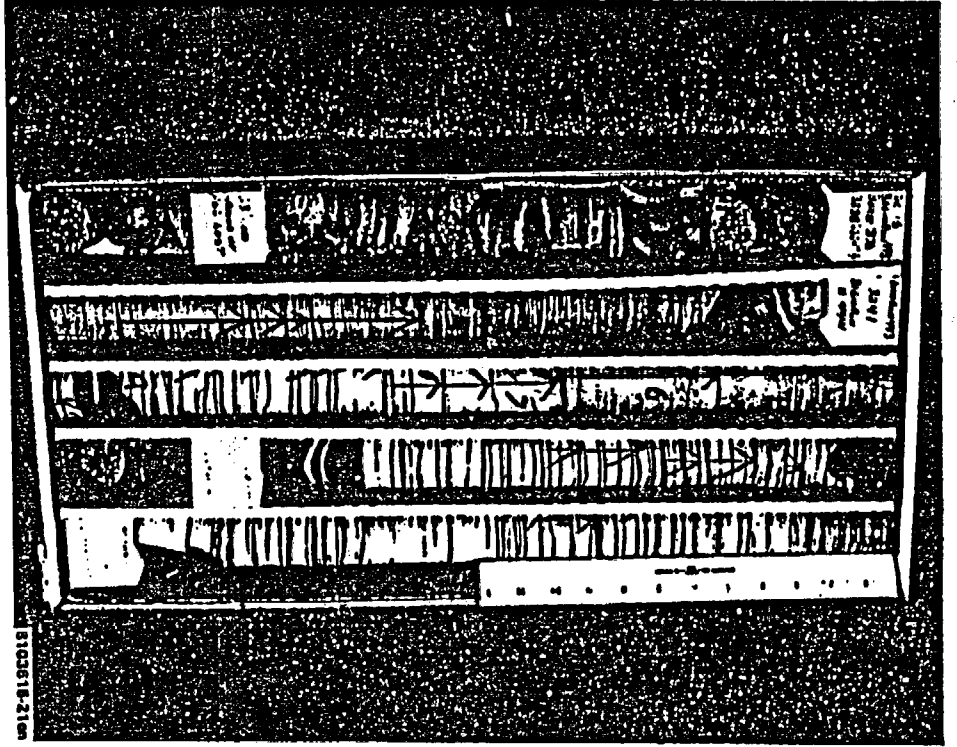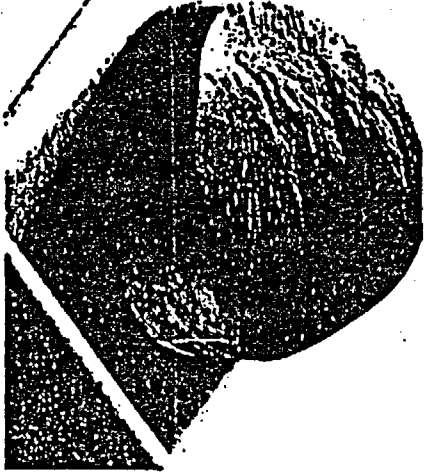
Figure 2.6-4(a). Examples of acoustic televiewer intervals
with borehole spalling in borehole RRL-6 (Paillet, 1985).

PS8407-195
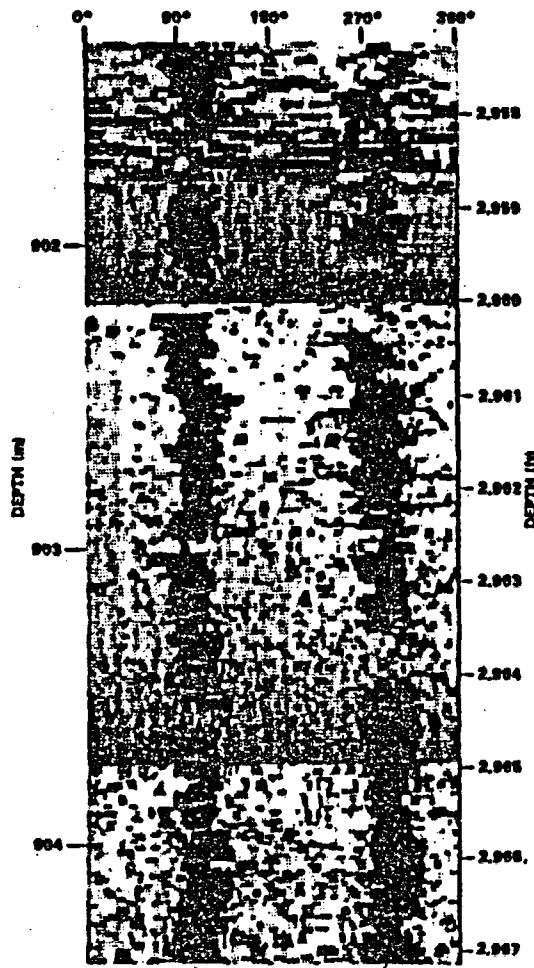
SPALLING
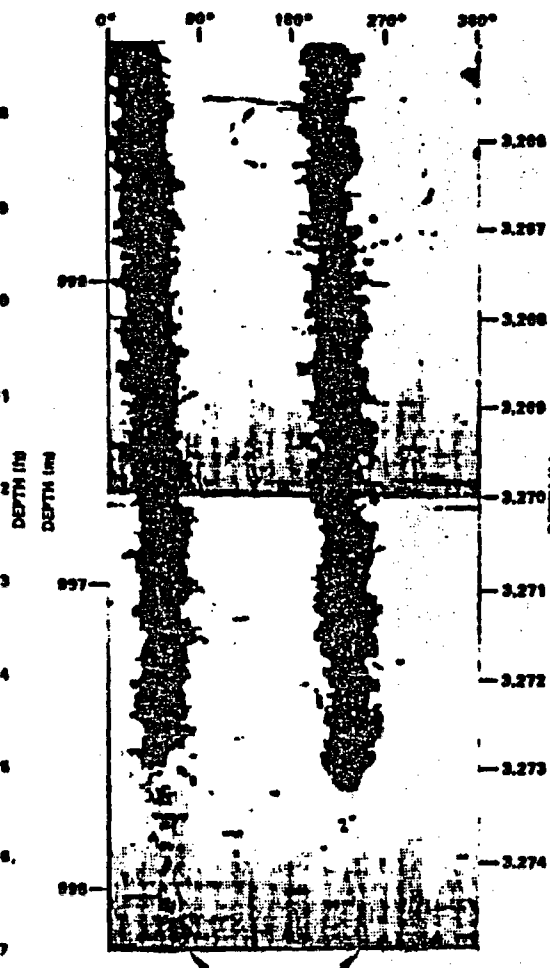
SPALLING
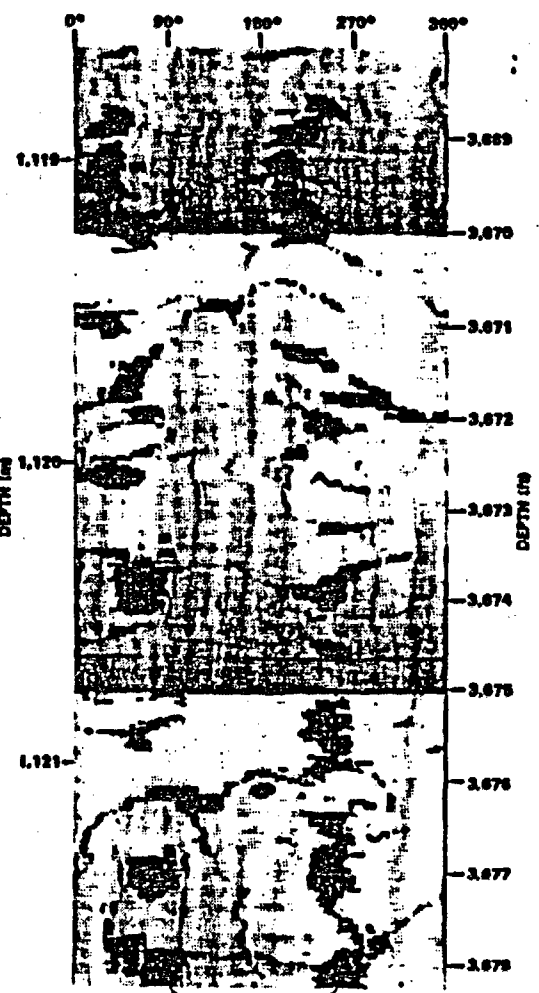
SPALLING

PS8407-196

Figure 2.6-4(b). Representation of horizontal section with borehole spalling.

BOREHOLE SPALLING

BOREHOLE

MINIMUM HORIZONTAL STRESS

MAXIMUM HORIZONTAL STRESS

-N-
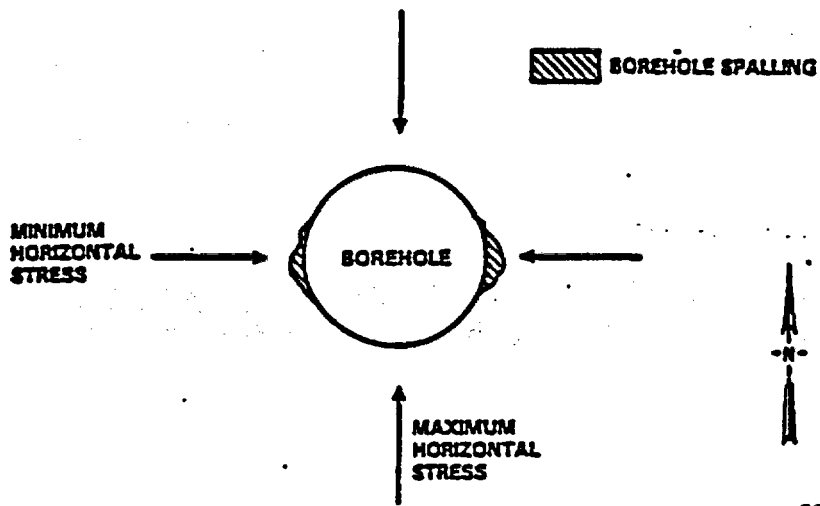
PS8407-196

Figure 2.6-5. Correlation between core disking and borehole
spalling in boreholes DC-4, RRL-6, and DC-12
(Paillet, 1985; Cross, 1985).

EXPLANATION OF FIGURE:

	TELEVIEWER	CORE LOG	
NO BREAKOUTS			NO DISKING NOTED BY CORE LOGGER
DISCONTINUOUS BREAKOUTS			DISCONTINUOUS DISKING ON CORE
CONTINUOUS BREAKOUTS			CONTINUOUS CORE DISKING

PS8407-187

Figure 2.6-6. Typical interval pressure and flow rate history
from the hydraulic fracturing tests at borehole RRL-2,
test depth 928 m (3,044 ft) (Rundle and Kim, 1983).

PS8407-199

FLOW RATE (L/min)
FLOW RATE (gal/min)

P_b-BREAKDOWN PRESSURE P_{Isi}-SHUT-IN PRESSURE

P_{Isi} P_{Isi}

P_{f2}-REOPENING PRESSURE P_{f2} P_{f2} P_{Isi}

BOREHOLE PRESSURE* (MPa)
BOREHOLE PRESSURE* (kip/in²)

1   2   3   4   5

*MEASURED AT SURFACE   ELAPSED TIME (min)
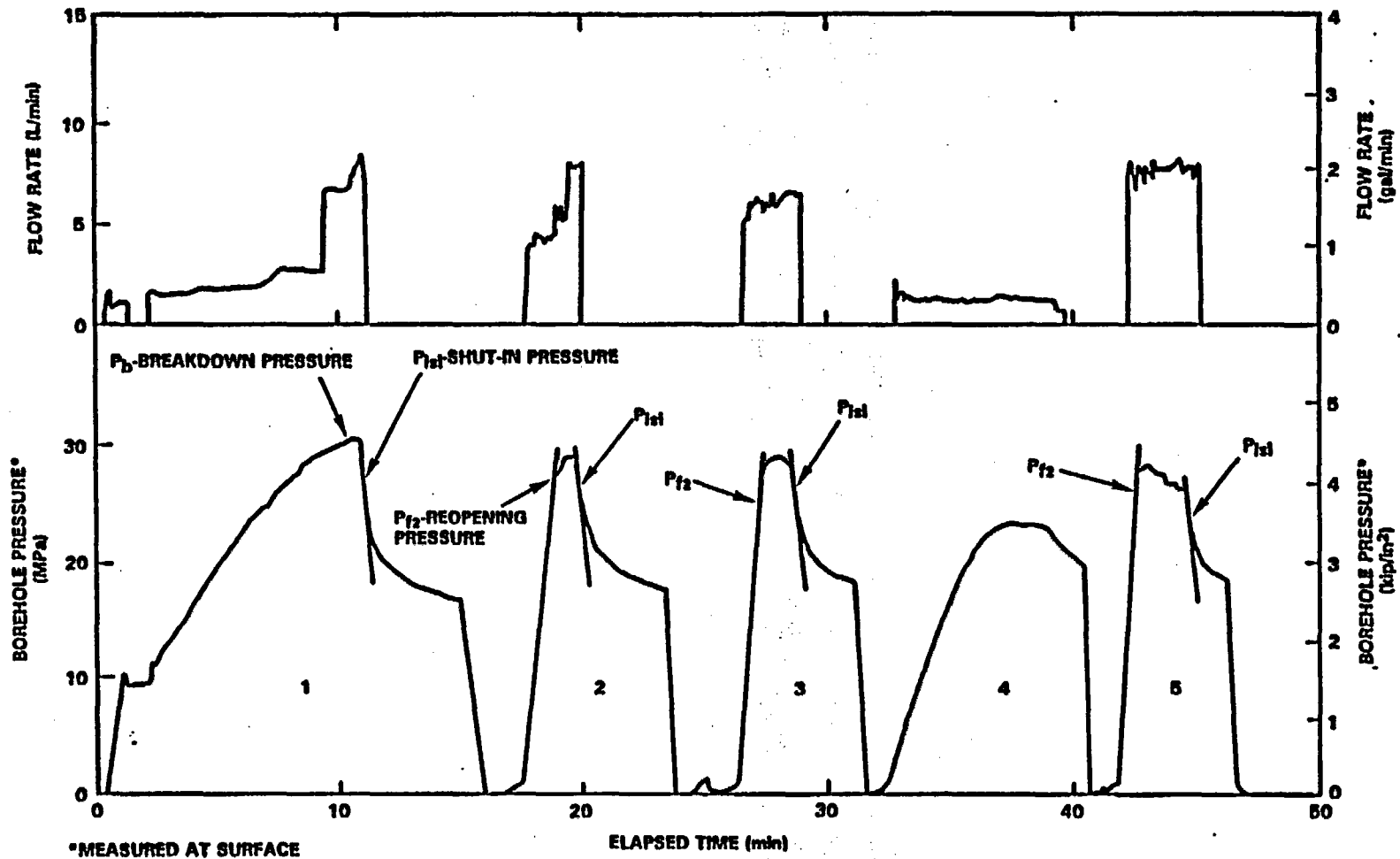
PS8407-199

PS8407-198

Figure 2.6-7. Typical fracture impression from the hydraulic fracturing tests at the Hanford Site.

0.9 m (3 ft)

360°

②

③

① LUG N. 23° E., 360°

ORIENTATION N. 21° W., S. 17° E.

④ DEPTH 924 m (3,030 ft)
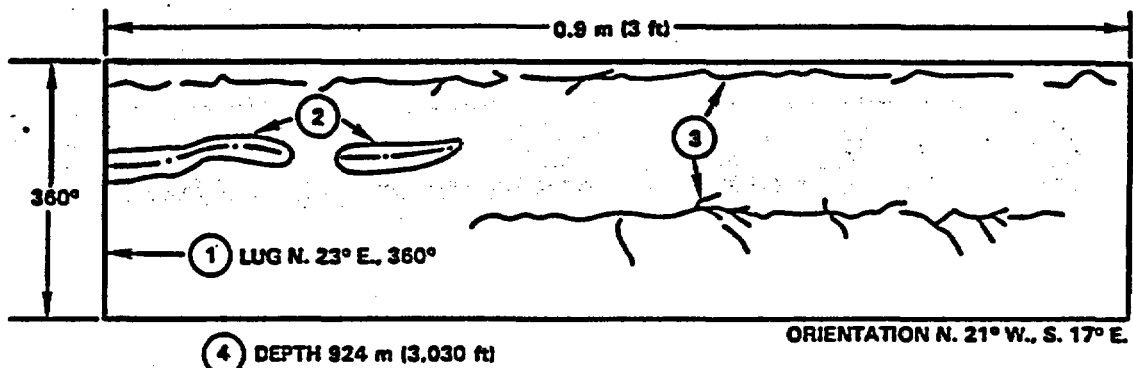
① INDICATES ORIENTATION OF THAT POINT ON THE RECORD AND THE DIRECTION TO THE SURFACE.

② BOREHOLE WALL SPALLING ZONES.

③ HYDRAULICALLY INDUCED FRACTURES.

④ DEPTH FROM SURFACE TO THE CENTER OF THE IMPRESSION INTERVAL AND ORIENTATIONS OF INDUCED FRACTURES.

PS8407-198

Figure 2.6-8. Expanded plot of interval pressure versus time for a
typical repressurization cycle at borehole RRL-6 (test
depth 1,008 m (3,306 ft)).

PS8407-200
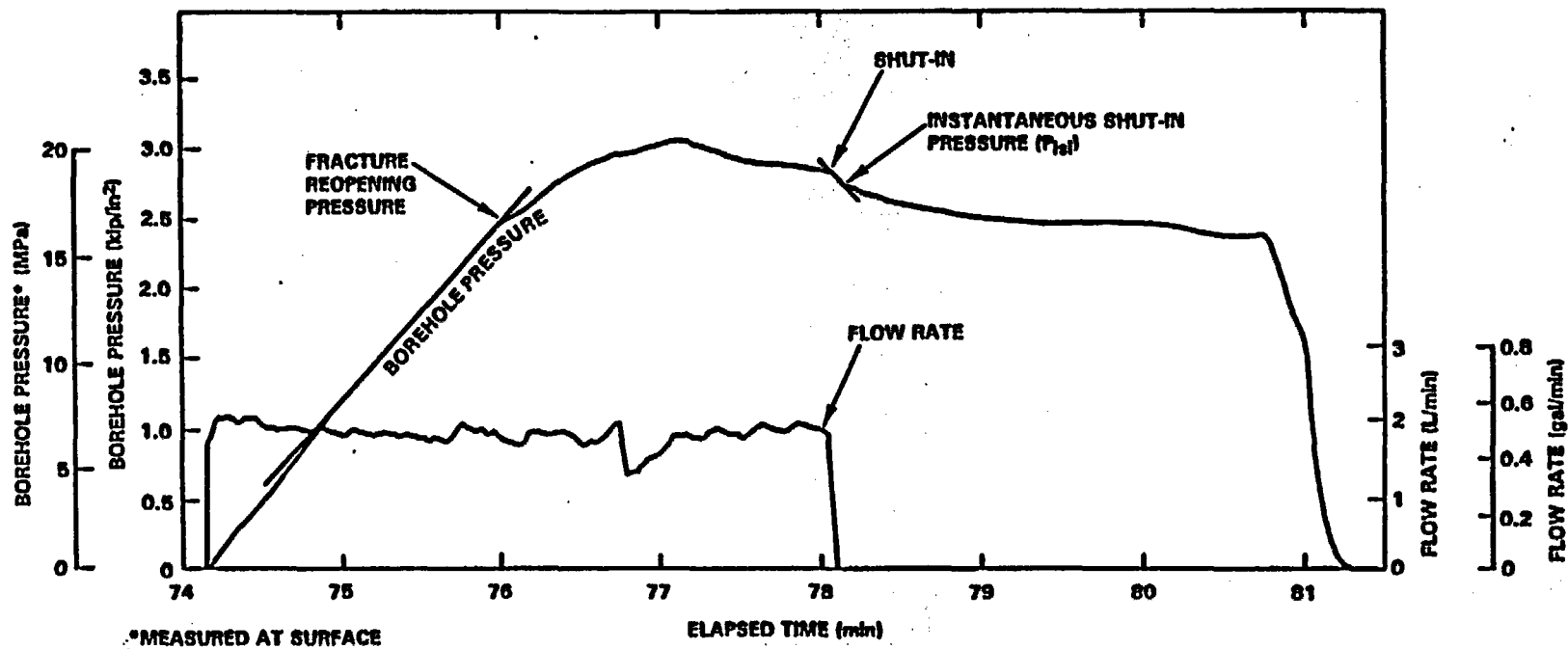
PS8407-200

Figure 2.6-9. Stress magnitudes as a function of depth in the reference repository location.

PS8407-201
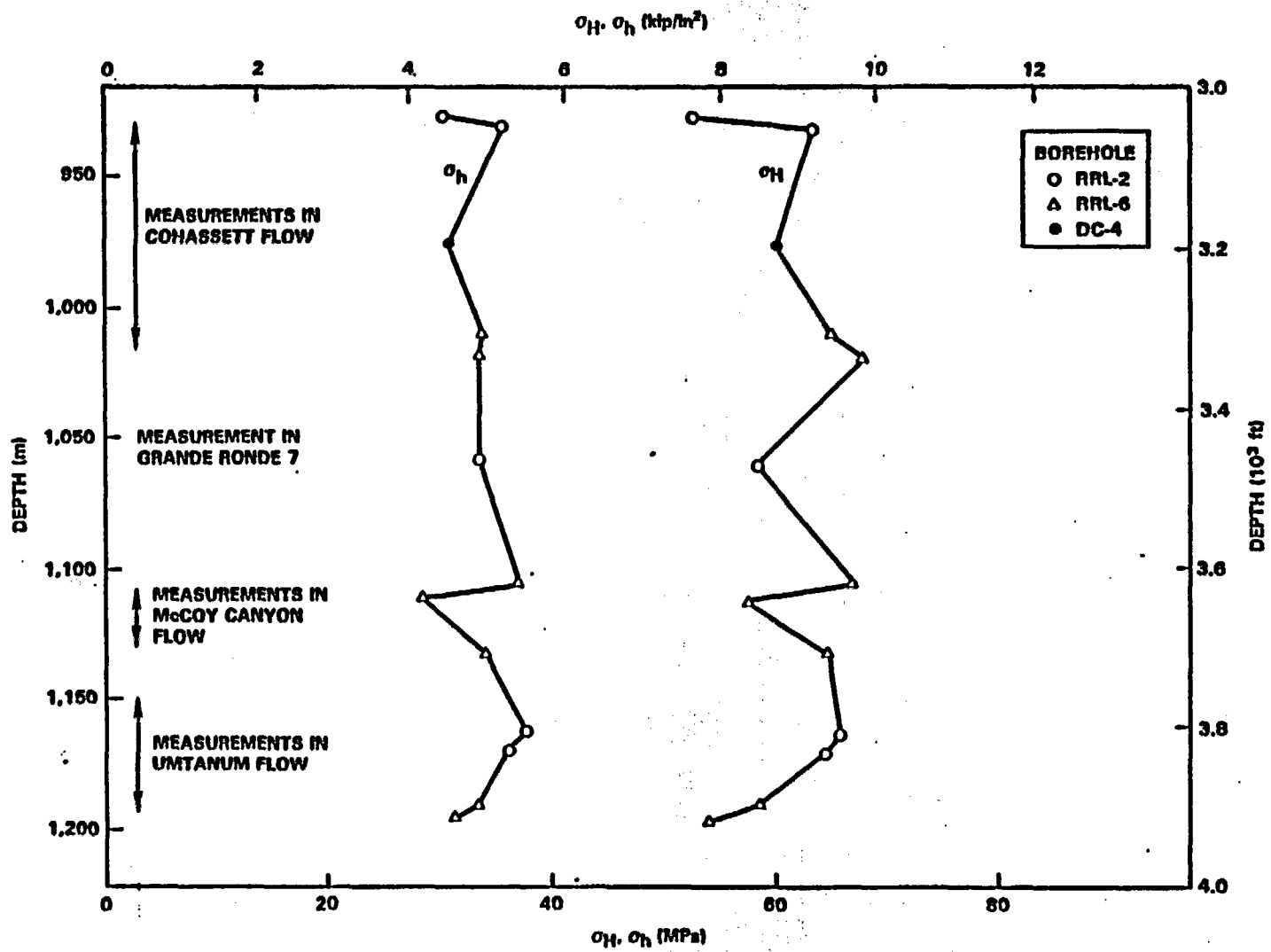
PS8407-201

PS8407-203

Figure 2.6-10. The ratio of average horizontal to vertical stress with depth
(after Hoek and Brown, 1980, p. 100).

STRESS RATIOS $k = \dfrac{\sigma_{h\,av}}{\sigma_v}$
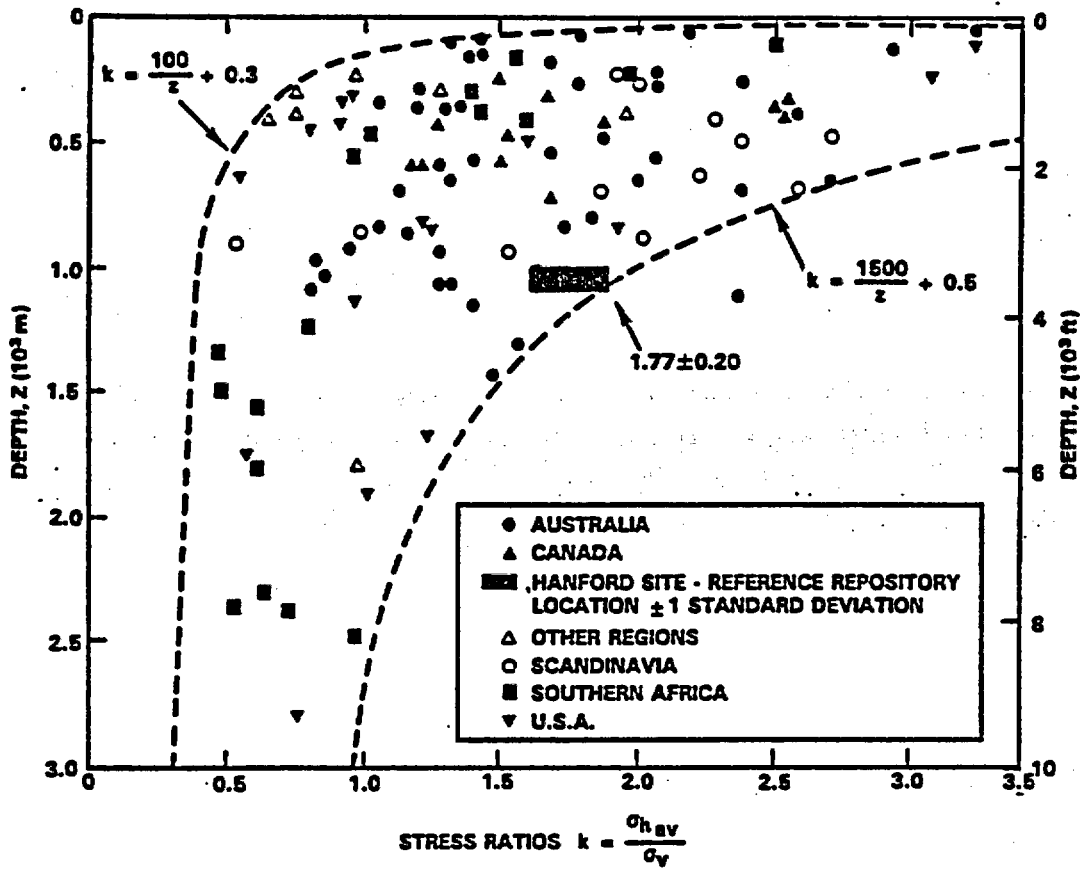
PS8407-203

Figure 2.6-11(a) and (b). Orientation of induced fractures
from hydraulic fracturing tests within the
reference repository location.

PS8407-204

RRL-2

RRL-6   (a)

DC-4

FREQUENCY

(b)
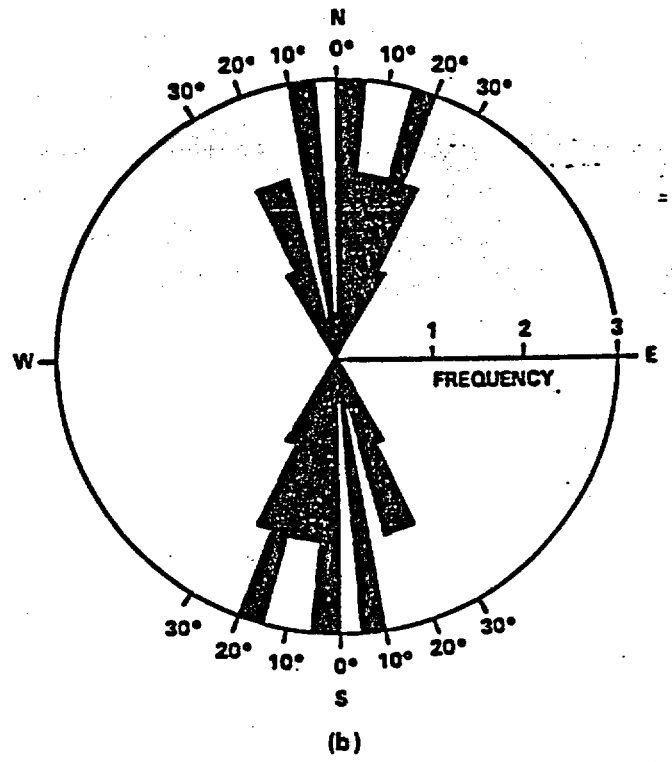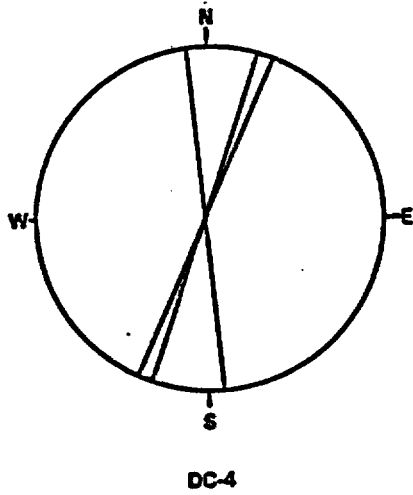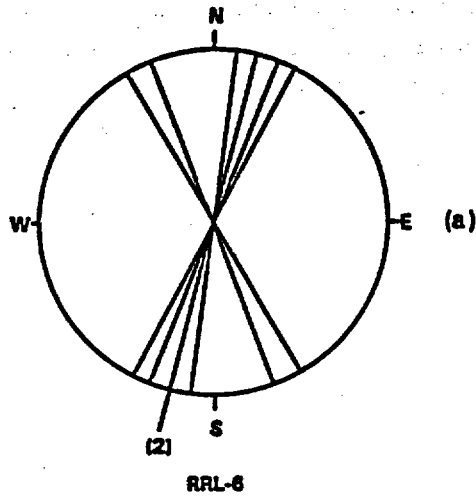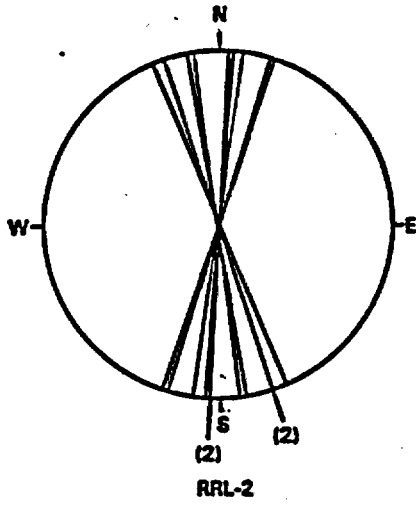
Figure 2.7-1. Stability of tunnel in relation
to vertical stress and uniaxial compressive
strength of intact rock (after Hoek and Brown,
1980).

PS8609-341

$P_z/\sigma_c = 0.1$ $P_z/\sigma_c = 0.2$ $P_z/\sigma_c = 0.3$ $P_z/\sigma_c = 0.4$ $P_z/\sigma_c = 0.5$

UNIAXIAL COMPRESSIVE STRENGTH OF INTACT ROCK, σ_c (MPa)

○ MINOR SPALLING
□ SEVERE SPALLING
▧ EXPECTED RANGE IN THE COHASSETT FLOW (MEAN ± STANDARD DEVIATION)

TO CONVERT MPa TO lbf/in², MULTIPLY BY 145.

VERTICAL APPLIED STRESS, P_z (MPa)
(OR MAXIMUM VIRGIN STRESS)

PS8609-341
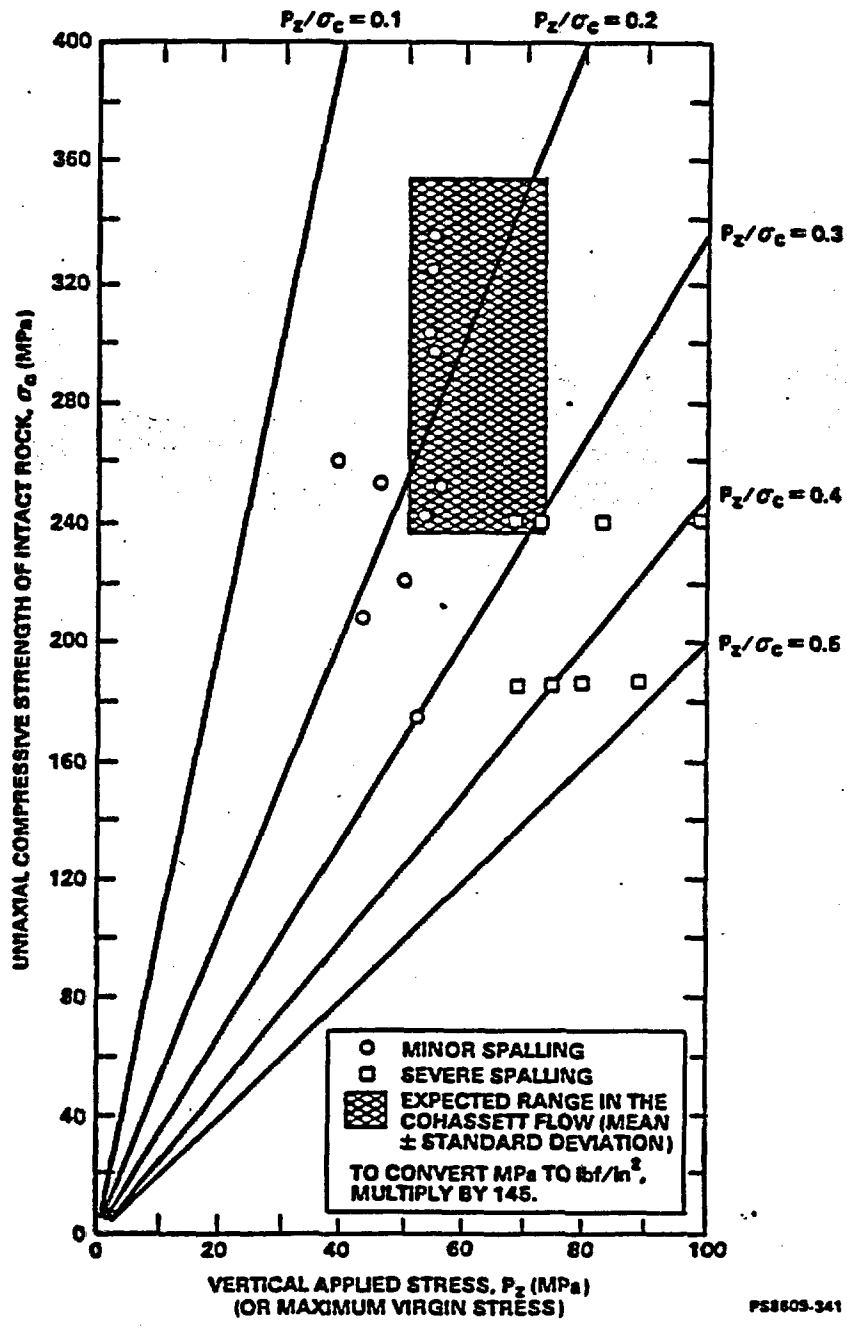
Figure 2.8-1.   Experimental tunnel (Ortlepp and Gay, 1984).

PS8508-52

(a)

STABILIZING PILLAR

73 FOOTWALL DRIVE

74 LEVEL

STABILIZING PILLAR

75 LEVEL   EXPERIMENTAL TUNNEL

76 LEVEL

77 LEVEL   MINED OUT

MINED OUT

0   100   200 METERS

(b)

EXPERIMENTAL TUNNEL

8.279   8.177   7.834   7.743   7.365

STRAINMETER
HOLE 2   STRAINMETER
                      HOLE 1   INITIALLY
                                                MINED OUT

3,100

EXTENSOMETER
HOLE   73 FOOTWALL
                                      DRIVE

PILLAR

3,150

EVENTUALLY MINED OUT

DEPTH BELOW GROUND SURFACE (m)

0   50   100 METERS

PS8508-52

Figure 2.8-2.   Rock mass quality chart with ranges of span/excavation
support ratio and rock mass quality values for the Cohassett flow
(after Barton, 1984).

PS8406-198

ENTABLATURE
(EXTREME MINIMUM)

ENTABLATURE
(DESIGN
RANGE)

ENTABLATURE
(EXTREME MAXIMUM)

EXCEPTIONALLY POOR	EXTREMELY POOR	VERY POOR	POOR	FAIR	GOOD	VERY GOOD	EXTREMELY GOOD	EXCEP- TIONALLY GOOD

EQUIVALENT DIMENSION = $\dfrac{\text{SPAN, DIAMETER, OR HEIGHT (m)}}{\text{EXCAVATION SUPPORT RATIO}}$

RANGE OF
POTENTIAL CONDITIONS

NO SUPPORT REQUIRED

SPAN	
EXCAVATION SUPPORT RATIO	
m	(ft)
6.1	(20.0)
4.7	(15.4)
4.3	(14.1)
3.3	(10.8)
3.1	(10.2)
2.3	(7.5)

COLONNADE
(EXTREME MINIMUM)

COLONNADE
(DESIGN RANGE)

COLONNADE
(EXTREME MAXIMUM)

NUMBERS SHOWN ON FIGURE
ARE SUPPORT CATEGORIES.

UNSHADED BOX EXTREME
USE FOR INTERSECTIONS.

ROCK MASS QUALITY (Q) = $\left[\dfrac{RQD}{J_n}\right] \times \left[\dfrac{J_r}{J_a}\right] \times \left[\dfrac{J_w}{SRF}\right]$

J_a = JOINT ALTERATION NUMBER
J_n = JOINT SET NUMBER
J_r = JOINT ROUGHNESS NUMBER
J_w = JOINT WATER-REDUCTION FACTOR
RQD = ROCK-QUALITY DESIGNATION
SRF = STRESS-REDUCTION FACTOR

PS8406-1988

Table 2.1-1. Summary of laboratory studies on basalt from
the Hanford Site (after South, 1985, p. 439)

(FULL PAGE -- 6085 TABLE)

Table 2.1-1. Summary of laboratory studies on basalt from the Hanford Site (after South, 1985, p. 439)

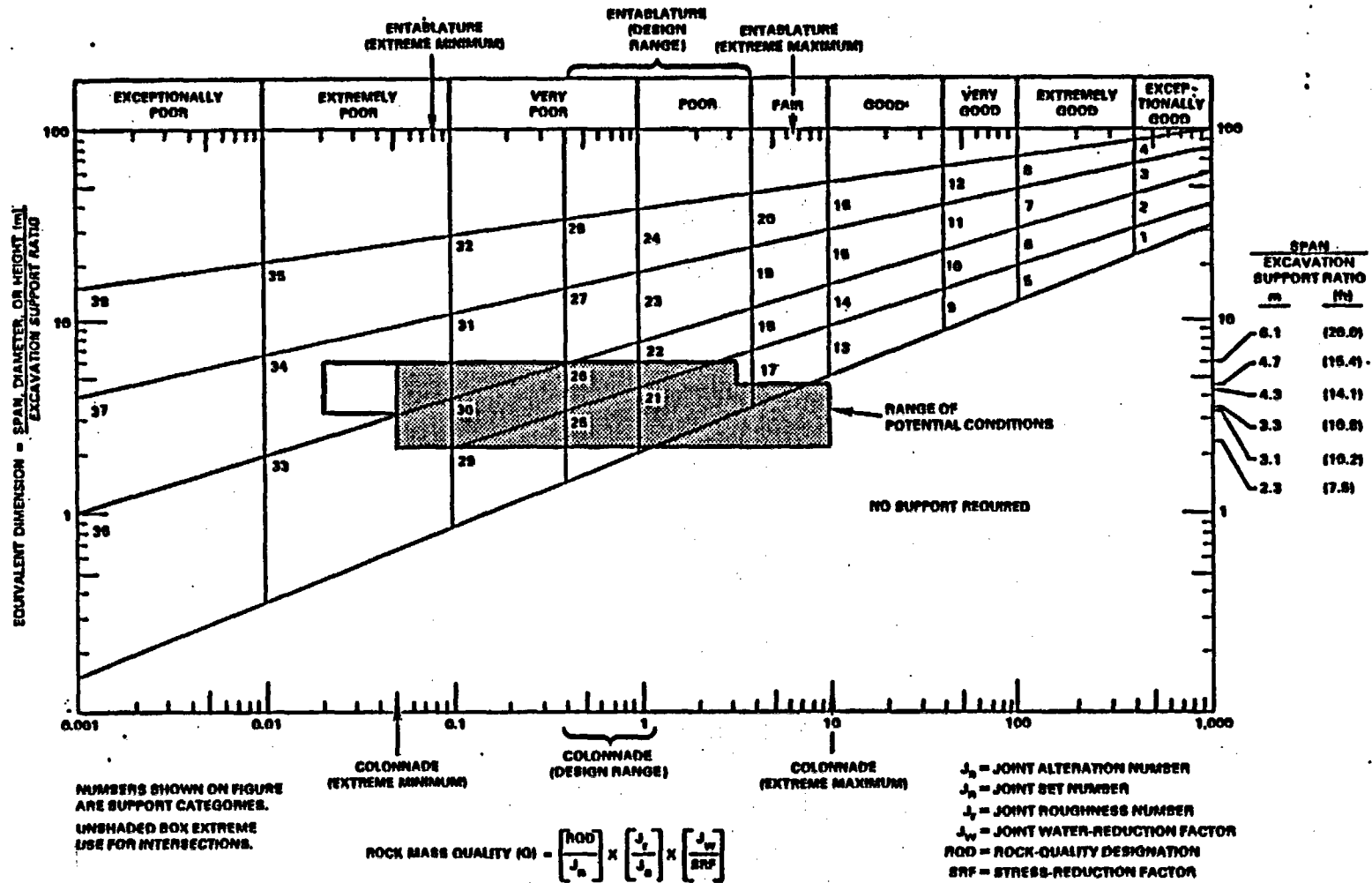| Borehole number	Flows tested	Tests performed	Reference	Laboratory
DC-2	Umtanum, Cohassett	UNX, BZ, TRX, MR, TRXJ, E, v, P, S, η, ρ_b, ρ_g, a, K	Rockwell (1978b)	CSM
DC-2	Umtanum	UNX, BZ, TRX, HTRX, MR, E, v, P, S, η, ρ_b, ρ_g, a, K, C_p, diff	FSI (1981a)	FSI
DC-4	Umtanum	HUNX, HTRX, a, K, C_p, creep, rock hardness, ρ_b, P, S	Miller (1979b)	CSM
DC-6	Umtanum	HUNX, HTRX, a, K, C_p, creep, rock hardness, C_p, P, S	Miller and Bishop (1979)	CSM
DC-8	Umtanum	HUNX, HTRX, a, K, C_p, creep, rock hardness, C_p, P, S	Miller (1979a)	CSM
DC-10	Pomona	UNX, BZ, TRX, MR, E, v, P, S, ρ_b, η, a, K, C_p	Duvall et al. (1978)	CSM
DC-11	Pomona	UNX, BZ, TRX, MR, TRXJ, E, v, P, S, η, ρ_b, a, K	Rockwell (1978)	CSM
DH-4	Umtanum; Grande Ronde 11, 13, 20, 21, 24, and 32	UNX, BZ, TRX, MR, TRXJ, E, v, P, S, ρ_b, a, K	Rockwell (1978)	CSM
DH-5	Umtanum, Grande Ronde 6	UNX, BX, TRX, MR, TRXJ, E, v, P, S, η, ρ_b, a, K	Rockwell (1978)	CSM
DH-5	Umtanum	a, K, C_p, ρ_b	Martinez-Baez and Amick (1978)	LBL
DDH-3	Frenchman Springs 1, Umtanum, Grande Ronde 13 and 14	UNX, BZ, TRX, MR, TRXJ, E, v, P, S, η, ρ_b, a, K	Rockwell (1978)	CSM
NSTF	Pomona	UNX, TRX, HTRX, BZ, MR, ρ_b, ρ_g, E, v, P, S, a, K, C_p, η, diff	FSI (1980a, 1980b, and 1981b)	FSI
RRL-2	Rocky Coulee, Cohassett, McCoy Canyon, Umtanum	UNX, TRX, BZ, E, v, P, S, ρ_b, η, ρ_g, MR	Hulstrom and Hanson (1982b)	BWIP
RRL-6	Cohassett, Umtanum	UNX, TRX, BZ, E, v, P, S, ρ_b, η, ρ_g	Hulstrom and Hanson (1983b)	BWIP
RRL-14	Cohassett, Umtanum	UNX, TRX, BZ, E, v, P, S, ρ_b, η, ρ_g	Hulstrom and Hanson (1983a)	BWIP

Test abbreviations

BZ	= Brazilian tensile		S	= S-wave velocity
C_p	= Specific heat		TRX	= Triaxial compressive strength
diff	= Thermal diffusivity		TRXJ	= Triaxial jointed compressive strength
E	= Young's modulus		UNX	= Uniaxial compressive strength
HTRX	= Heated triaxial compressive strength		a	= Thermal expansion
HUNX	= Heated uniaxial compressive strength		η	= Porosity
K	= Thermal conductivity		v	= Poisson's ratio
MR	= Modulus of rupture		ρ_b	= Bulk density
NSTF	= Near-Surface Test Facility		ρ_g	= Grain density
P	= P-wave velocity			

Laboratories

BWIP - Basalt Waste Isolation Project
CSM - Colorado School of Mines
FSI - Foundation Sciences, Inc.
LBL - Lawrence Berkeley Laboratory

Table 2.1-2. Comparison of the mechanical properties of
intact samples of similar rock types

(FULL PAGE -- 6085 TABLE)

Table 2.1-2. Comparison of the mechanical properties of intact samples of similar rock types

Rock type	Uniaxial compressive strength (MPa)	Elastic modulus (GPa)	Poisson's ratio	Tensile strength (MPa)	Comments	Reference
Basalt (Dresser, Wisconsin)	413[a]-479	82.1-88.5	0.26-0.27[b]	17.6-24.0	Dense unfractured intact samples	Krech et al. (1974, p. 11)
Basalt (Bacon Siphon, Washington)	81-293	22-80	0.09-0.31	--	Includes flow top and dense interior	Agapito et al. (1977, pp. 34-35)
Basalt (Nevada Test Site)	148	--	--	13.1[c]		Goodman (1980, p. 58)
Basalt (John Day Dam, Oregon)	355			14.5[c]		Goodman (1980, p. 58)
Basalt (Miocene, Oregon)	169 219			26.2[d]		Handin (1966, p. 273)
Basalt (Champion Copper Mine, Michigan)	230	61.5		26.2[d]		Windes (1949, p. 9)
Basalt (Ahmeek Copper Mine, Michigan)	258-358	70.3		[e]		Windes (1949, p. 10)

NOTE: To convert MPa to lbf/in^2, multiply by 145.
To convert GPa to kip/in^2, multiply by 145.

[a]Mean of 10 samples, range of mean from 3 groups.
[b]Dynamic Poisson's ratio.
[c]From point load test.
[d]Rupture strength.
[e]No tensile rupture strength reported

Table 2.1-3. Physical and mechanical properties of intact entablature
basalts from outside the reference repository location but
within the Hanford Site

Landscaped 860 Table

Table 2.1-3. Physical and mechanical properties of intact entablature basalts from outside the reference repository location but within the Hanford Site

| Property | Units | Grande Ronde Basalt | | | | Pomona flow entablature | |
| | | Umtanum flow only | | Excluding Umtanum flow | | | |
		Mean	Standard deviation	Mean	Standard deviation	Mean	Standard deviation
Brazilian tensile strength	MPA (kip/in^2)	11.9 (1.7)	6.9 (1.0)	17.2 (2.5)	5.1 (0.7)	19.4 (2.8)	3.8 (0.5)
Uniaxial compressive strength	MPA (kip/in^2)	212 (30.7)	106 (15.4)	--	--	356 (51.6)	42 (6.1)
Static elastic modulus	GPa $(10^3\ kip/in^2)$	71.0 (10.3)	20.0 (2.9)	64.8 (9.4)	16.0 (2.3)	83.4 (12.1)	8.3 (1.2)
Static Poisson's ratio		0.27	0.05	0.24	0.04	0.25	0.02
Bulk density	kg/m^3 (lb/ft^3)	2,780.0 (173.5)	50.0 (3.12)	2,780.0 (173.5)	50.0 (3.12)	2,850.0 (177.8)	30.0 (1.87)
Apparent porosity	%	1.1	0.4	3.4	1.3	0.7	0.4

NOTE: After Sublette (1983, Table 9, pp. 47-48).

Table 2.2-1. Testing of basalt discontinuities for the Basalt
Waste Isolation Project

Flow	Test	Reference
Pomona flow	Direct shear testing Jointed triaxial testing	Mitchell (1984a) Brechtel (1985)
Umtanum flow	Jointed triaxial with and without temperature variations	Miller (1979a, 1979b), Miller and Bishop (1979), Mitchell (1984b)
Grande Ronde Basalt undifferentiated	Jointed triaxial	CSM (1978), Mitchell (1984b)
Pomona flow	Intact, jointed, and multi-fractured uniaxial tests with and without temperature variations	FSI (1980a, 1980b, 1980c)

Table 2.2-2. Peak friction angle for various surface
conditions in rocks similar to basalt

(FULL PAGE -- 6085 TABLE)

Table 2.2-2. Peak friction angle for various surface conditions in rocks similar to basalt

Rock type	Normal stress		Peak angle of friction (°)	Comments	Source
	MPa	(lbf/in²)			
Lower Granite Basalt*	0.08	(12)	34.6	Sawed surface, lapped	Coulson (1971,
	0.84	(122)	37.6	with #600 grit, oven dry	p. 101)
	3.37	(488)	37.2		
	8.02	(1,163)	38.3		
Fine-grained	0.08	(12)	28.8	Sawed surface, lapped	Coulson (1971,
Grand Coulee Granite*	0.86	(124)	34.2	with #600 grit, oven dry	p. 101)
Fine-grained	0.11	(15)	43.6	Natural, undulating,	Barton (1973, p. 296)
Grand Coulee Granite	0.70	(102)	38.0	smooth, calcite and	
				zeolite present	
Coarse-grained	0.11	(16)	58.7	Natural, undulating, iron	Barton (1973, p. 296)
Grand Coulee Granite	0.69	(100)	45.6	staining, calcite and	
	2.07	(300)	50.8	epidote present	
Blackstone Granite	1.23	(178)	64.1	Rough, undulating,	Barton (1973, p. 296)
	1.40	(203)	69.0	artificial extension	
	1.72	(249)	71.7	fractures	
Granite	0.14	(21)	71.6	Rough, undulating,	Barton (1973, p. 296)
	0.34	(50)	69.2	artificial extension	
	0.64	(92)	70.6	fractures	
	1.37	(199)	56.3		
Gabbro			47.0	Natural joint, dry	Duncan (1969, p. 88)
Dolerite			52.0	Natural joint, dry	Duncan (1969, p. 88)
Basalt			47.0	Natural joint, dry	Duncan (1969, p. 88)
Granite			38.0	Artificial surface	Duncan (1969, p. 88)

*Peak angle of friction is the residual friction angle after large shear displacements for these cases.

Table 2.2-3. Shear and normal stiffness values derived
from the first loading cycle of triaxial tests on
joint samples from the Pomona Flow

	Stiffness GPa/mm (x 10^3 kip/in^2/in.)		
	Minimum	Average	Maximum
Normal stiffness hydrostatic loading			
Beginning	0.01 (0.038)	0.096 (0.353)	0.415 (1.527)
50% load	0.119 (0.439)	0.578 (2.129)	3.090 (11.379)
100% load	0.096 (0.352)	0.835 (3.074)	3.120 (11.490)
Shear stiffness 1st axial loading			
Beginning	0.009 (0.033)	0.130 (0.480)	0.414 (1.525)
50% load	0.017 (0.064)	0.373 (1.373)	1.825 (6.722)
100% load	0.005 (0.020)	0.113 (0.416)	0.427 (1.573)

NOTE: From Brechtel (1985, pp. 30-33).

Table 2.3-1. Test plans and operating procedures

Test plan or test description	Reference

Borehole jacking tests
  Goodman jack tests
  Modified Goodman jack
  tests
	Shuri et al. (1980)
	de la Cruz
	et al. (1982)

Jointed block test
  Step 1: single slot test under abmient temperature
  Step 2: ambient temperature test
  Step 3: elevated temperature test
	Cramer (1984)

Crosshole seismic testing	Moak and Wintczak (1980), Myer et al. (1983)

Table 2.3-2. Summary of large-scale compression tests

Landscaped 860 Table

Table 2.3-2. Summary of large-scale compression tests

Source	Rock type	Sample dimensions	Laboratory strength, MPa (kip/in^2)	Large-scale strength, MPa (kip/in^2)
Nose (1964)*	Granite	1.4 m x 1.8 m x 2.8 m (4.6 ft x 5.9 ft x 9.2 ft)	23-48 (3.4-7.0)	12-15 (1.7-2.2)
Jahns (1966)*	Iron ore	1 m x 1 m x 1 m (3.3 ft x 3.3 ft x 3.3 ft)	117 (17.0)	49 (7.1)
Gimm et al. (1966)*	Iron ore	1.4 m x 1.4 m x 1.5 m (4.6 ft x 4.6 ft x 5.0 ft)		
De Reeper (1966)*	Iron ore			50 (7.3)
Richter (1968)*	Iron ore	1.25 m x 1.5 m x 1.5 m (4.1 ft x 5.0 ft x 5.0 ft)	360 (52.2)	20 (2.9)
Georgi et al. (1970)*	Granite	1 m x 1 m x 1.2 m (3.3 ft x 3.3 ft x 3.9 ft)		13 (1.9)
Chaoui et al. (1970)*	Marble	0.7-m (2.3-ft) dia. x 1 m (3.3 ft)	10.5 (1.5)	3 (0.4)
Pratt et al. (1972)	Diorite	Up to 2.75 m per side (9.0 ft)	29 (4.2)	8 (1.2)
	Grano-diorite	Up to 2.75 m per side (9.0 ft)	144.8 (21.0)	25.0 (3.6)
Sundaram et al. (1983)	Granite	0.76-m (2.5-ft) dia. 1.5 m (5.0 ft) high	129-265 (19-38)	27.5 (4.0)
Thorp et al. (1983)	Granite	1-m (3.5-ft) dia. 2 m (6.6 ft) high	157-208 (22.8-30.2)	7.5 (1.1)

*Discussed in Bieniawski and Van Heerden (1975).

Table 2.3-3. Evaluation of rock mass strength from pillar observations

Source	Rock type	Pillar geometry	Laboratory strength, σ_L MPa (kip/in^2)	In situ strength, σ_c MPa (kip/in^2)
Agapito (1974)	Oil shale	18 m x 18 m x 18 m (60 ft x 60 ft x 60 ft)	90 (13.1)	22 (3.2)
Brady (1977)	Tuffaceous shales	10 m x 10 m x long (33 ft x 33 ft)	170 (24.7)	90 (13.1)
Coates et al. (1973)	Granodiorite	3 m x 30 m x 3 m (10 ft x 100 ft x 10 ft)	200 (29.0)	100 (14.5)
Petersen (1978)	St. Peter sandstone	6 m x 6 m x long (20 ft x 20 ft)	3.5 (0.5)	3.5 (0.5)
Russell et al. (1984)	Metamorphosed arenaceous sediments	10 m x 15 m x long (33 ft x 50 ft)	180 (26.1)	42 (6.1)

Table 2.3-4. In situ deformability modulus obtained by Goodman jack tests in the entablature zone of the Pomona flow at the Near-Surface Test Facility

Borehole orientation	Depth, m (ft)	In situ deformability modules, GPa (lbf/in^2)	Standard deviation, GPa (lbf/in^2)
Horizontal	1.5-13.7 (5-45)	18.75 (2.72×10^6)	1.86 (0.27×10^6)
Vertical	1.5-3 (5-10)	6.9 (1.0×10^6)	0.69 (0.10×10^6)
	6.1-7.6 (20-25)	13.1 (1.9×10^6)	1.93 (0.28×10^6)

NOTE: After Shuri et al. (1980, p. 11).

Table 2.3-5. In situ deformability modulus (obtained by nonlinear regression analysis) from modified Goodman jack tests in the colonnade zone of the Pomona flow at the Near-Surface Test Facility

Testing method	Number of data points	In situ deformability modulus, GPa (lbf/in^2)	Standard deviation, GPa (lbf/in^2)
NX-borehole Goodman jack, diametrical deformation	251	23 (3.4×10^6)	1.2 (0.17×10^6)
Modified Goodman jack, tangential strain	103	47 (6.8×10^6)	12 (1.73×10^6)

NOTE: From de la Cruz et al. (1982, p. 5).

Table 2.3-6. Pressure cycle summary for
step 2 of the jointed block test

Cycle	Horizontal load (σ_{xx}), MPa[a]	Vertical load (σ_{yy}), MPa	Axial load (σ_{zz}), MPa
1	1.00-3.75	1.50	1.50
2	1.00-6.50	2.50	2.50
3[b]	2.00-12.0	5.00	5.00
3R	2.00-12.5	5.00	5.00
4	1.50	1.00-3.75	1.50
5	2.50	1.00-6.50	2.50
6	5.00	2.00-12.5	5.00
7	5.00	2.00-9.00	5.00
8	2.00-9.00	5.00	5.00
9	2.00-9.00	5.00	5.00
10	5.00	2.00-9.00	5.00
11	2.50	2.50	1.25-5.00
12	5.00	5.00	1.25-5.00
13	9.00	9.00	2.00-5.00
14	1.00-5.00	1.00-5.00	1.00-5.00
15	2.50	2.50	1.25-5.00
16	1.00-5.00	1.00-5.00	1.00-5.00
17	2.00-9.00	5.00	5.00
18	1.00-6.50	2.50	2.50
19	1.00-3.75	1.50	1.50
20	5.00	2.00-9.00	5.00
21	1.50	1.00-3.75	1.50
22	0.50	0.50	0.50-5.00
	2.00	5.00	5.00
	2.00-9.00	5.00	5.00
23	5.00	5.00	1.00-5.00
	5.00-0.50	5.00-0.50	5.00
	0.50-9.00	0.50-5.00	5.00
24	9.00	9.00	1.00-5.00
	9.00-0.50	9.00-0.50	5.00
	0.50-9.00	0.50-9.00	5.00
25	0.50	0.50	0.50-5.00
	2.00	5.00	5.00
	2.00-9.00	5.00	5.00

NOTE: From Cramer and Kim (1985, pp. 100 and
101).
[a] To convert MPa to lbf/in^2, multiply by 145.
[b] Equipment problem prevented attainment of the
desired pressure of 12.5 MPa (1,812 lbf/in^2),
therefore rerun as Test 3R.

Table 2.3-7. Summary of modulus and Poisson's ratio values from horizontal and vertical loading

Loading cycle	Deviatoric stress	Nominal confining stress (MPa)[a]	E_{xx} (GPa)[b]	E_{yy} (GPa)[b]	ν_{xy}	ν_{yx}	ν_{xz}[c]	ν_{xy}[c]
1	σ_{xx}	1.50	9.40	--	--	0.13	0.19	--
2	σ_{xx}	2.50	11.5	--	--	0.15	0.24	--
3	σ_{xx}	5.00	15.4	--	--	0.04	0.29	--
3R	σ_{xx}	5.00	15.4	--	--	0.04	0.33	--
4	σ_{yy}	1.50	--	16.9	0.10	--	--	0.20
5	σ_{yy}	2.50	--	19.5	0.25	--	--	0.22
6	σ_{yy}	5.00	--	25.4	0.17	--	--	0.24
7	σ_{yy}	5.00	--	25.6	0.06	--	--	0.22
8	σ_{xx}	5.00	20.3	--	--	0.11	0.30	--
9	σ_{xx}	5.00	19.4	--	--	0.14	0.30	--
10	σ_{yy}	5.00	--	26.1	0.10	--	--	0.19
17	σ_{xx}	5.00	17.5	--	--	0.12	0.30	--
18	σ_{xx}	2.50	14.4	--	--	0.69	0.31	--
19	σ_{xx}	1.50	10.9	--	--	0.68	0.28	--
20	σ_{yy}	5.00	--	25.5	0.14	--	--	0.19
21	σ_{yy}	1.50	--	17.3	0.21	--	--	0.16

NOTE: From Cramer and Kim (1985, p. 315).
[a]To convert MPa to lbf/in^2, multiply by 145.
[b]To convert GPa to kip/in^2, multiply by 145.
[c]Strain in z-direction from MPBX anchor interval E02-E04.

Table 2.3-8. Summary of modulus and Poisson's ratio
results from axial loading of the jointed block test

Loading cycle	Confining stress (MPa)[a]	Deformability modulus[b], GPa[c]	Poisson's ratio	
			v_{xz}	v_{yz}
11	2.50	24.5	0.05	0.06
12	5.00	24.2	0.28	0.07
13	9.00	28.2	0.17	0.20
15	2.50	22.3	0.48	0.13
22	0.50	19.7	--	--
23	5.00	27.0	0.18	0.09
24	9.00	31.9	0.27	0.09
16	hydro-static	47.7	--	--

NOTE: After Cramer and Kim (1985, p. 324).
[a]To convert MPa to lbf/in^2, multiply by 145.
[b]Calculated using stress distribution obtained from modeling.
[c]To convert GPa to kip/in^2, multiply by 145.

Table 2.3-9. Basalt rock mass modulus measured
by different in situ tests

Method	Modulus (GPa)
Goodman jack[a]	
Horizontal	18.75
Vertical	13.1
Modified Goodman jack[b]	
From diametrial deformation	23
From tangental strain	47
Jointed block test	
Single slot at ambient temperature[c]	
From borehole deformation gages	44
From flat jack deformeter	40
Block at ambient temperature and low confinement[d]	
x-direction (horizontal) 1.5 MPa confinement	10.2
y-direction (vertical) 1.5 MPa confinement	17.1
z-direction (horizontal) 0.5 MPa confinement	19.7
Cross-hole seismic (dynamic moduli)[e]	
Vertical	80
Horizontal	50

NOTE: (1) To convert GPa to kip/in^2, multiply by 145.

(2) The modulus estimated by the empirical correlation of Equation 2.3-1 is 24 GPa.

[a]Shuri et al. (1980, p. 11).
[b]de la Cruz et al. (1982, p. 5).
[c]Cramer et al. (1985, p. 19).
[d]Cramer et al. (1985, pp. 27-28).
[e]Myer et al. (1983, p. 34).

Table 2.4-1. Summary of laboratory testing completed on
thermal and thermomechanical properties

(FULL PAGE -- 6085 TABLE)

Table 2.4-1. Summary of laboratory testing completed on thermal and thermomechanical properties

Stratigraphic unit	Core source	Number of samples and type of tests[a]	Testing laboratory[b]	Reference
Pomona flow	DB-5	2K, 1C	LBL	Martinez-Baez and Amick (1978)
	DC-10	3K, 3C, 3a	CSM	Duvall et al. (1978)
	DC-11	2K	CSM	CSM (1978)
	DB-5, DB-15	2K, 2C, 2a	PNL	Erickson and Krupka (1980)
	NSTF	20K, 20C, 20a	FSI	FSI (1980a, 1980b, 1981b)
	NSTF	6K, 3C, 2a	LBL	Myer (1982)
Umtanum flow	DH-5	2K, 2C	LBL	Martinez-Baez and Amick (1978)
	DC-2, DDH-3, DH-4, DH-5	6K, 6a	CSM	CSM (1978)
	DC-4	6a	CSM	Miller (1979a)
	DC-2	4K, 4C, 4a	FSI	FSI (1981a)
	RRL-2	5K, 3C, 2a	LBL	Myer (1982)
Cohassett flow	DC-2	3K, 3a	CSM	CSM (1978)
	RRL-2	6K, 3C, 2a	LBL	Myer (1982)
Grande Ronde Basalt, other flows	DDH-3, DH-4, DH-5	17K, 19a	CSM	CSM (1978)
	DB-5	2K, 1C	LBL	Martinez-Baez and Amick (1978)
	DC-6	6a	CSM	Miller and Bishop (1979)
	DC-8	9a	CSM	Miller (1979b)

Total numbers of tests:

Pomona flow	35K,	29C,	27a
Umtanum flow	17K,	9C,	18a
Cohassett flow	9K,	3C,	5a
Other Grande Ronde Basalt flows	19K,	1C,	34a
Total	80K,	42C,	84a

[a]Type of test
K = thermal conductivity
C = heat capacity
a = coefficient of thermal expansion

[b]Testing laboratory
LBL = Lawrence Berkeley Laboratory
CSM = Colorado School of Mines
PNL = Pacific Northwest Laboratory
FSI = Foundation Sciences, Inc.

Table 2.4-2. Thermal property test methods

Thermal property	Test method	Reference
Thermal conductivity	Transient comparator	CSM (1978)
	Steady-state comparator	Martinez-Baez and Amick (1978), Duval et al. (1978), Erikson and Krupka (1980), FSI (1980a, 1980b, 1981a, 1981b), Myer (1982)
Heat capacity	Copper-block drop calorimeter	Erikson and Krupka (1980)
	Adiabatic fluid calorimeter	FSI (1980a, 1980b, 1981a, 1981b)
	Adiabatic heating calorimeter	Duvall et al. (1978)
	Oxide analysis calculations	Martinez-Baez and Amick (1978), Erikson and Krupka (1980), Myer (1982)
Thermal expansion	Dilatometer	Duvall et al. (1978), CSM (1978), Miller and Bishop (1979), Miller (1979a, 1979b), Erikson and Krupka (1980)
	Strain gage	FSI (1980a, 1980b, 1981a, 1981b), Myer (1982)

Table 2.4-3. Pomona flow thermomechanical test results

Property	Number of samples	Mean	Standard deviation
Thermal conductivity (W/m·K)[a]	30	1.85	0.38
Thermal expansion coefficient (με/°C)	38	6.40	1.16
Heat capacity (J/kg·K; T is in °C)[b]	26	C = 845 + 0.519T	--

NOTE: From Sublette, 1983.
[a]To convert W/m·K to cal/cm·s·°C, divide by 418.4.
[b]To convert J/kg·K to cal/g°C, divide by 4,184.

Table 2.4-4. Umtanum flow thermomechanical test results

Property	Number of samples	Mean	Standard deviation
Thermal conductivity (W/m·K)[a]	11	1.71	0.48
Thermal expansion coefficient (με/°C)	9	6.51	0.33
Heat capacity (J/kg·K; T is in °C)[b]	9	C = 862 + 0.586T	--

NOTE: From Sublette (1983).
[a]To convert W/m·K to cal/cm·s·°C, divide by 418.4.
[b]To convert J/kg·K to cal/g°C, divide by 4,184.

Table 2.4-5. Cohassett flow thermomechanical test results

Property	Number of samples	Mean	Standard deviation
Thermal conductivity (W/m·K)[a]	6	1.51	0.15
Thermal expansion coefficient ($\mu\epsilon$/°C)	2	6.02	0.42
Heat capacity (J/kg·K; T is in °C)[b]	3	C = 766 + 0.816T	—

NOTE: After Sublette, 1983.

[a]To convert W/m·K to cal/cm·s·°C, divide by 418.4.

[b]To convert J/kg·K to cal/g°C, divide by 4,184.

Table 2.4-6. Thermal conductivity of similar rock

Rock	Thermal conductivity (W/m·K)*		
	Number	Mean	Range
Karoo dolerite (Orange Free State, South Africa)	9	2.0	1.7-2.3
Ventersdorp lava (Orange Free State, South Africa)	9	3.1	2.6-3.6
Ventersdorp lava (Transvall, South Africa)	15	3.0	2.7-3.3
Portage Lake lava (Calumet, Michigan)			
Dense flows	27	2.1	1.7-2.8
Amygdoloidal tops	10	2.7	2.3-3.8
Porphyrite and diabase (Grass Valley, California)	21	3.0	2.6-3.4

NOTE: From Clark (1966).
*To convert W/m·K to cal/cm·s·°C, divide by 418.4.

Table 2.4-7. Thermal expansion coefficient
of similar rock

Rock	Thermal expansion coefficient ($\mu\epsilon$/°C)	
	Number	Mean and standard deviation
Granites and rhyolites	21	8 ± 3
Andesites and diorites	4	7 ± 2
Basalts, gabbros, and diabase	10	5.4 ± 1

NOTE: From Clark (1966).

Table 2.4-8. The effect of saturated
porosity on thermal conductivity

Porosity (%)	Ratio of conductivities of saturated, porous rock to dry, nonporous rock
0	1.0
1	0.99
3	0.97
4	0.95

NOTE: From Roy et al. (1981, pp. 417-418) and computational brief No. _____.

Table 2.5-1. Procedures documents for
thermal and thermomechanical tests

Test name	Test plan document
Full-Scale Heater Test 1	Rockwell (1980a)
Full-Scale Heater Test 2	Rockwell (1980a)
Jointed block test	Cramer (1984)

Table 2.5-2. Large-scale thermal and thermochemical
properties of similar rocks

(oversized table)

Table 2.5-2. Large-scale thermal and thermomechanical properties of similar rocks

Rock type	Location	Test configuration	Thermal conductivity (W/m °C)	Heat capacity (J/kg °C)	Thermal expansion coefficient (10⁻⁶/ C)	Reference
Granite	Stripa	5-kW full-scale heater experiment	3.2-3.69	771-831	11.1	Jeffrey et al. (1979) Chan et al. (1980, p. 18)
Granite (Climax Stock)	Nevada Test	Single line heater and spent fuel test	3.6	--	--	Ramspott et. al (1982) Tammemagi and Chieslar (1985, p. 61)
Granitic Gneiss (block test)	Idaho Springs	Block test, line of heaters to simulate a planar heat source	3.8	--	6.07-9.86	Hardin et al. (1982, pp. 81 and 99)

Table 2.5-3. Thermal and thermo-
mechanical properties
used in design

Property	Design value, dense interior Cohassett flow
Thermal conductivity W/m °C	1.51
Heat capacity kj/kg °C	0.929 at 200 °C
Density kg/m³	2.80
Thermal expansion coefficient με/°C	6.02

NOTE: From Sublette (1983).

Table 2.6-1. Core disking percentages for the dense interiors of
horizons studied in boreholes RRL-2, RRL-6, and RRL-14

(FULL PAGE -- 6085 TABLE)

Table 2.6-1. Core disking percentages for the dense interiors of repository studied horizons in boreholes RRL-2, RRL-6, and RRL-14

Borehole	Rocky Coulee flow			Cohassett flow			McCoy Canyon flow			Umtanum flow		
	Dense interior, m (ft)	Disked (m)	Disked (%)	Dense interior, m (ft)	Disked, m (ft)	Disked (%)	Dense interior, m (ft)	Disked, m (ft)	Disked (%)	Dense interior, m (ft)	Disked, m (ft)	Disked (%)
RRL-2	46.6 (152.9)	9.1 (29.9)	19.5	45.1 (148.0)	10.3 (33.8)	22.8	31.4 (103.0)	14.7 (48.2)	46.8	25.3 (83.0)	17.4 (57.1)	68.9
RRL-6	46.2 (151.6)	38.5 (126.3)	83.3	43.3 (142.1)	3.8 (12.5)	8.8	30.5 (100.1)	8.1 (26.6)	26.6	41.8 (137.1)	23.1 (75.8)	55.3
RRL-14	30.5 (100.1)	20.8 (68.2)	68.2	35.7 (117.1)	22.8 (74.8)	63.9	33.2 (108.9)	17.7 (58.1)	53.3	39.0 (128.0)	36.9 (121.1)	94.6
Total	123.3 (404.5)	68.4 (224.4)		124.1 (407.2)	36.9 (121.1)		95.1 (312.0)	40.5 (132.9)		106.1 (348.1)	77.4 (253.9)	
Average percent disked			55.5			29.7			42.6			73.0

Note: From Long and WCC (1984, p. I-231).

Table 2.6-2. Calculated in situ stress, boreholes DB-15 and DC-12

(FULL PAGE -- 6085 TABLE)

Table 2.6-2. Calculated in situ stress within the reference repository location, boreholes RRL-2, RRL-6, and DC-4

Borehole	Test depth (m)	P₀ (MPa)	Maximum horizontal stress, σ$_H$	Minimum horizontal stress, σ$_h$ (MPa)	Vertical stress, σ$_v$ (MPa)	Fracture orientation	Stress ratios σ$_H$/σ$_h$	σ$_H$/σ$_v$
RRL-2								
Cohassett flow	924	8.3	52.6	30.3	23.0	N. 19° W.	1.73	2.28
	928	8.4	63.4	35.7	23.2	N. 04° E.	1.78	2.73
	945[a]	-	-	-	-	N. 17° E.	-	-
	947[a]	-	-	-	-	N. 03° E.	-	-
	967[a]	-	-	-	-	N. 19° W.	-	-
	970[a]	-	-	-	-	N. 16° E.	-	-
	991[a]	-	-	-	-	N. 23° W.	-	-
Grande Ronde 7	1,058	9.7	58.1	33.6	26.5	N. 08° W.	1.73	2.19
Umtanum flow	1,147[a]	-	-	-	-	N. 03° E.	-	-
	1,160	10.7	65.3	37.5	29.2	N. 08° E.	1.74	2.24
	1,166	10.7	63.9	35.5	29.4	N. 10° W.	1.80	2.17
RRL-6								
Cohassett flow	1,008	9.2	64.4	33.9	25.2	N. 28° E.	1.90	2.56
	1,017	9.3	67.4	33.4	25.4	N. 15° E.	2.01	2.66
	1,018[a]	-	-	-	-	N. 15° E.	-	-
McCoy Canyon flow	1,105	10.1	66.6	36.8	27.7	N. 08° E.	1.81	2.41
	1,109	10.1	56.9	28.4	27.8	N. 30° W.	2.00	2.05
	1,131	10.4	64.3	34.0	28.3	N. 22° E.	1.89	2.27
Umtanum flow	1,189	10.9	57.9	33.2	29.9	N. 21° W.	1.74	1.94
	1,195	11.0	53.6	31.0	30.0	[b]	1.73	1.78
DC-4								
Cohassett flow	921[a]	-	-	-	-	N. 18° E.	-	-
	966[a]	-	-	-	-	N. 23° E.	-	-
	976	8.6	59.9	30.8	24.4	N. 06° W.	1.95	2.45

NOTE: After Kim et al. (1986).
   To convert meters to feet, multiply by 3.28.
   To convert MPa to lbf/in², multiply by 145.

[a]Fracture orientation recorded; no stress magnitude.
[b]No fracture impression taken.
[c]Calculated assuming P₀ = static hydraulic head in the borehole.

Table 2.6-3. Calculated in situ stress within the reference repository
location, boreholes RRL-2, RRL-6, and DC-4

(FULL PAGE -- 6085 TABLE)

Table 2.6-3. Summary of mean stress values plus or minus standard deviation for each borehole within the reference repository location

Borehole	Number of tests	Mean depth m (ft)	Mean, σ_H, MPa(lbf/in²)	Mean, σ_h, MPa(lbf/in²)	Mean, σ_v, MPa(lbf/in²)	Mean fracture orientation	Mean stress ratios	
							σ_H/σ_h	σ_H/σ_v
DC-4	1	976 (3,201.3)	59.9 (8,685.5)	30.8 (4,466)	24.4 (3,538)	N. 12°E.[a] ±16°	1.95	2.45
RRL-6	7	1,174±74 (3,850.7±242.7)	61.6±5.4 (8,930±782)	33.0±2.4 (4,785±348)	27.8±1.9 (4,031±275.5)	N. 05° E. ±22°	1.87 ±0.11	2.24 ±0.33
RRL-2	5	1,047±119 (3,436±390)	60.6±5.3 (8,792±766)	34.5±2.7 (5,006±394)	26.3±3.1 (3,808±448)	N. 03° W.[b] ±14°	1.76 ±0.03	2.32 ±0.23
All RRL[c] holes combined	13	1,074±96 (3,522.7±314.9)	61.1±4.9 (8,857±713)	33.4±2.7 (4,843±362.5)	26.9±2.5 (3,900.5±362.5)	N. 02° E.[d] ±17°	1.83 ±0.11	2.29 ±0.28

NOTE: After Kim et al. (1986)

[a]Based on 3 impression tests.

[b]Based on 11 impression tests.

[c]RRL = reference repository location.

[d]Based on 21 impression tests.

Table 2.6-4. Summary of mean stress values plus or minus standard
deviation for each flow within the reference repository location

(FULL PAGE -- 6085 TABLE)

Table 2.6-4. Summary of mean stress values plus or minus standard deviation for each flow within the reference repository location.

Borehole	Number of tests	Mean depth m (ft)	Mean, σ_H, MPa(lbf/in²)	Mean, σ_h, MPa(lbf/in²)	Mean, σ_v, MPa(lbf/in²)	Mean fracture orientation	Mean stress ratios	
							σ_H/σ_h	σ_H/σ_v
Cohassett flow RRL-2 RRL-6 DC-4	5	970±44 (3,182±144)	61.5±5.7 (8,918±827)	32.8±2.2 (4,756±319)	24.2±1.1 (3,509±160)	N. 06° E.* ±17°	1.87 ±0.12	2.54 ±0.18
Grande Ronde 7 RRL-2	1	1,058 (3,470)	58.1 (8,425)	33.6 (4,872)	26.6 (3,857)	N. 08° W.	1.73	2.19
McCoy Canyon flow RRL-6	3	1,115±14 (3,657±46)	62.6±5.1 (9,077±740)	33.1±4.3 (4,800±624)	27.9±0.3 (4,046±44)	N. 00° E. ±27°	1.90 ±0.10	2.24 ±0.18
Umtanum flow RRL-2 RRL-6	4	1,178±17.1 (3,863±56)	60.2±5.4 (8,722±788)	34.3±2.8 (4,977±407)	29.6±0.4 (4,295±60)	N. 05° W. ±13°	1.75 ±0.03	2.03 ±0.21

NOTE: After Kim et al. (1986)

*Based on 13 tests.

Table 2.6-5. Comparison of hydraulic fracturing results in the Umtanum
flow from inside and outside the reference repository location

(FULL PAGE -- 6085 TABLE)

Table 2.6-5. Comparison of hydraulic fracturing results in the Umtanum flow from inside and outside the reference repository location

Location of boreholes	Number of test	Mean test depth m (ft)	Mean σ_H, MPa (lbf/in2)	Mean σ_h, MPa (lbf/in2)	Mean σ_v, MPa (lbf/in2)	Mean fracture orientation	Mean stress ratios σ_H/σ_h σ_H/σ_v
Outside the RRL* DC-12	6	1,024 ± 15 (3,351 ± 49)	61.2 ± 6.8 (8,874 ± 986)	34.8 ± 2.7 (5,046 ± 392)	26.2 ± 0.4 (3,799 ± 58)	N. 23° E. ± 21°	1.76 ± 0.08 2.33 ± 0.24
Inside the RRL RRL-2, RRL-6	4	1,177 ± 16 (3,863 ± 56)	60.2 ± 5.4 (8,722 ± 788)	34.3 ± 2.8 (4,977 ± 407)	29.6 ± 0.4 (4,295 ± 60)	N. 05° W. ± 13°	1.75 ± 0.03 2.03 ± 0.21

NOTE: After Kim et al. (1986)

*RRL = reference repository location.

Table 2.7-1. Summary of tunnel and shaft conditions where
spalling or rock burst occurred

(FULL PAGE -- 6085 TABLE)

Table 2.7-1. Examples of tunnel and shaft conditions where spalling or rock burst occurred

Site	Reference	Rock type	Geologic structure	Uniaxial compressive strength, MPa (kip/in²)	Depth, m (ft)	In situ stress, MPa (kip/in²)	Ratio in situ stress, strength	Failure	Rock support
Kan Etsu Tunnel, Japan Tunnel	Saito et al. (1983)	Quartz diorite	several joint sets	230 (33.4)	960 (3,150)	22.9 (3.3)	0.10	Rock burst	Face bolts of tunnel face
Brofjorden Tunnel, Sweden	Bergman and Stille (1983)	Granite	three joint sets, two vertical, one horizontal	200 (29.0)	60 (197)	15 (2.2)	0.075	Roof spall cave-in	Bolts and mesh
Vietas Tunnel, Sweden	Elfman (1969)	Siltstone and gneiss	one joint set	?	250 (820)	35 (5.1)	?	Horizontal compression failure	Rock bolts and net
South Africa Developments	Hoek and Brown (1980)	Massive quartzite	NA*	240 (34.8) 183 (26.5)		69 (10.0) 88 (12.8)	0.29 0.48		Steel girders on concrete walls Steel arches Steel arches
Ertan Hydropower Station, China	Bai et al. (1983) Shiwie and Guangyu (1982)	Basalt, syenite	NA	NA	Up to 200 (650)	Up to 64 (9.3)	?	Core disking, rock bursts in test galleries	NA
South Africa Shaft Station	Vasey (1983)	Granite	One joint set 10 m spacing (32.8 ft)	237 (34.4)	1,613 (5,290)	90 (13.1)	0.38	Splitting and bursting at close to shaft bottom	Lining installed
Caladay Shaft, Idaho	Blake (1984)	Quartzite		~185 (26.8)	1,400 (4,060)	NA	NA	Small rock burst (2-3 m³)	NA - Destress blasting used to alleviate problems
Thierry Shaft, Ontario	Blake (1984)	Granite		260 (37.7)	Up to 500 (1,640)	NA	NA	Spalling (<1 m³)	NA - Destress blasting
Silver Shaft, Idaho	Blake (1984)	Quartzite		300 (43.5)	Up to 1,900 (6,200)	NA	NA	Spalling	Split set - mesh

*NA = Not available.

Table 2.8-1. Excavations in basalt using drill-and-blast method
(sheet 1 of 2)

(FULL PAGE -- 6085 TABLE)

Table 2.8-1. Excavations in basalt using drill-and-blast method   (sheet 1 of 2)

Name	Structure type	Opening size, span	Location	Overburden depth	Rock support of basalt	
					Temporary	Final
Bacon Tunnel, second unit	Horseshoe-shaped tunnel	8.69-m (28.51-ft) finished diameter	Coulee City, WA	At tunnel crown 49.77 m (163.31), maximum 73.15 m (240.01 ft)	Steel set with timber backing, wall plate with 4-m (12-ft) rock bolts below wall plate, bolted as necessary and shotcreted	Entire tunnel fully lined, concrete 58-79 cm (198.3-239.2 ft)
Black Butte Dam, diversion tunnel	Circular tunnel section	7-m (72.97-ft) finished inside diameter	Orland, CA	--	Steel sets, 0.3-0.6-m (0.98-1.97) spacing (steel rib supports)	Concrete lined?
Burlington Northern Railroad tunnels	Tunnel	5 m (16.41 ft)	Pasco, WA	Up to 25 m (82.03 ft)	--	Two unlined, 19 fully concrete-lined
Cougar Dam, main diversion tunnel	Horseshoe-shaped tunnel	5.49 m (18.01 ft) wide x 6.10 m (20.01 ft) high	Williamette Basin, OR	--	Rock bolts	--
Cougar Dam, Rush Creek diversion tunnel	Horseshoe-shaped tunnel	2.44-m (8-ft) dia.	Williamette Basin, OR	--	None	None
Cougar Dam, Penstock Tunnel	Tunnel	4.57 m (14.99 ft) wide x 4.37 m (14.33 ft) high	Williamette Basin, OR	--	--	Rock bolts, 1.5-m (4.92 ft) pattern radiating across crown
Cougar Dam, outlet tunnel	Circular tunnel section	5.13-m (16.83-ft) dia.	Williamette Basin, OR	--	--	1.8-m (5.91-ft) rock bolts with no standard pattern
Foster Dam, diversion tunnel	Horseshoe-shaped tunnel	9.75 m (91.99 ft) high x 9.75 m (91.99 ft) wide	South Santiam River, OR	16.59-31.20 m (54.4-102.37 ft)	--	1.8-3.0-m (5.91-9.84-ft) rock bolts
Green Peter Dam, diversion tunnel	Horseshoe-shaped tunnel	8.9-m (29.2-ft) dia.	Middle Santiam River, OR	20.5-44.5 m (67.26-146 ft)	None	None
Highway No. 14, tunnels 1-5	U-shaped	7.62 m (25 ft) wide x 6.10 m (20.01 ft) high	Vancouver, WA	21-48 m (68.9-157.49 ft)	--	Fully lined with concrete
Highway No. 14, tunnel 6	U-shaped	7.62 m (25 ft) wide x 6.10 m (20.01 ft) high	Vancouver, WA	21-48 m (68.9-157.49 ft)	--	Rock bolts on 1.8-m (5.91 ft) spacing with wire mesh
Highway No. 14, tunnel 7	U-shaped	7.62 m (25 ft) wide x 6.10 m (20.01 ft) high	Vancouver, WA	21-48 m (68.9-157.49 ft)	--	Fully lined with timber R15 and lagging support
Krafla geothermal power plant	Underground power plant cavern	15 m (49.22 ft) high x 30 m (98.43 ft) long x 10 m (32.81 ft) wide	Krafla, Iceland	50 m (164.05 ft)	None	None
Keweenawan copper mines	Open advancing stopes	--	Keweenaw Peninsula, MI	Maximum 2,500 m (8,202.5 ft)	--	--
Lost Creek Lake, diversion tunnel	Horseshoe-shaped tunnel	6.86-m (22.51-ft) dia.	Medford, OR	46 m (150.93 ft)	Steel ribs where needed, 24- and 33-m (70- and 100-ft) rock bolts on 1.5-m (4.92 ft) centers throughout	Concrete-lined

Table 2.8-1. Excavations in basalt using drill-and-blast method
(sheet 2 of 2)

(FULL PAGE -- 6085 TABLE)

Table 2.8-1. Excavations in basalt using drill-and-blast method (sheet 2 of 2)

Name	Structure type	Opening size, span	Location	Overburden depth	Rock support of basalt	
					Temporary	Final
Lost Creek Lake, outlet tunnel	Circular tunnel	3.97-m (11.86-ft) dia.	Medford, OR	Maximum 76 m (249.76 ft) to top of dam embankment	Rock bolt in crown	Concrete-lined
Lucky Peak Dam, outlet tunnel	Circular tunnel	7-m (22.97-ft) dia.	Boise River, ID	70 m (229.67 ft)	None in massive, columnar, jointed basalt; circular steel ribs in soft weathered basalt	Concrete-lined
Mahi Hydel hydro-electric plant	Underground power plant cavern	45 m (147.65 ft) x 15 m (49.23 ft) x 30 m (32.81 ft)	Panam Basin, India	50 m (164.05 ft)	—	—
Near-Surface Test Facility	Test facility	7 m (23 ft) x 7 m (23 ft) 4.9 m (16 ft) x 8.5 m (28 ft)	Hanford Site, WA	Up to 82 m (270 ft)	Rock bolts	Concrete and steel portal sets Shotcrete
Poatina underground power station	Headrace tunnel circular	5.79-m (19-ft) dia.	Central Tasmania	—	None in competent-rock steel sets on 1.2-m (3.94-ft) centers in weathered rock	—
River Sog hydroelectric development	Circular intake tunnel	4.72-m (15.49-ft) dia.	Reykjavic, Iceland	—	—	Plate steel and concrete-lined
River Sog hydroelectric development	Horseshoe-shaped discharge tunnel	6.10-m (20.01-ft) dia.	Reykjavic, Iceland	—	—	Concrete-lined
River Sog hydroelectric development	Machine hall	43 m (141.08 ft) long x 12 m (39.37 ft) wide x 18 m (59.06 ft) high	Reykjavic, Iceland	—	—	Fully concrete-lined
River Sog hydroelectric development	Tailrace surge chamber	9 m (29.53 ft) high x 4.6 m (15.09 ft) wide	Reykjavic, Iceland	—	—	Fully concrete-lined
Snoqualmie Falls hydroelectric project	Unit 1 turbine chamber	61 m (200.14 ft) long x 12 m (39.37 ft) wide x 9 m (29.53 ft) high	Snoqualmie, WA	82 m (269.04 ft)	None	None
Snoqualmie Falls hydroelectric project	Unit 1 tailrace tunnel	3.66 m (12.01 ft) wide x 8.23 m (27 ft) high	Snoqualmie, WA	82 m (269.04 ft)	None	None
Snoqualmie Falls hydroelectric project	Unit 2 headrace tunnel circular	8.66-m (27-ft) dia.	Snoqualmie, WA	82 m (269.04 ft)	None	Fully lined with concrete for hydraulic purposes, rather than structural support
Vista Ridge tunnel	Half-circular section	15-m (49.22-ft) dia.	Portland, OR	—	—	Steel ribs on variable spacing
Underground fuel storage tanks, Pearl Harbor	Cylindrical tanks	30.5-m (100.07-ft) dia., 75-m (246.36-ft) dia.	Red Hill, HI	30.5 m (100.07 ft)	—	Heavily reinforced concrete to withstand pressure of stored fuels
Erton hydropower station	Main power house	63 m (206.7 ft) high x 27.5 m (90.23 ft) wide x 240 m (787.44 ft) long	Lower Yalong River, SW China	Up to 500 m (1,640.5 ft)	—	—
Kan Esto tunnel	Expressway tunnel	85 m² (925.36 ft²)	Tanigawa-Range, Japan	>1,000 m (3,281 ft)	Rock bolt ribs and face to stop rock burst	—

Table 2.8-2. Example of water inflows recorded during tunneling and mining
(sheet 1 of 2)

(Oversized table)

Table 2.8-2. Examples of water inflows recorded during tunneling and mining (sheet 1 of 2)

Location	Condition encountered	Recovery method	Reference
No. 4 main tunnel Tappi section of Seikan Tunnel, Japan	87.2 m^3/min of steady groundwater inflow	Drainage Grouting	Mochida (1979)
No. 5 main tunnel Yoshioka section of Seikan Tunnel, Japan	20.7 m^3/min of steady groundwater inflow	Drainage Grouting	Mochida (1979)
Yoshioka section of Seikan Tunnel, Japan	18,800 gal/min of instanteous groundwater inflow	Divert to tunnel with larger cross section, high-power pump brought in to increase drain capacity, bulkhead erected, bypath tunnel excavated, recovery to face	
Enasan Tunnel, Japan	Pressures up to 5 MPa, total quantity of water that flowed was 50 million tons	Pilot tunnel advanced ahead of main tunnel to full length, cross-sectional design changes such that height-bredth ratio was smaller, drainage drill holes, breasting and timbering of debris	Yano et al. (1979)
Shimo-Arai section of Haruna Tunnel, Japan	Average volume of water inflow for the wells ranges from 0.2-0.3 m^3/min to 1.0-1.5 m^3/min	Deep wells to lower groundwater level and to reduce volume of water inflow	Yokoyama (1979)
Linkoping, Sweden	Water leak of 20 m^3/h	Pilot tunnel followed by two side stopes, grout from pilot tunnel, shotcrete and post-grouting	Jansson (1979)

Table 2.8-2.   Example of water inflows recorded during tunneling and mining
(sheet 2 of 2)

(Oversized table)

Location	Condition encountered	Recovery method	Reference
	Leaks after blasting	Shotcrete and post-grouting	
	Inflow through cavern floor	Shielding curtain of vertical grout holes	
Lavera, France	Water leakage of 25 m^3/h	Grouting	Jansson (1979)
	Inflow of 300 m^3/h	Pumping Grouting	
Vexin, France	Leakage of 130 m^3/h	Shield of vertical holes drilled and grouted	Jansson (1979)
	Leakage of 30 m^3/h	Sludge suction lorry	
	Inflow of 470 m^3/h	Increase pump capacity, grout shield erected, water redirected	
Spirit Lake Drainage Tunnel, Washington	Peak inrush of 5.7 m^3/min falling to 4.2 m^3/min in 1 h and 0.4 m^3/min in 2 d		Patricio (1985)
Orange-Fish Tunnel, South Africa	Peak inrush of 333 m^3/min	Exploratory drilling, grouting from surface, dewatering pilot boreholes	Keyser and Krige (1978)
West Dreifontein, Transvaal, South Africa	Peak inflow of 267 m^3/min at 874 m depth	Emergency plugs, bulkhead doors, and grouting	Wolmarans and Guise-Brown (1978)

Table 2.8-3. Repository drift
dimensions (excavated)

Drift	Height, m (ft)	Width, m (ft)
Emplacement room Phase I Phase II	4.0 (13.2)	7.5 (24.5)
Panel entry, Panel crosscuts	3.3 (10.7)	4.5 (14.7)
Main entry	3.9 (12.7)	5.1 (16.7)

NOTE: After KE/PB (1986).

Table 2.8-4. Rock mass quality classification of repository
excavation in the Cohassett flow

(Oversized table)

Table 2.8-4. Rock mass quality classification of repository excavation in the Cohassett flow

Parameter	Parameter value Entablature	Parameter value Colonnade	Entablature Worst	Entablature Best	Colonnade Worst	Colonnade Best
Rock quality designation	30-50	70-90	30	50	70	90
Joint set number	3 joint sets to 3 joint plus random	2 joint sets plus random to 3 joint sets	12	9	9	6
Joint roughness number	smooth to rough, undulating	slickensided to smooth, undulating	2	3	1.5	2
Joint alteration number	softening or low friction clay mineral coatings, small quantities of swelling clay		4	4	4	4
Joint water reduction	minor to medium inflow or pressure	minor inflow	0.66	1.0	1.0	1.0
Stress reduction factor	high stress, tight tight structure ($\sigma_C/\sigma_1 = 4.6$)	mild rock burst ($\sigma_C/\sigma_1 = 4.7$)	1 2	0.5 (roof) 1 (walls)	6	4
Stress reduction factor (with thermal loading)	--	--	2 3	1 (roof) 2 (walls)	8	6
Rock mass quality rating (ambient)	--	--	0.8 0.4	8.3 (roof) 4.2 (walls)	0.5	1.9
Rock mass quality rating (thermal)	--	--	0.4 0.3	4.1 (roof) 2.1 (walls)	0.4	1.2
Class (ambient)	--	--	Very poor to fair rock		Very poor to poor rock	

NOTE: From Barton (1984), design ranges shown; Barton (1984) also states extreme values.

Table 2.8-5. Hydraulic conductivity of repository
intraflow zones

Zone	Conductivity	Reference
Dense interior	$<10^{-11}$ m/s (10^{-6} ft/d)	DOE 1985, p. 3-85
Flow top	10^{-5} - 10^{-9} m/s	DOE 1985, p. 3-88
	(10^{0} - 10^{-4} ft/d)	

Table 2.8-6. Quantity of water inflow adoped in design

Conditions	Source	Amount	Reference
Normal	Seepage into tunnels	5.8 L/s (91 gal/min)	2
		20 L/s (310 gal/min)	1
	Drilling water	32 L/s (500 gal/min)	1
	Leakage around shaft	26 L/s (410 gal/min)	1
Abnormal	Intersection of drift	158 L/s (2,500 gal/min)	1
	with fracture connected	219 L/s (3,400 gal/min)	2
	to aquifer		

NOTE: 1 = RKE/PB (1983, Sec. 8.11.3).
2 = Baker (1985, Fig. 7).

Table 2.9-1. Summary of rock mass property data used
for Site Characterization Conceptual Design
After KE/PB 1986

Parameter	Reference units	Value	Range
Mechanical properties			
Strength	MPa	σ_c = 305 m = 22.34 s = 0.00421	NA*
Modulus	GPa	38	20-55
Poisson's ratio	--	0.25	0.20-0.35
Thermal and thermomechanical properties			
Thermal conductivity	W/m °K	1.51	1.32-1.74
Heat capacity	kJ/kg °K	0.929	0.783-1.01
Coefficient of thermal expansion	x 10^{-6}/°K	6.02	5.72-6.31
Bulk density	g/cm^3	2,800.0	2,600.0-2,900.0
In situ conditions			
Vertical stress	MPa	24.2	NA*
Maximum horizontal stress	MPa	61.5	50.1-72.9
Minimum horizontal stress	MPa	32.8	28.4-37.2

*NA = not applicable.

Table 2.9-2. Correlation of Chapter 2 of Regulatory Guide 4.17 with the
Annotated Outline

Regulatory Guide 4.17	Annotated Outline for SCP
2. GEOENGINEERING	**2. GEOENGINEERING**
2.1 Mechanical Properties of Rock Units--Continua	2.1 Mechanical Properties of Rock--Intact Rock
2.2 Mechanical Properties of Rock Units--Large Scale	2.2 Mechanical Properties of Rock Units--Dicontinuities
2.3 Mechanical Properties of Units-Discontinua	2.3 Mechanical Properties of Rock Units--Large-scale
2.4 Thermal and Thermomechanical Properties--Laboratory Results	2.4 Thermal and Thermomechanical Properties--Intact Rock
2.5 Stress Field	2.6 Existing Stress Regime
2.6 Special Geoengineering Properties	2.7 Special Geoengineering Properties
2.7 Excavation Characteristics of Rock Mass	2.8 Excavation Characteristics of Rock Mass
	Additional Sections Added to the Annotated Outline
	2.0 Introduction
	2.5 Thermal and Thermomechanical Properties--Large Scale
	2.9 Summary